JSCSEN 86(3)213–340(2021)

ISSN 1820-7421(Online)

Journal of the Serbian Chemical Society

Electronic version

VOLUME 86

No 3

BELGRADE 2021

Available on line at

www.shd.org.rs/JSCS/

The full search of JSCS is available through

DOAJ DIRECTORY OF OPEN ACCESS JOURNALS

www.doaj.org

The **Journal of the Serbian Chemical Society** (formerly Glasnik Hemijskog društva Beograd), one volume (12 issues) per year, publishes articles from the fields of chemistry. The **Journal** is financially supported by the **Ministry of Education, Science and Technological Development of the Republic of Serbia.**

Articles published in the **Journal** are indexed in **Clarivate Analytics products: Science Citation Index-Expanded™** – accessed *via* **Web of Science®** and **Journal Citation Reports®**.

Impact Factor announced 2020: **1.097; 5-year Impact Factor**: **1.023**.

Articles appearing in the **Journal** are also abstracted by: **Scopus, Chemical Abstracts Plus (CAplus℠), Directory of Open Access Journals, Referativnii Zhurnal (VINITI), RSC Analytical Abstracts, EuroPub, Pro Quest** and **Asian Digital Library.**

Publisher:	**Serbian Chemical Society**, Karnegijeva 4/III, P. O. Box 36, 1120 Belgrade 35, Serbia tel./fax: +381–11–3370–467, E-mails: **Society** – shd@shd.org.rs; **Journal** – jscs@shd.org.rs Home Pages: **Society** – http://www.shd.org.rs/, **Journal** – http://www.shd.org.rs/JSCS/
Internet Service:	Contents, Abstracts and full papers (from Vol 64, No. 1, 1999) are available in the electronic form at the Web Site of the **Journal** (http://www.shd.org.rs/JSCS/).
Former Editors:	**Nikola A. Pušin** (1930–1947), **Aleksandar M. Leko** (1948–1954), **Panta S. Tutundžić** (1955**–**1961), **Miloš K. Mladenović** (1962–1964), **Đorđe M. Dimitrijević** (1965–1969), **Aleksandar R. Despić** (1969–1975), **Slobodan V. Ribnikar** (1975–1985), **Dragutin M. Dražić** (1986–2006).
Editor-in-Chief:	BRANISLAV Ž. **NIKOLIĆ**, Serbian Chemical Society (E-mail: jscs-ed@shd.org.rs)
Deputy Editor:	DUŠAN **SLADIĆ**, Faculty of Chemistry, University of Belgrade
Sub editors:	
Organic Chemistry	DEJAN **OPSENICA**, Institute of Chemistry, Technology and Metallurgy, University of Belgrade JÁNOS **CSANÁDI**, Faculty of Science, University of Novi Sad
Biochemistry and Biotechnology	OLGICA **NEDIĆ**, INEP – Institute for the Application of Nuclear Energy, University of Belgrade
Inorganic Chemistry	MILOŠ **ĐURAN**, Serbian Chemical Society
Theoretical Chemistry	IVAN **JURANIĆ**, Serbian Chemical Society
Physical Chemistry	LJILJANA **DAMJANOVIĆ-VASILIĆ**, Faculty of Physical Chemistry, University of Belgrade
Electrochemistry	SNEŽANA **GOJKOVIĆ**, Faculty of Technology and Metallurgy, University of Belgrade
Analytical Chemistry	SLAVICA **RAŽIĆ**, Faculty of Pharmacy, University of Belgrade
Polymers	BRANKO **DUNJIĆ**, Faculty of Technology and Metallurgy, University of Belgrade
Thermodynamics	MIRJANA **KIJEVČANIN**, Faculty of Technology and Metallurgy, University of Belgrade
Chemical Engineering	TATJANA **KALUĐEROVIĆ RADOIČIĆ**, Faculty of Technology and Metallurgy, University of Belgrade
Materials	RADA **PETROVIĆ**, Faculty of Technology and Metallurgy, University of Belgrade
Metallic Materials and Metallurgy	NENAD **RADOVIĆ**, Faculty of Technology and Metallurgy, University of Belgrade
Environmental and Geochemistry	VESNA **ANTIĆ**, Faculty of Agriculture, University of Belgrade
History of and Education in Chemistry	DRAGICA **TRIVIĆ**, Faculty of Chemistry, University of Belgrade
English Language Editors:	LYNNE **KATSIKAS**, Serbian Chemical Society VLATKA **VAJS**, Serbian Chemical Society JASMINA **NIKOLIĆ**, Faculty of Technology and Metallurgy, University of Belgrade
Technical Editors:	VLADIMIR **PANIĆ**, ALEKSANDAR **DEKANSKI**, VUK **FILIPOVIĆ**, Institute of Chemistry, Technology and Metallurgy, University of Belgrade
Journal Manager & Web Master:	ALEKSANDAR **DEKANSKI,** Institute of Chemistry, Technology and Metallurgy, University of Belgrade
Office:	VERA **ĆUŠIĆ**, Serbian Chemical Society

Editorial Board

From abroad: **R. Adžić**, Brookhaven National Laboratory (USA); **A. Casini**, University of Groningen (The Netherlands); **G. Cobb**, Baylor University (USA); **D. Douglas**, University of British Columbia (Canada); **G. Inzelt**, Etvos Lorand University (Hungary); **N. Katsaros**, NCSR "Demokritos", Institute of Physical Chemistry (Greece); **J. Kenny**, University of Perugia (Italy); **Ya. I. Korenman**, Voronezh Academy of Technology (Russian Federation); **M. D. Lechner**, University of Osnabrueck (Germany); **S. Macura**, Mayo Clinic (USA); **M. Spiteller**, INFU, Technical University Dortmund (Germany); **M. Stratakis**, University of Crete (Grecce); **M. Swart**, University de Girona (Cataluna, Spain); **G. Vunjak-Novaković**, Columbia University (USA); **P. Worsfold**, University of Plymouth (UK); **J. Zagal**, Universidad de Santiago de Chile (Chile).

From Serbia: **B. Abramović**, **V. Antić, V. Beškoski**, **J. Csanadi**, **Lj. Damjanović-Vasilić**, **A. Dekanski**, **V. Dondur**, **B. Dunjić**, **M. Đuran, S. Gojković**, **I. Gutman**, **B. Jovančićević**, **I. Juranić**, **L. Katsikas**, **M. Kijevčanin**, **V. Leovac**, **S. Milonjić**, **V.B. Mišković-Stanković, O. Nedić**, **B. Nikolić**, **J. Nikolić, D. Opsenica**, **V. Panić**, **M. Petkovska**, **R. Petrović**, **I. Popović**, **B. Radak**, T. **Kaluđerović Radiočić, N. Radović**, **S. Ražić**, **D. Sladić**, **S. Sovilj**, **S. Šerbanović**, **B. Šolaja**, **Ž. Tešić**, **D. Trivić, V. Vajs**.

Subscription: The annual subscription rate is **150.00 €** including postage (surface mail) and handling. For Society members from abroad rate is **50.00 €**. For the proforma invoice with the instruction for bank payment contact the Society Office (E-mail: shd@shd.org.rs) or see JSCS Web Site: http://www.shd.org.rs/JSCS/, option Subscription.

Godišnja pretplata: Za članove SHD: **2.500,00 RSD**, za penzionere i studente: **1000,00 RSD**, a za ostale: **3.500,00 RSD**:za organizacije i ustanove: **16.000,00 RSD**. Uplate se vrše na tekući račun Društva: **205-13815-62**, poziv na broj **320**, sa naznakom "pretplata za JSCS".

Nota: Radovi čiji su svi autori članovi SHD prioritetno se publikuju.

Odlukom Odbora za hemiju Republičkog fonda za nauku Srbije, br. 66788/1 od 22.11.1990. godine, koja je kasnije potvrđena odlukom Saveta Fonda, časopis je uvršten u kategoriju međunarodnih časopisa (**M-23**). Takođe, aktom Ministarstva za nauku i tehnologiju Republike Srbije, 413-00-247/2000-01 od 15.06.2000. godine, ovaj časopis je proglašen za publikaciju od posebnog interesa za nauku. **Impact Factor** časopisa objavljen 2020. godine iznosi **1,097**, a petogodišnji **Impact Factor 1,023**.

INSTRUCTIONS FOR AUTHORS (2021)

GENERAL

The *Journal of the Serbian Chemical Society* (the *Journal* in further text) is an international journal publishing papers from all fields of chemistry and related disciplines. Twelve issues are published annually. The Editorial Board expects the editors, reviewers, and authors to respect the well-known standard of professional ethics.

Types of Contributions

Original scientific papers	(up to 15 typewritten pages, including Figures, Tables and References) report original research which must not have been previously published.
Short communications	(up to 8 pages) report unpublished preliminary results of sufficient importance to merit rapid publication.
Notes	(up to 5 pages) report unpublished results of short, but complete, original research
Authors' reviews	(up to 40 pages) present an overview of the author's current research with comparison to data of other scientists working in the field
Reviews[a]	(up to 40 pages) present a concise and critical survey of a specific research area. Generally, these are prepared at the invitation of the Editor
Surveys	(about 25 pages) communicate a short review of a specific research area.
Book and Web site reviews	(1 - 2 pages)
Extended abstracts	(about 4 pages) of Lectures given at meetings of the Serbian Chemical Society Divisions
Letters to the Editor	report miscellaneous topics directed directly to the Editor

[a]Generally, Authors' reviews, Reviews and Surveys are prepared at the invitation of the Editor.

Submission of manuscripts

Manuscripts should be submitted using the **OnLine Submission Form**, available on the JSCS Web Site (**http://www.shd-pub.org.rs/index.php/JSCS**). The manuscript must be uploaded as a Word.doc or .rtf file, with tables and figures (including the corresponding captions – above Tables and below Figures), placed within the text to follow the paragraph in which they were mentioned for the first time.

Please note that **Full Names (**First Name, Last Name), **Full Affiliation** and **Country** (from drop down menu) of **ALL OF AUTHORS** (written in accordance with English spelling rules - the first letter capitalized) must be entered in the manuscript Submission Form (Step 3). Manuscript Title, authors' names and affiliations, as well as the Abstract, **WILL APPEAR** in the article listing, as well as in **BIBLIOGRAPHIC DATABASES (WoS, SCOPUS...)**, in the form and in the order entered in the author details

Graphical abstract

Graphical abstract is a one-image file containing the main depiction of the authors work and/or conclusion and must be supplied along with the manuscript. It must enable readers to quickly gain the main message of the paper and to encourage browsing, help readers identify which papers are most relevant to their research interests. Authors must provide an image that clearly represents the research described in the paper. The most relevant figure from the work, which summarizes the content, can also be submitted. The image should be submitted as a separate file in **Online Submission Form - Step 2**.

Specifications: The graphical abstract should have a clear start and end, reading from top to bottom or left to right. Please omit unnecessary distractions as much as possible.

- **Image size:** minimum of 500×800 pixels (W×H) and a minimum resolution of 300 dpi. If a larger image is sent, then please use the same ratio: 16 wide × 9 high. Please note that your image will be scaled proportionally to fit in the available window in TOC; a 150x240 pixel rectangle. Please be sure that the quality of an image cannot be increased by changing the resolution from lower to higher, but only by rescanning or exporting the image with a higher resolution, which can be set in usual "settings" option.
- **Font:** Please use Calibri and Symbol font with a large enough font size, so it is readable even from the image of a smaller size (150 × 240 px) in TOC.
- **File type:** JPG and PNG only.

No additional text, outline or synopsis should be included. Please do not use white space or any heading within the image.

Cover Letter

Manuscripts must be accompanied by a cover letter (strictly uploaded in **Online Submission Step 2**) in which the type of the submitted manuscript and a warranty as given below are given. The Author(s) has(have) to warranty that the manuscript submitted to the *Journal* for review is original, has been written by the stated author(s) and has not been published elsewhere; is currently not being considered for publication by any other journal and will not be submitted for such a review while under review by the *Journal*; the manuscript contains no libellous or other unlawful statements and does not contain any materials that violate any personal or proprietary rights of any other person or entity. All manuscripts will be acknowledged on receipt (by e-mail).

Illustrations

Illustrations (Figs, schemes, photos…) in TIF or EPS format (JPG format is acceptable for colour and greyscale photos, only), must be additionally uploaded (Online Submission Step 2) as a separate file or one archived (.zip, .rar or .arj) file. Figures and/or Schemes should be prepared according to the **Artwork Instructions -** http://www.shd.org.rs/JSCS/jscs-pdf/Artwork_Instructions.pdf!

For any difficulties and questions related to **OnLine Submission Form -** https://www.shd-pub.org.rs/index.php/JSCS/submission/wizard, please refer to **User Guide -** https://openjournal-systems.com/ojs-3-user-guide/ , Chapter **Submitting an Article -** https://openjournalsystems.com/ojs-3-user-guide/submitting-an-article/. If difficulties still persist, please contact JSCS Editorial Office at **JSCS@shd.org.rs**

A manuscript not prepared according to these instructions will be returned for resubmission without being assigned a reference number.

Conflict-of-Interest Statement*: Public trust in the peer review process and the credibility of published articles depend in part on how well a conflict of interest is handled during writing, peer review, and editorial decision making. A conflict of interest exists when an author (or the author's institution), reviewer, or editor has financial or personal relationships that inappropriately influence (bias) his or her actions (such relationships are also known as dual commitments, competing interests, or competing loyalties). These relationships vary from those with negligible potential to those with great potential to influence judgment, and not all relationships represent true conflict of interest. The potential for a conflict of interest can exist whether or not an individual believes that the relationship affects his or her scientific judgment. Financial relationships (such as employment, consultancies, stock ownership, honoraria, paid expert testimony) are the most easily identifiable conflicts of interest and the most likely to undermine the credibility of the journal, the authors, and of science itself. However, conflicts can occur for other reasons, such as personal relationships, academic competition, and intellectual passion.

Informed Consent Statement*: Patients have a right to privacy that should not be infringed without informed consent. Identifying information, including patients' names, initials, or hospital numbers, should not be published in written descriptions, photographs, and pedigrees unless the information is essential for scientific purposes and the patient (or parent or guardian) gives written informed consent for publication. Informed consent for this purpose requires that a patient who is identifiable be shown the manuscript to be published. Authors should identify Individuals who provide writing assistance and disclose the funding source for this assistance. Identifying details should be omitted if they are not essential. Complete anonymity is difficult to achieve, however, and informed consent should be obtained if there is any doubt. For example, masking the eye region in photographs of patients is inadequate protection of anonymity. If identifying characteristics are altered to protect anonymity, such as in genetic pedigrees, authors should provide assurance that alterations do not distort scientific meaning and editors should so note. The requirement for informed consent should be included in the journal's instructions for authors. When informed consent has been obtained it should be indicated in the published article.

Human and Animal Rights Statement* When reporting experiments on human subjects, authors should indicate whether the procedures followed were in accordance with the ethical standards of the responsible committee on human experimentation (institutional and national) and with the Helsinki Declaration of 1975, as revised in 2000 (5). If doubt exists whether the research was conducted in accordance with the Helsinki Declaration, the authors must explain the rationale for their approach, and demonstrate that the institutional review body explicitly approved the doubtful aspects of the study. When reporting experiments on animals, authors should be asked to indicate whether the institutional and national guide for the care and use of laboratory animals was followed.

---

*International Committee of Medical Journal Editors ("Uniform Requirements for Manuscripts Submitted to Biomedical Journals"), February 2006

PROCEDURE

All contributions will be peer reviewed and only those deemed worthy and suitable will be accepted for publication. The Editor has the final decision. To facilitate the reviewing process, authors are encouraged to suggest up to three persons competent to review their manuscript. Such suggestions will be taken into consideration but not always accepted. If authors would prefer a specific person not be a reviewer, this should be announced. The Cover Letter must be accompanied by these suggestions. Manuscripts requiring revision should be returned according to the requirement of the Editor, within 60 days upon reception of the reviewing comments by e-mail.

The *Journal* maintains its policy and takes the liberty of correcting the English as well as false content of manuscripts **provisionally accepted** for publication in the first stage of reviewing process. In this second stage of manuscript preparation by JSCS Editorial Office, the author(s) may be required to supply some **additional clarifications and corrections**. This procedure will be executed during copyediting actions, with a demand to author(s) to perform corrections of unclear parts before the manuscript would be published OnLine as **finally accepted manuscript (OLF Section of the JSCS website)**. Please note that the manuscript can receive the status of **final rejection** if the author's corrections would not be satisfactory.

When finally accepted manuscript is ready for printing, the corresponding author will receive a request for proof reading, which should be performed within 2 days. Failure to do so will be taken as the authors agree with any alteration which may have occurred during the preparation of the manuscript for printing.

Accepted manuscripts of active members of the Serbian Chemical Society (all authors) have publishing priority.

MANUSCRIPT PRESENTATION

Manuscripts should be typed in English (either standard British or American English, but consistent throughout) with 1.5 spacing (12 points Times New Roman; Greek letters in the character font Symbol) in A4 format leaving 2.5 cm for margins. For Regional specific, non-standard characters that may appear in the text, save documents with Embed fonts Word option: *Save as -> (Tools) -> Save Options… -> Embed fonts in the text.*

The authors are requested to seek the assistance of competent English language expert, if necessary, to ensure their English is of a reasonable standard. The Serbian Chemical Society can provide this service in advance of submission of the manuscript. If this service is required, please contact the office of the Society by e-mail (jscs-info@shd.org.rs).

Tables, figures and/or schemes must be embedded in the main text of the manuscript and should follow the paragraph in which they are mentioned for the first time. **Tables** must be prepared with the aid of the **WORD table function**, without vertical lines. The minimum size of the font in the tables should be **10 pt**. Table columns must not be formatted using multiple spaces. Table rows must not be formatted using any returns (enter key; ↵ key) and are **limited to 12 cm width**. Tables should not be incorporated as graphical objects. **Footnotes to Tables** should follow them and are to be indicated consequently (in a single line) in superscript letters and separated by semi-column.

Table caption must be placed above corresponding Table, while **Captions of the Illustrations** (Figs. Schemes...) must follow the corresponding item. **The captions, either for Tables or Illustrations**, should make the items comprehensible without reading of the main text (but clearly referenced in), must follow numerical order (Roman for Tables, Arabic for Illustrations), and should not be provided on separate sheets or as separate files.

High resolution Illustrations (named as Fig. 1, Fig. 2… and/or Scheme 1, Scheme 2…) in **TIF or EPS format** (JPG format is acceptable for photos, only) **must be additionally uploaded as a separate files or one archived (.zip, .rar) file.**

Illustrations should be prepared according to the ARTWORK INSTRUCTIONS - http://www.shd.org.rs/JSCS/jscs-pdf/Artwork_Instructions.pdf. **!**

All pages of the manuscript must be numbered continuously.

DESIGNATION OF PHYSICAL QUANTITIES AND UNITS

IUPAC recommendations for the naming of compounds should be followed. SI units, or other permissible units, should be employed. The designation of physical quantities must be in italic throughout the text (including figures, tables and equations), whereas the units and indexes (except for indexes having the meaning of physical quantities) are in upright letters. They should be in Times New Roman font. In graphs and tables, a slash should be used to separate the designation of a physical quantity from the unit

(example: p / kPa, j / mA cm^{-2}, t / °C, T_0 / K, τ / h, ln (j / mA cm^{-2})…). Designations such as: p (kPa), t [min]…, are not acceptable. However, if the full name of a physical quantity is unavoidable, it should be given in upright letters and separated from the unit by a comma (example: Pressure, kPa; Temperature, K; Current density, mA cm^{-2}…). Please do not use the axes of graphs for additional explanations; these should be mentioned in the figure captions and/or the manuscript (example: "pressure at the inlet of the system, kPa" should be avoided). The axis name should follow the direction of the axis (the name of y-axis should be rotated by 90°). Top and right axes should be avoided in diagrams, unless they are absolutely necessary.

Latin words, as well as the names of species, should be in *italic*, as for example: *i.e.*, *e.g.*, *in vivo*, *ibid*, *Calendula officinalis* L., *etc*. The branching of organic compound should also be indicated in *italic*, for example, *n*-butanol, *tert*-butanol, *etc*.

Decimal numbers must have decimal points and not commas in the text (except in the Serbian abstract), tables and axis labels in graphical presentations of results. Thousands are separated, if at all, by a comma and not a point.

Mathematical and chemical equations should be given in separate lines and must be numbered, Arabic numbers, consecutively in parenthesis at the end of the line. All equations should be embedded in the text Complex equations (fractions, integrals, matrix…) should be prepared with the aid of the **Microsoft Equation 3.0** (or higher) or **MathType** (Do not use them to create simple equations and labels). **Using the Insert -> Equation option, integrated in MS Office 2010 and MS Office 2013, as well as insertion of equation objects within paragraph text IS NOT ALLOWED.**

ARTICLE STRUCTURE

- TITLE PAGE;
- MAIN TEXT – including Tables and Illustrations with corresponding captions;
- SUPPLEMENTARY MATERIAL (optional**)**

Title page

- **Title** in bold letters, should be clear and concise, preferably 12 words or less. The use of non-standard abbreviations, symbols and formulae is discouraged.
- AUTHORS' NAMES in capital letters with the full first name, initials of further names separated by a space and surname. Commas should separate the author's names except for the last two names when 'and' is to be used. In multi-affiliation manuscripts, the author's affiliation should be indicated by an Arabic number placed in superscript after the name and before the affiliation. Use * to denote the corresponding author(s).
- *Affiliations* should be written in italic. The e-mail address of the corresponding author should be given after the affiliation(s).
- *Abstract:* A one-paragraph abstract written of 150 – 200 words in an impersonal form indicating the aims of the work, the main results and conclusions should be given and clearly set off from the text. Domestic authors should also submit, on a separate page, an Abstract - Izvod, the author's name(s) and affiliation(s) in Serbian (Cyrillic letters). (Домаћи аутори морају доставити Извод (укључујући имена аутора и афилијацију) на српском језику, исписане ћирилицом, иза Захвалнице, а пре списка референци.) For authors outside Serbia, the Editorial Board will provide a Serbian translation of their English abstract.
- *Keywords:* Up to 6 keywords should be given. Do not use words appearing in the manuscript title
- RUNNING TITLE: A one line (maximum five words) short title in capital letters should be provided.

Main text – should have the form:

- **INTRODUCTION,**
- **EXPERIMENTAL (RESULTS AND DISCUSSION),**
- **RESULTS AND DISCUSSION (EXPERIMENTAL),**
- **CONCLUSIONS,**
- **NOMENCLATURE (optional) and**
- ***Acknowledgements*: If any.**
- REFERENCES (Citation of recent papers published in chemistry journals that highlight the significance of work to the general readership is encouraged.)

The sections should be arranged in a sequence generally accepted for publication in the respective fields. They subtitles should be in capital letters, centred and NOT numbered.

- The INTRODUCTION should include the aim of the research and a concise description of background information and related studies directly connected to the paper.
- The EXPERIMENTAL section should give the purity and source of all employed materials, as well as details of the instruments used. The employed methods should be described in sufficient detail to enable experienced persons to repeat them. Standard procedures should be referenced and only modifications described in detail. On no account should results be included in the experimental section.

Chemistry

Detailed information about instruments and general experimental techniques should be given in all necessary details. If special treatment for solvents or chemical purification were applied that must be emphasized.

Example: Melting points were determined on a Boetius PMHK or a Mel-Temp apparatus and were not corrected. Optical rotations were measured on a Rudolph Research Analytical automatic polarimeter, Autopol IV in dichloromethane (DCM) or methanol (MeOH) as solvent. IR spectra were recorded on a Perkin-Elmer spectrophotometer FT-IR 1725X. ^{1}H and ^{13}C NMR spectra were recorded on a Varian Gemini-200 spectrometer (at 200 and 50 MHz, respectively), and on a Bruker Ultrashield Advance III spectrometer (at 500 and 125 MHz, respectively) employing indicated solvents (*vide infra*) using TMS as the internal standard. Chemical shifts are expressed in ppm (δ / ppm) values and coupling constants in Hz (J / Hz). ESI-MS spectra were recorded on Agilent Technologies 6210 Time-Of-Flight LC-MS instrument in positive ion mode with CH_3CN/H_2O 1/1 with 0.2 % HCOOH as the carrying solvent solution. Samples were dissolved in CH_3CN or MeOH (HPLC grade purity). The selected values were as follows: capillary voltage = 4 kV, gas temperature = 350 °C, drying gas flow 12 L min^{-1}, nebulizer pressure = 310 kPa, fragmentator voltage = 70 V.The elemental analysis was performed on the Vario EL III- C,H,N,S/O Elemental Analyzer (Elementar Analysensysteme GmbH, Hanau-Germany). Thin-layer chromatography (TLC) was performed on precoated Merck silica gel 60 F254 and RP-18 F254 plates. Column chromatography was performed on Lobar LichroPrep Si 60 (40-63 μm), RP-18 (40-63 μm) columns coupled to a Waters RI 401 detector, and on Biotage SP1 system with UV detector and FLASH 12+, FLASH 25+ or FLASH 40+ columns pre packed with KP-SIL [40-63 μm, pore diameter 6 nm (60 Å)], KP-C18-HS (40-63 μm, pore diameter 9 nm (90 Å) or KP-NH [40-63 μm, pore diameter 10 nm (100 Å)] as adsorbent. Compounds were analyzed for purity (HPLC) using a Waters 1525 HPLC dual pump system equipped with an Alltech, Select degasser system, and dual λ 2487 UV-VIS detector. For data processing, Empower software was used (methods A and B). Methods C and D: Agylent Technologies 1260 Liquid Chromatograph equipped with Quat Pump (G1311B), Injector (G1329B) 1260 ALS, TCC 1260 (G1316A) and Detector 1260 DAD VL+ (G1315C). For data processing, LC OpenLab CDS ChemStation software was used. For details, see Supporting Information.

1. Synthesis experiments

Each paragraph describing a synthesis experiment should begin with the name of the product and any structure number assigned to the compound in the Results and Discussions section. Thereafter, the compound should be identified by its structure number. Use of standard abbreviations or unambiguous molecular formulas for reagents and solvents, and of structure numbers rather than chemical names to identify starting materials and intermediates, is encouraged.

When a new or improved synthetic method is described, the yields reported in key experimental examples, and yields used for comparison with existing methods, should represent amounts of isolated and purified products, rather than chromategraphically or spectroscopically determined yields. Reactant quantities should be reported in weight and molar units and for product yields should be reported in weight units; percentage yields should only be reported for materials of demonstrated purity. When chromatography is used for product purification, both the support and solvent should be identified.

2. Microwave experiments

Reports of syntheses conducted in microwave reactors must clearly indicate whether sealed or open reaction vessels were used and must document the manufacturer and model of the reactor, the method of monitoring the reaction mixture temperature, and the temperature-time profile. Reporting a wattage rating or power setting is not an acceptable alternative to providing temperature data. Manuscripts describing work done with domestic (kitchen) microwave ovens will not be accepted except for studies where the unit is used for heating reaction mixtures at atmospheric pressure.

3. Compound characterization

The Journal upholds a high standard for compound characterization to ensure that substances being added to the chemical literature have been correctly identified and can be synthesized in known yield and purity by the reported preparation and isolation methods. For **all new** compounds, evidence adequate to establish both **identity** and **degree of purity** (homogeneity) must be provided.

Identity *- Melting point.* All homogeneous solid products (*e.g.* not mixtures of isomers) should be characterized by melting or decomposition points. The colors and morphologies of the products should also be noted.

Specific rotations. Specific rotations based on the equation $[\alpha]^t; D = (100\ \alpha) / (l\ c)$ should be reported as unitless numbers as in the following example: $[\alpha]^{20}$; D = -25.4 (c 1.93, $CHCl_3$), where c / g mL^{-1} is concentration and l / dm is path length. The units of the specific rotation, (deg mL) / (g dm), are implicit and are not included with the reported value.

Spectra/*Spectral Data.* Important IR adsorptions should be given.

For all new diamagnetic substances, NMR data should be reported (^1H, ^{13}C, and relevant heteronuclei). ^1H NMR chemical shifts should be given with two digits after the decimal point. Include the number of protons represented by the signal, signal multiplicity, and coupling constants as needed (*J* italicized, reported with up to one digit after the decimal). The number of bonds through which the coupling is operative, ^xJ, may be specified by the author if known with a high degree of certainty. ^{13}C NMR signal shifts should be rounded to the nearest 0.01 ppm unless greater precision is needed to distinguish closely spaced signals. Field strength should be noted for each spectrum, not as a comment in the general experimental section. Hydrogen multiplicity (C, CH, CH_2, CH_3) information obtained from routine DEPT spectra should be included. If detailed signal assignments are made, the type of NOESY or COSY methods used to establish atom connectivity and spatial relationships should be identified in the Supporting Information. Copies of spectra should also be included where structure assignments of complex molecules depend heavily on NMR interpretation. Numbering system used for assignments of signals should be given in the Supporting Information with corresponding general structural formula of named derivative.

HPLC/LCMS can be substituted for biochemistry papers where the main focus is not on compound synthesis.

HRMS/*elemental analysis.* To support the molecular formula assignment, HRMS data accurate within 5 ppm, or combustion elemental analysis [carbon and hydrogen (and nitrogen, if present)] data accurate within 0.5 %, should be reported for new compounds. HRMS data should be given in format as is usually given for combustion analysis: calculated mass for given formula following with observed mass: (+)ESI-HRMS *m*/*z*: [molecular formula + H]$^+$ calculated mass, observed mass. Example: (+)ESI-HRMS *m*/*z*: calculated for [$C_{13}H_8BrCl_2N + H^+$] 327.92899, observed 327.92792.

NOTE: in certain cases, a crystal structure may be an acceptable substitute for HRMS/elemental analysis.

Biomacromolecules. The structures of biomacromolecules may be established by providing evidence about sequence and mass. Sequences may be inferred from the experimental order of amino acid, saccharide, or nucleotide coupling, from known sequences of templates in enzyme-mediated syntheses, or through standard sequencing techniques. Typically, a sequence will be accompanied by MS data that establish the molecular weight.

Example: Product was isolated upon column chromatography [dry flash (SiO_2, eluent EA, EA/MeOH gradient 95/5 → 9/1, EA/MeOH/NH_3 gradient 18/0.5/0.5 → 9/1/1, and flash chromatography (Biotage SP1, RP column, eluent MeOH/H_2O gradient 75/25 → 95/5, N-H column, eluent EA/Hex gradient 6/3 → EA). was obtained after flash column chromatography (Biotage SP NH column, eluent hexane/EA 4:6 → 2:6). Yield 968.4 mg (95 %). Colorless foam softens at 96-101 °C. $[\alpha]^{20}$; D = +0,163 (c =2.0×10^{-3} g/mL, CH_2Cl_2). IR (ATR): 3376w, 2949m, 2868w, 2802w, 1731s, 1611w, 1581s, 1528m, 1452m, 1374s, 1331w, 1246s, 1171m, 1063w, 1023m, 965w, 940w, 881w, 850w, 807w, cm^{-1}. ^1H NMR (500 MHz, $CDCl_3$, δ): 8.46 (*d*, 1H, J = 5.4, H-2'), 7.89 (*s*, 1H, J = 2.0, H-8'), 7.71 (*d*, 1H, J = 8.9, H-5'), 7.30 (*dd*, 1H, J_1 = 8.8, J_2 = 2.1, H-6'), 6.33 (*d*, 1H, J = 5.4, H-3'), 6.07 (*s*, HN-Boc, exchangeable with D_2O), 5.06 (*s*, 1H, H-12), 4.92-4.88 (*m*, 1H, H-7), 4.42 (*bs*, H-3), 3.45 (*s*,CH_3-N), 3.33 (*bs*, H-9'), 3.05-2.95 (*m*, 2H, H-11'), 2.70-2.43 (*m*, 2H, H-24) and HN, exchangeable with D_2O), 2.07 (*s*, CH_3COO), 2.04 (*s*, CH_3COO), 1.42 (*s*, 9H, $(CH_3)_3$C-N(Boc)), 0.88 (*s*, 3H, CH_3-10), 0.79 (*d*, 3H,J = 6.6, CH_3-20), 0.68 (*s*, 3H, CH_3-13). ^{13}C NMR (125 MHz, $CDCl_3$, δ): 170.34, 170.27, 151.80, 149.92, 148.87, 134.77, 128.36, 125.11, 121.43, 117.29, 99.98, 75.41, 70.82, 50.43, 49.66, 47.60, 47.33, 44.97, 43.30, 41.83, 41.48, 37.65, 36.35, 35.44, 34.89,

34.19, 33.23, 31.24, 28.79, 28.35, 27.25, 26.45, 25.45, 22.74, 22.63, 21.57, 21.31, 17.85, 12.15. (+)ESI-HRMS (*m/z*): calculated for $[C_{45}H_{67}ClN_4O_6 + H]^+$ 795.48219, observed 795.48185. Combustion analysis for $C_{45}H_{67}ClN_4O_6$: Calculated. C 67.94, H 8.49, N 7.04; found C 67.72, H 8.63, N 6.75. HPLC purity: method A: RT 1.994, area 99.12 %; method C: RT 9.936, area 98.20 %.

Purity **-** Evidence for documenting compound purity should include one or more of the following:

a) Well-resolved high field 1D ^{1}H NMR spectrum showing at most only trace peaks not attributable to the assigned structure and a standard 1D proton-decoupled ^{13}C NMR spectrum. Copies of the spectra should be included as figures in the Supporting Information.
b) Quantitative gas chromatographic analytical data for distilled or vacuum-transferred samples, or quantitative HPLC analytical data for materials isolated by column chromatography or separation from a solid support. HPLC analyses should be performed in two diverse systems. The stationary phase, solvents (HPLC), detector type, and percentage of total chromatogram integration should be reported; a copy of the chromatograms may be included as a figure in the Supporting Information.
c) Electrophoretic analytical data obtained under conditions that permit observing impurities present at the 5 % level.

HRMS data may be used to support a molecular formula assignment **but cannot be used as a criterion of purity**.

4. Biological Data

Quantitative biological data are required for all tested compounds. Biological test methods must be referenced or described in sufficient detail to permit the experiments to be repeated by others. Detailed descriptions of biological methods should be placed in the experimental section. Standard compounds or established drugs should be tested in the same system for comparison. Data may be presented as numerical expressions or in graphical form; biological data for extensive series of compounds should be presented in tabular form. Tables consisting primarily of negative data will not usually be accepted; however, for purposes of documentation they may be submitted as supporting information. Active compounds obtained from combinatorial syntheses should be resynthesized and retested to verify that the biology conforms to the initial observation.

Statistical limits (statistical significance) for the biological data are usually required. If statistical limits cannot be provided, the number of determinations and some indication of the variability and reliability of the results should be given. References to statistical methods of calculation should be included. Doses and concentrations should be expressed as molar quantities (*e.g.*, mol/kg, μmol/kg, M, mM). The routes of administration of test compounds and vehicles used should be indicated, and any salt forms used (hydrochlorides, sulfates, *etc.*) should be noted. The physical state of the compound dosed (crystalline, amorphous; solution, suspension) and the formulation for dosing (micronized, jet-milled, nanoparticles) should be indicated. For those compounds found to be inactive, the highest concentration (*in vitro*) or dose level (*in vivo*) tested should be indicated.

- The RESULTS AND DISCUSSION should include concisely presented results and there significance discussed and compared to relevant literature data. The results and discussion may be combined or kept separate.
- The inclusion of a CONCLUSION section, which briefly summarizes the principal conclusions, is recommended.
- NOMENCLATURE is optional but, if the authors wish, a list of employed symbols may be included.
- REFERENCES should be numbered sequentially as they appear in the text. Please note that any reference numbers appearing in the Illustrations and/or Tables and corresponding captions must follow the numbering sequence of the paragraph in which they appear for the first time. When cited, the reference number should be superscripted in Font 12, following any punctuation mark. In the reference list, they should be in normal position followed by a full stop. Reference entry must not be formatted using Carriage returns (enter key; ↵ key) or multiple space key. The formatting of references to published work should follow the *Journal'*s style as follows:

Journals[a]:	A. B. Surname1, C. D. Surname2, *J. Serb. Chem. Soc.* **Vol** (Year) first page Number (https://doi.org/doi)[b]
Books:	A. B. Surname1, C. D. Surname2, *Name of Book*, Publisher, City, Year, pp. 100-101 (https://doi.org/doi)[b]
Compilations:	A. B. Surname1, C. D. Surname2, in *Name of Compilation*, A. Editor1, C. Editor2, Ed(s)., Publisher, City, Year, p. 100 (https://doi.org/doi)[b]
Proceedings:	A. B. Surname1, C. D. Surname2, in *Proceedings of Name of the Conference or Symposium*, (Year), Place of the Conference, Country, *Title of the Proceeding*, Publisher, City, Year, p. or Abstract No. 100
Patents:	A. B. Inventor1, C. D. Inventor2, (Holder), Country Code and patent number (registration year)
Chemical Abstracts:	A. B. Surname1, C. D. Surname2, *Chem. Abstr*. CA 234 567a; For non-readily available literature, the Chemical Abstracts reference should be given in square brackets: [C.A. 139/2003 357348t] after the reference
Standards:	EN ISO 250: *Name of the Standard* (Year)
Websites:	Title of the website, URL in full (date accessed)

[a] When citing Journals, the International Library Journal abbreviation is required. Please consult, *e.g.*, https://images.webofknowledge.com/WOK46/help/WOS/A_abrvjt.html

[b] doi should be replaced by doi number of the Article, for example: http://dx.doi.org/10.2298/JSC161212085B (as active link). If doi do not exist, provide the link to the online version of the publication.

Only the last entry in the reference list should end with a full stop.

The names of all authors should be given in the list of references; the abbreviation *et al.* may only be used in the text. The original journal title is to be retained in the case of publications published in any language other than English (please denote the language in parenthesis after the reference). Titles of publications in non-Latin alphabets should be transliterated. Russian references are to be transliterated using the following transcriptions:

ж→zh, х→kh, ц→ts, ч→ch, ш→sh, щ→shch, ы→y, ю→yu, я→ya, э→e, й→i, ь→’.

Supplementary material

Authors are encouraged to presentthe information and results non-essential to the understanding of their paper as SUPPLEMENTARY MATERIAL (can be uploaded inStep 4 of Online Submission). This material may include as a rule, but is not limited to, the presentation of analytical and spectral data demonstrating the identity and purity of synthesized compounds, tables containing raw data on which calculations were based, series of figures where one example would remain in the main text, etc. The Editorial Board retain the right to assign such information and results to the Supplementary material when deemed fit. Supplementary material does not appear in printed form but can be downloaded from the web site of the JSCS.

Mathematical and chemical equations should be given in separate lines and must be numbered, Arabic numbers, consecutively in parenthesis at the end of the line. All equations should be embedded in the text Complex equations (fractions, integrals, matrix…) should be prepared with the aid of the Microsoft Equation 3.0 (or higher) or MathType (Do not use them to create simple equations and labels). Using the Insert -> Equation option, integrated in MS Office 2010 and MS Office 2013, as well as insertion of equation objects within paragraph text IS NOT ALLOWED.

Deposition of crystallographic data

Prior to submission, the crystallographic data included in a manuscript presenting such data should be deposited at the appropriate database. Crystallographic data associated with organic and metal-organic structures should be deposited at the Cambridge Crystallographic Data Centre (CCDC) by e-mail to **deposit@ccdc.cam.ac.uk**

Crystallographic data associated with inorganic structures should be deposited with the Fachinformationszentrum Karlsruhe (FIZ) by e-mail to **crysdata@fiz-karlsruhe.de**. A deposition number will then be provided, which should be added to the reference section of the manuscript.

For detailed instructions please visit the JSCS website:
https://www.shd-pub.org.rs/index.php/JSCS/Instructions

ARTWORK INSTRUCTIONS

JSCS accepts only **TIFF** or **EPS** formats, as well as **JPEG** format (only for colour and greyscale photographs) for electronic artwork and graphic files. **MS files** (Word, PowerPoint, Excel, Visio) **NOT acceptable**. Generally, scanned instrument data sheets should be avoided. Authors are responsible for the quality of their submitted artwork. Every single Figure or Scheme, as well as any part of the Figure (A, B, C…) should be prepared according to following instructions (every part of the figure, A, B, C…, must be submitted as an independent single graphic file):

TIFF

Virtually all common artwork and graphic creation software is capable of saving files in TIFF format. This 'option' can normally be found under 'the 'Save As...' or 'Export...' commands in the 'File' menu.

TIFF (Tagged Image File Format) is the recommended file format for bitmap, greyscale and colour images.

- Colour images should be in the RGB mode
- When supplying TIFF files, please ensure that the files are supplied at the correct resolution:
    1. Line artwork: minimum of 1000 dpi
    2. RGB image: minimum of 300 dpi
    3. Greyscale image: minimum of 300 dpi
    4. Combination artwork (line/greyscale/RGB): minimum of 500 dpi
- Images should be tightly cropped, without frame and any caption.
- If applicable please re-label artwork with a font supported by JSCS (Arial, Helvetica, Times, Symbol) and ensure it is of an appropriate font size.
- Save an image in TIFF format with LZW compression applied.
- It is recommended to remove Alpha channels before submitting TIFF files.
- It is recommended to flatten layers before submitting TIFF files.

Please be sure that quality of an image cannot be increased by changing the resolution from lower to higher, but only by rescanning or exporting the image with higher resolution, which can be set in usual "settings" facilities.

EPS

Virtually all common artwork creation software, such as Canvas, ChemDraw, CorelDraw, SigmaPlot, Origin Lab…, are capable of saving files in EPS format. This 'option' can normally be found under the 'Save As...' or 'Export...' commands in the 'File' menu.

For vector graphics, EPS (Encapsulated PostScript) files are the preferred format as long as they are provided in accordance with the following conditions:

- when they contain bitmap images, the bitmaps should be of good resolution (see instructions for TIFF files)
- when colour is involved, it should be encoded as RGB
- an 8-bit preview/header at a resolution of 72 dpi should always be included
- embed fonts should always included and only the following fonts should be used in artwork: Arial, Helvetica, Times, Symbol
- the vertical space between the parts of an illustration should be limited to the bare necessity for visual clarity
- no data should be present outside the actual illustration area
- line weights should range from 0.35 pt to 1.5 pt
- when using layers, they should be reduced to one layer before saving the image (Flatten Artwork)

JPEG

Virtually all common artwork and graphic creation software is capable of saving files in JPEG format. This 'option' can normally be found under 'the 'Save As...' or 'Export...' commands in the 'File' menu.

JPEG (Joint Photographic Experts Group) is the acceptable file format **only for colour and greyscale photographs**. JPEG can be created with respect to photo quality (low, medium, high; from 1 to 10), ensuring file sizes are kept to a minimum to aid easy file transfer. Images should have a minimum resolution of 300 dpi. Image width: minimum 3.0 cm; maximum 12.0 cm.

Please be sure that quality of an image cannot be increased by changing the resolution from lower to higher, but only by rescanning or exporting the image with higher resolution, which can be set in usual "settings" facilities.

SIZING OF ARTWORK

- JSCS aspires to have a uniform look for all artwork contained in a single article. Hence, it is important to be aware of the style of the journal.
- Figures should be submitted in black and white or, if required, colour (charged). If coloured figures or photographs are required, this must be stated in the cover letter and arrangements made for payment through the office of the Serbian Chemical Society.
- As a general rule, the lettering on an artwork should have a finished, printed size of 11 pt for normal text and no smaller than 7 pt for subscript and superscript characters. Smaller lettering will yield a text that is barely legible. This is a rule-of-thumb rather than a strict rule. There are instances where other factors in the artwork, (for example, tints and shadings) dictate a finished size of perhaps 10 pt. Lines should be of at least 1 pt thickness.
- When deciding on the size of a line art graphic, in addition to the lettering, there are several other factors to address. These all have a bearing on the reproducibility/readability of the final artwork. Tints and shadings have to be printable at the finished size. All relevant detail in the illustration, the graph symbols (squares, triangles, circles, *etc*.) and a key to the diagram (to explain the explanation of the graph symbols used) must be discernible.
- The sizing of halftones (photographs, micrographs,...) normally causes more problems than line art. It is sometimes difficult to know what an author is trying to emphasize on a photograph, so you can help us by identifying the important parts of the image, perhaps by highlighting the relevant areas on a photocopy. The best advice that can be given to graphics suppliers is not to over-reduce halftones. Attention should also be paid to magnification factors or scale bars on the artwork and they should be compared with the details inside. If a set of artwork contains more than one halftone, again please ensure that there is consistency in size between similar diagrams.

General sizing of illustrations which can be used for the Journal of the Serbian Chemical Society:

- Minimum fig. size: 30 mm width
- Small fig. size - 60 mm width
- Large fig. size - 90 mm width
- Maximum fig. size - 120 mm width

Pixel requirements (width) per print size and resolution for bitmap images:

	Image width	A	B	C
Minimal size	30 mm	**354**	**591**	**1181**
Small size	60 mm	**709**	**1181**	**2362**
Large size	90 mm	**1063**	**1772**	**3543**
Maximal size	120 mm	**1417**	**2362**	**4724**

A: 300 dpi > RGB or Greyscale image
B: 500 dpi > Combination artwork (line/greyscale/RGB)
C: 1000 dpi> Line artwork

The designation of physical quantities and graphs formatting

The designation of physical quantities on figures must be in italic, whereas the units are in upright letters. They should be in Times New Roman font. In graphs a slash should be used to separate the designation of a physical quantity from the unit (example: p / kPa, t °C, T_0 / K, τ / h, ln (j / mA cm^{-2})…). Designations such as: p (kPa), t [min]…, are not acceptable. However, if the full name of a physical quantity is unavoiable, it should be given in upright letters and separated from the unit by a comma (example: Pressure, kPa, Temperature, K…). Please do not use the axes of graphs for additional explanations; these should be mentioned in the figure captions and/or the manuscript (example: "pressure at the inlet of the system, kPa" should be avoided). The axis name should follow the direction of the axis (the name of y-axis should be rotated by 90°). Top and right axes should be avoided in diagrams, unless they are absolutely necessary. Decimal numbers must have decimal points and not commas in the axis labels in graphical presentations of results. Thousands are separated, if at all, by a comma and not a point.

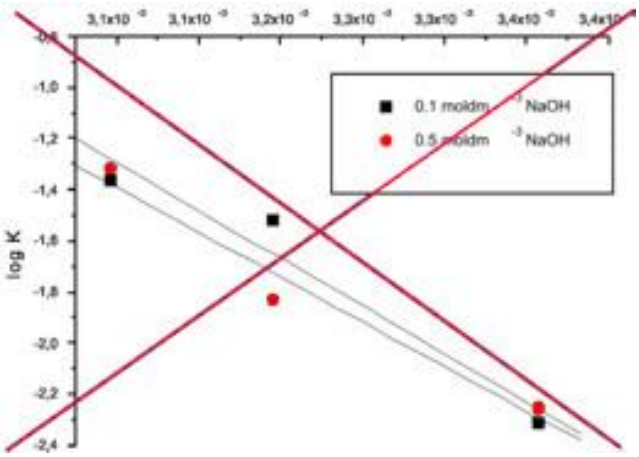

INCORRECT

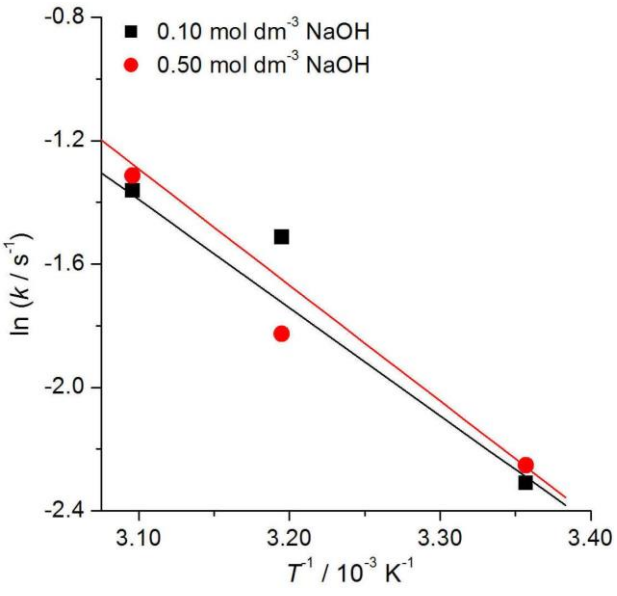

CORRECT

Journal of the Serbian Chemical Society
JSCS-info@shd.org.rs • www.shd.org.rs/JSCS

J. Serb. Chem. Soc. Vol. 86, No. 3 (2021)

CONTENTS*

Published by the Serbian Chemical Society
Karnegijeva 4/III, P.O. Box 36, 11120 Belgrade, Serbia
Printed by the Faculty of Technology and Metallurgy
Karnegijeva 4, P.O. Box 35-03, 11120 Belgrade, Serbia

* For colored figures in this issue please see electronic version at the Journal Home Page: http://www.shd.org.rs/JSCS/

Journal of the Serbian Chemical Society
JSCS-info@shd.org.rs • www.shd.org.rs/JSCS
J. Serb. Chem. Soc. *86* (3) 213–246 (2021)
JSCS–5417
Survey

SURVEY

3,4-Dihydro-2*H*-1,3-benzoxazines and their oxo-derivatives – Chemistry and bioactivities

NABAWEYA ABD EL-SALAM SHARAF EL-DIN*

Department of Pharmaceutical Chemistry, Faculty of Pharmacy, Tanta University, El Giesh Street, 31527, Tanta, Egypt

(Received 30 May, revised 3 December 2018, accepted 11 January 2019)

Abstract: 3,4-Dihydro-2*H*-1,3-benzoxazines derivatives are a significant class of heterocycles with particular awareness due to their remarkable biological activities in humans, plants and animals, and also their natural occurrence. Alteration in the benzoxazine skeleton and their comparative chemical simplicity and accessibility, make these compounds suitable sources of other bioactive compounds, resulting in the discovery of a wide set of these compounds that have broad biological activity, such as antifungal, antibacterial, anti-HIV, anticancer, anticonvulsant, anti-inflammatory, *etc*. Subsequently, this review gives herein a brief overview of the chemistry and bioactivities of derivatives of 3,4--dihydro-2*H*-1,3-benzoxazine monomers and their oxo-derivatives.

Keywords: 1,3-benzoxazines; synthesis; reactions; biological activities.

CONTENTS

* E-mail: nsharafd@gmail.com
https://doi.org/10.2298/JSC180530001S

1. INTRODUCTION

1,3-Benzoxazine is a bicyclic skeleton in which an oxazine ring is annulated with a benzene ring. A number of isomeric structures are possible depending on the positions and the degree of oxidation of the ring system. The two isomeric structures **1** and **2** (2*H*- and 4*H*-1,3-benzoxazine) in addition to 2,3-dihydro-2*H*--1,3-benzoxazine (**3**) are illustrated in Fig. 1.[1] This survey is focused on 3,4--dihydro-2*H*-1,3-benzoxazines and their oxo-derivatives.

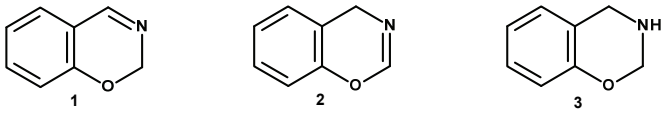

2*H*-1,3-benzoxazine 4*H*-1,3-benzoxazine 3,4-Dihydro-2*H*-1,3-benzoxazine

Fig. 1. Chemical structures of 1,3-benzoxazines.

3,4-Dihydro-2*H*-1,3-benzoxazines exist in two basic conformations, the semi-chair (A) and semi-boat (B) structures, as shown in Fig. 2. According to the orientation of the substituent at the nitrogen atom, each conformation exists in another two forms.[2]

On the other hand, the dihydro-1,3-benzoxazine monomers are synthesized not only by traditional Mannich condensation methods[3,4] of phenol, amine, and formaldehyde, but also by cycloaddition[5,6] and other methods. Interestingly,

several works have been performed to investigate the reactant ratios,[7,8] reactant structures,[9,10] solvent effect,[11] temperatures of reaction,[12] and reaction duration.[13]

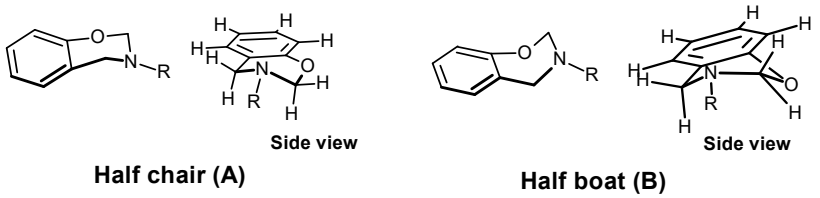

Fig. 2. Conformations of 3,4-dihydro-2*H*-1,3-benzoxazines.[2]

All previous studies[14,15] demonstrated that these factors play an important role in the synthesis and the properties of benzoxazine (such as, low yield and poor purity), resulting in limitation of the development of benzoxazine chemistry. Consequently, these problems need further efforts and studies.[10,16]

Furthermore, the benzoxazine nucleus is not only present in many pharmacologically active molecules, medicinally significant derivatives and natural products, but also they have been used as intermediates for the synthesis of other heterocyclic-scaffold bioactive compounds.[17] Furthermore, several 1,3-benzoxazines (Fig. 3) show interesting biological and pharmaceutical properties.[18,19] Moreover, these derivatives are very valuable in the chemistry of natural products due to the formation of acetal glycosides in plant[20] which act as a plant's own resistance factor towards insects, pests, fungi and other microbial diseases.[21] In this frame, the collected data in this survey is focused on the 3,4-dihydro-2*H*--1,3-benzoxazine monomers and their one-derivatives chemistry and bioactivities.

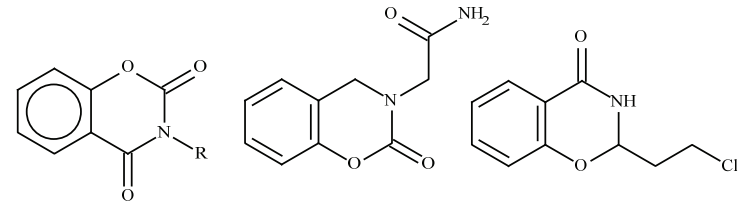

Fig. 3. 1,3-Benzoxazines with biological and pharmaceutical properties.

2. SYNTHESIS OF 1,3-BENZOXAZINE DERIVATIVES

*2.1. Synthesis of 3,4-dihydro-2*H*-1,3-benzoxazines*

3,4-Dihydro-2*H*-1,3-benzoxazines have been synthesized through the one-pot Mannich reaction of a substituted phenol with formaldehyde and aliphatic or aromatic monoamines/diamines (Scheme 1).[22] The importance of the role of the basicity of the amine on the rate of the reaction was found.[13,23] Thus a weakly basic amine will react faster than a strongly basic amine.[24]

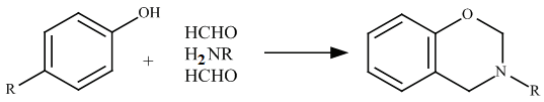

Scheme 1. Synthesis of 1,3-benzoxazines by a Mannich reaction.

This synthetic method could be performed either in solvent,[25] such as dioxane/water,[26] absolute ethanol,[27,28] methanol,[29] *etc*., or solventless.[30,31] The use of an organic solvent increases the cost of the products and causes some environmental problems. Furthermore, the solvent residue in the products leads to problems during the handling of the benzoxazine synthesis. To overcome these drawbacks, the solventless synthesis was developed under melt condition.[32] The reaction mechanism and kinetics of this method were suggested by Liu and Ishida for the preparation large quantities of benzoxazine monomers.[24]

Moreover, the influence of substituent attached to phenol or aniline on the stability of the oxazine ring and the equilibrium constant has been investigated and studied in the literature.[24,26]

In the solventless method[30,33] all the reactants are mixed together, heated, and maintained at above their melting point using paraformaldehyde to maintain the reaction stoichiometry.[30] Additionally, in the case of reactants with high melting points, it is necessary to use toluene or 1,4-dioxane as solvents.[34] Better yield and purity were obtained using two-step methods by reaction of an aliphatic amine and formaldehyde at low temperature first before adding the phenol derivative.[32]

On the other hand, the kinetics and details of 3,4-dihydro-3-phenyl-2*H*-1,3--benzoxazine synthesis by the Mannich reaction were investigated.[16] It was observed that *N*-hydroxymethyl aniline (HMA) is considered the key intermediate. HMA then reacts with phenol to give a second intermediate (**4**) that reacts with formaldehyde to form benzoxazines. However, HMA reacts with other intermediates and reactants to form byproducts, as shown in Scheme 2. Thus, this research observed that the formation and the mechanism of benzoxazines synthesis besides the formation of byproducts will need further investigations.[16]

In addition, due to the presence of water, polar solvents and the high temperatures used, the formation of oligomers are considered the main drawbacks in benzoxazine synthesis by the Mannich reaction.[10,32]

To minimize the previous drawbacks in the synthetic methods to 3,4--dihydro-3-phenyl-2*H*-1,3-benzoxazine monomers *via* Mannich condensation, numerous efforts have focused on two approaches: the use of a suitable synthetic method or the use a catalyst.

Herein, the different synthetic approaches for these derivatives have been studied as described in Scheme 3a–c.[35]

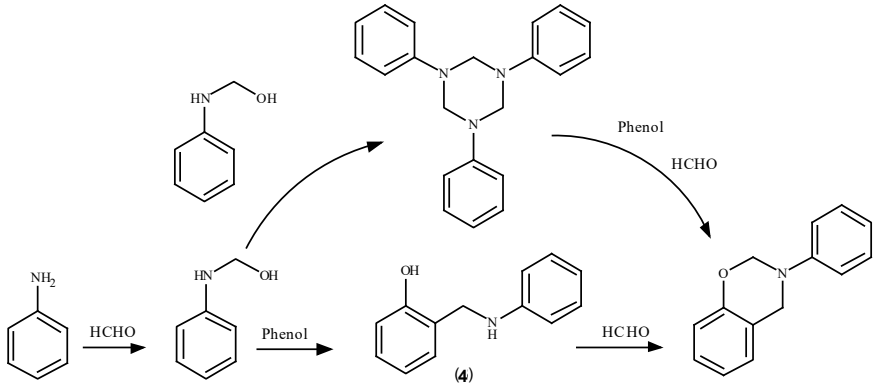

Scheme 2. Possible pathways for the synthesis of benzoxazines by the Mannich reaction.[16]

From the previous, there are three general synthetic methods for the preparation of benzoxazine monomers, one-pot, two-step and three-step Mannich reactions.

2.1.1. One-step Mannich condensation

Traditionally, benzoxazine synthesis was realized using the one-pot multi-component reactions of Burke.[3] This method has been generalized and studied because of its simplicity and diversity of substituents on both the phenol and the amine. For example, nitro,[35] halogenic,[36] cyano,[37] aldehyde,[38] carboxy,[39] alkenyl,[40] maleimide[41] groups, *etc.* could be adopted onto benzoxazine by using functional phenols/amines, leading to the production of a large variety of functional benzoxazines. Furthermore, by the use of bisphenol and/or diamine compounds, bifunctional benzoxazines could be obtained.[42] Another advantage of the solvent-free, one-pot method is that it avoids solvent residues, which may cause serious defects during processing, saves on solvent and its recovery costs, and there is no worry about the solubility of raw materials in an organic solvent.[32] As example, compound **5** was prepared in a one-step Mannich reaction (Fig. 4).[43]

Moreover, one-pot reactions are simple, easy to handle and avoid isolation and purification of intermediates, maximize the yield, minimize solvent, and enhance the greenness of the transformations.[44] Consequently, they have become a popular tool in the synthesis of complex heterocyclic molecules.[45]

A modification of the one-pot Mannich reaction was developed *via* the oxidative hydroxylation of arylboronic acids and subsequent coupling with paraformaldehyde and amines in good to excellent yields with a variety of functional groups, Scheme 4.[46]

The synthesis of dihydro-1,3-benzoxazines were obtained *via* one-pot condensation of α- or β-naphthol, aniline and formaldehyde using thiamine hydrochloride as catalyst.[47]

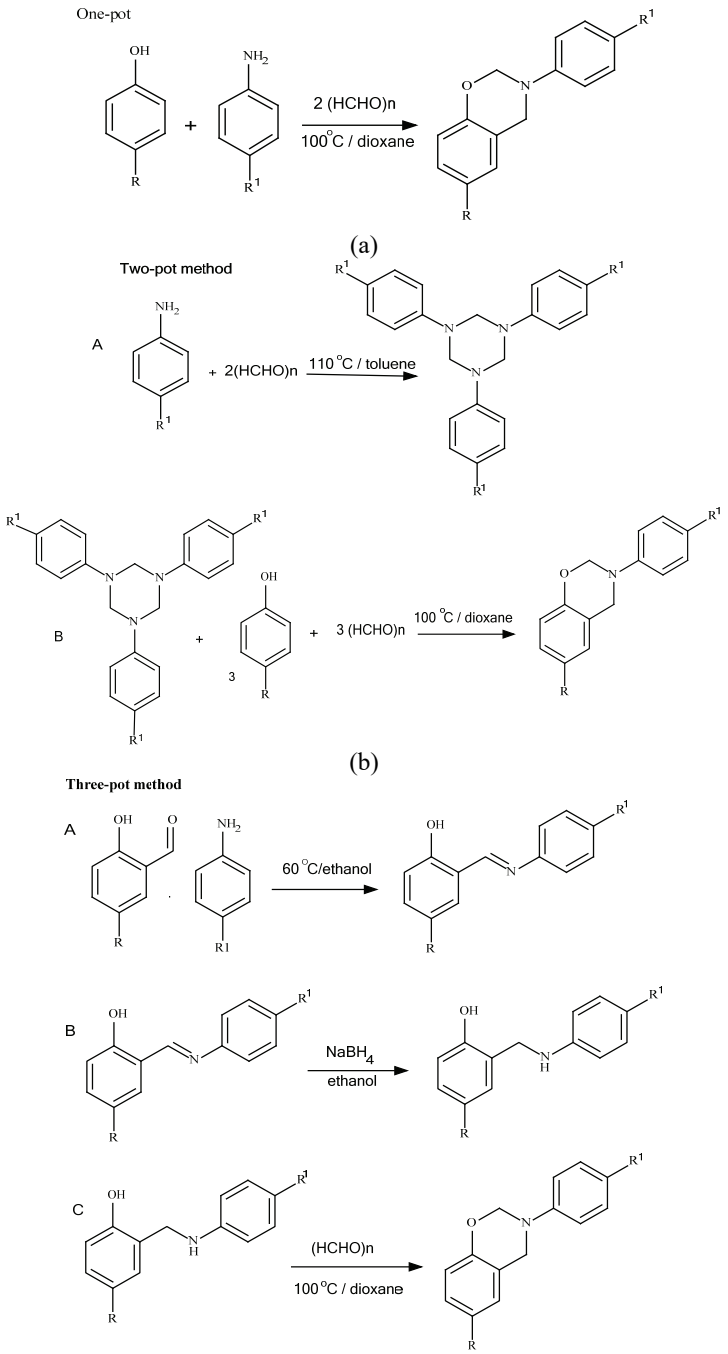

Scheme 3. Illustration of the one-pot (a), two-pot (b) and three-pot (c) synthetic method for the preparation of benzoxazine.

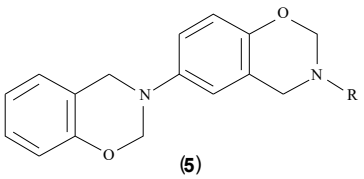

(**5**)

Fig. 4. Structure of compound **5**.

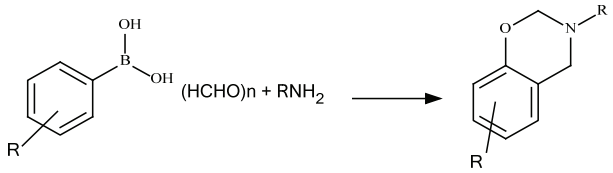

Scheme 4. Synthesis of 1,3-benzoxazines using arylboronic acids.

The preparation of a novel tetrafunctional oxazine monomer (**6**) containing 1,3-benzoxazine and fluorene-oxazine was performed through a one-step Mannich condensation reaction (Fig. 5).[48]

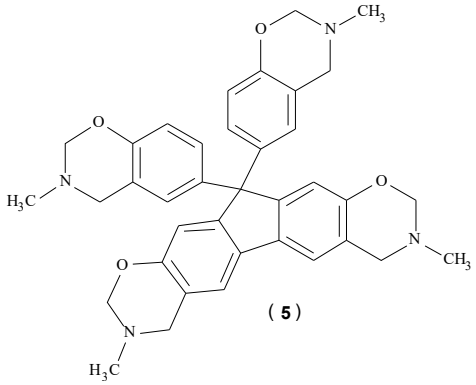

(**5**)

Fig. 5. Structure of compound **6**.

Additionally, benzoxazine monomers were synthesized in high purity and good yield through one-pot reactions from the reaction of bisphenol A with paraformaldehyde and isomeric butylamines, as indicated in Scheme 5.[49]

The Brønsted acidic ionic liquid [HMIm]BF_4 was used as a nonvolatile ecofriendly solvent and catalytic reagent for the one-pot green synthesis of isoxazolyl-3,4-dihydro-2*H*-1,3-benzoxazines (**7**, Fig. 6). This method afforded excellent yields in short reaction times, and avoids multistep synthesis.[50]

Moreover, 3,4-dihydro-2*H*-1,3-benzoxazines were synthesized in one pot by the directed *ortho*-lithiation of phenols.[51]

2.1.2. Two-step Mannich condensation

On the other hand, the two-step synthesis, first described by Holly and Cope,[52] is performed in solvent. The reaction by this method proceeds by first

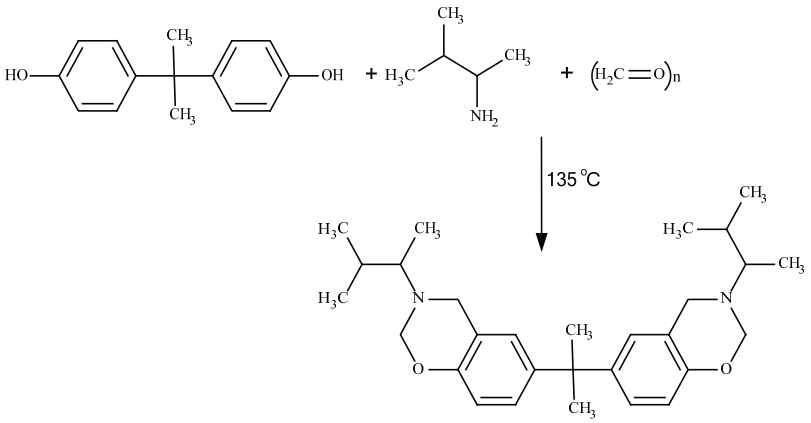

Scheme 5. Synthesis of benzoxazines from bisphenol A.

adding amine to formaldehyde at lower temperatures to form an *N*,*N*-dihydroxymethylamine, which then reacts with the labile hydrogen of the hydroxyl group on the *ortho*-position of the phenol at an elevated temperature to form the oxazine ring.[53] The slow reaction rate and the large amount of solvent required for the synthesis due to the poor solubility of the reacting compounds are considered the disadvantages of this procedure, in addition to increasing the costs of the products and creating environmental problems. To overcome these drawbacks, the solvent-free synthesis was developed.[32]

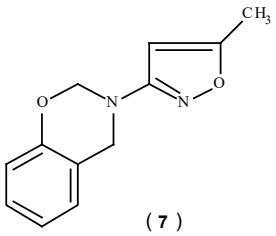

(**7**)

Fig. 6. Structure of compound **7**.

Thereafter, the two-step reaction involved the formation of perhydrotriazine (intermediate) in the reaction of formaldehyde with benzylamine. This intermediate reacts with phenol and formaldehyde in acidic condition to give benzoxazines (Scheme 6).[13] This method has been generalized with the proposed mechanism in the literature.[10]

Additionally, another way was reported through the formation of bis(alkoxymethyl)alkylamine as intermediate, which was obtained in the reaction of alkyl amine with alcohol (Scheme 7).[54]

Notably, these methods cannot be used in the presence of a primary amine similar as one-pot methods. However, these methods were enabled in cases of reactive phenolic compounds, such as hydroxybenzaldehyde and hydroxybenzoic

acid, allowing a primary amine to be used. Due to the diversity of substituents on both the phenol and the amine, a large variety of functional benzoxazines could be produced.

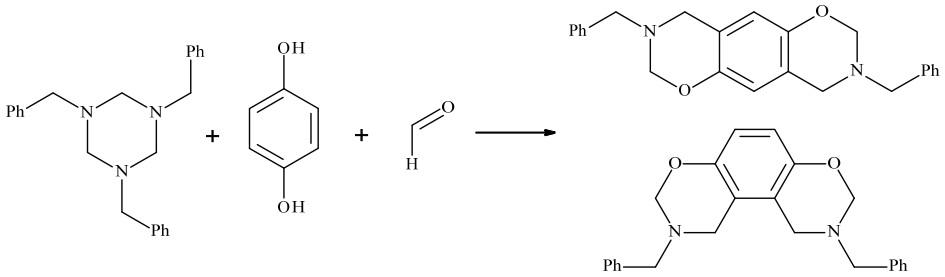

Scheme 6. Synthesis of benzoxazines with 1,3,5-hexahydrotriazine.

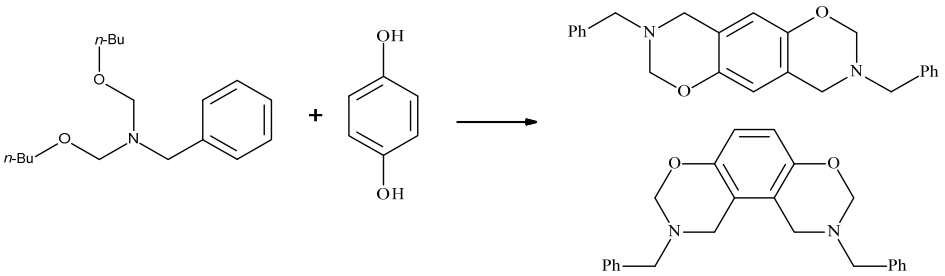

Scheme 7. Synthesis of benzoxazines with bis(alkoxymethyl)alkylamine.

In the synthesis of benzoxazine in a two-step reaction, the first step involved the formation of 1,3,5-tris(pentafluorophenyl)perhydro-1,3,5-triazine, then the reaction between the acid-promoted cleavage of the perhydrotriazine with substituted phenol and formaldehyde occurred. The latter step is considered the rate determining step reaction.[55]

Furthermore, 1,3,5-triphenylhexahydro-1,3,5-triazine (**8**, Fig. 7) was formed as intermediate during the solventless synthesis of benzoxazines. This triazine could be used as an amine source instead of the direct use of a primary amine.[10,56]

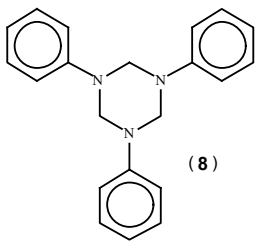

(**8**)

Fig. 7. Structure of compound **8**.

2.1.3. Three-step Mannich reaction

Brurke suggested a reaction pathway for a Mannich condensation, *i.e.*, initially, *N*,*N*-dihydroxymethylamine (**9**) is formed that is then converted into a *N*-hydroxymethyl Mannich base (**10**), which finally reacts with phenol to generate 1,3-benzoxazines (Scheme 8).[42,57,58]

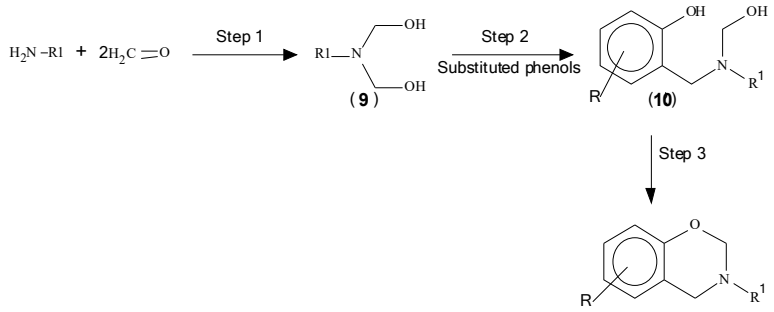

Scheme 8. Three-step Mannich reaction for the synthesis of 1,3-benzoxazines.

Moreover, a three-step method was developed by imine formation between salicylaldehyde and the selected primary amine as first step. The second step is the reduction of this imine into secondary amine and finally, ring closure using formaldehyde.[59]

The advantage of this method is the ability to control each step and the usage of amines that are incompatible in classical methods. Furthermore, the use of this method avoids the formation of undesirable oligomeric or polymeric species, thus leading to a simple workup and improving the yield and purity of the final product. As an example, salicylaldehyde[59] or 4-aminophenol can be used as the phenol or amine source, respectively. In addition, free phenol-containing benzoxazines can also be synthesized easily by this method. Moreover, asymmetrical benzoxazine derivatives can easily be obtained by choosing a suitable salicylaldehyde.[60]

Furthermore, 1,3-benzoxazine derivatives were formed *via* dehydration of methylene glycol to formaldehyde, which reacts with a Mannich base as indicated in Scheme 9.[26]

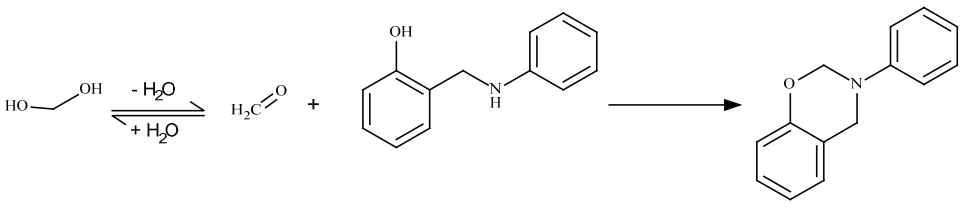

Scheme 9. Three-step Mannich reaction for the synthesis of 1,3-benzoxazines.

Salicylaldehyde was condensed with primary aromatic amines to give imine compounds which on reduction with $NaBH_4$, yielded intermediate **11** at room temperature (Fig. 8). Compound **11** subsequently undergoes ring-closure reaction with paraformaldehyde in toluene at 60 °C to give benzoxazine monomer by a three-pot method. [27,58]

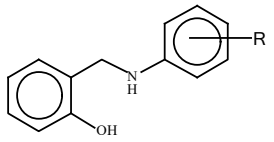

(**11**)

Fig. 8. Structure of compound **11**.

Furthermore, the kinetics of the reaction between 2-[(phenylamino)methyl]-phenol (phenol-aniline based Mannich base) and formaldehyde to benzoxazine has been studied. The results showed that the reaction occurs rapidly and the reverse reaction occurs *via* hydrolysis of the benzoxazine to the Mannich base.[26]

Moreover, a di-functional benzoxazine was prepared in the reaction of 1,2-bis-(*ortho*-hydroxybenzylamino)ethane (**12**, Fig. 9) with formaldehyde.[61] The advantage of this synthesis is the flexible substitution of functional groups on the oxazine ring. In addition, another substitution on the oxazine ring could be achieved by ring closure of salicylaldehyde with various aldehydes (aliphatic or aromatic) instead of formaldehyde.[62] Moreover, the oxazine ring could be closed by the reaction of salicylaldehyde not only with aldehydes but also with methylene bromide.[63] Furthermore, this method enhances the formation of benzoxazine monomer only because its intramolecular cyclization permits the reaction conditions to moderate, leading to the minimization of side reactions caused by high temperatures. However, in the case of a one-pot method, sometimes relatively high temperature are required to close the oxazine ring leading to the formation of undesirable oligomeric or polymeric species.

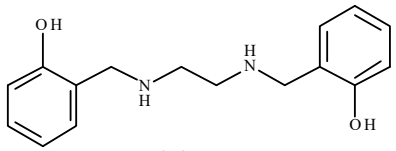

(**12**)

Fig. 9. Structure of compound **12**.

On the other hand, for further limitation on the drawbacks of Mannich methods, many catalysts have been used for the growing number of benzoxazines syntheses. As example, 2,3-diaryl-3,4-dihydro-*2H*-1,3-benzoxazines have been prepared in high yields from *o*-(arylaminomethyl)phenols and aromatic aldehydes in the presence of $SnCl_4$.[27] In addition, the condensation of hexakis(methoxy-methyl)melamine (HMMM) with mono- or di-substituted phenols in *p*-xylene

catalyzed by di-nonylnaphthalenedisulfonic acid[64] gave 1,3-benzoxazines. Finally, I_2/H_2O_2-promoted intramolecular C–O bond formation reaction of a variety of 1-(aminoalkyl)-2-naphthols or 2-(aminoalkyl)phenols yielded the corresponding 1,3-oxazines. The reaction is simple, economic, and proceeds at room temperature in ethanol as solvent.[65]

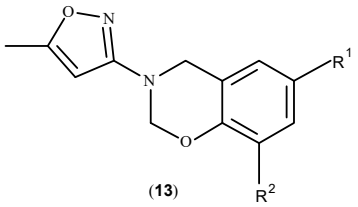

(13)

Fig. 10. Structure of compound **13**.

2.2. Synthesis of a sulfone-scaffold benzoxazine monomer

On the other hand, the formation of byproducts (oligomers or polymers) in Mannich reactions has been considered beneficial in many industrial usages in spite of being considered a drawback in the preparation of benzoxazine monomers. Thus, 3,4-dihydro-2*H*-1,3-benzoxazines can yield polymeric structures through ring-opening of the cyclic monomers. These polymeric structures are commercially important and widely applied in the areas of coatings, adhesives, microelectronics, aerospace, *etc*.[66,67] One example of commercially importance are polysulfones (PSU), a class of polymers with excellent features, *e.g*., thermal stability, durability in harsh conditions, oxidation, pH and temperature resistance, ease of process ability and good film properties.[68,69]

Sulfone-scaffold 3,4-dihydro-2*H*-1,3-benzoxazines (**14**) were prepared in high purity from 4,4′-diaminodiphenyl sulfone (**15**),[70,71] 4,4′-sulfonylbisphenol (**16**)[25] or polysufone[72] and paraformaldehyde and phenol using a high boiling point, nonpolar solvent, see Fig. 11.

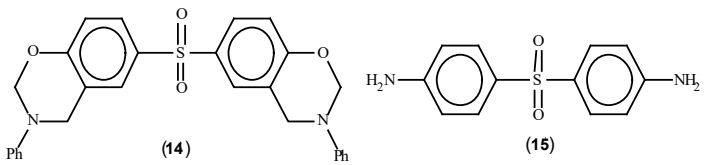

(14)

(15)

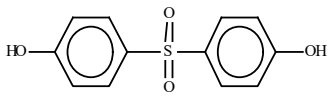

(16)

Fig. 11. Sulfone-based 1,3-benzoxazines, 4,4′-diaminodiphenyl sulfone and 4,4′-sulfonylbisphenol.

2.3. Synthesis of bio-based benzoxazine monomer

Interestingly, the raw materials for the synthesis of benzoxazine derivatives are almost always derived from petroleum oil. With the fast consumption of petroleum oil and the increasingly serious environmental pollution, the utilization of bio-based feedstock for the green preparation of these derivatives has gained more attention in all domains.[73,74]

In the synthesis of benzoxazines, renewable starting materials are used due to their availability, low toxicity, and relatively low cost. Thus, naturally occurring phenols, such as chavicol,[75] guaiacol,[76] cardanol[77,78]and lignocelluloses,[79,80] are used in the synthesis of 1,3-benzoxazines (Fig. 12).

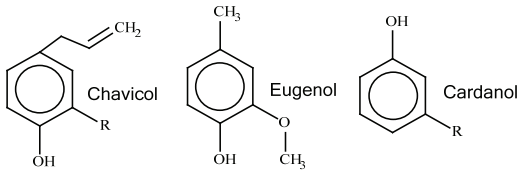

Fig. 12. The structures of some naturally occurring phenols.

*2.4. Synthesis of 4*H*-1,3-benzoxazin-2-ones*

The benzoxazinones were prepared in the one-pot reaction of 2-naphthol, an aldehyde and urea in the presence of various catalysts such as iodine (Scheme 10), P_2O_5 and $Yb(OTf)_3$,[81] cellulose sulfuric acid,[82] cyanuric chloride,[83] phosphomolybdic acid,[84] pyridinium-based ionic liquid,[85] thiamine hydrochloride,[86] zinc triflate,[87] montmorillonite K10,[88] zinc oxide,[89] TMSCl/NaI,[90] guanidine hydrochloride,[91] *etc*.

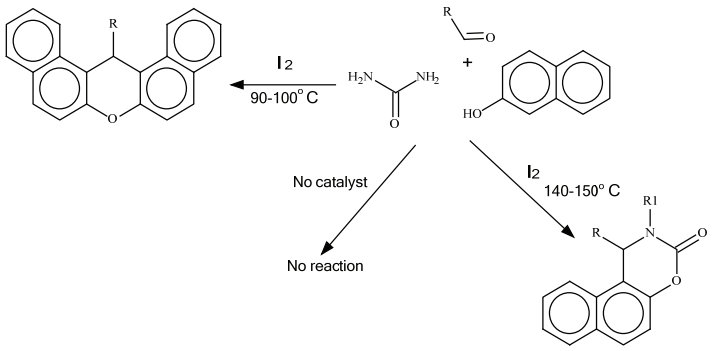

Scheme 10. One-pot Mannich reaction using iodine as catalyst.

On the other hand, by condensation of (aminoalkyl)naphthols with phosgene[92] or 1,1′-carbonyl diimidazole[93] in the presence of triethylamine, 2*H*-1,3--oxazin-2-one derivatives were produced in moderate yields. In addition, 1,3-

-benzoxazin-2-ones (**17**, Fig. 13) were prepared by reaction of 2-hydroxyphenyl-substituted enones and isocyanates using bisguanidinium salt as catalyst.[94]

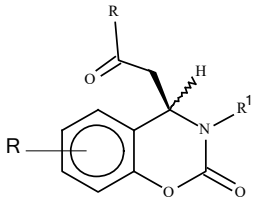

(**17**)

Fig. 13. Structure of compounds **17**.

Furthermore, 2*H*-1,3-benzoxazine-2-ones were synthesized in the reaction of substituted salicylaldehydes with a primary amine and an aldehyde. As example, spiropyrans based on benzoxazinone (**18**) were synthesized in the reaction of compound (A) with compound (B) using protonated acetic acid $[MeC(OH)_2]^+ClO_4^-$ as catalyst, as indicated in Scheme 11.[95]

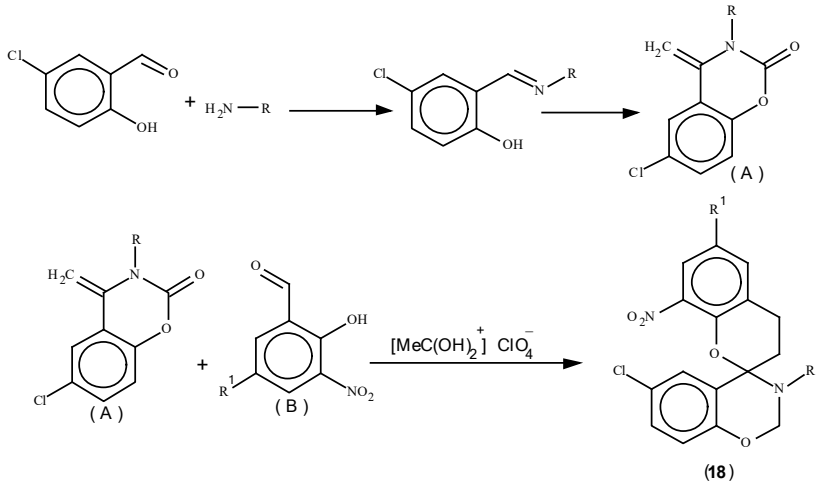

Scheme 11. Synthesis of spiropyrans based on 2*H*-1,3-benzoxazin-2-one.

In addition, 3,4-dihydro-2*H*-1,3-oxazin-2-ones were synthesized by intramolecular cyclization of aryl carbamates, which were produced from the reaction of aryl isocyanate and the corresponding 2-(nitroethenyl)phenol under basic conditions.[96]

Via the reaction of salicylaldehyde/2-hydroxyacetophenone or its hydrazones and substituted urea or substituted semicarbazide under solventless microwave irradiation,[97] 2*H*-1,3-benzoxazin-2-ones were synthesized in a one-pot method (Scheme 12).

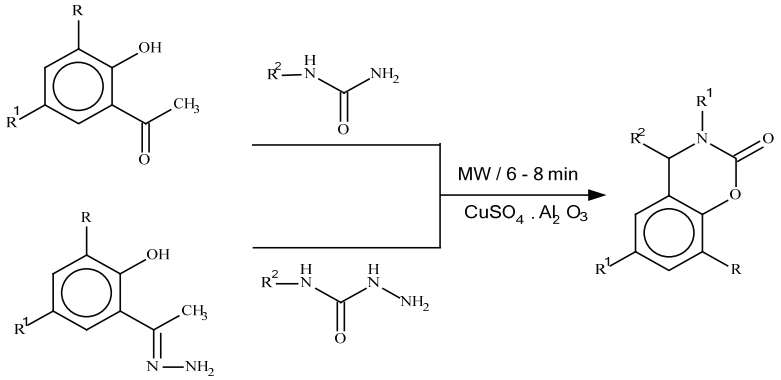

Scheme 12. Synthesis of 2*H*-1,3-benzoxazin-2-ones from salicylaldehyde/2-hydroxyacetophenone.

*2.5. Synthesis of 2*H*-1,3-benzoxazin-4-one*

In the condensation of an acid halide with salicylamides in the presence of pyridine using boiling xylene as solvent, substituted 2*H*-1,3-benzoxazin-4-ones were formed in one-step. They were also formed in a two-step method by refluxing the salicylamide with aroyl chloride in pyridine followed by cyclization of the isolated intermediate by hydrogen chloride.[98]

Furthermore, by carbonylation-cyclization of *ortho*-halophenols and cyanamide[99] or by treatment of the corresponding 2-hydroxycarboxamides with a formaldehyde/formic acid mixture,[100] the corresponding 4*H*-1,3-benzoxazin-4--ones were synthesized. 2-(Trichloromethyl) and 2-(dichloromethylene)-2*H*-1,3-benzoxazine derivatives were obtained *via* intramolecular cyclization of *N*-(*α*-aryloxytrichloroethyl)imidoyl chlorides through dehydrochlorination.[101] Additionally, 2-aryl-2-(trifluoromethyl)-2,3-dihydro-4*H*-benzoxazin-4-ones were synthesized *via* intramolecular thermal cyclization of 3-alkoxyphenyl *N*-(1-aryl-2,2,2-trifluoroethylidene)carbamates, which were produced in the reaction of 1-aryl-2,2,2-trifluoroethyl isocyanates with 3-alkoxyphenols (Scheme 13).[102]

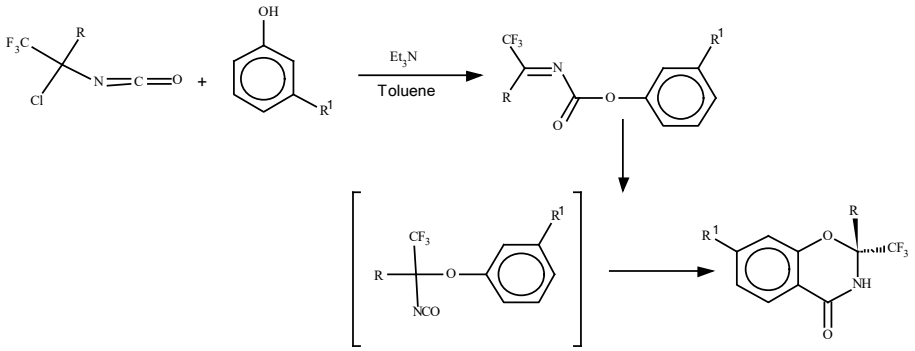

Scheme 13. Synthesis of 2-aryl-2-(trifluoromethyl)-2,3-dihydro-4*H*-benzoxazin-4-ones.

Moreover, 2,3-dihydro-4*H*-1,3-benzoxazin-4-ones have been synthesized by intermolecular cyclization reactions of *o*-halobenzamides, LiOH and dichloromethane using copper-catalyzed tandem reaction.[103]

*2.6. Synthesis of 2*H*-1,3-benzoxazine-2,4 (3*H*)-diones*

The 2*H*-1,3-benzoxazine-2,4(3*H*)-diones were synthesized from the reaction of acardic acids with triphosgene,[104] from the reaction of phthaloyl chlorides with acetone oxime[105] or from the reaction of salicylate esters with isocyanates.[106]

Reaction of 2-hydroxybenzonitrile with isocyanates[107] using triethylamine as catalyst has been performed to obtain the target compounds as in Scheme 14.

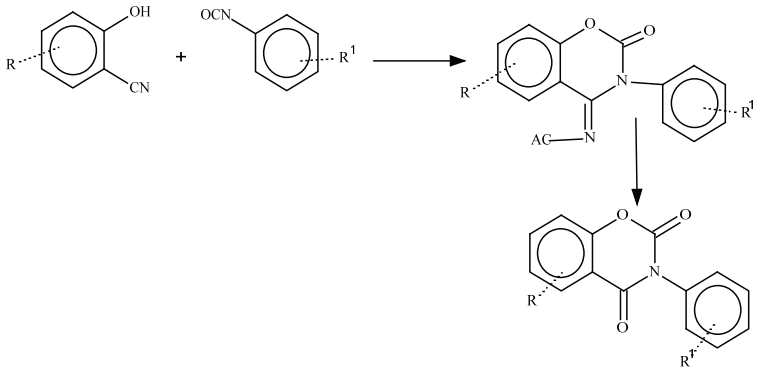

Scheme 14. Synthesis of 2*H*-1,3-benzoxazine-2,4(3*H*)-diones from 2-hydroxybenzonitrile and isocyanates.

3. CHEMISTRY OF 1,3-BENZOXAZINE DERIVATIVES

3.1. Unusual behavior of ortho-functional benzoxazines

The formation of intramolecular five-membered ring H-bond between the NH of the amide group and the oxygen of the oxazine ring (Fig. 14) is considered as unusual behavior of *ortho*-functional benzoxazines.[108]

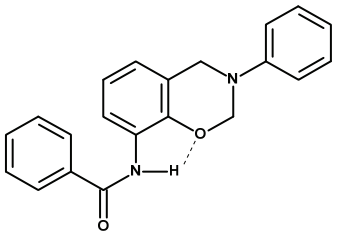

Fig. 14. The intramolecular five-membered ring H-bond in benzoxazines.

Furthermore, it was observed that, *o*-methyl-substituted benzoxazine dimers, as shown in Fig. 15,[109,110] trimers or tetramers exhibit intramolecular hydrogen bonding.[111]

Interestingly, the *o*-substituted benzoxazine dimers are used as novel ligands for rare earth metal ions, *e.g.*, the Ce(III) ion. It was found that, the substituted groups on the *para*-positions of benzoxazine dimers do not affect the formation of complexes.[112]

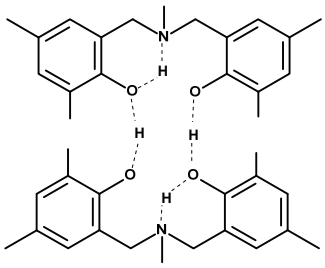

Fig. 15. The molecular structure of a pair of methyl benzoxazine dimers.

3.2. Ring opening of benzoxazines

The dihydro-derivatives are more stable than the 1,3-benzoxazines towards acidic agents. The ring opening ability depends on the basicity of the oxygen and nitrogen atoms.[113] In compounds with an active hydrogen, such as indoles, carbazole, imides, and aliphatic nitro compounds, even phenol (Scheme 15),[114,115] thiols (Scheme 16)[116] or carboxylic acids,[117] auto-ring opening occurs as shown in Schemes 15–17. The benzoxazines ring opening begins with protonation of oxygen and nitrogen atoms,[118] as indicated in Scheme 17.

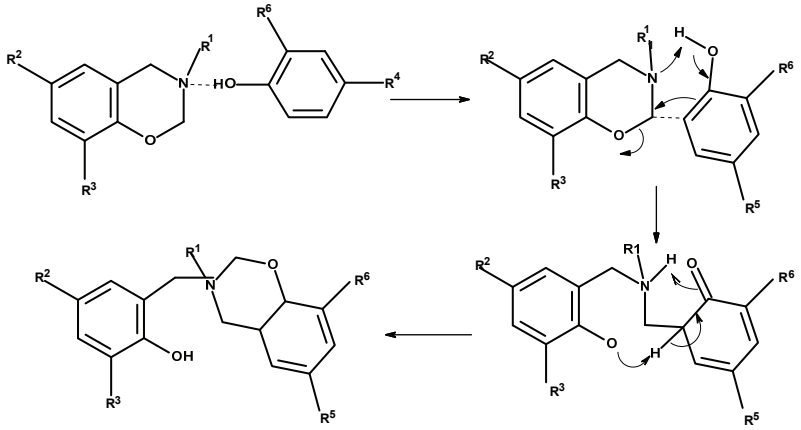

Scheme 15. The mechanism of benzoxazines ring opening.

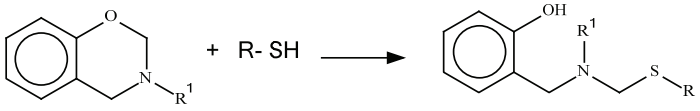

Scheme 16. The auto-ring opening reaction of 1,3-benzoxazines.

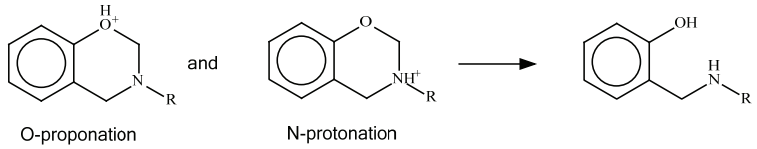

Scheme 17. The benzoxazines ring opening by protonation of oxygen and nitrogen atoms.

Furthermore, ring opening is promoted by irradiation with UV radiation (Scheme 18),[119,120] resulting in the formation of two chromophoric systems (the 3*H*-indolium cation and the 4-nitrophenolate anion moiety).[119]

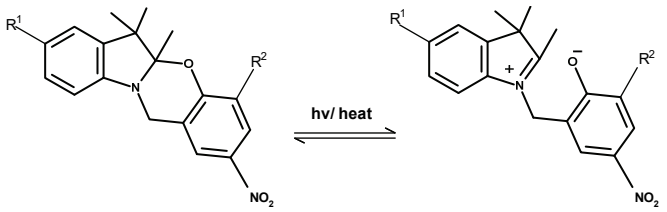

Scheme 18. Ring opening of 1,3-oxazine ring upon irradiation.

In addition, the ring opening reaction of substituted benzoxazine would readily occur by heating due to the resonance stabilization of the iminium ion, as indicated in Scheme 19.[121]

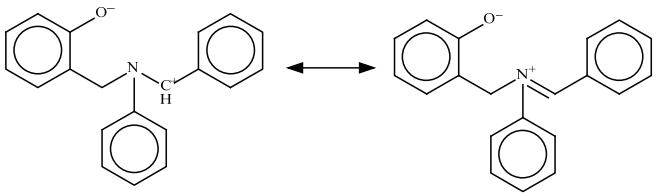

Scheme 19. The resonance stabilization of the iminium ion.

3.3. Ring-chain tautomerism

The 1-(substituted phenyl)-3-aryl-2,3-dihydro-1*H*-naphth[1,2-e][1,3]oxazines undergo ring–chain tautomerism, resulting in predominately the *trans*- (**19**) over the *cis*-configuration (**20**) through compound (**21**), as shown in Scheme 20.[122]

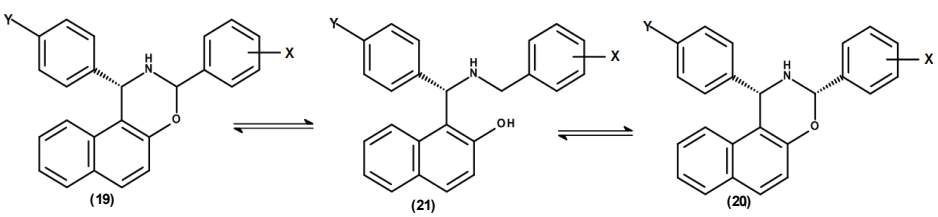

Scheme 20. Naphthoxazines epimerization.

4. REACTIONS OF 1,3-BENZOXAZINE DERIVATIVES

4.1. Hydrolysis with HCl

The benzoxazine derivatives (**22**) are hydrolyzed by HCl to give 2-amino-pyridine (**23**) or *N*-2-pyridylsalicylamide (**24**) depending on the concentration of the acid, as indicated in Scheme 21.[123]

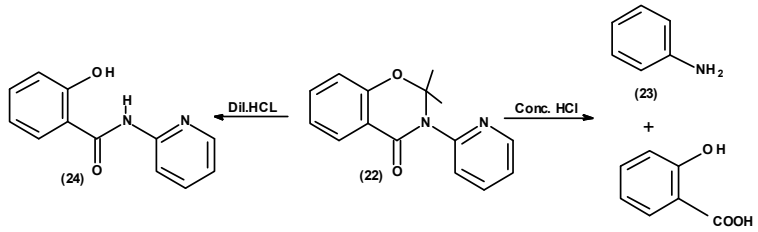

Scheme 21. Effect of acids on benzoxazine derivatives.

4.2. Salt formation

The formation salts of 1,3-benzoxazines has been realized by acidic cyclization of disalicylamide[124] or by acylation of (*o*-aminophenyl)diphenylmethanol with carboxylic acids in the presence of perchloric acid,[125] producing l,3-benzoxazinium perchlorate **25**, Fig. 16.

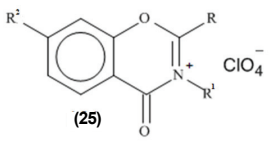

Fig. 16. Structure of compound **25**.

4.2.1. Reactions of 4-oxo-4*H*-1,3-benzoxazinium salts

Interestingly, 4-oxo-4*H*-1,3-benzoxazinium perchlorate **26** reacts with the dialdehyde potassium 3,5-diformyl-2,4-dihydroxybenzoate **27** in glacial acetic acid yielding the spiropyran of the 1,3-benzoxazine series through the formation of the intermediate styryl salt **28**. This intermediate has been isolated and then cyclized under the action of triethylamine in anhydrous diethyl ether to yield compound **29**, as shown in Scheme 22.[126,127]

4.3. Reaction with alkyl halides

1,3-Benzoxazine-2,4-dione was reacted with alkyl halide in the presence of K_2CO_3[128,129] yielding *N*-substituted derivatives (Scheme 23).

4.4. Nucleophilic substitution reaction

4.4.1. Reaction with pyridine *N*-oxide

2,3-Dihydro-2,2-dimethyl-3-(2-pyridyl)-4*H*-1,3-benzoxazin-4-one (**30**) was produced by refluxing the 4-chloro-derivative of benzoxazine (**31**) with two

moles of pyridine *N*-oxide in dichloromethane through a nucleophilic substitution reaction followed by rearrangement[123] (Scheme 24).

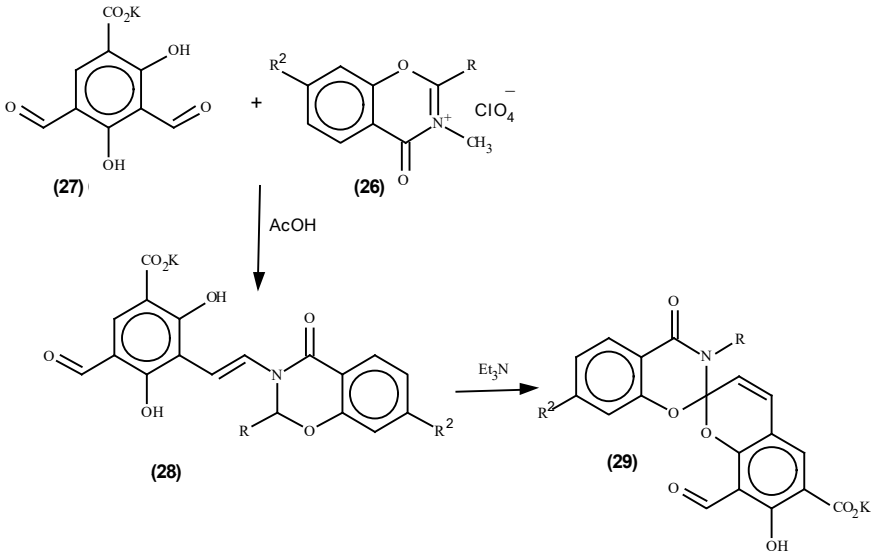

Scheme 22. Reaction of 4-oxo-4*H*-1,3-benzoxazinium salts with 3,5-diformyl-2,4-dihydroxybenzoate.

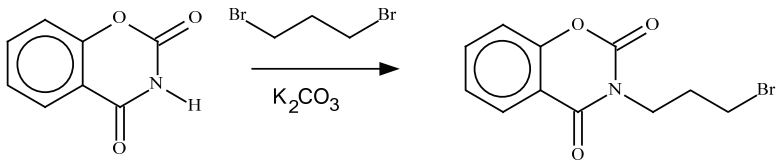

Scheme 23. Reaction of 1,3-benzoxazine-2,4-dione with alkyl halides.

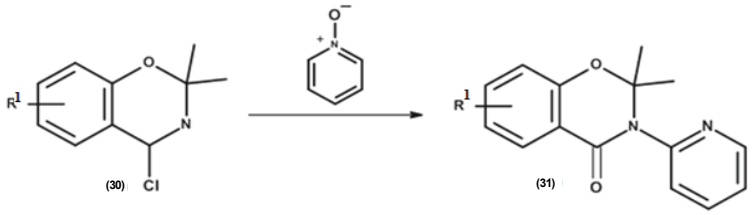

Scheme 24. Reaction of substituted-1,3-benzoxazines with pyridine *N*-oxide.

4.4.2. Reaction with organometalic compounds

2,3-Dihydro-2,2-dimethyl-1,3-benzoxazin-4-one derivatives react with organometallic compounds by nucleophilic substitution as shown in Scheme 25.[130]

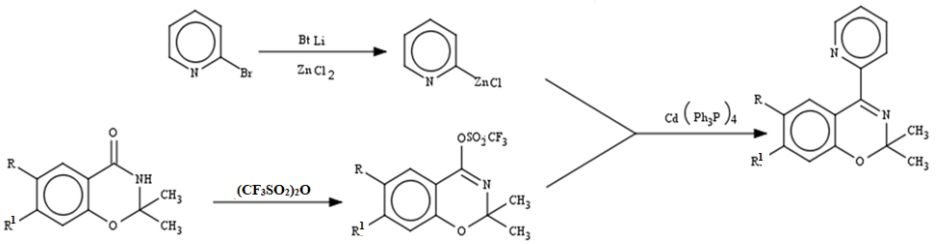

Scheme 25. Reaction of 1,3-benzoxazin-4-ones with organometalic compounds.

5. BIOLOGICAL ACTIVITIES

Benzoxazinone and its derivatives are a significant class of heterocyclic compounds, because many of these derivatives display diverse biological activities.

5. 1. Antiviral therapy

Elbasvir (**32**, Fig. 17)[131,132] is potent inhibitor of the HCV NS5A protein and is used in combination with grazoprevir for the treatment of the hepatitis C virus (HCV) NS3/4A.[133] In addition, grazoprevir/elbasvir plus ribavirin were examined as a new treatment option for patients after failure of triple therapy containing an earlier-generation protease inhibitor.[134]

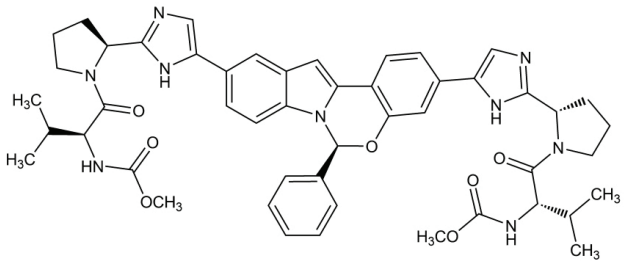

Fig. 17. Structure of elbasvir (**32**).

5.2. Anti-tuberculosis activity

The antimycobacterial activity of various substituted 3-phenyl-2*H*-1,3-benzoxazine-2,4(3*H*)-dithiones and 3-phenyl-2*H*-benzoxazine-2,4(3*H*)-diones have been studied using a quantum molecular similarity approach. The replacement of the oxo-group by the thioxo-group in position 4 on the benzoxazin-2,4-dione ring increases the activity, as well as the similar replacement in position 2.[135,136] *In vitro* antimycobacterial activity against *Mycobacterium tuberculosis*, *M. avium* and two strains of *M. kansasii* were studied. Furthermore, the antimycobacterial activity increased with replacement of the carbonyl group by the thiocarbonyl group in the starting 3-(4-alkylphenyl)-2*H*-1,3-benzoxazine-2,4(3*H*)-diones.[137,138]

5.3. Fungicidal and pesticide activities

A series of 2,3-disubstituted-3,4-dihydro-2*H*-1,3-benzoxazines was prepared by reaction of aza-acetalizations of aromatic aldehydes with *2*-(*N*-substituted aminomethyl)phenols in the presence of trimethylsilyl chloride (TMSCl). The fungicidal activities were evaluated, and some of these compounds exhibited activity against *Rhizoctonia solani*.[62] Additionally, a series of 2,3-diaryl-3,4--dihydro-2*H*-1,3-benzoxazines was prepared in high yields from *o*-arylamino-methylphenols and aromatic aldehydes in the presence of $SnCl_4$. Their fungicidal activities were investigated. Some of the products showed good fungicidal activities against *R. solani*.[27] Furthermore, novel naphtho[1,2-*e*][1,3]oxazines bearing an arylsulfonamide moiety were synthesized and evaluated for their anticancer and antifungal activities.[139]

Moreover, substituted 8-hydroxy-3-phenyl-2*H*-1,3-benzoxazine-2,4-(3*H*)--diones were synthesized by cyclization of the corresponding dihydroxy-*N*-phenylbenzamides with methyl chloroformate. Thionation of the compounds was performed using Lawesson's reagent. All compounds were tested *in vitro* for their antifungal activity against eight test strains. The compounds showed moderate activity.[140]

In addition, the compounds 3,4-dihydro-4-methyl-3-nonyl-2*H*-1,3-benzoxazines and 3-decyl-3,4-dihydro-4-methyl-2*H*-1,3-benzoxazines were studied and investigated as pesticides.[141]

5.4. Anticovulsive activities

2,4-Dioxo-2*H*-1,3-benzoxazine-3(4*H*)-butanoic acid (BXDBA) shows good anticonvulsive activity and its ability to block bicuculline-induced convulsions suggests that it could be a $GABA_A$ mimetic drug.[142,143]

5.5. Antibacterial activities

Substituted *N*-[(benzylamino)thioxomethyl]-2-hydroxybenzamides were synthesized using sodium bicarbonate and benzyl amine with 2-thioxo-substituted-1,3-benzoxazines. These derivatives were investigated as antibacterial and antifungal agents.[144]

Moreover, a series of 3,3′-(1,2-ethanediyl)-bis[3,4-dihydro-2*H*-1,3-benzoxazine derivatives (**33**, Fig. 18) was synthesized *via* an eco-friendly Mannich-type condensation-cyclization reaction of phenols or naphthols with formaldehyde and primary amines in water at ambient temperature. *In vitro* antimicrobial activity of the synthesized compounds was assessed against six pathogenic fungi, two Gram-negative and two Gram-positive bacteria. Some of the screened compounds showed significant *in vitro* antimicrobial effects.[145]

Benzofuranyl-1,3-benzoxazines and benzofuranyl-1,3-benzoxazin-2-ones were synthesized *via* coupling benzofuran with 1,3-benzoxazines and 1,3-benzo-

xazin-2-ones through –CONH– and –$COCH_2$– bridges, respectively. The antimicrobial activity of these compounds was reported.[146]

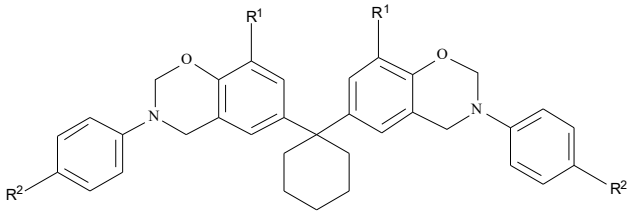

(33)

Fig. 18. Structure of compound **33**.

5.6. Anticancer activities

Furthermore, naphtho[1,2-*e*][1,3]oxazines bearing a arylsulfonamide moiety, synthesized *via* a one-pot method, showed remarkable activities against MCF-7 (breast) and HCT116 (colon) cancers.[139] In addition, 1,3-benzoxazines having a flavone moiety at the 3-position also showed activities against MCF-7.[147]

2*H*-1,3-Oxazine-2,6(3*H*)-dione (3-oxauracil) exhibited cytotoxic activity against the tested cancer cell lines (pancreatic, colon, neuroendocrine and non-small cell lung). These derivatives were studied as an inhibitor of selected neoplastic cell growth *in vivo*.[148]

In addition, a series of modified hexacyclic camptothecin derivatives containing a 1,3-oxazine ring was synthesized. All compounds were assayed *in vitro* against nine human cancer cell lines. Some of these compounds showed about 13-fold greater potency than camptothecin, and about six-fold greater potency than topotecan toward HEPG-2. Furthermore, the *N*-alkyl-substituted derivatives were more potent than the *N*-aryl- and *N*-benzyl-substituted compounds.[149]

The synthesis of 6-aryl, 8-aryl, and 8-aryl-6-chloro-2-morpholino-1,3-benzoxazines with potent activity against PI3K and DNA-PK was studied. A compound with the 8-(naphthalen-1-yl) scaffold showed strong anti-proliferative activity against A498 renal cancer cells, which warrants further investigation.[150]

5.7. Antihypertinsive activities

The antihypertensive and cardiovascular properties of a new potassium channel opener, TCV-295 (**34**), were studied in rats and dogs. In conscious, spontaneously hypertensive rats (SHR), TCV-295 reduced blood pressure (BP) with a low dose dependence and with slow onset of action being observed.[151]

An efficient process for potassium channel opener TCV-295, based on 4-(2--pyridyl)-2*H*-1,3-benzoxazine ring formation from 2-(*o*-hydroxybenzoyl)pyridine derivative by the NH_4I/piperidine/2,2-dimethoxypropane system and subsequent selective pyridine-*N*-oxidation using dimethyldioxirane, was examined.[152]

In addition, to explore K^+ channel openers, a series of 1,3-benzoxazine derivatives with a 2-pyridine-1-oxide group at C4 (**34**, Fig. 19) was synthesized by one-pot 1,3-benzoxazine skeleton formation and using a palladium(0)-catalyzed carbon–carbon bond formation reaction of imino-triflates with organozinc reagents. The compounds were tested for vaso-relaxant activity using $BaCl_2$-induced and high KCl-induced contraction of rat aorta to identify potential K^+ channel openers, and also for oral hypotensive effects in spontaneously hypertensive rats.[130]

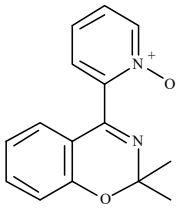

(34)

Fig. 19. Structure of compound **34**.

5.8. Antimalarial activities

A series of 6-(2-chloroquinolin-3-yl)-4-(substituted phenyl)-6*H*-1,3-oxazin-2-amines was synthesized and evaluated *in vitro* for antimalarial efficacy against chloroquine sensitive (MRC-02) and chloroquine resistant (RKL9) strains of *Plasmodium falciparum.*[153]

The antimalarial activities of the resulting benzoxazines, their isosteric tetrahydroquinazoline derivatives, and febrifugine-based quinazolin-4-ones were examined *in vitro* (against *P. falciparum*) and *in vivo* (against *P. berghei*).[138]

5.9. Antidiabetic and hypolipidaemic activity

A series of 5-{{4-[2-(4-oxo-2*H*-1,3-benzoxazin-3(4*H*)-yl)ethoxy]phenyl}methyl}thiazolidine-2,4-diones was synthesized and investigated for their plasma glucose and plasma triglyceride lowering activity. In addition the synthesized 2,4-thiazolidinedione derivatives of 1,3-benzoxazinone were evaluated for their antidiabetic and hypolipidaemic potential. For example, DRF-2519 (**35**, Fig. 20) showed potent dual PPAR activation.[154]

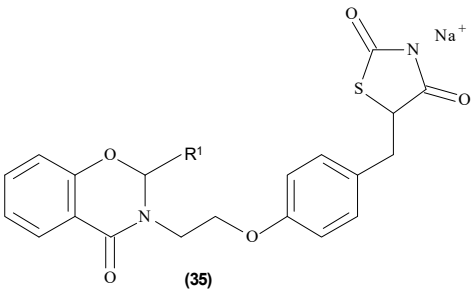

(35)

Fig. 20. Structure of compound **35**.

5.10. Receptor antagonist activity

The synthesis and pharmacology of benzoxazines (**36**, Fig. 21) were investigated as highly selective antagonists at M_4 muscarinic receptors.[155]

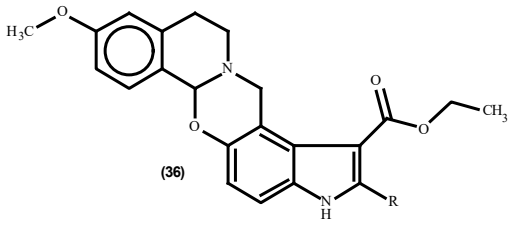

Fig. 21. Structure of compound **36**.

5.11. Antidepressant activity

It was found that 1,3-benzoxazine-2,4-diones (**37**, Fig. 22) have binding affinities for the 5-HT_{1A} and 5-HT_7 receptors.[128] Furthermore, the benzoxazine derivative caroxazone (**38**, Fig. 23), was investigated *in vitro* and *in vivo* as antidepressant (Ro 11-1163) and as a specific and short-acting MAO-A inhibitor.[156]

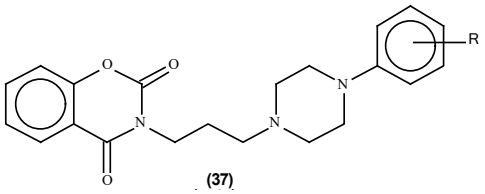

Fig. 22. Structure of compound **37**.

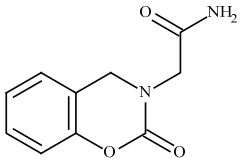

Fig. 23. Structure of compound **38**.

5.12. Anti-platelet aggregation activity

A series of 2,8-disubstituted benzoxazinones (**39**, Fig. 24) was synthesized and studied as anti-platelet aggregation agents *via* inhibition of superoxide anion generation and inhibition of neutrophile elastase release assays. It was found that, the synthesized compounds were more potent than aspirin on arachidonic acid-induced platelet aggregation.[157,158]

5.13. Miscellaneous activities

In addition, other benzoxazine compounds have anti-inflammatory activities, *e.g.*, compounds **40** and **41**,[30] and analgesic and antipyretic properties, such as

chlorthenoxazin (**42**), Fig. 25.[19,30] Furthermore, these derivatives are used as specific inhibitors of the Tissue Factor (TF)/Factor Via (Via)-induced pathway of coagulation, as reported in the literature.[159]

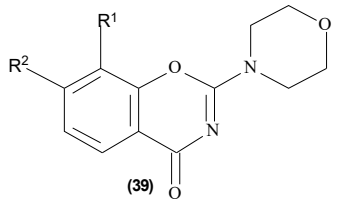

Fig. 24. Structure of compound **39**.

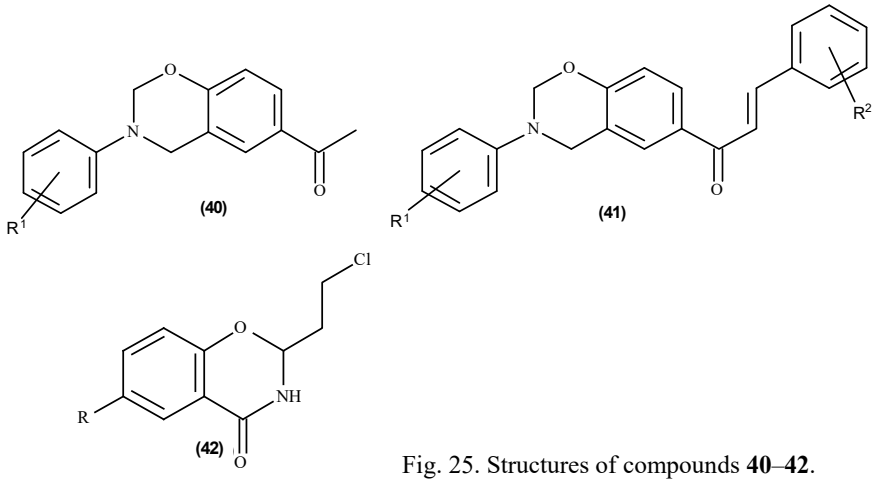

Fig. 25. Structures of compounds **40**–**42**.

CONCLUSIONS

In conclusion, the synthetic potential and transformations of 3,4-dihydro-2*H*--1,3-benzoxazines remain largely of interest. The 3,4-dihydro-2*H*-1,3-benzoxazines are flexible and tough, which lead the molecules to have diverse workable site for substitution. In addition, they exhibit a wide range of biological activities, such as herbicides and agricultural microbiocides, and they show diverse pharmacological activities, such as antitumor agents, antiretroviral therapy, anti-tubercular activity, antibacterial activity, anti-inflammatory activity, anti-convulsant activity, *etc*. On the other hand, the growth of drug resistance is considered a major problem in medicine and to overcome this status, the synthesis of new classes of compounds is a requisite. Consequently, the data collected in this review could be used to provide novel benzoxazine derivatives that could be utilized for the development of new compounds to overcome resistance of drugs for various diseases.

ИЗВОД

ХЕМИЈА И БИОЛОШКА АКТИВНОСТ 3,4-ДИХИДРО-2*H*-1,3-БЕНЗОКСАЗИНА И ЊИХОВИХ ОКСО-ДЕРИВАТА

NABAWEYA ABD EL-SALAM SHARAF EL-DIN

Department of Pharmaceutical Chemistry, Faculty of Pharmacy, Tanta University, El Giesh street, 31527, Tanta, Egypt

Деривати 3,4-дихидро-2*H*-1,3-бензоксазина су природни производи и значајна класа хетероцикличних једињења посебно због њихове изузетне активности у хуманој медицини, фитофармацији и ветерини. Услед могућности за надградњу бензоксазинске структуре, компаративне хемијске једноставности и доступности, ова једињења су подесан извор за нова биоактивна једињења. Резултати тога су истраживање и открића велике групе ових једињења која показују широк опсег биолошких активности, као што су антифунгална, антибактеријска, анти-ХИВ, антиканцерска, релаксациона, антиинфламаторна и др. Овај прегледни чланак даје кратак приказ деривата 3,4-дихидро-2*H*-1,3-бензоксазина и њихових оксо-деривата, хемијску реактивност и биоактивност.

(Примљено 30. маја, ревидирано 3. децембра 2018, прихваћено 10. јануара 2019)

REFERENCES

1. L. Lázár, F. Fülöp, *1,3-Oxazines and their benzo derivatives*, in *Comprehensive Heterocyclic Chemistry III*, Vol. 8, Elsevier Ltd., Amsterdam, 2008, p. 373 (http://dx.doi.org/10.1016/B978-008044992-0.00705-7)
2. J. B. Chylińska, T. Urbański, *J. Heterocycl. Chem.* **1** (1964) 93 (http://dx.doi.org/10.1002/jhet.5570010208)
3. W. J. Burke, *J. Am. Chem. Soc.* **71** (1949) 609 (http://dx.doi.org/10.1021/ja01170a063)
4. R. F. Ahn, J. S. Hahm, D. G. Heaney, H. Wilkins, *Bull. Korean Chem. Soc.* **15** (1994) 329 (http://dx.doi.org/10.1002/chin.199508203)
5. Y. Wu, G. Qiao, H. Liu, L. Zhang, Z. Sun, Y. Xiao, H. Guo, *RSC Adv.* **5** (2015) 84290 (http://dx.doi.org/10.1039/c5ra12401h)
6. H. Sugimoto, S. Nakamura, T. Ohwada, *Adv. Synth. Catal.* **349** (2007) 669 (http://dx.doi.org/10.1002/adsc.200600508)
7. W. J. Burke, R. P. Smith, C. Weatherbee, *J. Am. Chem. Soc.* **74** (1952) 602 (http://dx.doi.org/10.1021/ja01123a007)
8. S. Chirachanchai, A. Laobuthee, S. Phongtamrug, *J. Heterocycl. Chem.* **46** (2009) 714 (http://dx.doi.org/10.1002/jhet.130)
9. X. Wang, F. Chen, Y. Gu, *J. Polym. Sci., Part A: Polym. Chem.* **49** (2011) 1443 (http://dx.doi.org/10.1002/pola.24566)
10. Z. Brunovska, J. P. Liu, H. Ishida, *Macromol. Chem. Phys.* **200** (1999) 1745 (http://dx.doi.org/10.1002/(SICI)1521-3935(19990701)200:7<1745::AID-MACP1745>3.0.CO;2-D)
11. J. Liu, X. Lu, Z. Xin, C. Zhou, *Langmuir* **29** (2013) 411 (http://dx.doi.org/10.1021/la303730m)
12. W. J. Burke, M. J. Kolbezen, C. Wayne Stephens, *J. Am. Chem. Soc.* **74** (1952) 3601 (http://dx.doi.org/10.1021/ja01134a039)
13. W. J. Burke, C. R. Hammer, C. Weatherbee, *J. Org. Chem.* **26** (1961) 4403 (http://dx.doi.org/10.1021/jo01069a053)
14. Y. Cheng, J. Yang, Y. Jin, D. Deng, F. Xiao, *Macromolecules* **45** (2012) 4085 (http://dx.doi.org/10.1021/ma3004218)

15. H. C. Chang, C. H. Lin, Y. W. Tian, Y. R. Feng, L. H. Chan, *J. Polym. Sci., A: Polym. Chem.* **50** (2012) 2201 (http://dx.doi.org/10.1002/pola.25993)
16. C. X. Zhang, Y. Y. Deng, Y. Y. Zhang, P. Yang, Y. Gu, *Chin. Chem. Lett.* **26** (2015) (http://dx.doi.org/10.1016/j.cclet.2014.12.005)
17. A. Váradi, T. C. Palmer, P. R. Notis, G. N. Redel-Traub, D. Afonin, J. J. Subrath, G. W. Pasternak, C. Hu, I. Sharma, S. Majumdar, *Org. Lett.* **16** (2014) 1668 (http://dx.doi.org/10.1021/ol500328t).
18. J. D. Edwards, J. Pailermo, U.S. 8,293,281 (2012)
19. P. Zhang, E. A. Terefenko, A. Fensome, Z. Zhang, Y. Zhu, J. Cohen, R. Winneker, J. Wrobel, J. Yardley, *Bioorg. Med. Chem. Lett.* **12** (2002) 787 (http://dx.doi.org/10.1016/S0960-894X(02)00025-2)
20. D. Sicker, M. Schulz, *Stud. Nat. Prod. Chem.* **27** (2002) 185 (http://dx.doi.org/10.1016/S1572-5995(02)80037-0)
21. H. Varshney, A. Ahmad, A. Rauf, F. M. Husain, I. Ahmad, *J. Saudi Chem. Soc.* **21** (2017) S394 (http://dx.doi.org/10.1016/j.jscs.2014.04.008)
22. W. J. Burke, C. Weatherbee, *J. Am. Chem. Soc.* **72** (1950) 4691 (http://dx.doi.org/10.1021/ja01166a094)
23. H. P. Higginbottom, U.S. 4,501,864 (1985)
24. H. Ishida, J. P. Liu, in *Handbook of Benzoxazine Resins*, H. Ishida, T. Agag, Eds., Elsevier, Amsterdam, 2011, pp. 85–102 (http://dx.doi.org/10.1016/B978-0-444-53790-4.00047-3)
25. Y. Liu, Z. Yue, J. Gao, *Polymer* **51** (2010) 3722 (http://dx.doi.org/10.1016/j.polymer.2010.06.009)
26. Y. Deng, Q. Zhang, H. Zhang, C. Zhang, W. Wang, Y. Gu, *Ind. Eng. Chem. Res.* **53** (2014) 1933 (http://dx.doi.org/10.1021/ie402978s).
27. Z. Tang, W. Chen, Z. Zhu, H. Liu, *J. Heterocycl. Chem.* **48** (2011) 255 (http://dx.doi.org/10.1002/jhet.533)
28. A. U. G. Gabbas, M. B. Ahmad, N. Zainuddin, N. A. Ibrahim, *Asian J. Chem.* **28** (2016) 1304 (http://dx.doi.org/10.14233/ajchem.2016.19666)
29. Y. Omura, Y. Taruno, Y. Irisa, M. Morimoto, H. Saimoto, Y. Shigemasa, *Tetrahedron Lett.* **42** (2001) 7273 (http://dx.doi.org/10.1016/S0040-4039(01)01491-5)
30. M. Akhter, S. Habibullah, S. M. Hasan, M. M. Alam, N. Akhter, M. Shaquiquzzaman, *Med. Chem. Res.* **20** (2011) 1147 (http://dx.doi.org/10.1007/s00044-010-9451-x)
31. M. R. Vengatesan, S. Devaraju, D. Kannaiyan, J. K. Song, M. Alagar, *Polym. Int.* **62** (2013) 127 (http://dx.doi.org/10.1002/pi.4337)
32. H. Ishida, US 5,543,516 (1996)
33. O. A. Attanasi, M. S. Behalo, G. Favi, D. Lomonaco, S. E. Mazzetto, G. Mele, I. Pio, G. Vasapollo, *Curr. Org. Chem.* **16** (2012) 2613 (http://dx.doi.org/10.2174/138527212804004616)
34. K. Chiou, E. Hollanger, T. Agag, H. Ishida, *Macromol. Chem. Phys.* **214** (2013) 1629 (http://dx.doi.org/10.1002/macp.201300032)
35. R. Andreu, J. A. Reina, J. C. Ronda, *J. Polym. Sci., A: Polym. Chem.* **46** (2008) 3353 (http://dx.doi.org/10.1002/pola.22677).
36. P. Velez-Herrera, H. Ishida, *J. Fluorine Chem.* **130** (2009) 573 (http://dx.doi.org/10.1016/j.jfluchem.2009.04.002)
37. H. Qi, H. Ren, G. Pan, Y. Zhuang, F. Huang, L. Du, *Polym. Adv. Technol.* **20** (2009) 268 (http://dx.doi.org/10.1002/pat.1261).

38. Q. Ran, Q. Tian, C. Li, Y. Gu, *Polym. Adv. Technol.* **21** (2009) 170 (http://dx.doi.org/10.1002/pat.1412).
39. S. Q. R. Mahfud, T. Agag, H. Ishida, S. Shaikh, *J. Colloid Interface Sci.* **407** (2013) 339 (http://dx.doi.org/10.1016/j.jcis.2013.06.042)
40. T. Agag, T. Takeichi, *Macromolecules (Washington, DC, U.S.)* **36** (2003) 6010 (http://dx.doi.org/10.1021/ma021775q)
41. H. Ishida, S. Ohba, *Polymer* **46** (2005) 5588 (http://dx.doi.org/10.1016/j.polymer.2005.04.080)
42. *Handbook of Benzoxazine Resins*, H. Ishida, T. Agag, Eds., Elsevier, Amsterdam, 2011 (http://dx.doi.org/10.1016/C2010-0-66598-9).
43. M. Imran, B. Kiskan, Y. Yagci, *Tetrahedron Lett.* **54** (2013) 4966 (https://doi.org/10.1016/j.tetlet.2013.07)
44. Y. Hayashi, *Chem. Sci.* **7** (2016) 866 (http://dx.doi.org/10.1039/C5SC02913A)
45. R. Ruijter, E. Scheffelaar, R. Orru, *Angew. Chem. Int. Ed.* **50** (2011) 6234 (http://dx.doi.org/10.1002/anie.201006515)
46. J. Liu, G. Yuan, *Tetrahedron Lett.* **58** (2017) 1470 (http://dx.doi.org/10.1016/j.tetlet.2017.02.081)
47. V. D. Dhakane, S. S. Gholap, U. P. Deshmukh, H. V. Chavan, B. P. Bandgar, *C. R. Chim.* **17** (2014) 431 (http://dx.doi.org/10.1016/j.crci.2013.06.002)
48. T. Zhang, J. Wang, T. Feng, H. Wang, N. Ramdani, M. Derradji, X. Xu, W. Liu, T. Tang, *RSC Adv.* **5** (2015) 33623 (http://dx.doi.org/10.1039/c5ra02839f)
49. J. Wang, H. Wang, J. T. Liu, W. Bin Liu, X. De Shen, *J. Therm. Anal. Calorim.* **114** (2013) 1255 (http://dx.doi.org/10.1007/s10973-013-3081-8)
50. R. Eligeti, G. R. Kundur, S. R. Atthunuri, N. R. Modugu, *Green Chem. Lett. Rev.* **5** (2012) 699 (http://dx.doi.org/10.1080/17518253.2012.700736)
51. A. R. Katritzky, Y. J. Xu, R. Jain, *J. Org. Chem.* **67** (2002) 8234 (http://dx.doi.org/10.1021/jo020176e)
52. F. W. Holly, A. C. Cope, *J. Am. Chem. Soc.* **66** (1944) 1875 (http://dx.doi.org/10.1021/ja01239a022)
53. W. J. Burke, J. L. Bishop, E. L. M. Glennie, W. N. Bauer, *J. Org. Chem.* **30** (1965) 3423 (http://dx.doi.org/10.1021/jo01021a037)
54. D. L. Fields, J. B. Miller, D. D. Reynolds, *J. Org. Chem.* **27** (1962) 2749 (http://dx.doi.org/10.1021/jo01055a011)
55. J. Liu, *Synthesis, characterization, reaction mechanism and kinetics of 3,4-dihydro-2*H*--1,3-benzoxazine and its polymer*, 1995 (https://etd.ohiolink.edu/!etd.send_file?accession=case1062775094&disposition=inline)
56. M. A. Espinosa, V. Cádiz, M. Galià, *J. Appl. Polym. Sci.* **90** (2003) 470 (http://dx.doi.org/10.1002/app.12678)
57. N. N. Ghosh, B. Kiskan, Y. Yagci, *Prog. Polym. Sci.* **32** (2007) 1344 (http://dx.doi.org/10.1016/j.progpolymsci.2007.07.002)
58. C.-H. Chen, K.-W. Lee, C.-H. Lin, T.-Y. Juang, *Polymers (Basel)* **10** (2018) 411 (http://dx.doi.org/10.3390/polym10040411)
59. R. Andreu, J. C. Ronda, *Synth. Commun.* **38** (2008) 2316 (http://dx.doi.org/10.1080/00397910802138629)
60. M. Imran, B. Kiskan, Y. Yagci, *Tetrahedron Lett.* **54** (2013) 4966 (http://dx.doi.org/10.1016/j.tetlet.2013.07.041)
61. J. H. Billman, L. C. Dorman, *J. Med. Chem.* **6** (1963) 701 (http://dx.doi.org/10.1021/jm00342a016)

62. Z. Tang, Z. Zhu, Z. Xia, H. Liu, J. Chen, W. Xiao, X. Ou, *Molecules* **17** (2012) 8174 (http://dx.doi.org/10.3390/molecules17078174)
63. A. U. G. Gabbas, M. B. Hj Ahmad, N. Zainuddin, N. A. Ibrahim, *Polimery (Warsaw, Pol.)* **62** (2017) 86 (http://dx.doi.org/10.14314/polimery.2017.086).
64. R. P. Subrayan, F. N. Jones, *Chem. Mater.* **10** (1998) 3506 (http://dx.doi.org/10.1021/CM980284A)
65. M. Deb, P. Borpatra, P. Saikia, P. Baruah, *Synlett* **28** (2016) 461 (http://dx.doi.org/10.1055/s-0036-1589717)
66. H. Ishida, D. J. Allen, *J. Polym. Sci., B: Polym. Phys.* **34** (1996) 1019 (http://dx.doi.org/10.1002/(SICI)1099-0488(19960430)34:6<1019::AID-POLB1>3.0.CO;2-T)
67. H. Y. Low, H. Ishida, *Polym. Degrad. Stab.* **91** (2006) 805 (http://dx.doi.org/10.1016/j.polymdegradstab.2005.05.030)
68. C. Dizman M. A. Tasdelen, *Polym. Int.* **62** (2013) 991 (http://dx.doi.org/https://doi.org/10.1002/pi.4525)
69. B. Van der Bruggen, *J. Appl. Polym. Sci.* **114** (2009) 630 (http://dx.doi.org/10.1002/app.30578)
70. T. Agag, L. Jin, H. Ishida, *Polymer* **50** (2009) 5940 (http://dx.doi.org/10.1016/j.polymer.2009.06.038)
71. M. Liu, Z. Hao, S. Lv, J. Huang, C. Liao, C. Run, *Polymer* **57** (2015) 29 (http://dx.doi.org/10.1016/j.polymer.2014.12.005)
72. C. Dizman, C. Altinkok, M. A. Tasdelen, *Des. Monomers Polym.* **20** (2017) 293 (http://dx.doi.org/10.1080/15685551.2016.1257379)
73. M. J. H. Worthington, R. L. Kucera, J. M. Chalker, *Green Chem.* **19** (2017) 2748 (http://dx.doi.org/10.1039/C7GC00014F)
74. M. A. Rahman, H. N. Lokupitiya, M. S. Ganewatta, L. Yuan, M. Stefik, C. Tang, *Macromolecules (Washington, DC, U.S.)* **50** (2017) 2069 (http://dx.doi.org/10.1021/acs.macromol.7b00001)
75. L. Dumas, L. Bonnaud, M. Olivier, M. Poorteman, P. Dubois, *Eur. Polym. J.* **81** (2016) 337 (http://dx.doi.org/10.1016/j.eurpolymj.2016.06.018)
76. G. A. Phalak, D. M. Patil, S. T. Mhaske, *Eur. Polym. J.* **88** (2017) 93 (http://dx.doi.org/10.1016/j.eurpolymj.2016.12.030)
77. E. Calò, A. Maffezzoli, G. Mele, F. Martina, S. E. Mazzetto, A. Tarzia, C. Stifani, *Green Chem.* **9** (2007) 754 (http://dx.doi.org/10.1039/b617180j)
78. B. Lochab, I. K. Varma, J. Bijwe, *J. Therm. Anal. Calorim.* **107** (2012) 661 (http://dx.doi.org/10.1007/s10973-011-1854-5)
79. Y. Sun, J. Cheng, *Bioresour. Technol.* **83** (2002) 1 (http://dx.doi.org/10.1016/S0960-8524(01)00212-7)
80. V. Menon, M. Rao, *Prog. Energy Combust. Sci.* **38** (2012) 522 (http://dx.doi.org/10.1016/j.pecs.2012.02.002)
81. M. Sharma, S. Manohar, D. S. Rawat, *J. Heterocycl. Chem.* **49** (2012) 589 (http://dx.doi.org/10.1002/jhet.825)
82. A. Kumar, M. K. Gupta, M. Kumar, *RSC Adv.* **2** (2012) 7371 (http://dx.doi.org/10.1039/c2ra20848b)
83. F. Nemati, A. Beyzai, *J. Chem.* **2013**, 2013, Article ID 365281 (http://dx.doi.org/10.1155/2013/365281).
84. A. Chaskar, V. Vyavhare, V. Padalkar, K. Phatangare, H. Deokar, *J. Serb. Chem. Soc.* **76** (2011) 21 (http://dx.doi.org/10.2298/JSC100410016C)

85. D. Fang, L.-f. Yang, J.-m. Yang, *Res. Chem. Intermed.* **39** (2013) 2505 (http://dx.doi.org/10.1007/s11164-012-0776-6)
86. M. Lei, L. Ma, L. Hu, *Synth. Commun.* **41** (2011) 3424 (http://dx.doi.org/10.1080/00397911.2010.518278)
87. A. Hajra, D. Kundu, A. Majee, *J. Heterocycl. Chem.* **46** (2009) 1019 (http://dx.doi.org/10.1002/jhet.180)
88. S. Kantevari, S.V. Vuppalapati, R. Bantu, L. Nagarapu, *J. Heterocycl. Chem.* **47** (2010) 313 (http://dx.doi.org/10.1002/jhet.312)
89. G. B. Dharma Rao, M. P. Kaushik, A. K. Halve, *Tetrahedron Lett.* **53** (2012) 2741 (http://dx.doi.org/10.1016/j.tetlet.2012.03.085)
90. G. Sabitha, K. Arundhathi, K. Sudhakar, B. S. Sastry, J. S. Yadav, *J. Heterocycl. Chem.* **47** (2010) 272 (http://dx.doi.org/10.1002/jhet.328)
91. A. Olyaei, M. Sadeghpour, M. Zarnegar, *Chem. Heterocycl. Compd.* **49** (2013) 1374 (http://dx.doi.org/10.1007/s10593-013-1387-x).
92. I. Szatmári, A. Hetényi, L. Lázár, F. Fülöp, *J. Heterocycl. Chem.* **41** (2004) 367 (http://dx.doi.org/10.1002/jhet.5570410310)
93. C. Cimarelli, G. Palmieri, E. Volpini, *Can. J. Chem.* **82** (2004) 1314 (http://dx.doi.org/10.1139/v04-100)
94. S. Guo, X. Liu, B. Shen, L. Lin, X. Feng, *Org. Lett.* **18** (2016) 5070 (http://dx.doi.org/10.1021/acs.orglett.6b02522)
95. I. V. Ozhogin, I. V. Dorogan, B. S. Lukyanov, E. L. Mukhanov, V. V. Tkachev, A. V. Chernyshev, M. B. Lukyanova, S. M. Aldoshin, V. I. Minkin, *Tetrahedron Lett.* **57** (2016) 2382 (http://dx.doi.org/10.1016/j.tetlet.2016.04.054)
96. N. Latif, N. Mishriky, F. Assad, *Aust. J. Chem.* **35** (1982) 1037 (http://dx.doi.org/10.1071/CH9821037)
97. L. D. S. Yadav, B. S. Yadav, V. K. Rai, *Tetrahedron Lett.* **45** (2004) 5351 (http://dx.doi.org/10.1016/j.tetlet.2004.05.084)
98. A. Mustafa, A. Eldin, A. A. Hassan, *J. Am. Chem. Soc.* **79** (1957) 3846 (http://dx.doi.org/10.1021/ja01571a059)
99. L. Åkerbladh, S. Y. Chow, L. R. Odell, M. Larhed, *ChemistryOpen* **6** (2017) 620 (http://dx.doi.org/10.1002/open.201700130)
100. F.Fülöp, K.Pihlaja, I.Huber, G.Bernáth, B.Ribár, G.Argay, A. Kálmán, *Tetrahedron*, **48**(1992) 4963(https://doi.org/10.1016/S0040-4020(01)81589-1)
101. P. P. Onys'ko, K. A. Zamulko, O. I. Kyselyova, Y. A. Syzonenko, *Heterocycl. Commun.* **23** (2017) 421 (http://dx.doi.org/10.1515/hc-2017-0102)
102. M. V. Vovk, A. V. Bol'But, A. N. Chernega, *J. Fluorine Chem.* **116** (2002) 97 (http://dx.doi.org/10.1016/S0022-1139(01)00561-9)
103. X. Chen, W. Hao, Y. Liu, *Org. Biomol. Chem.* **15** (2017) 3423 (http://dx.doi.org/10.1039/C7OB00625J)
104. I. Chen Resck, M. L. dos Santos, L. A. Soares Romeiro, *Heterocycles* **65** (2005) 311 (http://dx.doi.org/10.3987/COM-04-10261)
105. R. A. Izydore, J. T. Jones, B. Mogesa, I. N. Swain, R. G. Davis-Ward, D. L. Daniels, F. F. Kpakima, S. T. Spaulding-Phifer, *J. Org. Chem.* **79** (2014) 2874 (http://dx.doi.org/10.1021/jo402708j)
106. P. Boontheung, P. Perlmutter, *Tetrahedron Lett.* **39** (1998) 2629 (http://dx.doi.org/10.1016/S0040-4039(98)00223-8)
107. J. Petridou-Fischer, E. P. Papadopoulos, *J. Heterocycl. Chem.* **20** (1983) 1159 (http://dx.doi.org/10.1002/jhet.5570200506)

108. P. Froimowicz, K. Zhang, H. Ishida, *Chem. – Eur. J.* **22** (2016) 2691 (http://dx.doi.org/10.1002/chem.201503477)
109. G. R. Goward, I. Schnell, S. P. Brown, H. W. Spiess, H.-D. Kim, H. Ishida, *Magn. Reson. Chem.* **39** (2001) S5 (http://dx.doi.org/10.1002/mrc.931)
110. H. D. Kim, H. Ishida, *Macromol. Symp.* **195** (2003) 123 (http://dx.doi.org/10.1002/masy.200390113)
111. G. R. Goward, D. Sebastiani, I. Schnell, H. W. Spiess, H. D. Kim, H. Ishida, *J. Am. Chem. Soc.* **125** (2003) 5792 (http://dx.doi.org/10.1021/ja029059r)
112. W. Wattanathana, C. Veranitisagul, N. Koonsaeng, A. Laobuthee, in *Advanced and Emerging Polybenzoxazine Science and Technology*, H. Ishida, P. Froimowicz, Eds., Elsevier, Amsterdam, 2017, p. 75 (http://dx.doi.org/10.1016/B978-0-12-804170-3.00006-8)
113. N. K. Sini, T. Endo, *Macromolecules (Washington, DC, U.S.)* **49** (2016) 8466-8478 (http://dx.doi.org/10.1021/acs.macromol.6b01965)
114. Y.-C. Su, D.-R. Yei, F.-C. Chang, *J. Appl. Polym. Sci.* **95** (2005) 730 (http://dx.doi.org/10.1002/app.21244)
115. K. S. Santhosh Kumar, C. P. Reghunadhan Nair, K. N. Ninan, *Thermochim. Acta* **441** (2006) 150 (http://dx.doi.org/10.1016/j.tca.2005.12.007)
116. T. Urbaniak, M. Soto, M. Liebeke, K. Koschek, *J. Org. Chem.* **82** (2017) 4050 (http://dx.doi.org/10.1021/acs.joc.6b02727)
117. R. Andreu, J. A. Reina, J. C. Ronda, *J. Polym. Sci., A: Polym. Chem.* **46** (2008) 6091 (http://dx.doi.org/10.1002/pola.22921)
118. P. Chutayothin, H. Ishida, *Macromolecules (Washington, DC, U.S.)* **43** (2010) 4562 (http://dx.doi.org/10.1021/ma901743h)
119. V. Voiciuk, K. Redeckas, V. Martynaitis, R. Steponavičiute, A. Šačkus, M. Vengris, *J. Photochem. Photobiol., A* **278** (2014) 60 (http://dx.doi.org/10.1016/j.jphotochem.2013.12.022)
120. Y. Prostota, P. J. Coelho, J. Pina, J. Seixas De Melo, *J. Photochem. Photobiol., A* **216** (2010) 59 (http://dx.doi.org/10.1016/j.jphotochem.2010.09.006)
121. S. Ohashi, F. Cassidy, S. Huang, K. Chiou, H. Ishida, *Polym. Chem.* **7** (2016) 7177 (http://dx.doi.org/10.1039/C6PY01686C)
122. I. Szatmári, T. A. Martinek, L. Lázar, A. Koch, E. Kleinpeter, K. Neuvonen, F. Fülöp, *J. Org. Chem.* **69** (2004) 3645 (http://dx.doi.org/10.1021/jo0355810)
123. K. Wachi, A. Terada, *Chem. Pharm. Bull. (Tokyo)* **28** (1980) 465 (http://dx.doi.org/10.1248/cpb.28.465)
124. Y. I., Ryabukhin, L. N. Faleeva, V. G. Korobkova, *Chem. Heterocycl. Compd.* **19** (1983) 332 (http://dx.doi.org/10.1007/BF00513273)
125. E. V. Gromachevskaya, T. P. Kosulina, A. L. Chekhun, V. G. Kul'nevich, *Chem. Heterocycl. Compd.* **29** (1993) 465 (http://dx.doi.org/10.1007/BF00529889)
126. I. V. Ozhogin, V. V. Tkachev, B. S. Lukyanov, G. V. Shilov, E. L. Mukhanov, G. T. Vasilyuk, S. M. Aldoshin, V. I. Minkin, *Dokl. Chem.* **477** (2017) 244 (http://dx.doi.org/10.1134/S0012500817110040)
127. B. S. Luk'yanov, Y. I. Ryabukhin, G. N. Dorofeenko, L. E. Nivorozhkin, V. I. Minkin, *Chem. Heterocycl. Compd.* **14** (1978) 122 (http://dx.doi.org/10.1007/BF00945321)
128. P. Kowalski; J. Jaśkowska; A. Bojarski, B. Duszyńska, *J. Heterocycl. Chem.* **45** (2008) 209 (http://dx.doi.org/10.1002/jhet.5570450125)
129. G. David, B. William, R. E Bay, U.S. 6,399,798 (2002)
130. S. Yamamoto, S. Hashiguchi, S. Miki, Y. Igata, T. Watanabe, M. Shiraishi, *Chem. Pharm. Bull. (Tokyo)* **44** (1996) 734 (http://dx.doi.org/10.1248/cpb.44.734)

131. C. A. Coburn, P. T. Meinke, W. Chang, C. M. Fandozzi, D. J. Graham, B. Hu, Q. Huang, S. Kargman, J. Kozlowski, R. Liu, J. A. McCauley, A. A. Nomeir, R. M. Soll, J. P. Vacca, D. Wang, H. Wu, B. Zhong, D. B. Olsen, S. W. Ludmerer, *ChemMedChem* **8** (2013) 1930 (http://dx.doi.org/10.1002/cmdc.201300343)
132. I. K. Mangion, C. Chen, H. Li, P. Maligres, Y. Chen, M. Christensen, R. Cohen, I. Jeon, A. Klapars, S. Krska, H. Nguyen, R. A. Reamer, B. D. Sherry, I. Zavialov, *Org. Lett.* **16** (2014) 2310 (http://dx.doi.org/10.1021/ol500971c)
133. S. Zeuzem, R. Ghalib, K. R. Reddy, P. J. Pockros, Z. B. Ari, Y. Zhao, M. N. Robertson, *Ann. Intern. Med.* **163** (2015) 1 (http://www.ncbi.nlm.nih.gov/pubmed/25909356?dopt=AbstractPlus)
134. X. Forms, S. C. Gordon, E. Zuckerman, E. Lawitz, J. L. Calleja, H. Hofer, C. Gilbert, J. Palcza, A. Y. M. Howe, M. J. DiNubile, M. N. Robertson, J. Wahl, E. Barr, M. Buti, *J. Hepatol.* **63** (2015) 564 (http://dx.doi.org/10.1016/j.jhep.2015.04.009)
135. A. Gallegos, R. Carbó-Dorca, R. Ponec, K. Waisser, *Int. J. Pharm.* **269** (2004) 51 (http://dx.doi.org/10.1016/j.ijpharm.2003.08.013)
136. P. Nemeček, J. Mocák, J. Lehotay, K. Waisser, *Chem. Pap.* **67** (2013) 305 (http://dx.doi.org/10.2478/s11696-012-0278-4)
137. E. Petrlíková, K. Waisser, H. Divišová, P. Husáková, P. Vrabcová, J. Kuneš, K. Kolář, J. Stolaříková, *Bioorg. Med. Chem.* **18** (2010) 8178 (http://dx.doi.org/10.1016/j.bmc.2010.10.017)
138. S. Gemma, C. Camodeca, M. Brindisi, S. Brogi, G. Kukreja, S. Kunjir, E. Gabellieri, L. Lucantoni, A. Habluetzel, D. Taramelli, N. Basilico, R. Gualdani, F. Tadini-Buoninsegni, G. Bartolommei, M. R. Moncelli, R. E. Martin, R. L. Summers, S. Lamponi, L. Savini, I. Fiorini, R. E. Martin, R. L. Summers, S. Lamponi, L. Savini, I. Fiorini, *J. Med. Chem.* **55** (2012) 10387 (http://dx.doi.org/10.1021/jm300831b)
139. S. G. Mansouri, H. Zali-Boeini, K. Zomorodian, B. Khalvati, R. H. Pargali, A. Dehshahri, H. A. Rudbari, M. Sahihi, Z. Chavoshpour, *Arab. J. Chem.* (2017), in press (http://dx.doi.org/10.1016/j.arabjc.2017.10.009)
140. P. Skála, M. Macháček, M. Vejsová, L. Kubicová, J. Kuneš, K. Waisser, *J. Heterocycl. Chem.* **46** (2009) 873 (http://dx.doi.org/10.1002/jhet.156)
141. N. A. Shakil, A. Pandey, M. K. Singh, J. Kumar, S. K. Awasthi, Pankaj, C. Srivastava, M. K. Singh, R. P. Pandey, *J. Environ. Sci. Health, Part B* **45** (2010) 108 (http://dx.doi.org/10.1080/03601230903471852)
142. A. Capasso, A. Biondi, F. Palagiano, F. Bonina, L. Montenegro, P. de Caprariis, E. Pistorio, L. Sorrentino, *Eur. Neuropsychopharmacol.* **7** (1997) 57 (http://dx.doi.org/10.1016/S0924-977X(96)00390-2)
143. A. Capasso, C. Gallo, *Med. Chem. (Sharjah, United Arab Emirates)* **5** (2009) 343 (http://dx.doi.org/10.2174/157340609788681548)
144. T. Belz, S. Ihmaid, J. Al-Rawi, S. Petrovski, *Int. J. Med. Chem.* **2013** (2013) 1 (http://dx.doi.org/10.1155/2013/436397)
145. B. P. Mathew, A. Kumar, S. Sharma, P. K. Shukla, M. Nath, *Eur. J. Med. Chem.* **45** (2010) 1502 (http://dx.doi.org/10.1016/j.ejmech.2009.12.058)
146. R. K. Ujjinamatada, R. S. Appala, Y. S. Agasimundin, *J. Heterocycl. Chem.* **43** (2006) 437 (http://dx.doi.org/10.1002/jhet.5570430226)
147. V. Garg, A. Kumar, A. Chaudhary, S. Agrawal, P. Tomar, K. K. Sreenivasan, *Med. Chem. Res.* **22** (2013) 5256 (http://dx.doi.org/10.1007/s00044-013-0534-3)
148. L. Seal, D. Von Hoff, R. Lawrence, E. Izbicka, R. M. Jamison, *Invest. New Drugs* **15** (1997) 289 (http://dx.doi.org/10.1023/A:1005962224801)

149. S. Wang, Y. Li, Y. Liu, A. Lu, Q. You, *Bioorg. Med. Chem. Lett.* **18** (2008) 4095 (http://dx.doi.org/10.1016/j.bmcl.2008.05.103)
150. R. Morrison, J. M. A. Al-Rawi, I. G. Jennings, P. E. Thompson, M. J. Angove, *Eur. J. Med. Chem.* **110** (2016) 326 (http://dx.doi.org/10.1016/j.ejmech.2016.01.042)
151. K. Kusumoto, Y. Awane, T. Kitayoshi, S. Fujiwara, S. Hashiguchi, Z. Terashita, M. Shiraishi, T. Watanabe, *J. Cardiovasc. Pharmacol.* **24** (1994) 929 (http://www.ncbi.nlm.nih.gov/pubmed/7898076)
152. H. Mizufune, H. Irie, S. Katsube, T. Okada, Y., Mizuno, M. Arita, *Tetrahedron* **57** (2001) 7501 (http://dx.doi.org/10.1016/S0040-4020(01)00728-1)
153. V. Tiwari, J. Meshram, P. Ali, J. Sheikh, U. Tripathi, *J. Enzyme Inhib. Med. Chem.* **26** (2011) 569 (http://dx.doi.org/10.3109/14756366.2010.539566)
154. G. R. Madhavan, R. Chakrabarti, K. A. Reddy, B. M. Rajesh, V. Balraju, P. B. Rao, R. Rajagopalan, J. Iqbal, *Bioorg. Med. Chem.* **14** (2006) 584 (http://dx.doi.org/10.1016/j.bmc.2005.08.043)
155. T. M. Böhme, C. E. Augelli-Szafran, H. Hallak, T. Pugsley, K. Serpa, R. D. Schwarz, *J. Med. Chem.* **45** (2002) 3094 (http://dx.doi.org/10.1021/jm011116o)
156. M. Da Prada, R. Kettler, H. H. Keller, W. E. Haefely, in *Satellite Symposium International Brain Research Organization (IBRO),* Mannheim, Germany, Karger Publishers, Basel, Switzerland, 1983, pp. 231–245 (http://dx.doi.org/10.1159/000407520)
157. A. Moretti, A. Caccia, C. Calderini, G. Menozzi, M. Amico, *Biochem. Pharmacol.* **30** (1981) 2728 (http://dx.doi.org/10.1016/0006-2952(81)90549-9)
158. P.-W. Hsieh, T.-L. Hwang, C.-C. Wu, F.-R. Chang, T.-W. Wang, Y.-C. Wu, *Bioorg. Med. Chem. Lett.* **15** (2005) 2786 (http://dx.doi.org/10.1016/j.bmcl.2005.03.104)
159. P. Jakobsen, B. Ritsmar Pedersen, E. Persson, *Bioorg. Med. Chem.* **8** (2000) 2095 (http://dx.doi.org/10.1016/S0968-0896(00)00129-2).

Journal of the Serbian Chemical Society
JSCS-info@shd.org.rs • www.shd.org.rs/JSCS
J. Serb. Chem. Soc. *86* (3) 247–256 (2021)
JSCS–5418
Original scientific paper

Synthesis and process optimization of Boscalid by catalyst Pd-PEPPSI-IPr$^{DtBu-An}$

JIAN XU, XIAO-BING LAN, LIN-JIAN XIA, YI YANG and GAO CAO*

School of Chemistry and Chemical Engineering, Guangdong Pharmaceutical University, Zhongshan, 528458, Guangdong Province, P. R. China

(Received 30 March 2020, revised 7 Januaray, accepted 11 January 2021)

Abstract: The purpose of this research was to reduce the amount of noble metal palladium catalyst and improve the catalytic performance in the Suzuki–Miyaura cross-coupling reaction, which is the key step in the synthesis of Boscalid. Taking *o*-bromonitrobenzene and *p*-chlorophenylboronic acid as raw materials, three kinds of Pd-PEPPSI-IPr catalysts were synthesized and employed in the Suzuki reaction, and then the biaryl product was subjected to reduction and condensation reaction to give Boscalid. Under the optimal reaction conditions, the result showed that the catalytic system exhibits highest catalytic efficiency under aerobic conditions, giving the 2-(4-chlorophenyl)nitrobenzene in over 99 % yield. Moreover, the Pd-PEPPSI-IPr$^{DtBu-An}$ catalyst was minimized to 0.01 mol%. The synthesis process was mild, the post-treatment was simple, and the production cost was reduced, which makes it suitable for industrial production.

Keywords: Boscalid; Suzuki reaction; Pd-PEPPSI-IPr$^{DtBu-An}$ synthesis.

INTRODUCTION

Boscalid has the advantages of low toxicity, high efficiency and no cross--resistance with other fungicides.[1] It has significant therapeutic effects on gray mold, black spot and powdery mildew.[2] It also has the advantages of rapid absorption, low environmental pollution, obvious therapeutic effect, resistance to rain erosion, rapid diffusion, safe crops, and long duration.[3] Boscalid was introduced into the market by BASF® in 2003, the current total production volume of this fungicide is more than 1000 t year^{-1}.[4] Boscalid has very broad application prospects in the world's agricultural sector. It would be of great value to develop a more efficient route suitable for the synthesis of Boscalid. Currently, the main production cost of Boscalid is the palladium catalyst that catalyzes the Suzuki reaction.[5,6] Cost reduction could be achieved by minimizing the amount of noble metal palladium catalyst and not using iodine-containing reagents. In accordance with the industrial synthesis method of Boscalid, the synthesis of 2-(4-chloro-

* Corresponding author. E-mail: cg@gdpu.edu.cn
https://doi.org/10.2298/JSC200330003X

phenyl)nitrobenzene with halogenated nitrobenzene as the raw material is low cost and the method is mature.[3,4,7,8] Although it is suitable for industrial production, a noble metal, such as $Pd(PPh_3)_4$, is necessary as a catalyst in the Suzuki reaction.[5,9] In the reduction path of the traditional method, palladium carbon hydrogenation is used although the cost is higher and the operation is very complicated.[10] In this study, Pd-PEPPSI-IPr$^{DtBu-An}$ (1,2-di(*tert*-butyl)acenaphthyl(DtBu-An)-based Pd-PEPPSI) catalyst was used to increase the catalytic efficiency in the key step of the Suzuki reaction, and a more economic reduction method was used to reduce the manufacturing cost of Boscalid (Scheme 1).

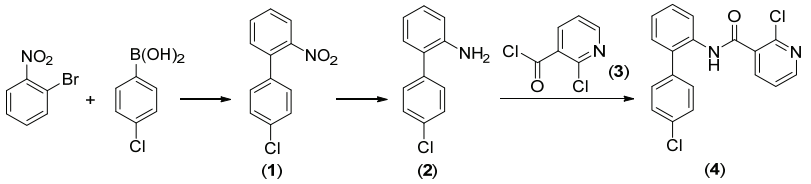

Scheme 1. The synthesis route of Boscalid (**4**).

EXPERIMENTAL

Materials and apparatus

o-Bromonitrobenzene and *p*-chlorophenylboronic acid were purchased from Shanghai DaRui Fine Chemical Co. Ltd. The ^{1}H- and ^{13}C-NMR spectra were measured in $CDCl_3$ using a Bruker Avance III HD 400 MHz spectrometer with tetramethylsilane (TMS) as the internal standard; chemical shifts are expressed in ppm. Melting points were determined on an X-4 apparatus. Thin layer chromatography (TLC) was performed on commercial GF_{254} silica-backed plates. The optimization of the reaction conditions was performed in a WATTECSTM WP-RH-1020 parallel reactor. Gas chromatographic analysis was performed on a Shimadzu GC-2010 plus chromatograph with a flame ionization detector. The mass spectra were recorded on a Thermo Scientific™ ISQ-7000 GC–MS.

Analytical and spectral data are given in Supplementary material to this paper.

Structure of the Pd-PEPPSI-IPr catalysts

Pd-PEPPSI-IPr$^{DtBu-An}$, Pd-PEPPSI-IPr^{An} and Pd-PEPPSI-IPr (Scheme 2) were synthesized according to literature reports.[11-13]

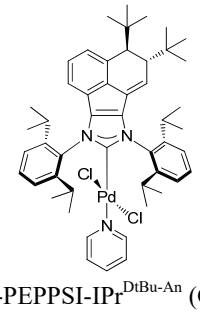

Pd-PEPPSI-IPr$^{DtBu-An}$ (**Cat1**)

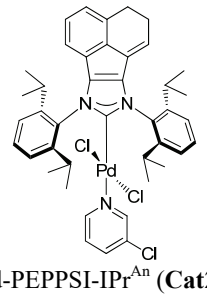

Pd-PEPPSI-IPr^{An} (**Cat2**)

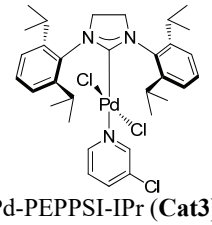

Pd-PEPPSI-IPr (**Cat3**)

Scheme 2. The structure of Suzuki–Miyaura cross-coupling catalysts.

*Synthesis of 2-chloronicotinoyl chloride (**3**)*

2-Chloronicotinic acid (2.36 g, 14.97 mmol) and thionyl chloride (10 mL) were added to a 50 mL single-mouth bottle and refluxed for 4 h. The tail gas was absorbed by an alkali sodium hydroxide solution. The reaction process was detected by TLC. When the consumption of 2-chloronicotinic acid was completed, the excess thionyl chloride was directly distilled off using a rotary evaporator, and then 10 mL anhydrous dichloromethane was added. A large amount of brown crystals precipitated on cooling the solution down to room temperature. The yield of the crystals was 2.64 g (98.5 %), m.p.: 56–57 °C.

*Synthesis of 2-(4-chlorophenyl)nitrobenzene (**1**)*

o-Bromonitrobenzene (20.20 g, 100 mmol), *p*-chlorophenylboronic acid (16.40 g, 105 mmol), anhydrous Na_2CO_3 (15.90 g, 150 mmol), anhydrous AcONa (2.46 g, 30 mmol) and TBAB (1.00 g) were added to C_2H_5OH/H_2O (3:1 volume ratio, 100 mL) as solvent in a 250 mL single port flask with a magnetic stir bar. A catalytic amount (0.01 mol % of **Cat1** (0.9 mg, 0.1 mmol) was added to the mixture, which was then stirred for 24 h at 90 °C. After completion of the reaction, the reaction mixture was cooled to room temperature, and 200 mL of ethyl acetate for extraction was added. The organic layer was separated and dried over anhydrous Na_2SO_4, filtered, and the filtrate was a yellow liquid. The filtrate was concentrated to give the crude product, then recrystallization from ethanol gave 23.17 g of pale yellow crystals, yield 99.2 %.

*Synthesis of the 2-(4-chlorophenyl)aniline (**2**)*

2-(4-Chorophenyl)nitrobenzene (9.35 g, 40 mmol) and ethyl acetate (100 mL) were added to a 250 mL three-necked flask and stirred to dissolve completely. Then zinc powder (15.70 g, 240 mmol) was added to the reaction mixture and the reactants were heated to the required temperature of 70 °C, and a mixed solution of 40 mL of concentrated hydrochloric acid and 20 mL of AcOH was added dropwise over a period of 1 h under a protection of N_2 atmosphere. After the reaction was finished (about 3 h), the reaction mixture was cooled to room temperature, ammonia water was added slowly to adjust pH 10. The mixture was allowed to stir for another 1 h at room temperature, and then 100 mL ethyl acetate was added for extraction. The aqueous phase was further extracted by 50 mL of ethyl acetate, and the organic phases were combined, dried over anhydrous Na_2SO_4 and filtered. Finally, the filtrate was concentrated to give a pale yellow oily liquid. The oily liquid 2-(4-chlorophenyl)aniline (8.00 g) was purified by column chromatography, yield 98%.

*Synthesis of the Boscalid (**4**)*

In a dry 250 mL three-necked flask, 2-(4-chlorophenyl)aniline (2.04 g, 10 mmol), dry dichloromethane (30 mL) and anhydrous K_2CO_3 (2.12 g, 20 mmol) were well stirred and then cooled to 10 °C. 2-Chloronicotinoyl chloride (2 mL) dissolved in dichloromethane (2.64 g) was added dropwise into the mixture. After completion of the dropwise addition, the reaction was continued at room temperature for 1 h. 2-(4-Chlorophenyl)aniline was monitored by TLC. The reaction was terminated when the raw material had been consumed or almost none remained, the solution was washed with 30 mL of water and 20 mL of 10 % hydrochloric acid, and finally with 30 mL of water. The organic phase was separated and dried over anhydrous Na_2SO_4. The filtrate was concentrated to give 3.43 g of crude yellow solid Boscalid in 100 % yield. Recrystallization from absolute ethanol gave 3.25 g of Boscalid in 95.04% yield.

RESULTS AND DISCUSSION

The reaction conditions were investigated and optimized with special regard to the Suzuki reaction, the type of reducing agent on the reduction reaction, the type of acid binding agent on the synthesis of Boscalid and the amount of 2-chloronicotinoyl chloride.

Optimization of the reaction conditions in the Suzuki reaction

First, the catalytic performance of **Cat1** in the Suzuki reaction was explored (Scheme 3). None of the solvents were further purified and the cross-coupling reaction was performed under aerobic conditions.

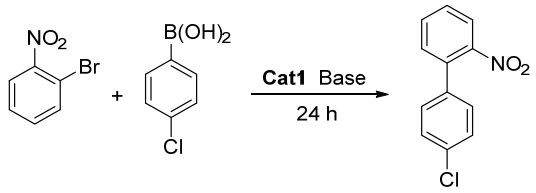

Scheme 3. Scheme for the Suzuki coupling reaction.

The reaction conditions, *i.e*., solvent, acid, base, reaction temperature, reaction time and catalyst dosage, were investigated. As shown in Table I, initially, in the conditions of C_2H_5OH/H_2O (3:1) as solvent and reaction for 24 h at 90 °C were considered. The amount of the catalyst used was 0.01 mol %. In addition, the effects of acid and alkali treatment on the coupling reaction were studied (entry 1-11, Table I). Under alkaline reaction conditions, the yield was higher than under acid reaction conditions. Unexpectedly, when AcONa and Na_2CO_3 were used in combination, the yield of the reaction reached 99.2 % (Table I, entry 3), while with K_2CO_3, Na_2CO_3, AcOK+Na_2CO_3, KOH and AcONa, the reactions were also successfully coupled with the yields of 21 to 88 % (entries 4–11, Table I).

The results indicated that the weak base Na_2CO_3 was the best in the reaction with AcONa. Subsequently, various solvents were screened (Table I, entries 12––18) and it was found that the solvent C_2H_5OH/H_2O (3:1) showed the highest yield. When the ratio of alcohol to water reached 6:1, the yield decreased to 86.57 % (Table I, entry 16).

When using a single solvent, such as EtOH, toluene, 1,4-dioxane, DMA, MeOH, THF, *etc*., the strategy did not yield the highest biaryl product. Moreover, the effect of a lowered temperature was not satisfactory giving a yield of 43.49 % (Table I, entry 19). Next, increasing the reaction temperature to 130 °C was tried, but the yield dropped to 77.75 % (Table I, entry 20). To our delight, under the optimal reaction conditions, lowering the amount of catalyst from 0.05 to 0.01 mol % gave little difference in the yield of 99 % (Table I, entries 3, 22, 23).

Nevertheless, further lowering of the amount of catalyst to 0.008 mol % reduced the yield to 86.11 % (Table I, entry 21). In conclusion, the superior Suzuki reaction conditions were obtained, that is, AcONa+Na_2CO_3 was used as the base, C_2H_5OH/H_2O (3:1) as the solvent, the amount of **Cat1** catalytic was 0.01 mol %, and reaction conditions were 90 °C for 24 h under aerobic conditions.

TABLE I. Optimization of the conditions in the Suzuki reaction; reaction conditions: *o*-bromonitrobenzene (1 mmol) and *p*-chlorophenylboronic acid (1.05 mmol) in TBAB (0.01 g) stirred at required temperature for 24 h

Entry	T / °C	Solvent	Acid	Base	$c_{\mathbf{Cat1}}$ / mol%	Yield, %
1	90	EtOH[a]	PivOH[c]	/	0.01	89.41
2	90	EtOH[a]	AcOH[d]	/	0.01	89.63
3	90	EtOH[a]	/	AcONa[e]+Na_2CO_3	0.01	99.20
4	90	EtOH[a]	/	K_2CO_3	0.01	21.77
5	90	EtOH[a]	/	Na_2CO_3	0.01	77.81
6	90	EtOH[a]	/	AcOK[f]+Na_2CO_3	0.01	62.19
7	90	EtOH[a]	/	AcOK[f]+K_2CO_3	0.01	76.70
8	90	EtOH[a]	/	AcONa[e]+K_2CO_3	0.01	79.87
9	90	EtOH[a]	/	KOH	0.01	28.11
10	90	EtOH[a]	/	AcOK[f]	0.01	76.37
11	90	EtOH[a]	/	AcONa[g]	0.01	88.27
12	90	Toluene	/	AcONa[e]+Na_2CO_3	0.01	23.28
13	90	DMA	/	AcONa[e]+Na_2CO_3	0.01	3.90
14	90	1,4-dioxane	/	AcONa[e]+Na_2CO_3	0.01	56.74
15	90	MeOH	/	AcONa[e]+Na_2CO_3	0.01	72.70
16	90	EtOH[b]	/	AcONa[e]+Na_2CO_3	0.01	86.57
17	90	THF	/	AcONa[e]+Na_2CO_3	0.01	37.45
18	90	EtOH	/	AcONa[e]+Na_2CO_3	0.01	93.54
19	60	EtOH[a]	/	AcONa[e]+Na_2CO_3	0.01	43.49
20	130	EtOH[a]	/	AcONa[e]+Na_2CO_3	0.01	77.75
21	90	EtOH[a]	/	AcONa[e]+Na_2CO_3	0.008	86.11
22	90	EtOH[a]	/	AcONa[e]+Na_2CO_3	0.02	99.30
23	90	EtOH[a]	/	AcONa[e]+Na_2CO_3	0.05	99.32

[a]$V_{(EtOH:H2O)}$ = 3:1 (3 mL); [b]$V_{(EtOH:H2O)}$ = 6:1 (3 mL); [c]60 % mol L^{-1} PivOH (0.1 mL); [d]30 % mol L^{-1} AcOH (4 drops); [e]30 % mol L^{-1} AcONa (0.1 mL); [f]AcOK (1.5 equiv); [g]AcONa (1.5 equiv.)

The catalytic efficiency of the four kinds of catalyst, $Pd(PPh_3)_4$, **Cat1**, **Cat2** and **Cat3** was tested under the optimized reaction conditions for *o*-bromonitrobenzene (1 mmol) and *p*-chlorophenylboronic acid (1.05 mmol) at 90 °C for 24 h. AcONa and Na_2CO_3 were used as the base, C_2H_5OH/H_2O (3:1) as the solvent, the amount of catalyst was 0.01 mol %. The results are presented in Table II.

As can be seen from the Table II, the catalytic performance of **Cat1** (99.20 %) was significantly better than that of **Cat2** (80.36 %), **Cat3** (70.85 %) and $Pd(PPh_3)_4$ (56.34 %). As shown in Fig. 1, the 1,2-di-*tert*-butyl group on **Cat1** provides steric hindrance to the axial position of the acenaphthyl on the back-

bone, which hinders the rotation of the C_{ar}–N bond, thereby protecting the Pd atom from exposure to air and preventing the formation of unreactive NHCs-Pd (O–O) peroxo complexes. It could be speculated that large substituents on the backbone would prolong the life of catalyst and increase the efficiency of the cross-coupling reaction. Therefore, **Cat1** was selected as the Pd source due to its high efficiency.

TABLE II. Synthesis of **1** promoted by Pd-PEPPSI-IPr

Entry	Catalyst	Amount of catalyst, mol%	Yield, %
1	None	0	34.25
2	$Pd(PPh_3)_4$	0.01	56.34
3	**Cat1**	0.01	99.20
4	**Cat2**	0.01	80.36
5	**Cat3**	0.01	70.85

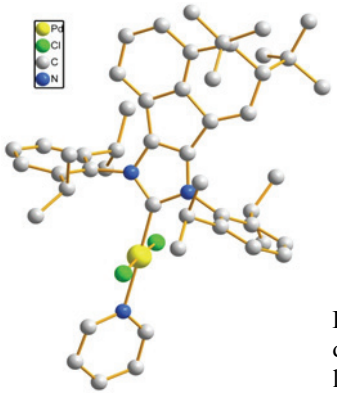

Fig. 1. X-Ray structure of **Cat1**. All H atoms are omitted and displacement ellipsoids are drawn at the 30 % probability level.

The effort of reducing agent on the reduction reaction

Hydrogen and Pd/C could be used as reducing agents for the reduction reaction, however, although the yield is extremely high, the reaction conditions are too harsh. Iron powder could also be used as the reducing agent for this reaction, the reaction conditions are mild, but considering that iron sludge pollutants, such as ferric hydroxide, are generated in the solution, the post-processing is more difficult.

In order to investigate the reduction reaction of 2-(4-chlorophenyl)nitrobenzene, zinc powder or iron powder were used as reducing agents at 70 °C for 4 h. The obtained results are presented in Table III.

As indicated in Table III, as the amount of reducing agent increases, the reduction yield of iron powder and zinc powder can reach up to 98 %. However, the post-processing is cumbersome in the course of the reaction with iron powder. Zinc hydroxide is more convenient to treat after the reduction reaction because it

can be dissolved in ammonia. As a result, zinc powder was chosen as the reducing agent, and at a reactant ratio of 1:6 gives **2** in excellent yield.

TABLE III. Effect of reducing agent on the reduction reaction

Entry	Reducing agent	The mole ratio	Product yield, %
1	Zn	1	20.36
2	Zn	4	83.59
3	Zn	6	98.34
4	Fe	6	97.85

The effort of the type of acid binding agent on the synthesis of Boscalid

Reaction conditions: 2-(4-chlorophenyl)aniline (10 mmol) and 2-chloronicotinoyl chloride(2.64 g) in acid binding agent (20 mmol) stirred at room temperature for 2 h.

In the last step, the coupling of acid **3** and amine **2** should be performed in anhydrous conditions. All reagents and solvents need to be anhydrous to avoid the decomposition of 2-chloronicotinoyl chloride, otherwise the synthesis yield of Boscalid will be affected. The advantage of choosing an inorganic base as the acid binding agent is to improve greatly the yield and purity of Boscalid.

It can be seen from the data in Table IV, the reaction yields are significantly increased by replacing the organic base by an inorganic base. When Na_2CO_3 and K_2CO_3 are used as acid binding agents, the reaction afforded almost the same yields, but Na_2CO_3 is cheaper than K_2CO_3. Therefore, Na_2CO_3 was chosen as the acid binding agent.

TABLE IV. Results of the type of the acid-binding agent on the yield of Boscalid

Entry	Acid binding agent	Yield, %
1	Et_3N	62.13
2	Na_2CO_3	95.04
3	K_2CO_3	94.58

The effort of amount of 2-chloronicotinoyl chloride

The results depicted in Table V show that the highest yield of Boscalid 95.04 % could be acquired when the amount of 2-chloronicotinoyl chloride is increased

TABLE V. Effect of the amount of 2-chloronicotinoyl chloride; reaction conditions: 2-(4-chlorophenyl)aniline (2.04 g) and Na_2CO_3 (20 mmol) stirred at room temperature for 2 h

Entry	Amount of **2**, mmol	Amount of **3**, mmol	Product yield, %
1	10	11(1:1.1)	56.66
2	10	12(1:1.2)	64.32
3	10	13(1:1.3)	74.18
4	10	14(1:1.4)	78.92
5	10	15(1:1.5)	95.04
6	10	16(1:1.6)	90.01

to 15 mmol, that is, with a 2-(4-chlorophenyl)aniline:2-chloronicotinoyl chloride ratio of 1:1.5.

CONCLUSIONS

The general route for the total synthesis of Boscalid has been widely reported in the literature, including three separate steps: Suzuki reaction, reduction reaction and condensation reactions. BASF® using *o*-chloronitrobenzene as the starting material, its reaction requires a large amount of expensive palladium catalysts and harsh conditions, such as high temperature, anhydrous and oxygen-free conditions, *etc.*[1] Glasnov *et al*.[5] reported a continuous and efficient method for synthesis of Boscalid, the Suzuki coupling reaction was catalyzed by $Pd(PPh_3)_4$, the reduction reaction under the catalysis of Pt/C, and condensation reaction under the conditions of microwave heating, the reaction conditions are harsh. Schwarze *et al*.[15] reported environmentally friendly solvents for the synthesis of Boscalid, the Suzuki reaction was catalyzed by water-soluble homogeneous Pd/ /SPhos, together with the easily recyclable heterogeneous $PtIr@TiO_2$, the condensation reaction under the conditions of triethylamine, the catalysts used are not easily available. Audun Drageset *et al*.[16] reported a three step continuous/ /semi-flow process for synthesis of Boscalid, the Suzuki coupling reaction was catalyzed by $Pd(PPh_3)_4$, in the reduction reaction $NaBH_4/CoSO_4{\cdot}7H_2O$ were used as reduction reagents, and condensation reaction under conditions of ethyl acetate as the reaction medium with pyridine as the amine base. It is not easy to separate the product. Balaram S. Takale *et al*.[17] reported a sustainable 1-pot, 3-step synthesis of Boscalid, the Suzuki coupling reaction was catalyzed by nanomicelles in water at a very low loading (0.07 ppm or 0.07 mol %) of $Pd(OAc)_2$. In the reduction reaction, carbonyl iron powder (CIP) was used, the acylation reaction was performed under the conditions of *i*-Pr_2Net. The catalysts of the method are not readily available.

In summary, Boscalid is synthesized in this paper through three-step reaction. In the first step of the Suzuki reaction, the optimum synthesis conditions are 0.01 mol % catalytic amount of Pd-PEPPSI-$IPr^{DtBu\text{-}An}$ catalyzed with *o*-bromonitrobenzene and *p*-chlorophenylboronic acid as raw materials, with C_2H_5OH/H_2O (3:1) as solvent, $AcONa+Na_2CO_3$ as the base, the phase transfer agent TBAB was added during the reaction, under aerobic conditions at 90 °C for 24 h. In the second step of the reduction reaction, the commonly used Pd/C was replaced by zinc powder to reduce costs and adapt to industrial production. In the last step of the coupling of acid **3** and amine **2**, compared with other synthesis usually carried out at high temperature or long time, in this paper sodium carbonate was used in a room temperature reaction for a short time. It could be seen from the experimental results that the reaction yields of each step were high, the reaction conditions were mild, using low-cost raw materials, and the amount of

catalyst used is small. This method for producing the bactericide Boscalid can reduce greatly the cost in industrial production, and is expected to promote industrial production.

SUPPLEMENTARY MATERIAL

Analytical and spectral data of the synthesized compounds are available electronically at the pages of journal website: https://www.shd-pub.org.rs/index.php/JSCS/index, or from the corresponding author on request.

Acknowledgment. The authors gratefully thank the special funds of key disciplines in construction from Guangdong and Zhongshan cooperating for the financial support.

ИЗВОД

ОПТИМИЗАЦИЈА СИНТЕЗЕ БОСКАЛИДА УПОТРЕБОМ КАТАЛИЗАТОРА PD-PEPPSI-IPr$^{DtBu-An}$

JIAN XU, XIAO-BINGLAN, LIN-JIAN XIA, YI YANG и GAO CAO

School of Chemistry and Chemical Engineering, Guangdong Pharmaceutical University, Zhongshan, 528458, Guangdong Province P. R. China

Циљ рада је био да се смањи количина паладијумског катализатора и да се унапреди његова каталитичка ефикасност у реакцији укрштеног Сузуки–Мијура (Suzuki–Miyaura), купловања која представља кључни корак у синтези Боскалида. Три типа Pd-PEPPSI-IPr катализатора су примењена у Сузукијевој реакцији купловања *o*-бромнитробензена и *p*-хлорфенилборонске киселине као полазних једињења. Добијени би-арилни производ је редукован и коришћен у реакцији купловања да би био добијен Боскалид. Под оптималним реакционим условима, резултати показују да каталитички систем има највећу каталитичку ефикасност под аеробним условима, при чему се 2-(4-хлорфенил)нитробензен добија у приносу од 99 %. Додатно, количина Pd-PEPPSI-IPr$^{DtBu-An}$ катализатора је смањена на 0,01 mol %. Реакциони услови су благи, обрада реакционе смеше је једноставна и трошкови производње су смањени, што поступак чини погодним за индустријску производњу.

(Примљено 30. марта 2020, ревидирано 7. јануара, прихваћено 11. јануара 2021)

REFERENCES

1. K. Eicken, K. Goetz, A. Harreus, A. Ammermann, G. Lorenz, A and H. Rang, (BASF AG, Ludwigshafen). European: Patent-EP0545099B (1993)
2. S. Engel, T. Oberding, (BASF AG, Ludwigshafen). Patent-WO2006/092429A1 (2006)
3. K. Eicken, M. Rack, F. Wetterich, E. Ammermann, G. Hardt, M. Rack, P. Schäfer, (BASF AG, Ludwigshafen). Patent-WO97/33846A (1997)
4. C. Torborg, M. Beller, *Adv. Synth. Catal.* **351** (2009) 3027 (https://doi.org/10.1002/adsc.200900587)
5. T. N. Glasnov, C. O. Kappe, *Adv. Synth. Catal.* **17** (2010) 3089 (https://doi.org/10.1002/adsc.201000646)
6. Y. P. Zhu, S. Sergeyev, P. Franck, R. A. Orru, B. U. W. Maes, *Org. Let.* **18** (2016) 4602 (https://doi.org/10.1021/acs.orglett.6b02247)
7. K. S. Manoj, P. M. Siba, G. L. Vinod, B. Ekambaram, *Green Chem.* **19** (2017) 2111 (https://doi.org/10.1039/C6GC03438A)
8. R. Dey, B. Sreedhar, B. C. Ranu, *Tetrahedron* **66** (2010) 2301 (https://doi.org/10.1016/j.tet.2010.02.011)

9. K. Eicken, M. Rack, F. Wetterich, E. Ammermann, G. Lorenz, S. Strathmann, (BASF AG, Ludwigshafen). German: Patent-DE19735224A1 (1999)
10. N. Takashi, R. A. Alexander, H. Shenlin, H. L. Bruce, *Beilstein. J. Org. Chem.* **12** (2016) 1040 (https://doi.org/10.3762/bjoc.12.99)
11. X. B, Lan, F. M. Chen, B. B. Ma, D. S. Shen, F. S. Liu, *Organometallics* **35** (2016) 3852 (https://doi.org/10.1021/acs.organomet.6b00723)
12. T. Tu, W. W. Fang J. Jiang, *Chem. Commun*. **47** (2011) 12358 (https://doi.org/10.1039/C1CC15503B)
13. J. O'B. Christopher, A. B. K. Eric, V. Cory, H. Niloufar, A. C. Gregory, L. Alan, C. H. Alan, G. O. Michael, *Chem. Eur. J.* **12** (2006) 4743 (https://doi.org/10.1002/chem.200690054)
14. F. X. Felpin, E. Fouquet, C. Zakri, *Adv. Synth. Catal.* **351** (2009) 649 (https://doi.org/10.1002/adsc.200800783)
15. I. Volovych, M. Neumann, M. Schwarze, *RSC Adv.* **6** (2016) 58279 (https://doi.org/10.1039/c6ra10484c)
16. A. Drageset, V. Elumalaia, H. R. Bjørsvik, *React. Chem. Eng*. **3** (2018) 550 (https://doi.org/10.1039/C8RE00049B)
17. B. S. Takale, R. R. Thakore, R. Mallarapu, F. Gallou, B. H. Lipshutz, *Org. Pro. Res. Dev.* **24** (2020) 101 (https://doi.org/10.1021/acs.oprd.9b00455).

Journal of the Serbian Chemical Society
JSCS-info@shd.org.rs • www.shd.org.rs/JSCS
J. Serb. Chem. Soc. 86 (3) S66–S69 (2021) *Supplementary material*

SUPPLEMENTARY MATERIAL TO

Synthesis and process optimization of Boscalid by catalyst Pd-PEPPSI-IPr$^{DtBu-An}$

JIAN XU, XIAO-BING LAN, LIN-JIAN XIA, YI YANG and GAO CAO*

School of Chemistry and Chemical Engineering, Guangdong Pharmaceutical University, Zhongshan, 528458, Guangdong Province, P. R. China

J. Serb. Chem. Soc. 86 (3) (2021) 247–256

SUPPORTING DATA AND ^{1}H- AND ^{13}C-NMR SPECTRA

2-(4-chlorophenyl)nitrobenzene ***(1)***

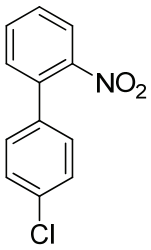

(**1**)

Yield: 99.2 %; m.p.: 67–68 °C; ^{1}H-NMR (400 MHz, $CDCl_3$, δ / ppm): 7.77 (1H, *dd*, J = 8.1 & 1.2 Hz, CH), 7.54 – 7.50 (1H, *m*, CH), 7.42 – 7.38 (1H, *m*, CH), 7.31–7.27 (3H, *m*, CH), 7.16–7.13 (2H, *m*, CH); ^{13}C-NMR (101 MHz, $CDCl_3$, δ / ppm): 149.0, 135.9, 135.1, 134.4, 132.4, 131.8, 129.2, 128.8, 128.5, 124.2; Mass spectrum (ESI$^+$) (*m*/*z*): 233 (M^+).

* Corresponding author. E-mail: cg@gdpu.edu.cn

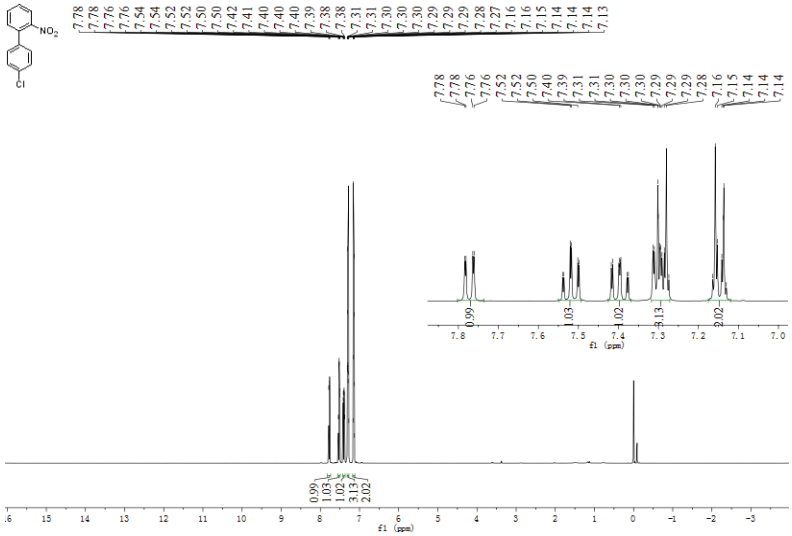

Fig. S-1. ^{1}H-NMR spectra of 2-(4-chlorophenyl)nitrobenzene (400 MHz, $CDCl_3$).

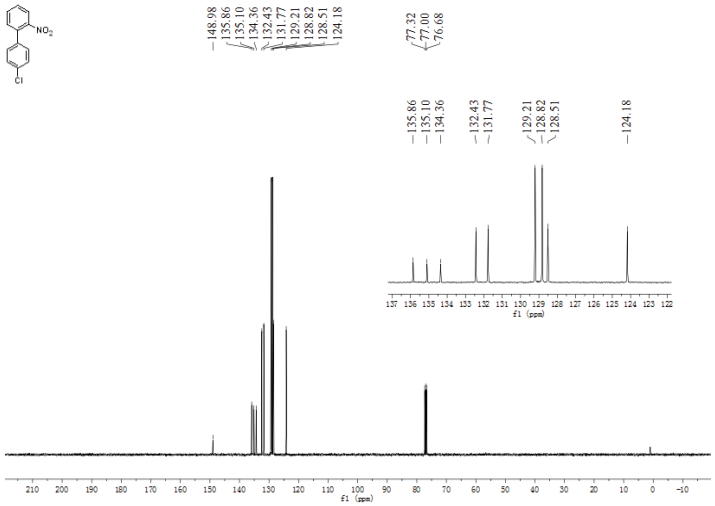

Fig. S-2. ^{13}C-NMR spectra of 2-(4-chlorophenyl)nitrobenzene (101 MHz, $CDCl_3$).

2-(4-Chlorophenyl)aniline ***(2)***

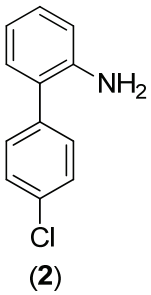

(**2**)

Yield: 98 %; ^{1}H-NMR (400 MHz, $CDCl_3$, δ / ppm): 7.31–7.27 (4H, *m*, CH), 7.08 – 7.04 (1H, *m*, CH), 6.99 (1H, *dd*, J = 7.6 & 1.6 Hz, CH), 6.75 – 6.71 (1H, *m*, CH), 6.67 – 6.64 (1H, *m*, CH), 3.65 (2H, *s*, NH_2); ^{13}C-NMR (101 MHz, $CDCl_3$, δ / ppm): 143.2, 137.8, 133.0, 130.4, 130.3, 128.9, 126.3, 118.8, 115.7; Mass spectrum (ESI$^+$) (*m*/*z*): 204 (M^+).

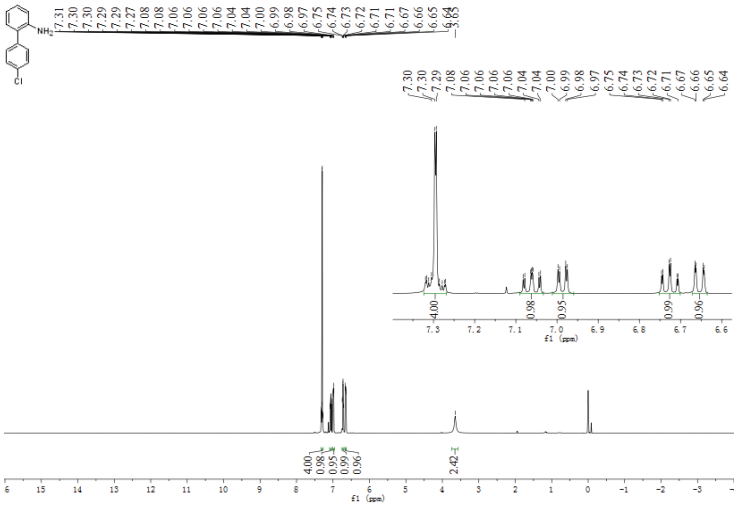

Fig. S-3. ^{1}H-NMR spectra of 2-(4-chlorophenyl)aniline (400 MHz, $CDCl_3$).

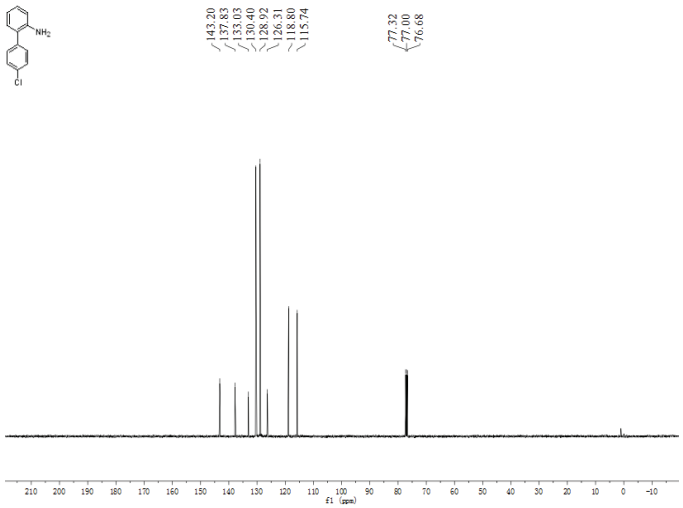

Fig. S-4. ^{13}C-NMR spectra of 2-(4-chlorophenyl)aniline (101 MHz, $CDCl_3$).

*Boscalid (**4**)*

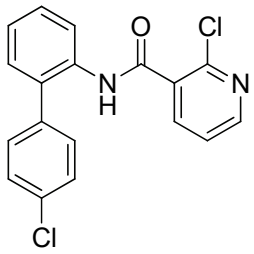

(**4**)

Yield: 95.04 %; m.p.: 145.8 – 146.8 °C (lit. value: 141.8 – 142.8 °C[14]); ^{1}H-NMR (400 MHz, $CDCl_3$, δ / ppm): 8.40–8.35 (2H, *m*, CH), 8.20 (*s*, 1H, NH), 8.07 (*dd,* 1H, *J* = 7.6, 2.0 Hz, CH), 7.47–7.39 (*m*, 3H, CH), 7.34 – 7.30 (*m*, 3H, CH), 7.27–7.25 (*m*, 2H, CH); ^{13}C-NMR (101 MHz, $CDCl_3$, δ / ppm): 162.5, 151.1, 146.6, 139.9, 136.2, 134.3, 134.2, 132.3, 131.0, 130.7, 130.2, 129.2, 128.8, 125.3, 122.8, 122.2; (M^+) mass spectrum (ESI^+) *m*/*z*: 343.

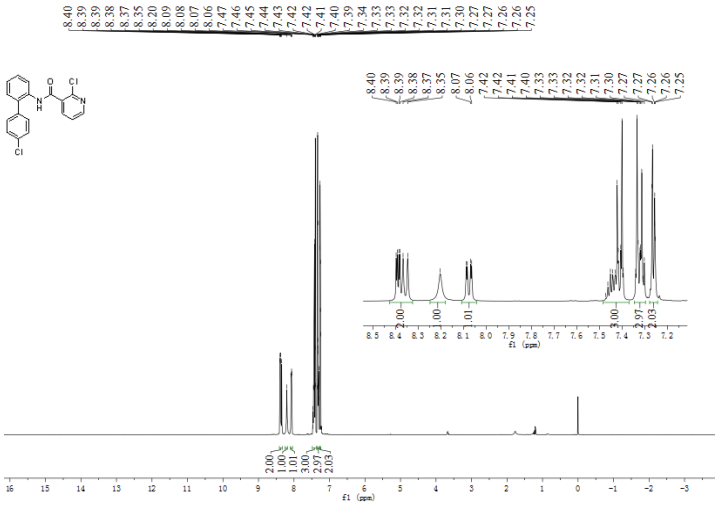

Fig. S-5. ^{1}H-NMR spectra of Boscalid (400 MHz, $CDCl_3$).

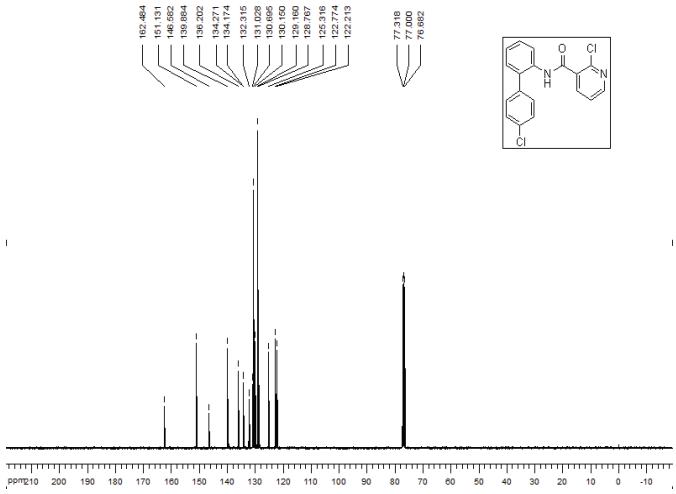

Fig. S-6. ^{13}C-NMR spectra of Boscalid (101 MHz, $CDCl_3$).

Journal of the Serbian Chemical Society
JSCS-info@shd.org.rs • www.shd.org.rs/JSCS
J. Serb. Chem. Soc. *86* (3) 257–267 (2021)
JSCS–5419
Original scientific paper

Phytochemical analysis of volatiles and biological activities of *Chaerophyllum bulbosum* L. essential oils

JELENA G. STAMENKOVIĆ*, ALEKSANDRA S. ĐORĐEVIĆ, GORDANA S. STOJANOVIĆ, VIOLETA D. MITIĆ and GORAN M. PETROVIĆ

University of Niš, Faculty of Science and Mathematics, Department of Chemistry, Višegradska 33, 18000 Niš, Serbia

(Received 20 October, revised and accepted 5 December 2020)

Abstract: The present study reports for the first time the chemical composition of the headspace volatiles (HS) and essential oils obtained from fresh *Chaerophyllum bulbosum* roots and aerial parts, as well as biological activities of the essential oils. Generally, monoterpene hydrocarbons were found to be the main class of all investigated samples, with (*E*)-*β*-ocimene being the most abundant component. The results of antibacterial assay showed that both investigated samples exhibit bactericidal activity against two tested Gram-positive bacteria (*Staphylococcus aureus* and *Bacillus subtilis subs. spizizenii*) while they were inactive against tested Gram-negative bacteria (*Escherichia coli* and *Salmonella abony)*. Regarding the antioxidant activity, it was found that the essential oils showed low antioxidant capacities in comparison with standard antioxidant compounds (such as butylated hydroxytoluene). The obtained results were expected given the fact that the main components in both samples were monoterpene hydrocarbons.

Keywords: chemical composition; GC/MS; antibacterial assay; antioxidant activity.

INTRODUCTION

Apiales, carrot order of flowering plants, consist of about 5,489 species. There are seven families in the order, of which the largest are *Apiaceae* (carrot or parsley family), *Araliaceae* (ginseng family) and *Pittosporaceae*. *Apiaceae*, also called *Umbelliferae* (the parsley family) comprising between 300 and 400 genera of plants distributed worldwide, principally in the north temperate regions of the world. Many species of the *Apiaceae* are poisonous, some are widely used vegetables, others are used as herbs and spices, while some species are grown for their ornamental value. The genus *Chaerophyllum* belongs to the *Apiaceae*, and includes about 40 species widespread in Europe, Asia and North America, six of

* Corresponding author. E-mail: jelena.stamenkovic@pmf.edu.rs
https://doi.org/10.2298/JSC201020080S

which are described in the flora of Serbia.[1] *Chaerophyllum bulbosum* L. which is known by several common names, including turnip-rooted chervil, tuberous--rooted chervil, bulbous chervil and parsnip chervil, is one of the vegetables that is more commonly grown in the past then it is today. This is a tall annual herb with fringelike divided leaves and large umbels of white flowers. The plant is cultivated on a small scale in parts of Europe for the edible root, which is similar to carrot. Because of its biochemical composition[2,3] and specific chestnut-like flavor,[4] tuberous-rooted chervil is considered as a "gourmet" vegetable. The root is characterized by the accumulation of starch and sucrose. It is interesting that at harvest time the root is not edible and traditionally, storage at 10 °C during four to five months is necessary to reach the stage at which it is edible. Storage enables changes in carbohydrate reserves responsible for taste. *C. bulbosum* is also reported to be a traditional medicinal plant used by locals in Eastern Turkey (the rhizomes were consumed raw to increase appetite, to treat diabetes and high cholesterol levels).[5]

Literature survey showed that there are several phytochemical investigations that have been published on *C. bulbosum*[2–9] with only a few reports regarding the essential oil isolated from air dried aerial parts of the plant.[10–12] It is interesting that even though the root is the only part of the plant that has an application in human diet, there are no data considering the chemical composition of the root essential oil, so this is the first report about the chemical composition, antimicrobial and antioxidant activity of the essential oil obtained from *C. bulbosum* roots as well as fresh aerial parts of the plant.

EXPERIMENTAL

Plant material

Root maturity is reached when leaves turn yellow in June. The plant material at flowering stage was collected on Vlasina plateau, Serbia, at an altitude of 1250 m, in July 2018. Around 75 plant individuals were collected at the same location in the diameter of approximately 150 m to give a composite sample. The plant material was identified by Bojan Zlatković and the voucher specimen was deposited in the Herbarium Moesiacum Niš (HMN), Department of Biology and Ecology, Faculty of Science and Mathematics, University of Niš, under the acquisition number 7232. The fresh plant material was divided into parts (aerial parts and root) and they were analyzed separately.

Headspace sample preparation

The fresh plant material was analyzed immediately after harvest. Five hundred mg of milled plant material was put into 20 mL HS vial and then soaked with 2 mL of distilled water. The sample was heated at 80 °C for 20 min with the following mixing program: shaking for 5 s, pause for 2 s. 500 μL of vapor generated from the samples was drawn out from the vial using a gas-tight syringe (90 °C) and injected directly in the chromatographic column *via* a transfer line (75 °C).

Hydrodistillation

Fresh samples (473 g of aerial parts and 636 g of roots) were subjected to hydrodistillation for 2.5 h using a Clevenger-type apparatus and yielded 0.15 and 0.02 mass% (based on the weight of fresh plant material) of essential oil, respectively. The obtained essential oils were decanted; extracted with hexane and treated with anhydrous magnesium sulfate to remove any residue of moisture, then filtered and solvent was evaporated in a stream of nitrogen. Samples were analyzed immediately after isolation.

Identification of volatile compounds

The samples were analyzed by a 7890/7000B GC/MS/MS triple quadrupole system in MS1 scan mode (Agilent Technologies, Santa Clara, CA, USA) equipped with a Combi PAL sampler and Headspace for G6501B/G6509B. A fused silica capillary column HP-5MS (5 % phenylmethylsiloxane, 30 m×0.25 mm, film thickness 0.25 μm; Agilent Technologies, Santa Clara, CA, USA) was used. The injector and interface operated at 250 and 300 °C, respectively. Temperature program: from 50 to 290 °C at a heating rate of 4 °C/min. The carrier gas was helium (99.9999 %) with a flow of 1.0 mL/min. The samples (500 μL) were injected for HS and of essential oil solutions (1 μL), prepared by mixing 20 μL of essential oil with 980 μL of *n*-hexane, were injected (split ratio 40:1) for liquid analyses. Post run: back flash for 1.89 min, at 280 °C, with helium pressure of 50 psi. MS conditions were as follows: ionization voltage of 70 eV, acquisition mass range 40–440, scan time 0.32 s. GC analysis equipped with FID detector was carried out under the same experimental conditions using the same column as described for the GC/MS. The relative percentage composition of the samples (analysis was performed in triplicate) was computed from the GC peak areas without any corrections. The median and standard deviation was performed as statistical analysis. Essential oil constituents were identified by comparison of their linear retention indices (relative to C_8-C_{32} *n*-alkanes on the HP-5MS column) with literature values and their MS with those from Adams,[13] Wiley 6, NIST11, Agilent Mass Hunter Workstation B.06.00 software and a homemade MS library with the spectra corresponding to pure substances and components of known essential oils by application of the automated mass spectral deconvolution and identification system (AMDIS software, ver. 2.1, DTRA/NIST, 2011).

Antibacterial activity

Antibacterial activity was evaluated against two Gram-positive and two Gram-negative bacteria by using the disk diffusion assay.[14] The Gram-positive bacteria used were: *Bacillus subtilis subsp. spizizenii* ATCC 6633 and *Staphylococcus aureus* ATCC 6538. The Gram-negative bacteria utilized in the assay were: *Escherichia coli* ATCC 8739 and *Salmonella abony* ATCC 6017. The inocula of the bacterial strains were prepared from overnight broth cultures and suspensions were adjusted to 0.5 McFarland standard turbidity. The suspensions of the tested microorganisms (0.1 mL) were spread on the solid Mueller-Hinton agar plates. All agar plates were prepared in 90 mm Petri dishes giving the final depth of 4 mm. Sterile filter paper disks (“Antibiotica Test Blättchen”, Macherey-Nagel, Düren, Germany, 9 mm in diameter) were impregnated with 30 μL of the essential oil (essential oils were dissolved in hexane at concentration of 100 mg/mL) and placed on the inoculated plates. These plates, after standing at 4 °C for 2 h, were incubated at 37 °C for 24 h. Chloramphenicol (30 μg) and streptomycin (10 μg) were used as positive reference standards to determine the sensitivity of a strain of each tested microbial species while disks containing hexane were used as the negative control. The diameters of the inhibition zones were measured in millimeters using a “Fisher-Lilly Antibiotic Zone Reader” (Fisher Scientific Co., USA). Each test was performed in triplicate.

Antioxidant activity

ABTS radical "scavenging" activity was performed according to the method of Re *et al.*[15] The ABTS radical was produced by the reaction of ABTS stock solution with potassium persulfate and the mixture was allowed to stand in the dark at room temperature for 12–16 h before use. The solution was then diluted by mixing 7 mL $ABTS^{\bullet+}$ solution with 120 mL methanol to obtain an absorbance of 0.7±0.02 units at 734 nm. An aliquot of each sample (0.1 mL), concentration 100 mg/mL, was mixed with 1.8 mL of diluted ABTS solution in the concentration of 7 mmol/L and diluted with methanol to a total volume of 4 mL. After 6 min at room temperature, the reduction in absorbance was measured at 734 nm. Results are expressed as mg of Trolox equivalents (TE) per mg of essential oil (mg TE per mg EO).

The quantitative assays of the essential oils (EO) on 2,2-diphenyl-1-picrylhydrazyl (DPPH) radicals were performed according to the method of Dimitrijević *et al.*[16] 1.5 mL of 100 mmol/L 2, 2-diphenyl-1-picrylhydrazylradical methanol solution, 0.1 mL of 100 mg/mL EO and 4 mL of methanol were shaken, left to react for 60 min in darkness, and the absorbance was measured at 515 nm, and expressed in μg of Trolox equivalents (TE) per mg of essential oil (μg TE/mg EO).

The ferric reducing antioxidant power (FRAP) assay was performed using method of Benzie and Strain.[17] 1 mL of FRAP reagent was mixed with 0.1 mL of EO, concentration 100 mg/mL, and diluted with water to a volume of 4 mL. After 5 min of incubation at 37 °C, the absorbance was recorded at 595 nm. The ferric ion reducing antioxidant power value was expressed as μg of Fe(II) equivalents per mg of essential oil (μg Fe/mg EO).

The reducing power (TRP) of essential oils was determined by the method of Oyaizu.[18] Reaction mixtures were prepared by mixing of EO (0.01 mL), 1 mL of 1 % $K_3[Fe(CN)_6]$, phosphate buffer (pH 6.6) and water. The mixtures were incubated at 50 °C for 30 min and after incubation 10 % trichloroacetic acid (1 mL) and $FeCl_3$ (0.6 mL) were added. The absorbance was measured at 700 nm against a blank sample and results were expressed as mg ascorbic acid equivalents per mg of essential oil (mg AAE/mg EO).

The cupric ion reducing antioxidant capacity (CUPRAC) assay was performed using the method of Apak *et al.*[19] This assay involved the addition of EO (0.1 mL), phosphate buffer (pH 7.0, 1 mL), neocuproine (7.5×10^{-3} mol/L), copper(II)chloride (0.01 mol/L) and dilution with water to a total volume of 4.1 mL. The mixture was left for 30 min at 25 °C and the absorbance was measured at 450 nm. Trolox was used as a standard and results were expressed as μg Trolox equivalents per mg of essential oil (μg TE/mg EO).

Trolox (TE) was used as a standard for ABTS, DPPH and CUPRAC assays, ascorbic acid (AAE) for TRP and fero sulfat for FRAP assay.

RESULTS AND DISCUSSION

Chemical composition

Chemical compositions of the hydrodistillated essential oils (EO) as well as the volatiles obtained by static headspace method (HS) of *C. bulbosum* were analyzed by GC and GC/MS, and the results are presented in Table I.

In general, monoterpene hydrocarbons were found to be the main class of all investigated samples, with (*E*)-*β*-ocimene being the most abundant component.

Headspace volatiles of the aerial parts of the plant consisted 100 % of monoterpene hydrocarbons with (*E*)-*β*-ocimene accounting 96.1 % of the sample. In

the root sample, for which twenty compounds were identified (representing 99.9 % of the total), the main class was also represented by monoterpene hydrocarbons (98.7 %) with (*E*)-*β*-ocimene (46.1 %), followed by limonene (14.9 %), *γ*-terpinene (12.5 %), *p*-cymene (11.1 %) and *α*-pinene (10.9 %) as the main components. Sesquiterpene hydrocarbons were also present but with the contribution of only 0.4 %.

TABLE I. Chemical compositions (average of triplicates±*SD*) of the *Chaerophyllum bulbosum* essential oils and headspace volatiles; compounds listed in order of elution on a HP--5MS column. *RI*: experimentally determined retention indices on the mentioned column by co-injection of a homologous series of *n*-alkanes C_8–C_{32}; *RA*: Adams retention indices; *: identified by NIST Chemistry WebBook Retention indices; tr: trace (<0.05 %); –: not detected. Headspace samples: HS1 – aerial parts, HS2 – root; essential oil samples: EO1 – aerial parts, EO2 – root

RI	*RA*	Compound	Content, %			
			HS1	HS2	EO1	EO2
928	924	*α*-Thujene	–	0.1±0.01	–	–
935	932	*α*-Pinene	0.3±0.02	10.9±1.05	0.4±0.02	2.0±0.2
950	946	Camphene	–	0.1±0.04	–	–
975	969	Sabinene	–	0.7±0.05	tr	0.9±0.05
978	974	*β*-Pinene	0.4±0.05	0.2±0.01	0.3±0.02	0.2±0.01
991	988	Myrcene	0.1±0.01	1.0±0.35	0.2±0.02	0.9±0.07
1004	998	*n*-Octanal	–	0.2±0.05	–	0.5±0.03
1006	1002	*α*-Phellandrene	–	tr	–	–
1018	1014	*α*-Terpinene	–	0.1±0.02	–	0.1±0.02
1026	1020	*p*-Cymene	0.6±0.05	11.1±0.55	0.8±0.02	3.3±0.54
1030	1024	Limonene	0.3±0.02	14.9±1.13	0.3±0.02	15.2±1.25
1039	1032	(*Z*)-*β*-Ocimene	0.4±0.05	0.9±0.32	1.6±0.24	1.0±0.03
1051	1044	(*E*)-*β*-Ocimene	96.1±2.17	46.1±1.15	91.5±1.18	38.5±0.95
1061	1054	*γ*-Terpinene	1.9±0.35	12.5±0.95	4.1±0.08	11.7±0.55
1091	1089	*p*-Cymenene	–	0.7±0.11	0.1±0.01	0.7±0.05
1121	1118	*cis*-*p*-Menth-2-en-1-ol	–	–	–	0.6±0.02
1140	1137	(*E*)-Epoxy-ocimene	–	–	–	1.6±0.16
1158	1157	(*E*)-2-Nonen-1-al	–	–	–	0.4±0.02
1178	1174	Terpinen-4-ol	–	–	–	0.3±0.01
1186	1184	Dill ether	–	–	–	0.2±0.01
1187	1184	Cryptone	–	–	–	tr
1191	1186	*α*-Terpineol	–	–	–	tr
1196	1195	*cis*-Piperitol	–	–	–	0.1±0.02
1198	1195	Methyl chavicol	–	–	–	0.2±0.02
1208	1207	*trans*-Piperitol	–	–	–	0.5±0.01
1220	1215	*trans*-Carveol	–	–	–	tr
1229	1232	Thymol, methyl ether	–	–	–	0.2±0.02
1234	1232*	Isothymol, methyl ether	–	–	–	0.7±0.05
1256	1249	Piperitone	–	–	–	tr
1260	1260	(*E*)-2-Decenal	–	–	–	0.2±0.04
1287	1287	Bornyl acetate	–	tr	–	0.4±0.01

TABLE I. Continued

RI	*RA*	Compound	Content, %			
			HS1	HS2	EO1	EO2
1293	1289	Thymol	–	–	–	tr
1315	1315	(*E*,*E*)-2,4-Decadienal	–	–	–	tr
1358	1356	Eugenol	–	–	–	tr
1379	1374	*α*-Copaene	–	–	–	tr
1382	1380	Daucene	–	–	–	0.2±0.02
1402	1396	*α*-Chamipinene	–	–	–	0.2±0.02
1415	1407	*α*-Barbatene	–	–	–	tr
1422	1413	*β*-Funebrene	–	0.1±0.04	–	2.3±0.34
1426	1419	*β*-Cedrene	–	–	–	0.5±0.05
1436	1429	*cis*-Thujopsene	–	–	–	0.1±0.02
1441	1436	Isobazzanene	–	–	–	tr
1444	1440	(*Z*)-*β*-Farnesene	–	–	–	tr
1452	1450	*β*-Barbatene	–	0.1±0.01	–	1.2±0.08
1456	1454	(*E*)-*β*-Farnesene	–	–	–	0.5±0.01
1461	1456*	Amorpha-4,11-diene	–	0.1±0.01	–	1.5±0.05
1483	1476	*β*-Chamigrene	–	–	–	0.5±0.03
1486	1484	Germacrene D	–	–	0.1±0.01	–
1496	1493	*α*-Zingiberene	–	–	–	tr
1499	1498	*β*-Alaskene	–	–	–	0.4±0.05
1501	1500	Bicyclogermacrene	–	–	0.2±0.01	–
1502	1501	Epizonarene	–	–	–	0.1±0.01
1512	1505	*β*-Bisabolene	–	0.1±0.02	–	1.5±0.12
1516	1512	*α*-Alaskene	–	–	–	0.5±0.02
1524	1517	Myristicin	–	–	–	5.1±0.64
1534	1530	Dauca-4(11),8-diene	–	–	–	0.3±0.02
1537	1532	*γ*-Cuprenene	–	–	–	0.2±0.01
1556	1555	Elemicin	–	–	–	0.2±0.01
1583	1577	Spathulenol	–	–	–	tr
1596	1589	*allo*-Cedrol	–	–	–	0.2±0.03
1608	1600	Cedrol	–	–	–	0.6±0.05
2034	2035	(*Z*)-Falcarinol	–	–	–	1.9±0.12
Number of constituents			8	20	12	57
Total identified			100	99.9	99.6	98.4
Monoterpenes hydrocarbon (MH)			100	99.3	99.3	74.5
Monoterpenes oxygenated (MO)			–	–	–	4.8
Sesquiterpenes hydrocarbon (SH)			–	0.4	0.3	9.8
Sesquiterpenes oxygenated (SO)			–	–	–	0.8
Others (O)			–	0.2	–	3.2
Phenylpropanoids (PP)			–	–	–	5.3

Similar situation was noticed regarding essential oil samples. In the essential oil obtained from the aerial parts, monoterpene hydrocarbons make up over 99 % of the sample with (*E*)-*β*-ocimene as the main component. Although, both of the samples were dominated by (*E*)-*β*-ocimene, two main features distinguished

essential oil obtained from the root; the number of identified constituents (fifty--seven *vs.* twelve) and the presence of the oxygenated fraction which was not even detected in aerial parts. In the root sample (*E*)-*β*-ocimene was present with the contribution of 38.5 %, followed by limonene (15.2 %) and *γ*-terpinene (11.7 %), unlike the aerial parts were (*E*)-*β*-ocimene make up over 90 % of the total (91.5 % to be exact). These differences could be attributed to the fact that the essential oils which have been isolated from root and aerial parts of the plant have significantly different chemical composition.

If we compare our results with the previously published results it is obvious that the composition of the essential oils of the aerial parts of the *C. bulbosum* collected from different geographic regions was found to be quite different. The analysis of the volatile fraction of *Chaerophyllum bulbosum* L. *ssp. bulbosum* (Apiaceae) growing wild in Greece demonstrated the presence of apiol (37 %), 3,7,11-trimethyldodeca-1,6,10-trien-3-ol (8.5 %), linalool (7.7 %), myristicine (6.9 %) and eugenol (5.8 %).[10] The essential oil of *C. bulbosum* from Iran had (*E*)-β-farnesene (22.3 %), (*Z*)-*β*-ocimene (18.8%), and myristicin (17.1%) as the major components in this oil. The other notable compounds in the oil of the plant were caryophyllene oxide (6.6 %), *allo*-ocimene (5.1%), and (*E*)-*β*-ocimene (4.0 %).[12] In the oil from the epigeal part of *C. bulbosum* grown in Azerbaijan,[11] linalool (18.3 %) and *α*-pinene (7.8 %) were predominant. Since this is the first report considering the chemical composition of the essential oil obtained from the root, comparison cannot be done.

The differences in chemical composition can be explained by many factors including genetic variation, plant ecotype or variety, plant nutrition, application of fertilizers, geographic location of the plants, climate conditions, seasonal variations, stress during growth or maturity and the post-harvest drying and storage.[20] All these factors influence one another so it is difficult to say with certainty which of these factors have the greatest effect on the chemical composition of essential oils.

Antibacterial activity

The results of antibacterial assay showed that both investigated samples exhibit inhibitory activities against two tested Gram-positive bacteria (Table II).

Root essential oil showed bactericidal activity against *Staphylococcus aureus* and *Bacillus subtilis subs. spizizenii* (diameter of zone of inhibition 10 and 16 mm, respectively), while diameter of zone of inhibition for aerial parts oil was 12 and 14 mm, respectively. Chloramphenicol (30 μg) and streptomycin (10 μg) were used as positive reference standards, and diameter of zone of inhibition for chloramphenicol against *Staphylococcus aureus* and *Bacillus subtilis subs. spizizenii* was 24 and 28 mm, respectively, while the diameter of zone of inhibition for streptomycin was 14 and 24 mm, respectively. Previous studies of the essen-

tial oil obtained from epigeal parts of *C. bulbosum* from Iran[12] also showed significant activity against Gram-positive bacteria, (*Staphylococcus aureus*, *Bacillus anthracis* and *Streptococcus pyogenes*), moderate inhibitory activity against *Escherichia coli*, and inactivity against *Klebsiella pneumonia* and *Pseudomonas aeruginosa*.

TABLE II. Antibacterial activity of *Chaerophyllum bulbosum* essential oils and positive controls; values are the mean inhibition zone of three replicates including disc; Bc: bactericidal activity; Bs: bacteriostatic activity; n.a.: not active. Active amounts: *C. bulbosum* root and aerial parts essential oils (30 µg/disc), chloramphenicol (30 µg/disc), streptomycin (10 µg/disc). Hexane used to dissolve the samples, was employed as negative control and didn't have any activity. Essential oil samples: EO1 – aerial parts, EO2 – root

Sample	Zone of inhibition, mm							
	B. spizizenii		*S. aureus*		*S. abony*		*E. coli*	
	Bc	Bs	Bc	Bs	Bc	Bs	Bc	Bs
EO1	14	n.a.	12	n.a.	n.a.	n.a.	n.a.	n.a.
EO2	16	n.a.	10	n.a.	n.a.	n.a.	n.a.	n.a.
Chloramphenicol	28	n.a.	24	n.a.	25	n.a.	28	n.a.
Streptomycin	24	n.a.	14	n.a.	17	n.a.	16	n.a.

These differences in antibacterial activity can be explained by the fact that our and their sample has significantly different chemical composition. Obtained results showed that the antibacterial activities of the same plant species differed significantly depending on taxonomic characteristics as well as biological characteristics of the tested bacteria.

Antioxidant activity

This is the first report on the evaluation of the antioxidant activity of *C. bulbosum* essential oils. The antioxidant activity was evaluated by five different methods: DPPH, ABTS, total reducing power (TRP), ferric reducing antioxidant power (FRAP), and cupric reducing antioxidant capacity (CUPRAC). The results are given in Table III.

TABLE III. Antioxidant activity of *Chaerophyllum bulbosum* essential oils; values are means ± *SD* (*n* = 3). Essential oil samples: EO1 – aerial parts, EO2 – root

Sample	ABTS µg TE / mg EO	DPPH µg TE / mg EO	TRP µg AAE / mg EO	FRAP µg Fe / mg EO	CUPRAC µg TE / mg EO
EO1	0.3±0.04	1.34±0.04	0.163±0.003	0.162±0.006	6.1±0.2
EO2	0.85±0.02	1.30±0.02	0.379±0.009	0.512±0.008	7.79±0.08

Since there are no any data regarding antioxidant activity of *C. bulbosum* essential oils, the obtained results were compared with activity of the commercial standard antioxidants and it was found that both essential oils showed low antioxidant capacities in comparison with standard antioxidant compounds.

Free radical scavenging activity of samples was investigated by DPPH and ABTS assays. According to the results obtained, DPPH "scavenging" radical capacity of samples were similar (1.30±0.02 and 1.34±0.04 μg TE/mg oil for the root and aerial parts, respectively), while the antioxidant capacity estimated in terms of the $ABTS^{\bullet+}$ radical scavenging activity, was 0.85±0.02 and 0.30±0.04 μg TE / mg oil, respectively. Reducing power of the samples was estimated by FRAP and CUPRAC assays. The results of FRAP assay, expressed as μg Fe / mg of essential oils, indicates that the root essential oil was almost 4 times more active than aerial parts essential oil (0.512±0.008 and 0.162±0.006 μg Fe / mg EO). The higher CUPRAC capacity was observed for root sample (7.97±0.08 mg TE / / mg EO) then for aerial parts (6.1±0.2 mg TE / mg EO). The total reducing power of the oil was found to be 0.379±0.009 μg AAE / mg oil for the root sample and 0.163±0.003 μg AAE/mg oil for the aerial parts.

Given the fact that the main components in both samples were monoterpene hydrocarbons, it is not unexpected that the oils exhibit no significant antioxidant activity.[21]

CONCLUSION

This is the first report about the chemical composition, antimicrobial and antioxidant activity of the essential oils obtained from *C. bulbosum* roots as well as fresh aerial parts of the plant. In general, monoterpene hydrocarbons were found to be the main class of all investigated samples, with (*E*)-*β*-ocimene being the most abundant component. As can be seen from the results, (*E*)-*β*-ocimene make up over 90 % of the essential oil of *C. bulbosum* aerial parts which points to the fact that it can be used in perfumery industries. Comparison of ours with previously published results considering the antimicrobial activities led to the conclusion that the antibacterial activities of the same plant species depend on taxonomic characteristics as well as biological characteristics of the tested bacteria. Since there are no previously published investigations of the antioxidant activity, comparison cannot be done. On the other hand, low antioxidant activity of the examined samples was expected, since the major compounds in both samples were monoterpene hydrocarbons.

Acknowledgements. Financial support of the Ministry of Education, Science and Technological Development of Serbia (Grant No. 451-03-68/2020-14/200124) is gratefully acknowledged.

ИЗВОД

ФИТОХЕМИЈСКА АНАЛИЗА ИСПАРЉИВИХ КОМПОНЕНАТА И БИОЛОШКА АКТИВНОСТ ЕТАРСКИХ УЉА БИЉНЕ ВРСТЕ *Chaerophyllum bulbosum*

ЈЕЛЕНА Г. СТАМЕНКОВИЋ, АЛЕКСАНДРА С. ЂОРЂЕВИЋ, ГОРДАНА С. СТОЈАНОВИЋ, ВИОЛЕТА Д. МИТИЋ и ГОРАН М. ПЕТРОВИЋ

Универзитет у Нишу, Природно–математички факултет, Департман за хемију , Вишеградска 33, 18000 Ниш

У овом раду је, по први пут, испитиван хемијски састав лако испарљивих састојака и етарских уља изолованих из свежег корена и надземних делова биљне врсте *Chaerophyllum bulbosum* L. као и биолошка активност етарских уља. Испитивања су показала да су угљоводонични монотерпени доминантна класа једињења у свим испитваним узорцима, при чему је као главна компонента идентификован (*E*)-*β*-оцимен. Резултати антибактеријског теста показали су да оба испитивана узорка показују бактерицидно дејство на две тестиране Грам-позитивне бактерије (*Staphylococcus aureus* и *Bacillus subtilis subs. spizizenii*), док су Грам-негативне бактерије (*Escherichia coli* и *Salmonella abony*) биле резистентне. Што се тиче антиоксидативне активности, утврђено је да су етарска уља показала слабу антиоксидативну активност у поређењу са стандардним антиоксидативним једињењима. Добијени резултати су очекивани с обзиром на чињеницу да су главне компоненте у оба узорка угљоводонични монотерпени.

(Примљено 20. октобра, ревидирано и прихваћено 5. децембра 2020)

REFERENCES

1. V. Nikolić, in: *Flora SR Srbije*, Vol. 5, M. Josifović, Ed., Srpska Akademija Nauka i Umetnosti, Belgrade, 1973, p. 327 (in Serbian)
2. J. Billot, C. Hartmann, N. Imbault, C. Joseph, J. Y. Péron, *Rev. Gen. Froid.* **4** (1989) 344
3. O. J. Ayala Garay, M. Briard, J. Granger, J. Y. Péron, *Umbelliferae Improv. Newslett.* **9** (1999) 20 (https://www.researchgate.net/profile/Oscar_J_Garay/publication/330401135_-Phenologic_development_and_carbon_reserves_within_tuberous_rooted_chervil/links/5c3e4211a6fdccd6b5b0447a/Phenologic-development-and-carbon-reserves-within-tuberous-rooted-chervil.pdf)
4. J. Y. Péron, *Acta Hort.* **242** (1989) 123 (ISBN 9789066054035)
5. R. Polat, U. Cakilcioglu, F. Satıl, *J. Ethnopharmacol.* **148** (2013) 951 (https://doi.org/10.1016/j.jep.2013.05.050)
6. S. Ivanov, M. Zlatanov, E. Ivanova, K. Aitzetmüller, *Eur. J. Lipid Sci. Technol.* **101** (1999) 307 (https://doi.org/10.1002/(SICI)1521-4133(199908)101:8<307::AID-LIPI307>3.0.CO;2-%23)
7. O. J. Ayala Garay, M. Briard, J. Y. Péron, V. Planchot, *Acta Hortic.* **598** (2003) 227 (https://wwwlib.teiep.gr/images/stories/acta/Acta%20598/598_33.pdf)
8. J. Y. Péron, M. Briard, *Acta Hortic.* **598** (2003) 235 (https://doi.org/10.17660/ActaHortic.2003.598.34)
9. D. Brković, Lj. Čomić, S. Solujić-Sukdolak, *Kragujevac J. Sci.* **28** (2006) 65 (https://www.pmf.kg.ac.rs/KJS/volumes/kjs28/kjs28brkoviccomic65.pdf)
10. E. Kokkalou, E. Stefanou, *Pharm. Acta Helv.* **64** (1989) 133 (https://pubmed.ncbi.nlm.nih.gov/2755958/)
11. S. A. Mamedova, É. R. Akhmedova, *Chem. Nat. Compd.* **27** (1991) 248 (https://doi.org/10.1007/BF00629777)

12. Sh. Masoudi, A. Faridchehr, S. Alizadehfard, N. Zabarjadshiraz, F. Chalabian, R. Taghizadfarid, A. Rustaiyan, *Chem. Nat. Compd.* **47** (2011) 829 (https://doi.org/10.1007/s10600-011-0076-1)
13. R. P. Adams, *Identification of Essential Oil Components by Gas Chromatography/Mass Spectrometry*, 4th ed. Allured Publ. Corp., Carol Stream, IL 2007 (ISBN-13: 978-1932633214, ISBN-10: 1932633219)
14. G. Petrović, J. Stamenković, I. Kostevski, G. Stojanović, V. Mitić, B. Zlatković, *Chem. Biodivers.* **14** (2017) (https://doi.org/10.1002/cbdv.201600367)
15. R. Re, N. Pellegrini, A. Proreggente, A. Pannala, M. Yang, *Free Radical Biol. Med.* **26** (1999) 1231 (https://doi.org/10.1016/S0891-5849(98)00315-3)
16. M. Dimitrijević, V. Stankov-Jovanović, J. Cvetković, T. Mihajilov-Krstev, G. Stojanović, V. Mitić, *Anal. Methods.* **7** (2015) 4181 (https://pubs.rsc.org/en/content/getauthorversionpdf/c4ay03011g)
17. I. F. F. Benzie, J. J. Strain, *Anal. Biochem.* **239** (1996) 70 (https://doi.org/10.1006/abio.1996.0292)
18. M. Oyaizu, *Jpn. J. Nutr.* **44** (1986) 307 (http://dx.doi.org/10.5264/eiyogakuzashi.44.307)
19. R. Apak, K. Güçlü, M. Özyürek, B. B. Oğlu, M. Bener, *Methods Mol. Biol.* **477** (2008) 163 (https://doi.org/10.1007/978-1-60327-517-0_14)
20. A. Barra, *Nat. Prod. Commun.* **4** (2009) 1147 (https://doi.org/10.1177/1934578X0900400827)
21. G. Ruberto, M. T. Baratta, *Food Chem.* **69** (2000) 167 (https://doi org/10.1016/S0308-8146(99)00247-2).

Journal of the Serbian Chemical Society
JSCS-info@shd.org.rs • www.shd.org.rs/JSCS
J. Serb. Chem. Soc. *86* (3) 269–282 (2021)
JSCS–5420
Original scientific paper

Catalytic investigation of Pd(II) complexes over Heck–Mizoroki reaction: Tailored synthesis, characterization and density functional theory

SATYENDRA N. SHUKLA[1]*, PRATIKSHA GAUR[1], SANJAY S. BAGRI[1], RIPUL MEHROTRA[2] and BHASKAR CHAURASIA[1]

[1]*Coordination Chemistry Research Lab, Department of Chemistry, Government Science College, Jabalpur (M.P.) 482001, India and* [2]*Instituto de Quimica Rosario Area Inorganica Facultad de Cs. Bioquimicas y Farmaceuticas Universidad Nacional de Rosario Suipacha 531 S2002LRK Rosario, Argentina*

(Received 2 September, revised 18 November, accepted 20 November 2020)

Abstract: Tailored reaction of Schiff base ligands with palladium(II) chloride and imidazole afford three complexes of formula $[Pd^{(II)}(L)(imdz)_2]Cl$, which are L = 2-((*E*)-(*p*-lylimino)methyl)-6-methoxyphenol (complex **1**), 2-methoxy--6-((*E*)-(phenylimine)methyl)phenol (complex **2**) and 2-((*E*)-(4-chlorophenyl-imino)methyl)-6-methoxyphenol (complex **3**). Compounds were characterized with elemental analysis, molar conductance, electronic spectroscopy, ESI-MS, FT-IR, TGA, ^{1}H-NMR and ^{13}C-NMR. Molecular structure and different quantum chemical parameters were calculated using the B3LYP basis set of density functional theory with the standard 6-311+G (d, 2p) level. The catalytic potential of **1-3** was examined over Heck-Mizoroki reaction and found in order of **1** > **2** > **3**.

Keywords: Schiff base Pd(II) derivative; spectroscopic characterization; molecular modeling; thermogravimetric analysis; cross-coupling reaction.

INTRODUCTION

The cross-coupling reactions leading to C–C bond formation have emerged recently as a remarkably significant preparative strategy for the synthesis of various class of organic compounds.[1] The catalytic introduction of C–C bond to any organic moiety is one of the most popular methods for the synthesis of large complex organic molecules.[2] These methods have been successfully employed in the synthesis of many natural products, bioactive compounds and materials. Despite the presence of several other C–C bond formation reactions, like Suzuki, Sonogashira, Tsuji-Trost, Negishi and Hiyama-coupling reactions, Heck–Mizoroki reaction has attained significant position during the last ten years due to vari-

* Corresponding author. E-mail: ccrl_2004@rediffmail.com; sns1963_1@rediffmail.com
https://doi.org/10.2298/JSC200902075S

ous applications, *viz.* pharmaceuticals, agrochemicals, synthetic fragrances, cosmetics, detergents, and other commercial derivatives.[3–6]

The palladium-catalyzed Heck–Mizoroki cross-coupling reaction has drawn much attention due to high efficiency, chemoselectivity and mild reaction conditions.[7] The remarkable ability of palladium complexes to assemble C–C bonds between suitable functionalized substrates remain a growing area of research.[8] The well-accepted mechanism for this reaction (Fig. 1) is based on the intermediate species involving Pd(0)/Pd(II); however, other possibilities cannot be ruled out.[9] Schiff base metal-derivatives have displayed a wide range of applications, *i.e.*, pharmaceutical, industrial and catalysis.[10] Anchoring of a Schiff base complex by a suitable ligand may be used as a strategy to tune the catalytic activity of complexes.[11] Since, imidazole is an electron-rich heterocyclic nucleus with a wide range of applications in medicinal chemistry, non-linear optics and as a catalyst in industrial uses, it was selected as an anchoring ligand.[12]

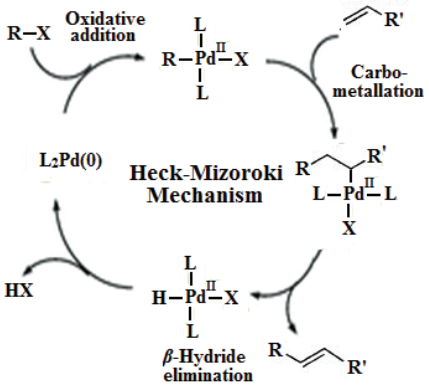

Fig. 1. General mechanism of Heck–Mizoroki reaction.

The present study is an attempt to synthesize an efficient catalyst and investigate the role of palladium intermediates formed in the Heck-Mizoroki mechanism.[13] Although some studies have been done in the field, a lot still remains to be investigated.[14] Therefore, we have synthesized Schiff base ligands through condensation of 4-hydroxy-3-methoxy-benzaldehyde popularly known as *o*-vanillin with selected amines. The resulting ligands in combination with imidazole as a complementary ligand yielded the novel three Pd(II) derivatives. Thus, we herein, report new palladium(II) Schiff base complex as an efficient catalyst in Heck-Mizoroki cross-coupling reaction. Density functional theory (DFT) is a computational quantum mechanical modelling method used to investigate the electronic structure of many-body systems, in a particular molecules. DFT was used to optimize the geometry of synthesized compounds in the gaseous phase. The probable mechanism of the catalysis and energy profile diagram was also elucidated. A general scheme for the synthesis of ligands and complexes is given in Fig. 2.

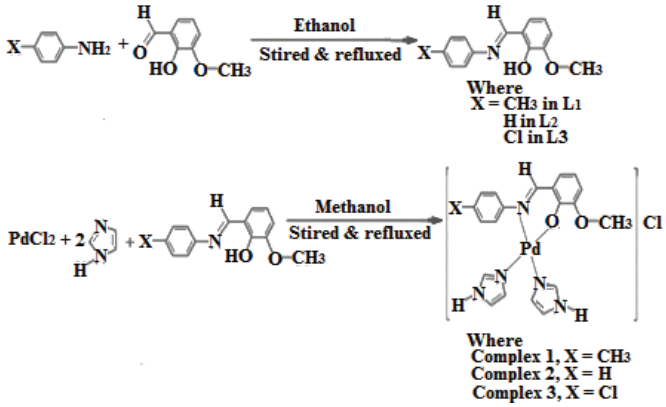

Fig. 2. Scheme for the synthesis of ligands and complexes

EXPERIMENTAL

Materials and methods

Palladium(II) chloride and other starting materials were purchased from E. Merck, India/ /Sigma Aldrich and used as received. Analytical reagent grade solvents were used. Conductivity measurements were carried out at 25 °C on an EI-181 conductivity bridge with dipping type cell. ESI-MS spectra were recorded on Agilent-6520(QTOF) mass spectrometer. FT-IR spectra were recorded in KBr pellets on Shimadzu-8400 PC. Electronic absorption spectra were recorded with EI-2305, double beam spectrophotometer equipped with a PC. ^{1}H-NMR and ^{13}C-NMR spectra were recorded in DMSO-d_6 on Agilent-700-vnmrs 700. The metal contents were analyzed gravimetrically by the literature procedure.[15] For the catalytic investigation, degassed solvents were used with bubbling nitrogen for 50 min.

Synthesis of Schiff base ligands 2-((E)-(p-tolylimino)methyl)-6-methoxyphenol (L_1)/2-methoxy-6-((E)-(phenylimino)methyl)phenol (L_2)/2-((E)-(4-chlorophenylimino)methyl)-6-methoxy phenol (L_3)

Ligands were prepared according to the method reported in the literature.[16–18] The solids obtained in each case were filtered off, washed several times with ethanol and recrystallized with hot methanol to yield orange/yellow crystals which were dried over anhydrous calcium chloride in desiccators under vacuum.

Synthesis of complexes[Pd(L)(imdz)$_2$]Cl; where L = Schiff base ligand L_1/L_2/L_3

Palladium(II) chloride (0.177 g, 0.001 mol) and imidazole (0.136 g, 0.002 mol) were mixed in 25 mL methanol and stirred at room temperature for 30 min to 1 h. Schiff base ligand, **SB** (0.001 mol) dissolved in 25 mL hot methanol was added to the above reaction mixture. The resulting reaction mixture was stirred for 2–3 h in an inert atmosphere. A brown/ /light brown/dark brown solid was separated after refluxing the reaction mixture for 6–8 h, which was filtered, washed with diethyl ether, and dried in vacuum. Unfortunately, after several attempts, we did not find any crystal suitable for single-crystal XRD.

DFT calculation

Density functional theory (DFT) was employed to achieve more insight into the molecular structure. It was carried out using the method of B3LYP with 6-311++G(d,p) basis set

for all nonmetallic atoms and Los Alamos National Laboratory 2 double zeta (LANL2DZ) basic set for the central metal atoms in the gas phase.[19] Gaussian-09 software package was employed to carry out all the quantum chemical calculations.[20] Optimized structural parameter of the compounds such as bond lengths, bond angles and dihedral angles were calculated with the atom numbering scheme of the molecule. Several quantum chemical parameters have been calculated.[21] The ^{1}H-NMR and ^{13}C-NMR Chemical Shifts of the molecule were calculated by the gauge-independent atomic orbital (GIAO) method and compared with the experimental results. DFT was employed to study the energy profiles of the full catalytic cycle of complex **1** for the Heck- Mizoroki reaction.

Catalytic activity over Heck–Mizoroki reaction

The solvent mixture (DMF:H_2O in 1:1 ratio) used in reaction was degassed through the Freeze-pump-claw method.[22] A three-neck round bottom flask equipped with water condenser, magnetic stir bar and N_2-inlet was charged with degassed DMF: H_2O (100 mL), potassium carbonate (0.75 mmol) and complex (**1**–**3**, 0.4 μmol). The styrene (0.6 mmol) and aryl halide (0.5 mmol) were added by glass syringe through a rubber septum. The mixture was allowed to stir at ~80 °C for 8 h and then cooled to room temperature. It was further filtered through the bed of silica. The reaction progress was monitored periodically by TLC. The product was extracted with ethyl acetate (3×10 mL). The combined organic phase was washed with brine (2×10 mL) and dried over Na_2SO_4. The solvent was removed under reduced pressure to afford impure residue. The residue obtained was purified through column chromatography on silica gel eluting with ethyl acetate. Column chromatography was performed to obtain a purified product. The pure compound was obtained by eluting the column by ethyl acetate:hexane (5:95 volume ratio) solvent mixture.

RESULTS AND DISCUSSION

Spectral characterization of complexes

Stoichiometries of the complexes were in agreement with elemental analyses data. Molar conductance (Λ_m) for complexes in 10^{-3} M concentration in DMSO was in the range 16–19 Ω^{-1} cm^2 mol^{-1} indicative of their 1:1 electrolytic nature.[23] ESI-MS spectra of complexes exhibit several peaks. However, a pseudo-molecular ion peak for [M+H$^+$] was inevitably present in each case, which indicates the molecular mass. ESI-MS spectrum of complex **1** is shown in Supplementary material to this paper, Fig. S-1. This shows a signal for [M$^+$], confirming 1:1 electrolytic nature of complex **1**, probably due to dissociation in solution as below:

$$[Pd^{II}L_1(imdz)_2]Cl \rightarrow [Pd^{II}L_1(imdz)_2]^+ + Cl^-$$

In the FT-IR spectra of complexes, the band observed at ~3217 cm^{-1}, assigned for –OH vibration in ligands completely vanished and a new band at lower frequency appeared at ~534 cm^{-1}, which was assigned to Pd–O.[24] The appearance of this band indicates the bonding of metal with phenolic oxygen. The band due to azomethine HC=N groups was shifted downwards in complexes and observed at ~1602 cm^{-1}, which confirms the coordination of azomethine nitrogen with metal. The coordination of azomethine nitrogen with metal was

further ascertained by the appearance of a band at a lower frequency at ~450 cm^{-1}, assign to Pd–N vibration stretching.[25] The experimental FT-IR spectrum of complex **1** was compared with the theoretical I.R. spectrum and presented in Table S-I (Supplementary material). Since the DFT calculation generally overestimates the vibrational frequencies due to the neglect of crystal packing effects and anharmonicity, as well as incompleteness of the basis set and dynamic electronic correlation, the calculated frequencies slightly deviated from the experimental values of the normal vibrations. Therefore, we have derived scaling factors and applied to the theoretical data to get a satisfactory value. On comparison, it was observed that the in the theoretical spectra after scaling peak for ν(C–H), ν(HC=N), $\nu(C–O)_{sym}$, $\nu(C–O)_{asym}$, $\nu(C–H_3)_{in\ plane}$, $\nu(C–H_3)_{out\ plane}$, ν(Pd–O) and ν(Pd–N) were observed with a deviation of 0.1 %. The calculated scaling factor for complex **1** is 1.000 (R^2 = 0.999) over a complete range of the spectrum. From Table S-I, it can be observed that most of the unscaled vibrations become closer to the experimental value after scaling. The experimental and theoretical FT-IR spectrum of complex **1** is shown in Fig. S-2 of the Supplementary material.

Complexes are diamagnetic as expected for d^8 configuration.[26] In electronic spectra, the lowest energy band at ~703 nm was assigned to $^1A_{1g} \rightarrow {}^3A_{2g}$ (ν_1) transition. However, bands at ~605, ~440 and ~400 nm were attributed to $^1A_{1g} \rightarrow {}^1A_{2g}$ (ν_2), $^1A_{1g} \rightarrow {}^1E_g$ (ν_3) and $^1A_{1g} \rightarrow {}^1B_{1g}$ (ν_4) transitions, indicating square-planar geometry around Pd(II) ion.[27] The spectrum of complex **1** is given in Fig. S-3 of the Supplementary material.

The coordination of the azomethine HC=N group was confirmed by the downfield shifting of the azomethine proton signal in complexes by δ 0.08––0.09 ppm. This downfield shifting of azomethine proton in Pd(II) complex was attributed to the discharge of the electronic cloud towards the Pd(II) ion. The hydroxyl OH proton signal at $\delta \approx$ 13.30 ppm in the ligands disappeared in the spectra of Pd(II) complexes, indicating the deprotonation and the coordination of oxygen with the metal ion. The ^{1}H-NMR spectrum of the complexes shows doublet centred at $\delta \approx$ 10.85 ppm for two protons attributed to the –NH of two imidazole ring. A doublet at $\delta \approx$ 7.30 ppm for two C–H protons and a multiplet centred at $\delta \approx$ 7.25 ppm for four protons were assigned to other C–H protons of the imidazole ring.[30] The two double doublets centred at $\delta \approx$ 7.10 ppm, $\delta \approx$ 6.90 ppm ($J \approx$ 8 and ≈ 2.5 Hz) and a triplet centred at $\delta \approx$ 6.77 ppm ($J \approx$ 8.0 Hz) were attributed to aromatic protons of vanillin moiety. However, in complex **1** and **3**, a multiplet centred at $\delta \approx$ 7.20 ppm for four protons was attributed to toluidine/ /chloroaniline moiety. In complex **2**, a multipletcentred at $\delta \approx$ 7.22 ppm for five protons was assigned for aniline moiety. In addition to this, in complexes, a signal at $\delta \approx$ 3.45 ppm was assigned for protons of methoxy group. In complex **1**, a signal at $\delta =$ 2.22 ppm was assigned for methyl proton. The theoretical chemical shift values were calculated by the GIAO method using TMS-HF/6-31G(d)

GIAO and TMS-B3LYP/6-311+G(2d, p) GIAO level theory. The correlation coefficients of ^{1}H-NMR were determined as 0.979 and 0.985 as given in Fig. S--4A and B of the Supplementary material. For $\mathbf{L}_1$, ^{1}H-NMR $\delta_{cal} = 1.135\delta_{exp}$ - 1.193 (R^2 = 0.979). For complex **1**, ^{1}H-NMR $\delta_{cal} = 0.987\delta_{exp}$ - 0.196 (R^2 = = 0.985). It was evident from the correlation graph that a good correlation exists in theoretical and experimental δ values. ^{1}H-NMR of the spectrum of complex **1** is shown in Fig. S-5 of the Supplementary material.

In ^{13}C-NMR spectrum signal at $\delta \approx$ 160.0 ppm in ligand assigned for azomethine group was downfield shifted by δ = 3.4 - 6.2 ppm in the complexes confirming the transfer of one lone pair electron from nitrogen to metal and coordination of azomethine-N to metal. In complexes, the two signals appeared at $\delta \approx$ 135.0 ppm were assigned for the two imidazole ring carbon atom. The remaining four imidazole carbon resonate at $\delta \approx$ 120.0 ppm. In complex **1** and **3**, the six signals observed between δ = 156.6 - 130.0 ppm were attributed to vanillin moiety of the ligand. In complex **2**, the six signals of vanillin carbon appeared between δ = 153.1 - 126.6 ppm. However, the remaining six signals observed between δ = 129.0 - 111.1 ppm were ascribed for six-carbon of toluidine/aniline/ /*p*-chloroaniline ring moiety. A signal in complexes observed between δ = 55.8 - - 52.6 ppm was assigned for methoxy carbon. In complex **1**, a signal at δ = 20.5 ppm was due to methyl carbon of vanillin moiety. The correlation coefficients of ^{13}C-NMR for $\mathbf{L}_1$ and complex **1** were determined as 0.977 and 0.999, as shown in Fig. S-6A and B of the Supplementary material. It was evident from the correlation graph that a good correlation exists in theoretical and experimental δ values. The ^{13}C-NMR spectrum of complex **1** is shown in Fig. S-7 of the Supplementary material.

TGA of complexes (Fig. 3A, B and C) were carried out in the temperature range of 30–900 °C at the heating rate of 10 °C/min in a nitrogen atmosphere. The TGA curves of these complex displayed a similar two steps degradation pattern. In each case, the first step was the partial decomposition of ligand and one imidazole unit along with one Cl^-. In the second step, the loss of the remaining one imidazole unit occurs. In complex **1**, a weight loss of 64 % (calcd. 63.34 wt.%) in the temperature range ~255–350 °C was attributed to the first step of decomposition. In second step the loss of remaining one imidazole unit occurs in the temperature range of 350–530 °C, with a weight loss of 13 % (calcd. 12.45 wt.%). In complex **2**, a weight loss of 62.52 % (calcd. 62.22 wt.%) in the temperature range ~330–370 °C was attributed for the first step decomposition. In the second step the loss of remaining one imidazole unit occurs in the temperature range of 370–500 °C with a weight loss of 13.46 % (calcd. 13.51 wt.%). In complex **3,** a weight loss of 64.93 % (calcd. 64.64 wt.%) in the temperature range ~330–390 °C was the first step of decomposition. In the second step loss of remaining one imidazole unit occurs in the temperature range of 390–500 °C, with a

weight loss of 12.38 % (calcd. 12.61 wt.%). A very unusual gain of weight in complex **1** between 500–600 °C is ascribed to the oxidation of the remaining Pd to PdO. In the end, a metallic oxide residue was formed as PdO (calcd. 22.45 wt.%).[28–30]

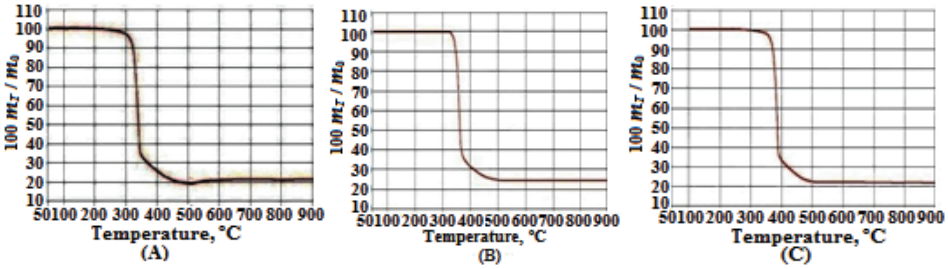

Fig. 3. TGA curve of complexes: A) **1**, B) **2** and C) complex **3**.

Quantum chemical calculations

Mulliken atomic charge and molecular electrostatic potential analysis (MEP). The calculated Mulliken atomic charge values of selected atoms were listed in Table S-II of the Supplementary material. Mulliken atomic charge plots of rest of the ligands and complexes were given in Fig. S-8 of the Supplementary material. From results, it was observed that in ligands the hydrogen attached with the electronegative oxygen exhibits the highest positive charge of ~ +0.4000. However, the highest negative charge of ~ –0.6800 was present on highly shielded oxygen. However, in complexes **1**–**3**, the highest positive charge of ~ +0.4700 was present at Pd metal centre. The other electronegative atoms such as phenolic oxygen and azomethine nitrogen consist of a negative Mulliken charge because of high electron density on these atoms. The imidazole ring is an electron-rich moiety, and its N atoms possess the negative Mulliken charge. The Mulliken charge values of electropositive carbon and electronegative oxygen/nitrogen are also higher than ligand, probably due to the occurrence of back bonding of π-electrons during complexation. This result is consistent with the molecular electrostatic potential map.[31]The molecular electrostatic potential (MEP) is a particularly useful descriptor in understanding sites for electrophilic and nucleophilic reactions as well as hydrogen-bonding interactions. The molecular electrostatic potential, (r), at a given point r (x, y, z) in the vicinity of a molecule is defined in terms of the interaction energy between the electrical charge generated from the molecule electrons and nuclei. To predict the electrophilic and nucleophilic reactive sites for the title molecule, MEP was calculated using the B3LYP/LanL2DZ method with the 6-31++G(d,p) basis set and optimized geometries. The negative (red) regions of MEP were related to electrophilic reactivity and the positive (blue) regions to nucleophilic reactivity. The MEP maps of ligands and complexes were shown in Fig. S-9 of the Supplementary material. The electrostatic potential in $\mathbf{L}_1$

ranges between $–5.7\times10^{–2}$ to $5.7\times10^{–2}$ a.u. and in $\mathbf{L}_2$ it ranges from $–5.6\times10^{–2}$ to $5.6\times10^{–2}$ a.u. Similarly, in $\mathbf{L}_3$, potential value is found between $–6.1\times10^{–2}$ to $6.1\times10^{–2}$ a.u. The electrostatic potential in complex **1** range between $–9.2\times10^{–2}$ to $9.2\times10^{–2}$ a.u. and in complex **2**, it ranges from $-9.7\times10^{–2}$ to $9.7\times10^{–2}$ a.u. Similarly, in complex **3**, potential value is found between $-9.8\times10^{–2}$ to $9.8\times10^{–2}$ a.u. Different colours represent the different values of the electrostatic potential at the surface. The potential increases in the order: red<orange<yellow<green<<blue.[32] It was observed that the positive areas are present on less electronegative atom such as hydrogen, carbon, and central metal atoms. On the other hand, the negative areas are confined on more electronegative O, and N. These electronegative moieties worked as a donor atom of the ligand.

Molecular modelling and computational study. The quantum chemical parameters were calculated and listed in Table S-III. The highest occupied molecular orbital (HOMO) and the lowest unoccupied molecular orbital (LUMO) are named as frontier molecular orbitals (FMO). The HOMO and LUMO of $\mathbf{L}_1$ and complex **1** is shown in supplementary Fig. S-10 of the Supplementary material. The HOMO and LUMO energies and energy gap, ΔE of ligands and complexes were given above in Table S-III. From the calculated energies of the highest occupied molecular orbital (HOMO) and lowest unoccupied molecular orbital (LUMO), it may be concluded that:

1. The difference of FMO_s energies in complexes are for E_{HOMO} is in the order $\mathbf{L}_3>\mathbf{L}_2>\mathbf{L}_1>\mathbf{3}>\mathbf{1}>\mathbf{2}$ and for E_{LUMO} the order is $\mathbf{3}>\mathbf{2}>\mathbf{1}>\mathbf{L}_3>\mathbf{L}_1>\mathbf{L}_2$**.**
2. Complex **2** has low values of the energy gap (ΔE) suggesting high reactivity.
3. Complex **1** exhibit a high value of the dipole moment, which may favour their dipole-dipole interactions between molecules.

Bond length and bond angle. The optimized structures of the complexes with the atomic numbering scheme were determined. The bond lengths (Å) and bond angles (in degree) obtained from the geometry optimized structures are given in Tables S-IV and S-V. The molecular structure of complexes exhibits almost square planar geometry around the metal centre, as revealed from the calculated bond lengths and bond angles. The C=N, C–O and C–C bond lengths become slightly longer in complexes than the bonds formed with ligands. Ligands were coordinated *via* imine nitrogen by the shifting of electron density of imine and phenolic oxygen because of the removal of phenolic hydrogen. Formation of two new bonds Pd–N and Pd–O takes place. The C–O bond distance in all complexes becomes longer due to the formation of Pd–O bond, which makes the C–O bond weaker. This elongation in Pd–N and Pd–O bond lengths caused a slight distortion from the regular square planar geometry.

Thus, based on the elemental analysis, ESI-MS, molar conductance, electronic spectra, FT-IR, ^{1}H-NMR, ^{13}C-NMR, TGA and DFT studies, the optimized structures of the ligands and complexes are given in Fig. 4A–F.

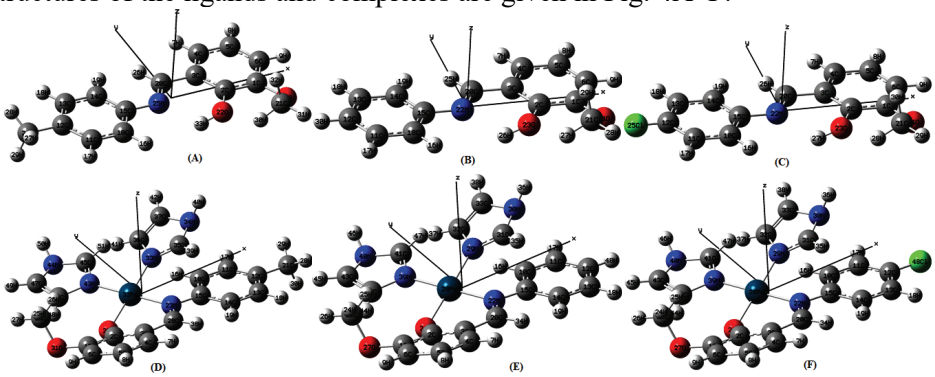

Fig. 4. DFT optimized structure of: A) $\mathbf{L}_1$, B) $\mathbf{L}_2$, C) $\mathbf{L}_3$, and complexes: D) **1**, E) **2** and F) **3.**

Catalytic activity

Catalytic potential for the synthesized complexes was examined over Heck–Mizoroki C–C cross-coupling reaction (Fig. 5) at various reaction conditions of temperature, base, solvent and catalyst loading. The results obtained are summarized in Table S-VI.

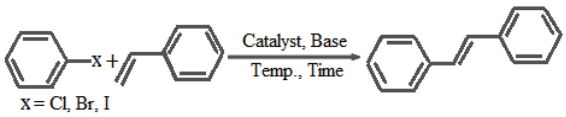

Fig. 5. Scheme for catalytic activity optimization.

*Effect of catalyst loading/base/solvent and temper*ature. It is ideal to have good yields using a minimal amount of catalysts. Hence, this study examined the effect of catalyst loading (0.1–0.6 μmol). It was observed that the highest yield of a coupling product was obtained when 0.4 μmol of the complex **1** was employed as a catalyst. Higher product conversion with an increased amount of catalyst may probably due to the increased availability of more basic sites, which can be linked to the dispersion of more active species.[33] However, with the increasing catalyst concentration above 0.4 μmol, no appreciable increase in product yield was observed. The yield of products at different catalyst concentration is shown in Fig. 6A.

The role of a base is to neutralize the acid and consequently the exchange of a hydrogen atom with an aryl or vinyl group occurs. Hence, to study the effect of the base in Heck–Mizoroki reaction, the reaction was carried out in the presence of different bases such as K_2CO_3, Na_2CO_3, CH_3COONa, NaOH and KOH. It

was observed from Fig. 6B that K_2CO_3 is the most effective base in the catalytic conversion, probably due to its higher solubility in comparison to others.

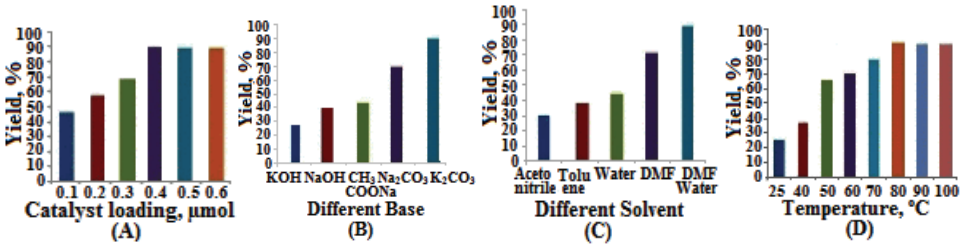

Fig. 6. Heck–Mizoroki reaction; A) effect of catalyst loadings, B) effect of different base, C) effect of different solvents, D) effect of temperature.

It was observed that the mixed solvent such as DMF+H_2O (1:1) gives good quantitative yield. The polar aprotic solvents such as the DMF give a lower yield. However, in acetonitrile solvent, lowest yield of product was obtained, as shown in Fig. 6C. Heck–Mizoroki reaction is a temperature-sensitive reaction, and therefore it is necessary to study the reaction at different temperature ranges from 25–100 °C. It was observed that, at room temperature, very little catalytic conversion takes place, and with the rise of temperature the yield increases. The maximum yield was observed at an optimum temperature of 80 °C. With further increase of the temperature, no appreciable increase in yield was observed. The temperature effect can be explained by the influence on the equilibrium between different forms of Pd participating in the reaction. For example, the low-temperature decrease provides the increase of the stability of palladium complexes in solution. In contrast, higher temperature increases the rate of Pd reduction. The percentage yield at different reaction temperature is shown in Fig. 6D.

With the optimized reaction conditions in hand, the scope of the Heck––Mizoroki reaction was extended to a variety of substituted aryl halides (XC_6H_4Y; where X = Br/Cl/I and Y = H/ CHO/OCH_3). It was interesting to observe that the yield of the product is almost the same in the case of bromo and iodobenzene. However, in the case of aryl bromide substituted with electron-withdrawing aldehydes group (Table S-VII, entry 4) higher yield was observed in comparison to a substrate with an electron-donating methoxy group (Table S-VII, entry 5). The reaction of chlorobenzene, in comparison to bromobenzene/iodobenzene, failed in providing good yield under optimized conditions presumably owing to less reactivity of C–Cl bond due to higher bond energy. Turn over frequency (*TOF*) of catalysts was also calculated, and it ranges between 36.3–302.5 h^{-1}. *TOF* values are higher than the reported *TOF* values in similar complexes.[34] The catalytic activity of the complex **1** was quite good in comparison to previously reported catalysts for Heck–Mizoroki coupling reaction in terms of temperature, cat-

alyst loading, base and solvents.[35] In our case catalyst gave better yields at moderate temperature using less amount of catalyst in the DMF–water medium. ^{1}H--NMR and ^{13}C-NMR characterized the resulting products.

Energy profile diagram. DFT calculations were performed at the B3LYP/6--31G level of theory to evaluate the formation of alkene *via* C–C cross-coupling reaction using chelated palladium Schiff base complex **1** as a catalyst. The overall computed energy profile diagram of this reaction is displayed in Fig. 7. The energy profile diagram shows that the complete Heck–Mizoroki reaction proceeds *via* four major steps, *viz.* reductive elimination, oxidative addition, migratory insertion and *β*-hydride elimination. The first step involves the elimination followed by the reduction of Pd(II) to Pd(0). Reductive elimination is a facile step with an energy barrier of 2.0116 eV. The next step involves the addition of Ph-Br and oxidation of metal center Pd(0) to Pd(II) with the energy of 2.4116 eV. After that, the formation of high energy π-complex $\mathbf{TS}_1$ takes place which later gets stabilized by 1.0386 eV and forms a stable sigma intermediate $\mathbf{TS}_2$. Sigma complex further changes into a new higher energy state $\mathbf{TS}_3$ by the migratory insertion mechanism. In the last step, *β*-hydride elimination occurs, and a final cross-coupled product was obtained. The energy profile of reaction obtained from the DFT calculation clearly shows that π-complex $\mathbf{TS}_1$ is situated at the top in comparison to $\mathbf{TS}_2$ and $\mathbf{TS}_3$. The less stable energetically $\mathbf{TS}_3$ is more favourable for easy conversion into the product. There has been considerable evidence that oxidative addition does not limit the rate of Heck–Mizoroki reactions.[36] Further evidence from the gas-phase computational studies indicates that the rate-determining step in a palladium (II/IV) cycle involving iodobenzene would be the oxidative addition of iodobenzene to palladium. Since the actual rate-determining step in the Heck–Mizoroki reaction of aryl iodides is not oxidative addition, this indicates that palladium (II/IV) cycle is not running. In the present situation, we suggest olefin coordination as a rate-limiting step, due to wide energy gap in between **3** and **4** in the energy profile diagram of the catalytic cycle. The probable mechanism of Heck-Mizoroki reaction is shown in Fig. S-11 of the Supplementary material.

CONCLUSION

Three novel mixed ligand complexes of Pd(II) containing imidazole as anchoring ligand and Schiff base as N, O donor, have been synthesized by the tailored synthesis and characterized. For a better insight into molecular structure, quantum chemical calculations have been performed. The geometry of compounds was optimized by DFT. The complexes have square planar complexes geometry with slight distortion in both bond length and bond angle. The theoretical parameters have shown an excellent agreement with the experimental results and hence proved the reliability of the employed level of theory. The

resulting complexes exhibit quite good catalytic activity in comparison to those reported in the literature. The complex **1** exhibited excellent catalytic activity with the substrate containing bromo/iodo substituent. However, when the bromo substituent is in combination with aldehydes in the substrate, it exhibits higher catalytic activity in comparison to the combination of bromo and methoxy group. It was also observed from the DFT that the proposed intermediate is the π-complex which exhibit higher energy than σ-intermediate and it is situated at the top of the energy profile. Hence, it can be concluded that this catalytic system tolerates various functional group on the phenyl ring and could be further exploited for the design of promising catalytic material.

SUPPLEMENTARY MATERIAL

Physical, analytical and spectral data for the synthesized compounds are available electronically from http://www.shd.org.rs/JSCS/, or from the corresponding author on request.

Acknowledgements. The authors are grateful to the Principal, Government Science College, Jabalpur and Head, Chemistry Department, for providing necessary laboratory facilities. We sincerely thanks SAIF, CDRI, Lucknow, for recording ESI-MS, ^{1}H-NMR, ^{13}C-NMR and IISERBhopal for recording TGA. One of us (SSB) is also grateful to the UGC-New Delhi, for financial support through RGNF (Award letter no. F1-17.1/2017--18/RGNF-2017-18-SC-MAD 43228/(SAIII/Website).

ИЗВОД

КАТАЛИТИЧКА ИСПИТИВАЊА Pd(II) КОМПЛЕКСА ПОМОЋУ HECK–MIZOROKI РЕАКЦИЈЕ: СИНТЕЗА, КАРАКТЕРИЗАЦИЈА И ТЕОРИЈА ФУНКЦИОНАЛА ГУСТИНЕ

SATYENDRA N. SHUKLA[1], PRATIKSHA GAUR[1], SANJAY S. BAGRI[1], RIPUL MEHROTRA[2] И BHASKAR CHAURASIA[1]

[1]*Coordination Chemistry Research Lab, Department of Chemistry, Government Science College, Jabalpur (M.P.) 482001, India u* [2]*Instituto de Quimica Rosario Area Inorganica Facultad de Cs. Bioquimicas y Farmaceuticas Universidad Nacional de Rosario Suipacha 531 S2002LRK Rosario, Argentina*

У реакцијама Шифових база као лиганада са паладијум(II)-хлоридом и имидазолом добијена су три комплекса опште формуле [Pd(II)(L)(imdz)$_2$]Cl; L је 2-((*E*)-(*p*-алилимино)метил)-6-метоксифенол (комплекс **1**), 2-метокси-6-((*E*)-(фенилимин)метил)фенол (комплекс **2**) и 2-((*E*)-(4-хлорофенилимино)метил)-6-метоксифенол (комплекс **3**). Комплекси су окарактерисани на бази резултата елементалне микроанализе, моларне проводљивости, електронске спектроскопије, ESI-MS, FT-IR, TGA, ^{1}H-NMR и ^{13}C-NMR спектара. Молекулска структура и различити квантнохемијски параметри су одређени помоћу B3LYP базисног сета теорије функционала густине са стандардним 6-311+G(d,2p) нивоом. Каталитичка способност комплекса **1**–**3** испитивана је на основу Heck–Mizoroki реакције, при чему је нађено да се њихова каталитичка способност мења у низу **1**>**2**>**3**.

(Примљено 2. септембра, ревидирано 18 новембра, прихваћено 20. новембра 2020)

REFERENCES

1. K. C. Nicolaou, P. G. Bulger, D. Sarlah, *Angew. Chem. Int. Ed.* **44** (2005) 4442 (https://doi.org/10.1002/anie.200500368)

2. C. Jia, T. Kitamura, Y. Fujiwara, *Acc. Chem. Res.* **34** (2001) 633 (https://dx.doi.org/10.1021/ar000209h)
3. A. Balanta, C. Godard, C. Claver, *Chem. Soc. Rev.* **40** (2011) 4973 (https://dx.doi.org/10.1039/c1cs15195a)
4. A. R. Hajipour, F. Rafiee, *J. Organomet. Chem*. **696** (2011) 2669 (https://dx.doi.org/10.1016/j.jorganchem.2011.03.023)
5. A. Dewan, U. Bora, G. Borah, *Tet. Lett.* **55** (2014) 1689 (https://dx.doi.org/10.1016/j.tetlet.2014.01.041)
6. F. Bakkali, S. Averbeck, D. Averbeck, M. Idaomar, *Food Chem. Toxicol.* **46** (2008) 446 (https://dx.doi.org/10.1016/j.fct.2007.09.106)
7. M. Esmaeilpour, J. Javidi, *J. Chin. Chem. Soc.* **62** *(*2015) 614 (http://dx.doi.org/10.1002/jccs.201500013)
8. R. F. Heck, *J. Am. Chem. Soc*. **90** (1968) 5518 (https://doi.org/10.1021/ja01022a034)
9. J. P. Genet, M. Savignac, *J. Organomet. Chem*. **576** (1999) 305 (https://doi.org/10.1021/ja01022a034)
10. M. Sankarganesh, N. Revathi, J. D. Raja, K. Sakthikumar, G. G. V. Kumar, J. Rajesh, M. Rajalakshmi, L. Mitu, *J. Serb. Chem. Soc.* **84** (2019) 291 (https://dx.doi.org/10.2298/JSC180609080)
11. H. O. Oloyede, J. A. O. Woods, H. Gorls, W. Plass, A. O. Eseola, *J. Mol. Struct.* **1199** (2020) 1 (https://dx.doi.org/10.1016/j.molstruc.2019.127030)
12. H. A. Doung, M. Cross, *J. Org. Lett.* **6** (2004) 4679 (https://dx.doi.org/10.1021/ol048211m)
13. P. J. Knowles, A. Whiting, *Org. Biomol. Chem*. **5** (2007) 31 (https://dx.doi.org/10.1039/b611547k)
14. C. S. Letizia, J. Cocchiara, J. Lalko, A. M. Api, *Food Chem. Toxicol.* **41** (2003) 943 (https://dx.doi.org/10.1016/S0278-6915(03)00015-2)
15. G. H. Jeffery, J. Bassett, J. Mendham, R. C. Denney, *Vogel's Textbook of Quantitative Inorganic Analysis*, 5th ed., John Wiley & Sons, Inc. New York, 1989
16. Y. Y. Yu, H. D. Xian, J. F. Liu, G. L. Zhao, *Molecules* **14** (2009) 1747 (https://dx.doi.org/10.3390/molecules14051747)
17. M. Amirnasar, A. H. Mahmoudkhani, A. Gorji, S. Dehghanpour, H. R. Bijanzadeh, *Polyhedron* **21** (2002) 2733 (https://dx.doi.org/10.1016/S0277-5387(02)01277-9)
18. N. Raman, Y. P. Raja, A. Kulandaisamy, *Proc. Indian Acad. Sci.* (*Chem. Sci.*) **113** *(*2001) 183
19. G. Y. Yeap, S. T. Ha, S. N. Ishizawa, K. L. Boey, W. A. K. Mahmood, *J. Mol. Struct.* **658** (2003) 87 (https://dx.doi.org/10.1016/S0022-2860 (03)00453-8)
20. Gaussian Inc., Wallingford, CT, 2009
21. M. Dehestani, L. Zeidabadinejad, *J. Serb. Chem. Soc.* **80** (2015) 1008 (https://dx.doi.org/10.2298/JSC150224027Z)
22. D. A. Vicic, G. D. Jones, *Experimental Methods and Techniques: Basic Techniques,* Elsevier Ltd., University of Arkansas, Fayetteville, AR, 2007
23. W. J. Geary, *J. Coord. Chem. Rev.* **7** (1971) 81 (https://dx.doi.org/10.1016/S0010-8545(00)80009-0)
24. E. G. Bakirdere, M. F. Fellah, E. Canpolat, M. Kaya, S. Gur, *J. Serb. Chem. Soc.* **81** (2016) 520 (https://doi.org/10.2298/JSC151030008B)
25. M. Shabbir, Z. Akhter, I. Ahmad, S. Ahmed, M. Shafiq, B. Mirza, V. Mckee, K. S. Munawar, A. R. Ashraf, *J. Mol. Struct*. **1118** (2016) 250 (https://dx.doi.org/10.1016/j.molstruc.2016.04.003)

26. A. A. Soliman, I. O. Alajrawy, A. F. Attabi, M. R. Shaaban, W. Linert, *Spectrochim. Acta, A* **152** (2016) 358 (https://dx.doi.org/10.1016/j.saa.2015.07.076)
27. Z. Leka, S. Grujic, Z. Tesic, S. Lukic, S. Skuban, S. Trifunovic, *J. Serb. Chem. Soc.* **69** (2004) 137 (https://doi.org/10.2298/JSC0402137L)
28. C. V. Barra, F. V. Rocha, A. V. G. Netto, R. C. G. Frem, A. E. Mauro, I. Z. Carlos, S. R. Ananias, M. B. Quilles, *J. Therm. Anal. Calorim.* **106** (2011) 489 (https://dx.doi.org/10.1007/s10973-011-1393-0)
29. S. A. Al-Jibori, M. M. Barbooti, M. H. S. Al-Jibori, B. K. Aziz, *J. Mater. Environ. Sci.* **8** (2017) 1365
30. V. G. Netto, A. M. Santana, A. E. Mauro, Regina C. G. Frem, *J. Therm. Anal. Calorim* **79** (2005) 339 (https://doi.org/10.1007/s10973-005-0061-7)
31. N. Yıldırım, N. Demir, G. Alpaslan, B. Boyacioglu, M. Yıldız, H. Unver, *J. Serb. Chem. Soc.* **83** (2018) 707 (https://dx.doi.org/10.2298/JSC171001009Y)
32. T. A. Mohamed, I. A. Shaaban, R. S. Farag, W. M. Zoghaib, M. S. Afifi, *Spectrochim. Acta, A* **135 (**2015) 417 (https://dx.doi.org/10.1016/j.saa.2014.07.018)
33. J. M. Collinson, Wilton-Ely, *J. Cat. Commun.* **87** (2016) 78 (https://dx.doi.org/10.1016/j.catcom.2016.09.006)
34. S. Layek, Anuradha. B. Agrahari, D. D. Pathak, *J. Organomet. Chem.* **846** *(*2017*)* 105 (https://dx.doi.org/10.1016/j.jorganchem.2017.05.049)
35. R. N. Prabhu, R. Ramesh, *Tetrahedron Lett*. **53** (2012) 5961 (https://dx.doi.org/10.1016/j.tetlet.2012.08.120)
36. C. S. Consorti, G. Ebeling, F. R. Flores, F. Rominger, *J. Adv. Synth. Catal.* **346** (2004) 617 (https://dx.doi.org/10.1002/adsc.200303228).

Journal of the Serbian Chemical Society
JSCS-info@shd.org.rs • www.shd.org.rs/JSCS
J. Serb. Chem. Soc. 86 (3) S70–S83 (2021) *Supplementary material*

SUPPLEMENTARY MATERIAL TO

Catalytic investigation of Pd(II) complexes over Heck–Mizoroki reaction: Tailored synthesis, characterization and density functional theory

SATYENDRA N. SHUKLA[1]*, PRATIKSHA GAUR[1], SANJAY S. BAGRI[1], RIPUL MEHROTRA[2] and BHASKAR CHAURASIA[1]

[1]*Coordination Chemistry Research Lab, Department of Chemistry, Government Science College, Jabalpur (M.P.) 482001, India and* [2]*Instituto de Quimica Rosario Area Inorganica Facultad de Cs. Bioquimicas y Farmaceuticas Universidad Nacional de Rosario Suipacha 531 S2002LRK Rosario, Argentina*

J. Serb. Chem. Soc. 86 (3) (2021) 269–282

ISOLATED YIELDS AND SPECTROSCOPIC DATA OF SYNTHESIZED COMPOUNDS

2-((E)-(p-tolylimino)methyl)-6-methoxyphenol (L_1)

M.p.: 102 ºC; Yield: 1.115 g (92.60 %). Electronic spectra λ_{max} / nm (ε / mol L^{-1} cm^{-1}) in DMSO: 240 (1220), 360 (385). Selected infrared absorption (KBr, cm^{-1}): ν(O-H), 3217; ν(C-H), 2931; ν(HC=N), 1627; ν(C=C), 1454; ν(C-O), 1265; $\nu(-OCH_3)_{asym}$, 1172; $\nu(-OCH_3)_{sym}$, 1091; $\gamma(C-H)_{in\ plane}$, 1057; $\gamma(C-H)_{out\ plane}$, 740. ^{1}H-NMR spectra (400 MHz, CH_3CN, δ / ppm): (O-H), 13.37 (s, 1H); δ (HC=N), 8.93 (s, 1H), δ $(Ar-H)_{p\text{-}toluidine}$, 7.32 (m, 2H), 7.27 (m, 2H), δ $(Ar-H)_{Vanillin}$, 7.23 (dd, J = 10.6 Hz, 2 Hz, 1H), 7.12 (dd, J = 10.8 Hz, 2.0 Hz, 1H), 6.89 (t, J = 10.4 Hz, 10.4 Hz, 1H); $(-OCH_3)$, 3.42 (s, 3H); $(-CH_3)$, 2.33 (s, 3H). ^{13}C-NMR spectra (400 MHz, CH_3CN, δ / ppm): $(>C=N)_{imine}$, 161.5, (C-OH), 151.7, (Ar-C),150.9 (C_1), 148.1 (C_2), 134.4 (C_3), 128.0 (C_4), 123.7 (C_5), 119.5 (C_6), 119.4 (C_8), 119.2 (C_9), 117.9 (C_{10}), 116.4 (C_{11}), 115.1 (C_{12}); $(O-CH_3)$,55.8; $(-CH_3)$, 20.1. ESI-Mass spectra, (*m/z)*: calculated for $[C_8H_8NO_2+H^+]^+$ = 151.099, $[C_{14}H_{12}NO+H^+]^+$ = 211.026, $[C_{15}H_{14}NO+H^+]^+$ = 225.032, $[C_{14}H_{12}NO_2+H^+]^+$ = 227.014, $[C_{15}H_{15}NO_2+H^+]^+$= 242.116, observed 241.286. Combustion analysis for $C_{15}H_{15}NO_2$: calcd. C 74.67, H 6.27, N 5.81 %. Found C 74.59, H 6.23, N 5.75 %.

2-methoxy-6-((E)-(phenylimino)methyl)phenol (L_2)

M.p.: 95 ºC; Yield: 0.982 g (86.51 %); Electronic spectra λ_{max} / nm (ε / mol L^{-1} cm^{-1}) in DMSO: 250 (1237), 360 (375). Selected infrared absorption

* Corresponding author. E-mail: ccrl_2004@rediffmail.com; sns1963_1@rediffmail.com

(KBr, cm^{-1}): *ν*(O-H), 3216; *ν*(C-H), 3034; *ν*(HC=N), 1619; *ν*(C=C), 1464; *ν*(C-O), 1271; $\nu(\text{-OCH}_3)_{asym}$, 1188; $\nu(OCH_3)_{sym}$, 1081. ^{1}H-NMR spectra (400 MHz, CH_3CN, *δ* / ppm): (O-H), 13.34, (s, 1H); (HC=N), 8.92 (s, 1H), (Ar-H), 7.28 (m, $5H)_{aniline}$, 7.20 (dd, J = 9.2 Hz, 2.5 Hz, 1H), 7.13 (dd, *J* = 8.4 Hz, 2.2 Hz, 1H), 6.78 (t, *J* = 8.0 Hz, 8.0 Hz, 1H), (-OCH_3), 3.45 (s, 3H). ^{13}C-NMR spectra (400 MHz, CH_3CN, *δ* / ppm): $(\text{>C=N})_{imine}$,159.2; (C-OH),153.0; (Ar-C),149.5 (C_1), 147.2 (C_2), 135.3 (C_3), 126.5 (C_4), 121.5 (C_5), 118.7 (C_6), 118.1 (C_8), 118.1 (C_9), 115.0 (C_{10}), 114.2 (C_{11}), 113.5 (C_{12}); (O-CH_3), 51.6. ESI-Mass spectra, (*m/z)*: calculated for $[C_8H_8NO_2+H^+]^+$ = = 151.485, $[C_{14}H_{12}NO+H^+]^+$ = 211.152, $[C_{13}H_{10}NO_2+H^+]^+$ = 213.053, $[C_{14}H_{13}NO_2+H^+]^+$ = 228.258, observed 227.351. Combustion analysis for $C_{14}H_{13}NO_2$: calcd. C 73.99, H 5.77, N 6.16 %.Found C 73.92, H 5.69, N 6.08 %.

2-((E)-(4-chlorophenylimino)methyl)-6-methoxy phenol (L_3)

M.p.: 175 ºC; Yield: 1.058 g (81.19 %); Electronic spectra λ_{max}/nm (*ε*/mol L^{-1} cm^{-1}) in DMSO: 245 (1228), 352 (392). Selected infrared absorption (KBr, cm^{-1}): *ν*(O-H), 3249; *ν*(C-H), 3137; *ν*(HC=N), 1613; *ν*(C=C), 1449; *ν*(C-O), 1248; $\nu(\text{-OCH}_3)_{asym}$, 1161; $\nu(\text{-OCH}_3)_{sym}$, 1092. ^{1}H-NMR spectra (400 MHz, CH_3CN, *δ* / ppm): (O-H), 13.32 (s, H); (HC=N), 8.91 (s, 1H), *δ* (Ar-H) 7.45 (m, $4H)_{chloroaniline}$, 7.23 (dd, *J* = 10.5 Hz, 2.4 Hz, 1H), 7.10 (dd, *J* = 9.5 Hz, 3.0 Hz, 1H), 6.95 (t, *J* = 8.4 Hz, 8.4 Hz, 1H); *δ* (-OCH_3), 3.49 (s, 3H); *δ* (-CH_3), 2.33 (s, 3H). ^{13}C-NMR spectra (400 MHz, CH_3CN, *δ* / ppm): $(\text{>C=N})_{imine}$, 157.3; (C-OH),152.3; (Ar-C), 151.7 (C_1), 147. 2 (C_2), 132.0 (C_3), 127.2 (C_4), 124.6 (C_5), 116.8 (C_6), 116.5 (C_8), 116.1 (C_9), 114.9 (C_{10}), 113.2 (C_{11}), 113.0 (C_{12}); (O-CH_3),55.0. ESI-Mass spectra, (*m/z)*: calculated for $[C_8H_8NO_2+H^+]^+$ = 151.359, $[C_{14}H_{12}NO_2+H^+]^+$ = 227.014, $[C_{13}H_9ClNO+H^+]^+$ = 231.026, $[C_{14}H_{12}ClNO_2+H^+]^+$ = 262.706, observed 261.725. Combustion analysis for $C_{14}H_{12}ClNO_2$: calcd. C 64.25, H 4.59, N 5.35 %. Found C 64.17, H 4.52, N 5.24 %.

[Pd(L_1)(imdz)$_2$]Cl (1)

A brown crystalline solid was obtained after recrystallization of impure solid from 1: 1: 2, acetonitrile: acetone: chloroform (v/v) solvent mixture, which was dried in a desiccator over anhydrous calcium chloride under vacuum. M.p.: >300 ºC; Color: brown, Yield: 0.381 g (73.69 %). Electronic spectra λ_{max} / nm (ε / mol L^{-1} cm^{-1}) in DMSO: 703 (29), 600 (98), 440 (286), 400 (421), 370 (759), 260 (1245). Molar conductance Λ_m at 25 ºC (Ω^{-1} cm^2 M^{-1}): 19 in DMSO. Selected infrared absorption (KBr, cm^{-1}): ν(C-H),2843; ν(HC=N), 1602; ν(C=C), 1472; ν(C-O), 1265; $\nu(H_3C\text{-}O)_{asy}$, 1178; $\nu(H_3C\text{-}O)_{sy}$, 1068; $\nu(H_3C)_{in\ plane}$, 1028; $\nu(H_3C)_{out\ of\ plane}$, 752; ν(Pd-O), 534; ν(Pd-N), 453. ^{1}H-NMR spectra (400 MHz, DMSO, *δ* / ppm): 10.94 (s, 2H, $(N\text{-}H)_{imdz}$), 8.99 (s, 1H, -HC=N), 7.34 (d, J = 8.4 Hz, $2H)_{imdz}$, 7.25 (m, $4H)_{imdz}$, (Ar-H), 7.15 (m, $4H)_{p\text{-}toluidene}$, 7.07 (d, *J* = 8.4

Hz, 1H)$_{vanillin}$, 6.90 (t, J = 8.0 Hz, 8.0 Hz, 1H)$_{vanillin}$, 6.77 (d, J = 7.2 Hz, 1H)$_{vanillin}$, 3.41 (s, 3H, -OCH_3), 2.22 (s, 3H, CH_3). ^{13}C-NMR spectra (400 MHz, dmso, δ / ppm): (>C=N)$_{imine}$, 165.1; (imd-C), 136.5, 136.4, 122.3, 122.1, 122.0, 122.0, (Ar-C), 156.6 (C_1), 150.5 (C_2), 147.8 (C_3), 145.1 (C_4), 131.3 (C_5), 130.0 (C_6), 129.9 (C_7), 116.1 (C_8), 114.5 (C_9), 114.5 (C_{10}), 113.4 (C_{11}), 113.1 (C_{12}); (O-CH_3), 55.8; (-CH_3), 20.5.ESI-Mass spectra, (*m/z)*: calculated for $[C_8H_8O_2N+H^+]^+$ = 151.090, $[C_{15}H_{15}O_2N+H^+]^+$ = 242.172, $[C_8H_7ClO_2$-$NPd+H^+]^+$ = 291.038, $[C_{15}H_{14}O_2NPd+H^+]^+$ =347.697, $[C_{15}H_{14}ClO_2NPd+H^+]^+$= 383.340, $[C_{14}H_{15}N_5O_2Pd+H^+]^+$ = 392.203, $[C_{18}H_{18}N_3O_2Pd+H^+]^+$ = 415.215, $[C_{14}$-$H_{15}ClN_5O_2Pd+H^+]^+$ = 428.210, $[C_{18}H_{18}ClN_3O_2Pd]^+$ = 450.001, $[C_{21}H_{22}N_5O_2Pd]^+$ = 482.857, $[C_{21}H_{22}ClN_5O_2Pd+H^+]^+$ = 519.304, observed 518.258. Combustion analysis for $C_{21}H_{22}ClN_5O_2Pd$: calcd. C 48.63, H 4.28, N 13.51, Pd 20.53 %. Found C 48.54, H 4.23, N 13.44, Pd 20.45 %.

[Pd(L_2)(imdz)$_2$]Cl (2)

The solid obtained was further recrystallized from 1:1:2, acetone: acetonitrile:chloroform (v / v) solvent mixture to yield light brown crystalline solid, which was dried in a desiccator over anhydrous calcium chloride under vacuum. M.p.: >300 ºC; Color: light brown, Yield: 0.345 g (68.59 %); Electronic spectra λ_{max} / nm (ε / mol L^{-1} cm^{-1}) in DMSO: 715 (37), 609 (91), 437 (295), 405 (408), 366 (743), 253 (1264). Molar conductance Λ_m at 25 °C (Ω^{-1} cm^2 M^{-1}): 16 in DMSO. Selected infrared absorption (KBr, cm^{-1}): ν(C-H)$_{arom}$, 2827; ν(HC=N), 1589; ν(C=C), 1438; ν(C-O), 1251; ν(H_3C-O)$_{asym}$, 1172; ν(H_3C-O)$_{sym}$, 1068; ν(Pd-O), 516; ν(Pd-N), 437. ^{1}H-NMR spectra (400 MHz, DMSO, δ / ppm): 10.80 (s, 2H, (N-H)$_{imdz}$), 8.99 (s, 1H, -HC=N), 7.38 (d, J = 8.8 Hz, 2H)$_{imdz}$, 7.27 (m, 4H)$_{imdz}$, (Ar-H), δ 7.22 (m, 5H)$_{aniline}$, 7.18 (dd, J = 9.8 Hz, 2.5 Hz, 1H)$_{vanillin}$, 6.97 (t, J = 8.4 Hz, 8.4 Hz, 1H)$_{vanillin}$, 6.69 (dd, *J = 9.6Hz, 2.2 Hz,* 1H)$_{vanillin}$, 3.48 (s, 3H, -OCH_3).^{13}C-NMR spectra (400 MHz, DMSO, δ / ppm): (>C=N)$_{imine}$, 162.6, (imd-C), 134.6, 134.4, 120.4,120.3, 120.2, 120.1, (Ar-C), 153.1 (C_1), 152.9 (C_2), 144.6 (C_3), 141.8 (C_4), 128.4 (C_5), 126.6 (C_6), 126.2 (C_7), 121.8 (C_8), 117.4 (C_9), 117.1 (C_{10}), 114.8 (C_{11}), 114.6 (C_{12}); (O-CH_3), 52.6. ESI-Mass spectra, (*m/z)*: calculated for $[C_8H_8O_2N+H^+]^+$ = 151.064, $[C_{14}H_{12}O_2N+H]^+$ = 228.258, $[C_8H_7ClO_2NPd+H^+]^+$ = 291.043, $[C_{14}H_{12}O_2NPd+H^+]^+$ = 333.654, $[C_{14}H_{12}ClO_2NPd+H^+]^+$ = 368.283, $[C_{14}H_{15}N_5O_2Pd+H^+]^+$ = 392.218, $[C_{14}H_{11}Cl_2O_2NPd+H^+]^+$ = 401.246, $[C_{14}H_{15}Cl$-$N_5O_2Pd+H^+]^+$ = 428.281, $[C_{20}H_{20}N_5O_2Pd+H^+]^+$ =469.158, $[C_{20}H_{20}ClN_5O_2Pd+H^+]^+$ = 505.035, observed 504.125. Combustion analysis for $C_{20}H_{20}ClN_5O_2Pd$: calcd. C 47.64, H 4.00, N 13.89, Pd 21.12 %. Found C 47.53, H 3.95, N 13.78, Pd 21.01 %.

[Pd(L_3)(imdz)$_2$]Cl (3)

M.p.: >300 ºC; Color: dark brown, Yield: 0.354 g (65.92 %); Electronic spectra λ_{max} / nm (ε / mol L^{-1} cm^{-1}) in DMSO: 711 (32), 605 (104), 445 (282), 403 (419), 375 (751), 248 (1270). Molar conductance Λ_m at 25 ˚C (Ω^{-1} cm^2 M^{-1}): 17 in DMSO. Selected infrared absorption (KBr, cm^{-1}): ν(C-H), 2889; ν(HC=N), 1581; ν(C=C), 1441; ν(C-O), 1247; ν(H_3C-O)$_{asym}$, 1178; ν(H_3C-O)$_{sym}$, 1060; ν(Pd-O), 530; ν(Pd-N), 457. ^{1}H-NMR spectra (400 MHz, DMSO, δ / ppm): 10.78 (s, 2H, (N-H)$_{imdz}$), 8.99 (s, 1H –HC=N), 7.37 (*d, J* = 8.0 Hz, 2H)$_{imdz}$, 7.25 (m, 4H)$_{imdz}$, (Ar-H), 7.20 (m, 4H)$_{chloroaniline}$, 7.15 (dd, *J* = 9.2 Hz, 2.2 Hz, 1H)$_{vanillin}$, 6.90 (t, *J* = 7.2 Hz, 7.2 Hz, 1H)$_{vanillin}$, 6.78 (dd, *J* = 7.4 Hz, 2.4 Hz, 1H)$_{vanillin}$, 3.54 (s, 3H, -OCH_3). ^{13}C-NMR spectra (400 MHz, DMSO, δ / ppm): (>C=N)$_{imine}$, 163.5; (imd-C), 137.6; δ 137.5; 122.3; 122.1; 122.0; 122.0; (Ar-C), 154.2 (C_1), 152.8 (C_2), 148.6 (C_3), 145.2 (C_4), 132.6 (C_5), 130.2 (C_6), 130.0 (C_7), 119.3 (C_8), 115.5 (C_9), 115.2 (C_{10}), 111.8 (C_{11}), 111.5 (C_{12}); (O-CH_3), 58.7. ESI-Mass spectra, (*m/z)*: calculated for $[C_8H_8O_2N+H^+]^+$ = 151.157, $[C_{14}H_{12}ClO_2N+H^+]^+$ = 262.106, $[C_8H_7ClO_2NPd+H^+]^+$ = 291.094, $[C_{14}H_{15}N_5O_2Pd+H^+]^+$ = 392.18, $[C_{17}H_{15}Cl_2N_3O_2Pd+H^+]^+$= 469.134, $[C_{20}H_{19}ClN_5O_2Pd+H^+]^+$ = 505.015, $[C_{20}H_{19}Cl_2N_5O_2Pd+H^+]^+$ = 539.723, observed 538.564. Combustion analysis for $C_{20}H_{19}Cl_2N_5O_2Pd$: calcd. C 44.59, H 3.55, N 13.00, Pd 19.75 %. Found C 44.51, H 3.48, N 12.89, Pd 19.67 %.

Coupling reaction product ((E)-1,2-diphenylethene)

M.p.: 134-135 °C. Color: white crystals. ^{1}H-NMR spectra (400 MHz, DMSO, δ / ppm): 7.614 (t, 2H), 7.239 (t, 2H), 7.293 (t, 2H); 7.287 (d, 2H); 7.267 (d, 2H); δ HC=CH, 4.13 (d, 2H). ^{13}C-NMR spectra (400 MHz, DMSO, δ / ppm): δ 136.99 ($C_{1,9}$); δ 127.27 ($C_{3,11}$); δ 126.12 ($C_{4,12}$); δ 127.62 ($C_{5,13}$); δ 128.67 ($C_{6,14}$); (HC= CH), δ 60.13.

Table S-I. Correlation of experimental FT-IR spectra with theoretical IR spectra for complex **1**

Assignment	Wavelength, cm^{-1}			Deviation, %
	Experimental	Theoretical		
		Unscaled	Scaled	
ν(O-H)	-	-	-	-
ν(C-H)	2843	2835	2840	0.1
ν(-CH=N)	1602	1610	1600	0.1
ν(C=C)	1427	1436	1425	0.1
ν(C-O)	1265	1267	1263	0.1
ν(C-O-C)$_{sym}$	1178	1171	1176	0.1
ν(C-O-C)$_{asym}$	1068	1070	1066	0.1
χ(C-H)$_{in\ plane}$	1028	1013	1026	0.1
χ(C-H)$_{out\ of\ plane}$	752	754	733	0.1
ν(M-O)	534	532	533	0.1
ν(M-N)	453	443	452	0.1

Table S-II. Selected Mulliken atomic charges of ligands and complexes

Atoms	Mulliken atomic charge					
	Ligand			Complex		
	L_1	L_2	L_3	1	2	3
C (connected to O)	(C2) 0.355	(C2) 0.396	(C2) 0.396	(C2) 0.396	(C2) 0.394	(C2) 0.384
C′ OCH_3 (connected to O)	(C1) 0.086	(C1) 0.075	(C1) 0.075	(C1) 0.076	(C1) 0.072	(C1) 0.052
C (connected to imine N)	(C20) 0.356	(C21) 0.354	(C20) 0.354	(C20) 0.343	(C20) 0.359	(C20) 0.350
H (connected to O)	(H33) 0.356	(H27) 0.356	(H27) 0.355	-	-	-
O	(O22) -0.687	(O23) -0.679	(O23) -0.679	(O22) -0.678	(O27) -0.656	(O21) -0.669
N (imine)	(N25) -0.671	(N25) -0.615	(N22) -0.615	(N23) -0.582	(N22) -0.582	(N24) -0.578
N (Imdz)	-	-	-	(N33) -0.655	(N29) -0.611	(N31) -0.674
N′ (Imdz)	-	-	-	(N43) - 0.640	(N39) -0.653	(N33) -0.654
Pd	-	-	-	1.324	1.331	1.340

Table S-III. The calculated quantum chemical parameters of ligands and complexes

Quantum parameter	Ligand			Complex		
	L_1	L_2	L_3	1	2	3
E_{HOMO} / eV	-5.937	-5.980	-6.271	-4.508	-3.986	-5.490
E_{LUMO} / eV	-2.029	-0.595	-2.236	-3.137	-3.197	-3.771
ΔE / eV	3.907	5.384	4.035	1.371	0.789	1.719
χ / eV	3.983	3.288	4.254	3.822	3.591	4.631
η / eV	1.953	2.692	2.017	0.685	0.394	0.859
Σ / eV^{-1}	0.511	0.371	0.495	1.458	2.534	1.163
μ / eV or Pi	-3.983	-3.288	-4.254	-3.822	-3.591	-4.319
2n	3.907	5.384	4.035	1.371	0.789	1.791
S / eV^{-1}	0.255	0.185	0.247	0.729	1.267	0.581
Ω / eV	4.061	2.007	4.485	10.657	13.347	12.472
ΔN_{max} / eV	2.038	1.221	2.108	5.575	6.103	5.386
E, TD- F / TD-KS	-785.615	-746.303	-856.915	-1378.681	-1339.642	-1354.039
Dipole moment, D	4.959	4.445	4.044	12.793	12.533	12.318

Table S-IV. Geometrically optimized bond lengths of ligands and complexes

Bonds	Bond length, Å					
	Ligand			Complex		
	L_1	L_2	L_3	1	2	3
C-O	(C2-O22) 1.431	(C2-O23) 1.430	(C2-O23) 1.435	(C2-O22) 1.431	(C2-O21) 1.435	(C2-O21) 1.437
H-O	(H33-O22)	(H27-H23)	(H27-O23)	-	-	-

	0.968	0.961	0.960			
C=N (imine)	(C20=N25) 1.298	(C21=N25) 1.293	(C20=N22) 1.297	(C20=N23) 1.299	(C20=N22) 1.298	(C20= N24) 1.299
C-O (O-CH_3)	(C21-O23) 1.430	(C22-O24) 1.430	(C21-O24) 1.430	(C24-O31) 1.430	(C23-O27) 1.434	(C23-O22) 1.431
C-Cl			(C12-Cl25) 1.761	-	-	(C12-Cl25) 1.760
Pd-O	-	-	-	(Pd32-O22) 1.942	(Pd28-O21) 1.942	(Pd30 -O21) 1.941
Pd -N	-	-	-	Pd32-N23 (phen) 1.981	Pd28-N22 (phen) 1.980	Pd30-N24 (phen) 1.980
Pd –N (Imdz)	-	-	-	Pd32 N33 1.978	Pd28-N29 1.977	Pd30-N31 1.976
Pd -N′ (Imdz)				Pd32 N43 1.979	Pd32-N39 1.976	Pd32-N33 1.974

Table S-V. Geometrically optimized bond angles of ligands and complexes

Angles	Bond angle, °					
	Ligand			Ligand		
	L_1	L_2	L_3	1	2	3
∠C-C-O	(∠C3-C2-O22) 119.999	(∠C3-C2-O23) 119.997	(∠C3-C2-O23) 119.994	(∠C3-C2-O22) 122.849	(∠C3-C2-O21) 122.842	(∠C3-C2-O21) 122.616
∠C-O-H	(∠C2-O22-H33) 109.471	(∠C2-O23-H27) 109.471	(∠C2-O23-H27) 109.471	-	-	-
∠C=N-C	(∠C3-C20-N25) 120.004	(∠C3-C21-N25) 120.007	(∠C3-C21-N22) 120.005	(∠C3-C22-N23) 123.139	(∠C3-C22-N22) 123.137	(∠C3-C20-N24) 123.142
∠H-C=N (imine)	(∠H26-C20-N25) 119.999	(∠H26-C21-N25) 119.998	(∠H26-C20-N22) 119.997	(∠H38-C20-N23) 118.400	(∠H34-C20-N22) 118.400	(∠H26-C20-N24) 118.925
∠C-O-C O-CH_3	(∠C1-O23-C21) 109.471	(∠C1-O24-C22) 109.472	(∠C1-O24-C21) 109.471	(∠C1-O31-C24) 109.492	(∠C1-O27-C23) 109.490	(∠C1-O22-C23) 109.471
∠N(imine)-Pd-O	-	-	-	(∠N23-Pd32-O22) 92.855	(∠N22-Pd28-O21) 92.848	(∠N24-Pd30-O21) 92.841
∠N-Pd-O (Imdz)	-	-	-	(∠N23-Pd32-O22) 92.855	(∠N22-Pd28-O21) 92.860	(∠N24-Pd30-O21) 92.853
∠N-Pd-N	-	-	-	(∠N43-Pd32-N33) 87.534	(∠N39-Pd28-N29) 87.534	(∠N39-Pd30-O31) 87.748
∠N(imdz-Pd-O	-	-	-	(∠N43-Pd32-O22) 125.874	(∠N39-Pd28-O21) 125.874	(∠N33-Pd30-O21) 125.425
∠N(imine)-Pd-N	-	-	-	(∠N23-Pd32-N33) 90.697	(∠N22-Pd28-N29) 90.695	(∠N24-Pd30-N31) 90.629

Table S-VI. Catalysis of Heck-Mizoroki reaction in different condition by complexes

Ent.	Catal load, μmol	Solv.	*T* / ° C	Base	*t* / h	Yield*, % 1	TOF, h^{-1}	Yield*, % 2	TOF, h^{-1}	Yield*, % 3	TOF, h^{-1}
1	0.1	DMF+ Water	80	K_2CO_3	8	44.656	302.5	42.285	287.5	39.476	267.5
2	0.2	DMF+ Water	80	K_2CO_3	8	57.633	195.62	54.637	185.62	51.524	175
3	0.3	DMF+ Water	80	K_2CO_3	8	68.326	158.25	62.392	166.25	58.518	136.62
4	0.4	DMF+	80	K_2CO_3	8	89.694	152.5	76.240	129.68	74.823	127.62

		Water									
5	0.5	DMF+ Water	80	K_2CO_3	8	89.308	121.5	76.005	103.25	74.661	127.18
6	0.6	DMF+ Water	80	K_2CO_3	8	89.246	101.03	76.404	86.45	74.856	87.16
7	0.4	DMF	80	K_2CO_3	8	72.519	123.12	69.725	118.43	68.214	112.8
8	0.4	Toluene	80	K_2CO_3	8	46.259	78.43	41.034	69.68	40.473	68.81
9	0.4	Aceto-nitrile	80	K_2CO_3	8	38.549	65.31	35.559	60.31	35.415	60.06
10	0.4	Water	80	K_2CO_3	8	29.746	50.31	28.854	48.81	27.964	47.56
11	0.4	DMF+ Water	25	K_2CO_3	8	24.572	44.06	22.554	38.18	19.863	46.06
12	0.4	DMF+ Water	40	K_2CO_3	8	35.877	60.56	34.168	57.81	21.468	36.31
13	0.4	DMF+ Water	50	K_2CO_3	8	65.568	111.31	62.359	105.93	59.216	100.62
14	0.4	DMF+ Water	60	K_2CO_3	8	69.847	118.8	68.526	116.31	62.163	105.68
15	0.4	DMF+ Water	70	K_2CO_3	8	78.442	133.1	73.056	124.06	71.225	120.93
16	0.4	DMF+ Water	90	K_2CO_3	8	89.524	152.31	76.164	129.37	74.001	125.68
17	0.4	DMF+ Water	100	K_2CO_3	8	89.512	152.18	76.408	129.62	74.614	126.93
18	0.4	DMF+ Water	80	Na_2CO_3	8	69.465	117.81	64.556	109.68	60.509	113.18
19	0.4	DMF+ Water	80	CH_3COONa	8	44.656	75.68	42.465	72.18	42.148	71.56
20	0.4	DMF+ Water	80	NaOH	8	39.694	67.56	35.469	60.6	31.968	54.06
21	0.4	DMF+ Water	80	KOH	8	28.989	49.06	26.989	45.68	24.382	41.31
22	0.4	DMF+ Water	80	K_2CO_3	2	31.297	212.75	30.857	208.75	28.957	196.25
23	0.4	DMF+ Water	80	K_2CO_3	4	61.846	210.12	60.761	189.37	55.872	189.37
24	0.4	DMF+ Water	80	K_2CO_3	6	65.648	148.75	61.299	139.2	58.469	132.08
25[#]	0.4	DMF+ Water	80	K_2CO_3	8	41.984	71.31	39.914	67.81	36.710	62.18
26[##]	0.4	DMF+ Water	80	K_2CO_3	8	-	-	-	-	-	

Reaction condition: Bromobenzene (0.5 mmol); Styrene (0.6 mmol); Potassium carbonate (0.75 mmol).
[*]Yield after column chromatography. [#]Only $PdCl_2$ used as catalyst. [##]Schiff base ligands as catalyst.

Table S-VII. Heck-Mizoroki reactions with different substituents catalyzed by complex **1** under optimized reaction conditions

Entry	X	Y	Catalyst loading, μmol	Solvents	*T* / ºC	Base	*t* / h	*Yield, %	TOF, h^{-1} Complex **1**
1	Cl	H	0.4	DMF+ Water	80	K_2CO_3	8	43.710	74.06
2	Br	H	0.4	DMF+ Water	80	K_2CO_3	8	89.694	152.5
3	I	H	0.4	DMF+	80	K_2CO_3	8	89.899	152.7

				Water					
4	Br	CHO	0.4	DMF+ Water	80	K_2CO_3	8	67.872	115.2
5	Br	OCH_3	0.4	DMF+ Water	80	K_2CO_3	8	59.660	101.25

Substituted aryl halides (0.5 mmol) (XC_6H_4Y; where X = Cl/ Br/ I and Y = H/ CHO/OCH_3). In each case styrene (0.6 mmol) and as base potassium carbonate (0.75 mmol) was used. *Yield after column chromatography

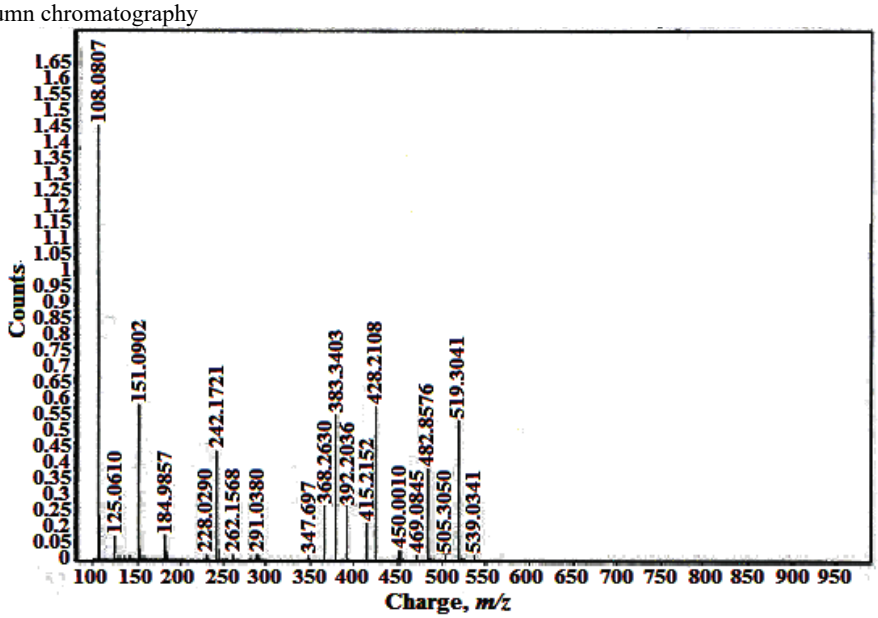

Fig. S-1. ESI-Mass spectrum of complex **1**.

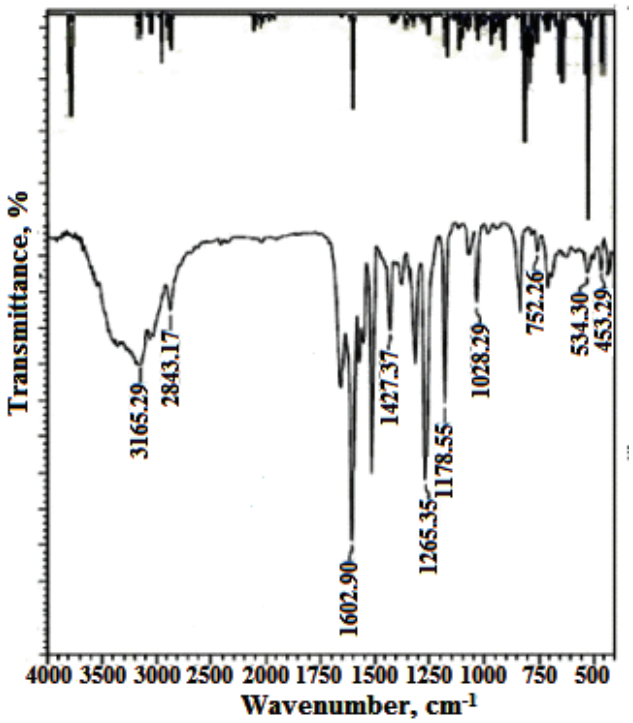

Fig. S-2. Experimental and theoretical FT-IR spectrum of complex **1**.

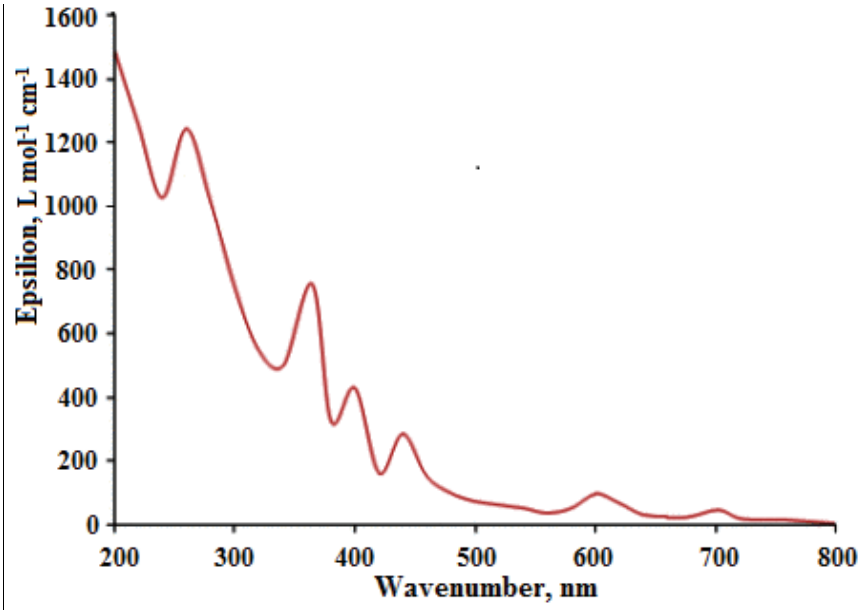

Fig. S-3. UV-Vis spectra spectrum of complex **1**.

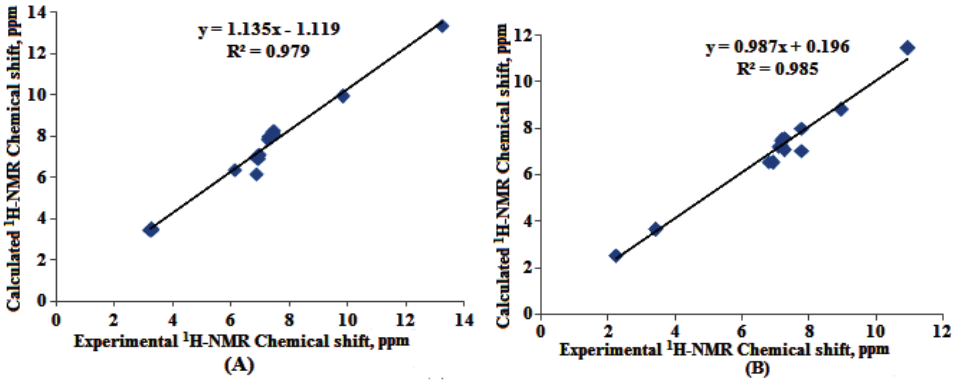

Fig. S-4. ^{1}H-NMR correlation diagram for (A) L_1 and (B) complex **1**.

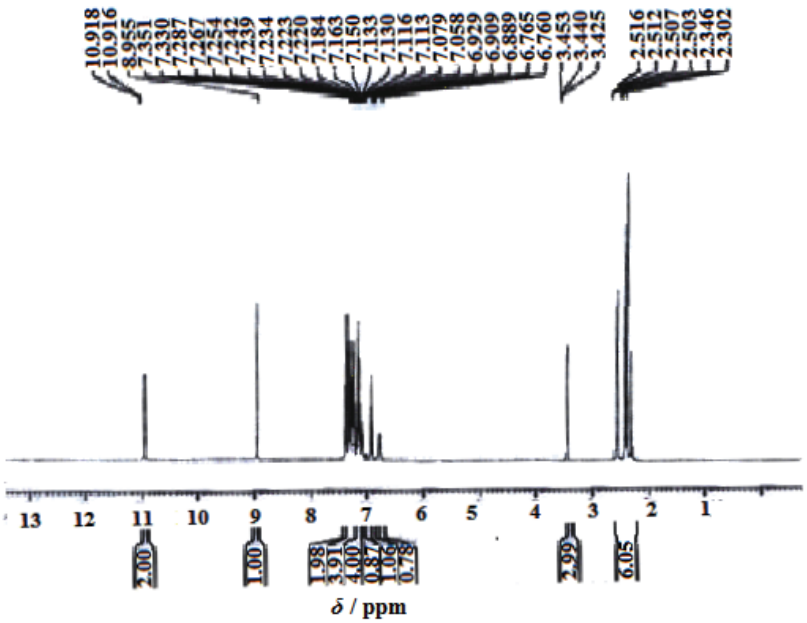

Fig. S-5. ^{1}H-NMR spectrum of complex **1**.

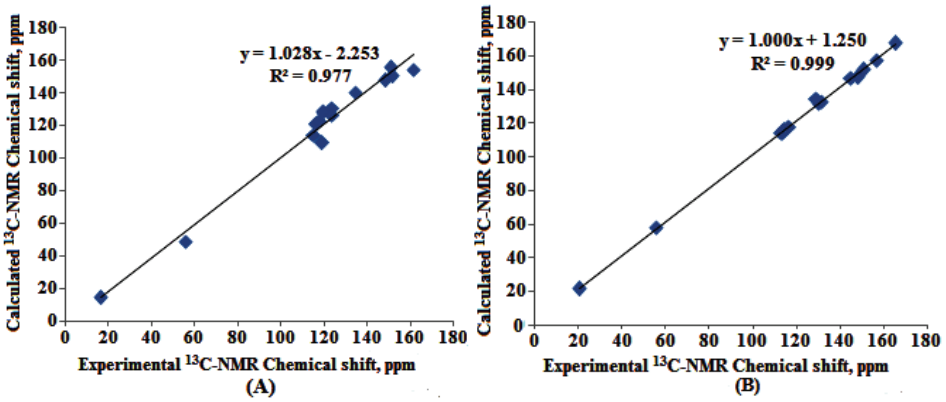

Fig. S-6. ^{13}C-NMR correlation diagram for (A) L_1 and (B) complex **1**.

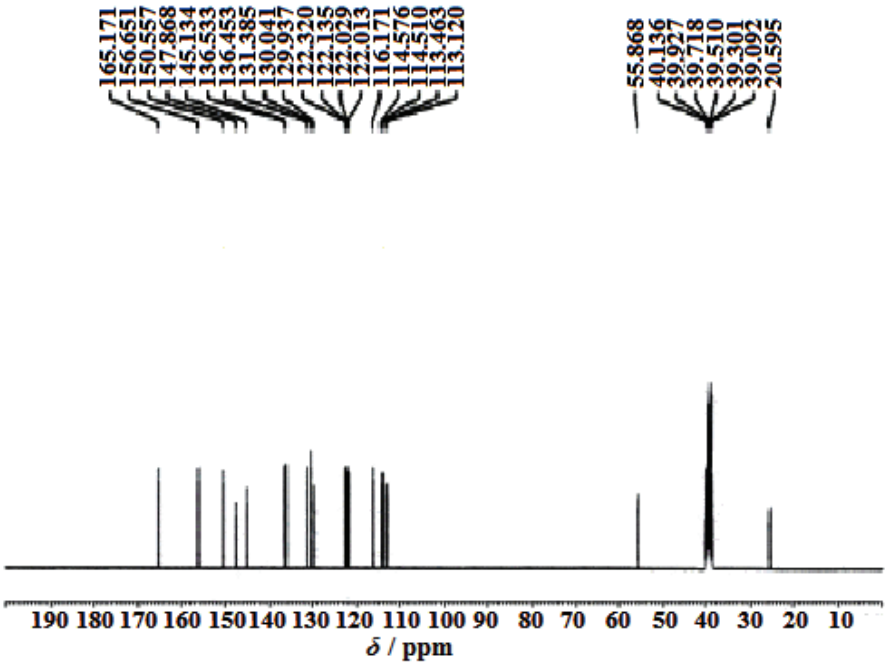

Fig. S-7. ^{13}C-NMR spectrum of complex **1**.

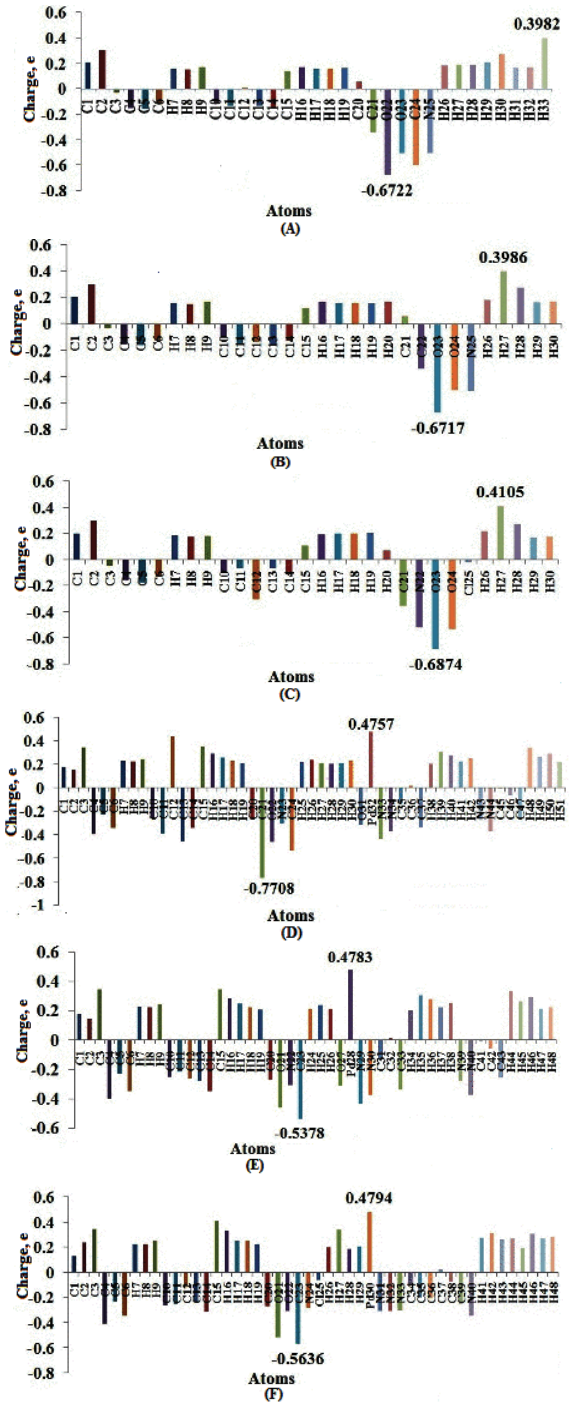

Fig. S-8. Mulliken atomic charge plot of $\mathbf{L}_1$, $\mathbf{L}_2$, $\mathbf{L}_3$, complexes **1**, **2** and **3**.

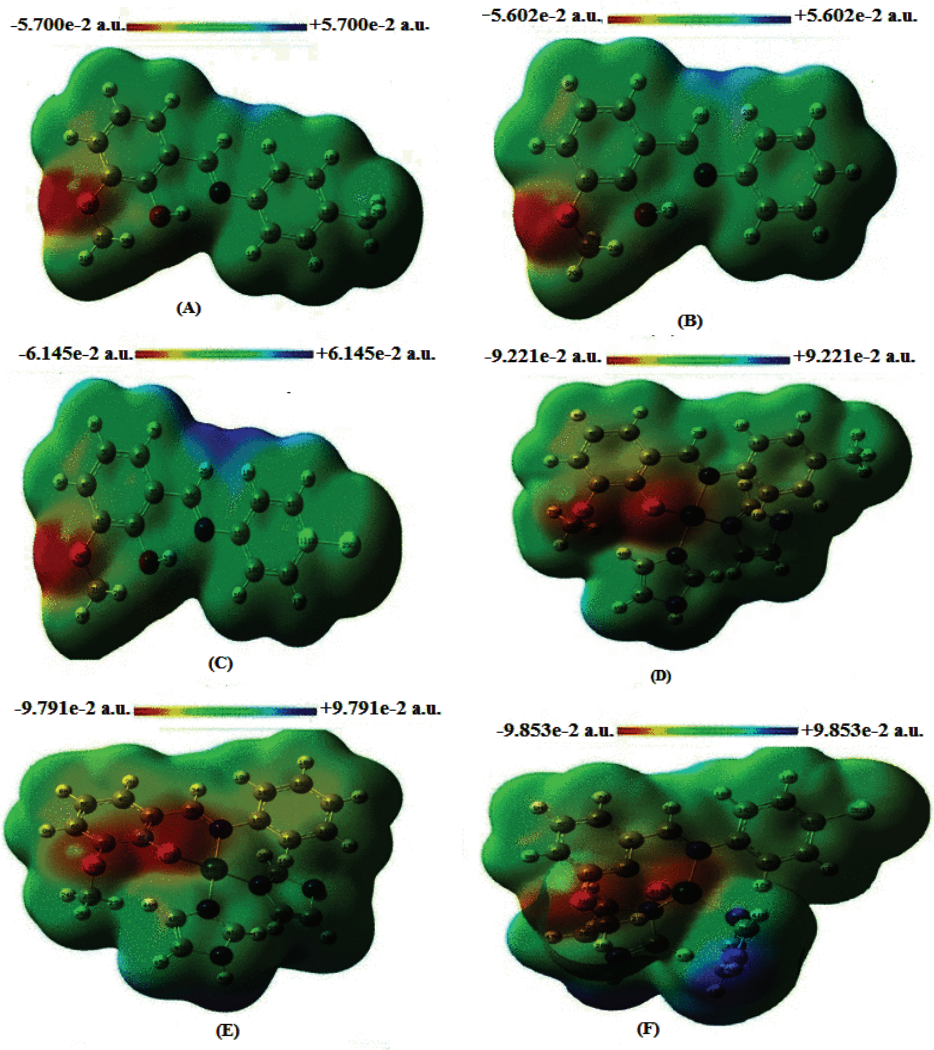

Fig. S-9. Molecular Electrostatic Potential of $\mathbf{L}_1$, $\mathbf{L}_2$, $\mathbf{L}_3$, complexes **1**, **2** and **3**.

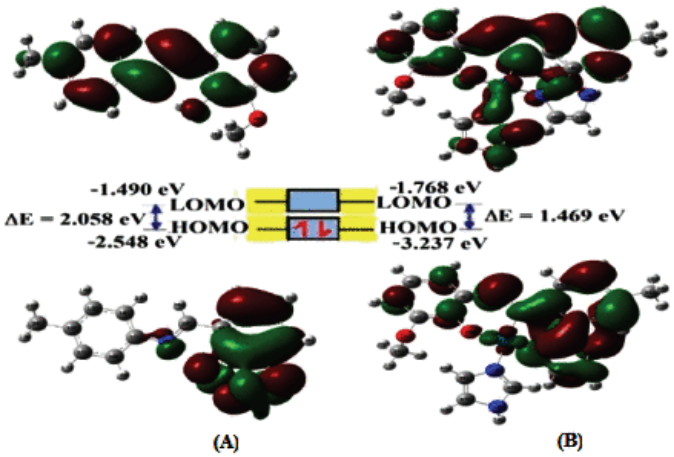

Fig. S-10. HOMO-LUMO structure with energy level diagram of (A) $\mathbf{L}_1$ (B) complex **1**.

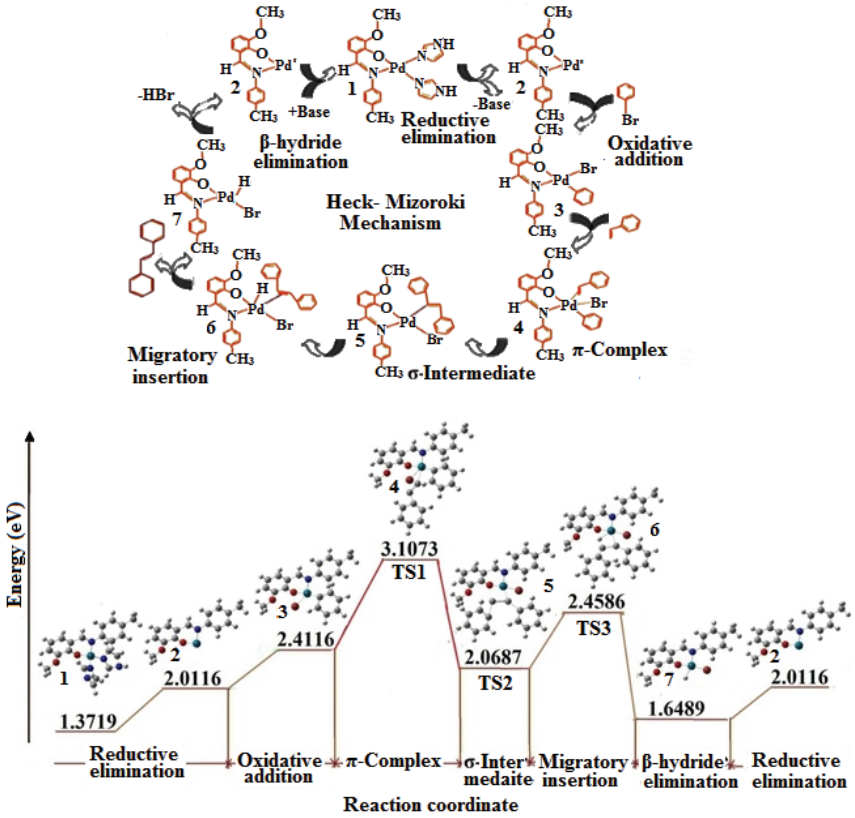

Fig. S-11. Proposed mechanism and energy profiles of *the* full catalytic species using complex **1**.

Journal of the Serbian Chemical Society
JSCS-info@shd.org.rs • www.shd.org.rs/JSCS
J. Serb. Chem. Soc. *86* (3) 283–297 (2021)
JSCS–5421
Original scientific paper

Density functional theory calculation of propane cracking mechanism over chromium (III) oxide by cluster approach

TOYESE OYEGOKE[1,2]*, FADIMATU NYAKO DABAI[1], ADAMU UZAIRU[3] and BABA EL-YAKUBU JIBRIL[1]

[1]*Chemical Engineering Department, Faculty of Engineering, ABU Zaria, Nigeria,* [2]*Laboratoire de Chimie, ENS Lyon, l'Universite de Lyon, 69007, Lyon, France and* [3]*Chemistry Department, Faculty of Physical Sciences, ABU Zaria, Nigeria*

(Received 21 May, revised 18 July, accepted 20 July 2020)

Abstract: The catalyst coking and production of undesired products during the transformation of propane into propylene have been the critical challenges in the on purpose approach of propylene production. The mechanism contributing to this challenge was theoretically investigated through the analysis of cracking reaction routes. The study carried out employed the use of a density functional theory and cluster approach in order to understand the reactions that promote coking of the catalyst and in the search for the kinetic and thermodynamic data of the reaction mechanism involved in the process over Cr_2O_3. The rate-determining step and feasible route that easily promote the production of small hydrocarbons like ethylene, methane, and many others were identified. The study suggests Cr-site substitution or co-feeding of oxygen can aid in preventing deep dehydrogenation in the conversion of propane to propylene. This information will help in improving the Cr_2O_3 catalyst performance and further increase the production yield.

Keywords: catalyst deactivation; olefins; rate-determining step; scission; first principle; coking.

INTRODUCTION

Light alkenes, such as ethylene and especially propylene, are among the essential feedstock or precursors for petrochemical industries, and their global demand (utilization) is increasing day after day.[1] Dehydrogenation involves the transformation of materials like alkanes, which are of low-value, to alkenes (or olefins), which are commonly known for being highly reactive and valuable; examples of the elementary reactions involved in the process includes hydrogen abstraction (that is, propane to propylene) and cracking (that is, propane into lighter hydrocarbons like ethylene). Products like ethylene and propylene do

* Corresponding author. E-mail: ToyeseOyegoke@gmail.com, Toyese.Oyegoke@ens-lyon.fr
https://doi.org/10.2298/JSC200521044O

serve as precursors to the production of aldehydes, alcohols, aromatics, and polymers productions.[2] Propylene is one of the most vital building blocks in the world petrochemical industry, where it finds applications in the production of propylene oxide, isopropanol, polypropylene and acrylonitrile.[3,4] Dehydrogenation is widely known as a highly endothermic process, which requires high temperatures (500 °C and above).[2,5] This kind of high reaction condition often promotes the production of undesired products via the cracking process, which ends up leading to the deactivation of the catalyst after being coked.

In the search for ways of alleviating this challenge that retards the life span of dehydrogenation catalysts, several research works have been carried out to get this problem addressed. For instance, Yan *et al.*[6] was able to employ the use of DFT calculation to study the effectiveness of the gallium oxide for the promotion of propane dehydrogenation. The study proposes a radical mechanism involved with the H abstraction from the propyl species, by Ga sites, and identified it as the rate-determining step. Besides, it was recognized that the propane dehydrogenation over Ga_2O_3(100) majorly takes the approach of direct dehydrogenation mechanism (DDH) and not the oxidative dehydrogenation (ODH) approach.

The study of Ming *et al.*[7] unveils that with the introduction of Sn on Pt catalyst, the alloyed surface was confirmed to have weakened the binding strength of propylene with the surface. The deductions made by Ming *et al.*[7] were found to be in line with Lauri and Karoliina[8] report, which indicated that alloying weakened the binding force of propylene and thereby prevent further dehydrogenation. This further increases the selectivity property of the catalyst[7]. Besides, Lauri and Karoliina's[8] study indicates that the low coking and high selectivity of Pt-Sn alloyed catalyst were due to the lack of active Pt step sites.

Further studies byTimothy[9] suggested that the introduction of Ga into the Pt surface has surface selectivity for olefins improved. It was also reported that PtGa exhibits better activity compared to PtSn alloyed surface.[9] Stephanie *et al.*[10] identified that the rise in hydrogen coverage reduces the binding force holding propylene to the Pt surface and increases the energy barriers towards the further dehydrogenation step. Oyegoke *et al.*[11] studies present that Cr was highly acidic and reactive, and the Cr site was confirmed to be active in the promotion of propane dehydrogenation. Furthermore, many other reports such as: Zhang *et al.*[12] studied V_2O_3; Eduard *et al.*[13] studied the palladium surface; Xie *et al.*[14] studied V_2O_3, etc., supported surface.

Theoretical studies in the literature have been concentrating mainly on the use of Pt catalyst with less attention for the appraisal of chromium oxide catalyst performance and how the catalyst can be improved. Hence, this analysis provides an insight into the thermodynamic and kinetic details of the reaction mechanism involved in the cracking of propane over a chromium oxide via combined use of the DFT and cluster approach. The deductions made from the results obtained

will allow a better understanding of how propane cracking can be inhibited when it is not desired in a reaction.

METHODOLOGY

Theoretical background

Computations were carried out with the use of the density functional theory (DFT) calculation method in the Spartan 18 software package. The calculations were run on an HP 15 Pavilion Notebook (Intel Core i3 Processor @ 1.8 GHz and 6 GB RAM).

The structures of reactant, catalyst, and different intermediate species were built and minimized via the use of the molecular mechanics (MMFF) method to remove strain energy. All the molecular mechanics optimized geometries were subjected to DFT calculation, and the B3LYP method was adopted, ensuring that the structures built do not show the presence of any negative imaginary frequency on the IR spectra result.

Literature confirms, 6-31G* and LANL2DZ basis set as one of the best sets for computations, when dealing with transition metals like chromium,[15] also more cost-effective computationally. Surveys reveal that the 6-31G* basis set is widely considered the best compromise in the terms of accuracy and speed and is the most frequently used basis set available for elements H–Kr. At the same time, heavy atoms are usually modeled *via* the use of the LANL2DZ basis set, which employs a capable core for all atoms larger than Ne[15].

The chromium (III) oxide catalyst cluster or slab used in this study was adopted from Brown *et al.*[16,] which was confirmed to be similar to the one used in the literature[17-19]. Research has shown that the IR spectrum of the cluster model obtained from a DFT study corresponds with the peaks obtained from the experimental analysis of chromium oxide IR spectrum. The study indicated that the cluster model is accurate and consistent.[16,18,20]

The properties of all concerned species were computed. This estimation was carried out via the use of the various statistical thermodynamic models and the use of output data obtained from density functional theory (DFT) computations carried out on Spartan 18. The DFT calculation presents input parameters such as the moment of inertia, total mass, and wavenumbers of the structures considered in this report, which were later used to calculate the free energies. The thermodynamic properties' model employed was adapted from the literature[21-23] and is presented in the Supplementary material to this paper. Besides, the chemical species' thermodynamic properties computations employed the use of the following conditions and models in the computation of Gibbs free energies:

a. Surface gas-phase species. The properties of gas-phase species were calculated accounting for all contributions such as translational, rotational, and vibrational motion effects to the overall species' free energies in the reaction steps:

$$G_{gas} = H_t + H_r + H_v + E_{elect} + ZPE - T(s_t + s_r + s_v) \quad (1)$$

b. Catalyst slab. In the case of the catalyst, all rotational and translation effects were assumed to be zero. This zero was due to the catalyst structure that was taken to be fixed (as a solid catalyst) in the estimation of the catalyst-free energies:

$$G_{cat} \approx E_{elect} + ZPE + H_v - T(s_v) \quad (2)$$

c. Species. The effect of vibrational motion was thoroughly taken. In contrast, two--thirds (2/3) translational and one half (1/2) rotational motion effects were considered in the calculation of free energies for the adsorbate (*i.e.*, the surface species) including the effect of surface configuration on the free energies:

$$G_{ads} = H_v + {}^2/_3H_t + ½H_r + E_{elect} + ZPE - T(s_v + {}^2/_3s_t + ½s_r + s_{config}) \quad (3)$$

An approximation model for 2D gas[24,25] was employed in the treatment of the adsorbate in studies as recommended by Campbell *et al.*,[24] where the adsorbate species account for the loss of a degree of freedom in both translational and rotation motion contributions, that is, hindered translator/hindered rotor approximation as an alternative harmonic oscillation approximation[26,27] which was reported to have underestimated the contribution of rotation and translational motion or effect in the computation of total free energies for adsorbates.

Reaction mechanism scheme

Here, the cracking of the propane was considered to be initiated with the physisorption of propane on the catalyst surface. Followed by the activation of the C–H bond in the propane on the catalyst (*i.e.*, assessing the effect across alpha-carbon and surface sites like Cr–Cr and Cr–O), along with the activation of propane across the C–H bond to give isopropyl (1-propyl or 2-propyl). After this, next step tends to evaluate the chance of the C–C bond scission of the adsorbed species of isopropyl. This study involves the thermodynamic feasibility of the different surface sites such as Cr–Cr, and Cr–O, leading to the production of adsorbed ethyl and methyl. Next was the association of H with methyl species, the further scission of C–H bond in methyl and ethyl species, to give adsorbed methyl (CH_3), methylene (CH_2) and ethylene (C_2H_4). They were evaluated as across different sets of surface sites aforementioned. It is diagrammatically presented in Fig. 1.

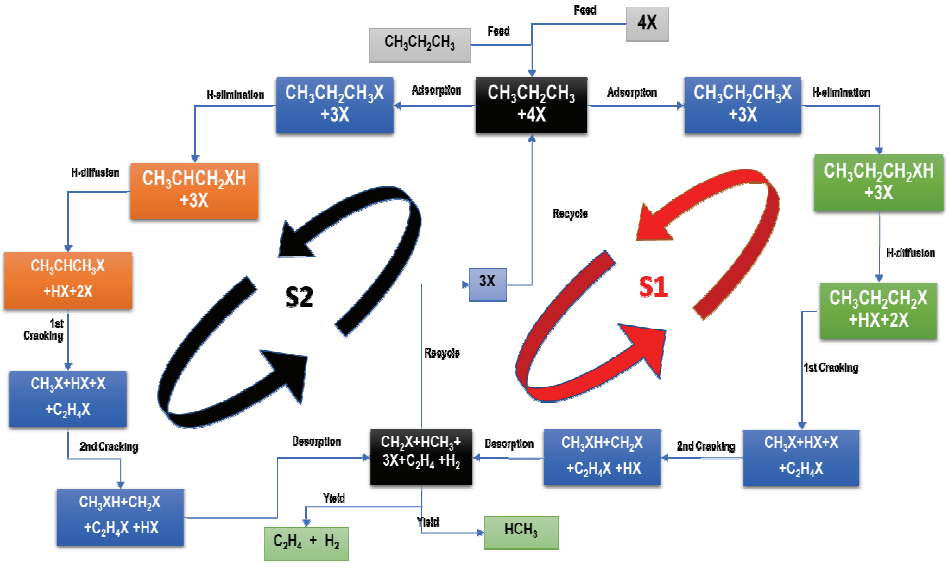

Fig. 1. A representation of the reaction routes studied.

The propane cracking mechanism is presented with the use of chemical equations, where sets of chemical reaction equations (reaction scheme) are employed to display the elementary reaction steps involved in the process in this study.

Propane activated at alpha-carbon (S1):

$$C_3H_8 + X \leftrightarrow CH_3CH_2CH_3X \quad (4)$$

$$CH_3CH_2CH_3X + X \leftrightarrow CH_3CH_2CH_2XH \quad (5)$$
$$CH_3CH_2CH_2XH + X \leftrightarrow CH_3CH_2CH_2X + HX \quad (6)$$
$$CH_3CH_2CH_2X + X \leftrightarrow CH_3X + CH_2CH_2X \quad (7)$$
$$CH_3X + HX \leftrightarrow CH_3XH + X \quad (8a)$$
$$CH_3X + X \leftrightarrow CH_2X + HX \quad (8b)$$
$$CH_3XH \leftrightarrow HCH_3 + X \quad (9a)$$
$$2HX \leftrightarrow H_2 + 2X \quad (9b)$$
$$CH_2CH_2X \leftrightarrow CH_2CH_2 + X \quad (9c)$$

Propane activated at beta-carbon (S2):

$$C_3H_8 + X \leftrightarrow CH_3CH_2CH_3X \quad (10)$$
$$CH_3CH_2CH_3X + X \leftrightarrow CH_3CHCH_3XH \quad (11)$$
$$CH_3CHCH_3XH + X \leftrightarrow CH_3CHCH_3X + HX \quad (12)$$
$$CH_3CHCH_3X + X \leftrightarrow CH_3X + CH_2CH_2X \quad (13)$$
$$CH_3X + HX \leftrightarrow CH_3XH + X \quad (14a)$$
$$CH_3X + X \leftrightarrow CH_2X + HX \quad (14b)$$
$$CH_3XH \leftrightarrow HCH_3 + X \quad (15a)$$
$$2HX \leftrightarrow H_2 + 2X \quad (15b)$$
$$CH_2CH_2X \leftrightarrow CH_2CH_2 + X \quad (15c)$$

It was noted that the isopropyl(s), *i.e.*, 1-propyl activated at the alpha-carbon (S1) or 2-propyl activated at the beta-carbon (S2), that propane can be activated in either ways. This study tries to identify the thermodynamically feasible path that best promotes propane cracking and to identify its potential rate-determining step across the chromium (III) oxide surface. The X represents catalyst surface sites, which could be chromium (Cr) or oxygen (O) sites.

RESULTS AND DISCUSSIONS

Findings from the study of the mechanism involved in the cracking of propane into small hydrocarbon over the chromium oxide catalyst are discussed here. The results obtained for the assessment of different surface sites (such as Cr–Cr and Cr–O), and the point of propane activation (at alpha and beta carbon) were evaluated. The set of results for the reaction energies, energy barrier, including the reaction profiles, was presented in different forms for the provision on insight on the feasible reaction path and the rate-determining step involved in the cracking of the propane.

In Figs. 1–4, the Cr–Cr and Cr–O denote sets of different catalyst surface sites while S1 and S2 imply activation at alpha-carbon and beta-carbon, respectively. The R depicts the reverse reaction while F represents forward reaction. Besides, ‘ads,’ ‘suf1’, ‘diff,’ ‘cra1’, ‘cra2’ and ‘des’ represent the six elementary reaction steps involved in the study, that is, adsorption, first abstraction, diffusion, cracking/scission, further scission of adsorbed species, and desorption respectively.

Reaction energies of the elementary reaction steps

All chemical processes or reactions involve energy changes. In some reactions, these energy changes could either be an increase or a decrease in the system's overall energy. In another reaction, we see it as a change in the temperature. In other reactions, this change is observed when a reaction starts to give off light or when a reaction begins with a presence of light. By the physical law (that is, the law of conservation of energy), it is well known that the total system energy must remain unchanged. Usually, a chemical reaction will release or absorb in the form of light, heat, or both.

Here, the results of the reaction energies are presented, displaying the quantity of energy lost or gained as the reaction proceeds in terms of increase and decrease. Figs. 1 and 2 present the sets of reactions energy collected for the elementary reaction making up the process. This energy lost or gain was obtained via use of the difference in the amounts of stored chemical energy between the products and the reactants for both forward and backward reactions.

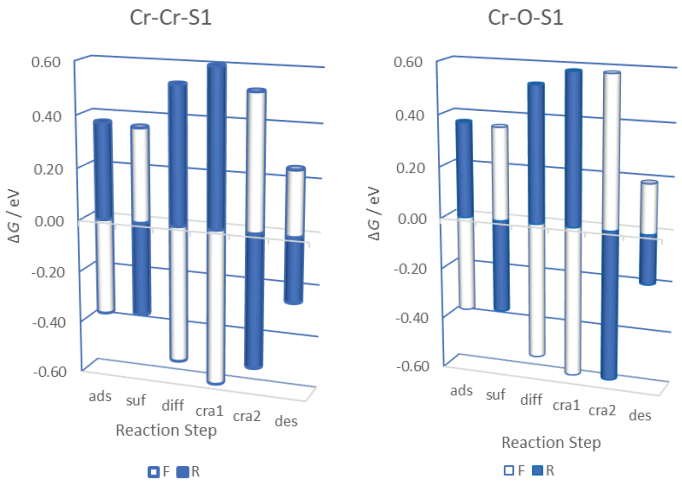

Fig. 2. Reaction energy, Δ*G* / eV, for the reaction path across: a) Cr–Cr and b) Cr–O sites activated at the alpha-carbon (S1) atom of the propane.

The study of the results presented for the forward (F) reactions in Fig. 2a for the propane cracking across Cr–Cr surface sites activated at alpha carbon (S1) indicated that propane adsorption (ads), H abstraction (suf), H diffusion (diff), cracking of isopropyl (cra1), second cracking (cra2) and desorption (des) steps displayed –0.37, 0.36, –0.53, –0.60, 0.52 and 0.25 eV, respectively. The results show that propane adsorption (ads), H diffusion (diff), and cracking of isopropyl (cra1) steps displayed negative reaction energies, which implies that they are exothermic steps. Whereas H abstraction (suf), second cracking (cra2), and des-

orption (des) steps displayed positive reaction energies, which indicated that they are endothermic steps.

The reaction energies of the elementary steps evaluated for Cr–O sites activated at alpha carbon (S1) displayed –0.37, 0.36, –0.53, –0.58, 0.58 and 0.19 eV for the forward (F, *i.e.*, while bars in Fig. 2b) reaction for propane adsorption (ads), H abstraction (suf), H diffusion (diff), cracking of isopropyl (cra1), second cracking (cra2) and desorption (des) steps respectively. Fig. 2b displays the results obtained for the evaluation of propane cracking across the Cr–O sites. The results displayed similar kind of negative reaction energies for the propane adsorption (ads), H diffusion (diff), and cracking of isopropyl (cra1) steps indicating that they are exothermic steps as well. Just as it was observed for the H abstraction (suf), second cracking (cra2) and desorption (des) step that showed positive reaction energy, which suggested that they are endothermic steps as well.

For propane activated at beta carbon (S2), studies across the Cr-Cr sites present the reaction energies of the elementary steps as -0.37, 0.26, -0.45, -0.58, 0.52 and 0.25 eV while Cr–O presents its reaction energies for its elementary reaction steps as -0.37, 0.34, -0.48, -0.61, 0.58 and 0.19 eV for the forward (F *i.e.* white bars in Fig. 3) reaction for propane adsorption (ads), H abstraction (suf), H diffusion (diff), cracking of isopropyl (cra1), second cracking (cra2) and desorption (des) steps respectively.

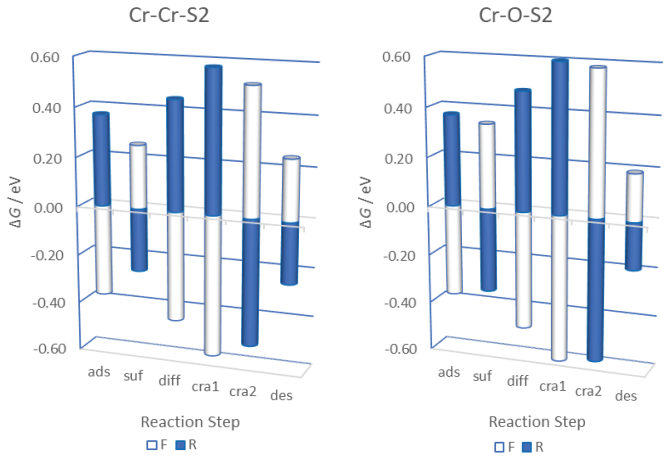

Fig. 3. Reaction energy, Δ*G* / eV, for the reaction path across: a) Cr–Cr and b) Cr–O sites activated at the beta-carbon (S2) atom of the propane.

Fig. 3 displays the results obtained in the evaluation of propane cracking across the Cr–Cr and Cr–O sites. The results displayed similar kind of negative reaction energies for the propane adsorption (ads), H diffusion (diff) and cracking of isopropyl (cra1) steps indicating that they are exothermic steps as well. Also, it

was observed that the H abstraction (suf), second cracking (cra2), and desorption (des) steps exhibited positive reaction energy, which suggested that they are endothermic steps.

The results obtained for H abstraction (suf) presented in Fig. 3 indicated that the reaction energy for Cr–Cr sites was lower when compared with that of the Cr–O sites. For H diffusion and first cracking step, the reaction energy for the Cr–Cr site was found to be less negative compared to Cr–O sites. The second cracking and desorption step showed that the reaction energy of the Cr–Cr site is much lower compared to Cr–O sites except for the desorption step, which was the reverse.

The assessment of the reaction energies across the different surface sites (depicting different reaction routes) indicated that all the propane adsorption (ads), H diffusion (diff), and cracking of isopropyl (cra1) steps are exothermic steps while the H abstraction (suf), second cracking (cra2) and desorption (des) steps were found to be endothermic steps.

The energy barrier of the elementary reaction steps

The results collected for this study are diagrammatically represented in Figs. 4 and 5. These figures display the results for the Cr–Cr and Cr–O sites, which indicate the different energy barriers for the different reaction steps in the cracking/scission of propane.

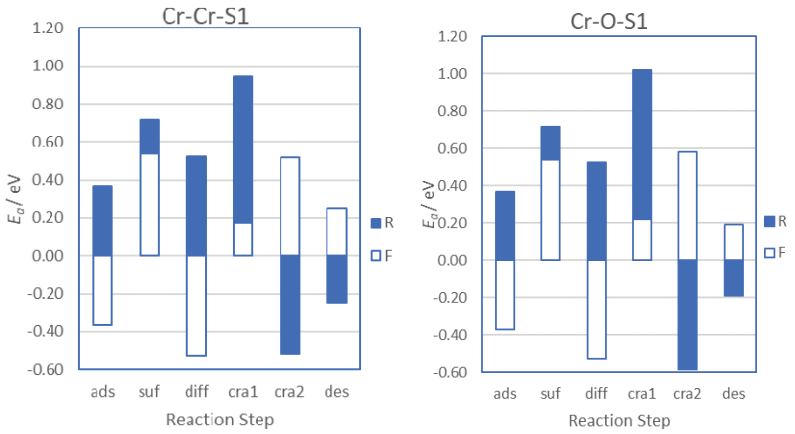

Fig. 4. Energy barrier, E_a / eV, for the surface reaction steps across: a) Cr–Cr and b) Cr–O sites activated at the alpha-carbon (S1) atom of the propane.

Fig. 4 shows that all the reaction steps involved in the propane adsorption (ads), and hydrogen diffusion (diff) indicated a negative energy barrier. The findings imply that they are barrierless steps, unlike the other steps like hydrogen abstraction (suf), first cracking (cra1), second cracking (cra2) and desorption (des) steps, which showed a positive activation energy (or energy barrier).

Further evaluation of the energy barriers across the Cr–Cr and Cr–O for the S1 route indicated that similar kind of energy barriers were displayed for adsorption (ads, *i.e.*, –0.37 eV), H abstraction (suf, *i.e.*, 0.54 eV), and H diffusion (diff, *i.e.*, 0.53 eV) but varying energy barriers for other steps. Nevertheless, the other steps, the 1st cracking (cra1) step for Cr–Cr site (0.17 eV) were found to show a lower energy barrier compared Cr–O (0.22 eV) while for the second cracking (cra2) and desorption (des) step, Cr–Cr site (0.52 and 0.25 eV) energy barrier was found to be higher than for the Cr–O sites (0.58 and 0.19 eV).

The assessment of the results presented for the energy barriers across the Cr–Cr and Cr–O sites in the route of S1 (that is, the path that activate propane at the beta-carbon atom) revealed that the energy barriers displayed for adsorption (ads), H abstraction (suf), H diffusion (diff), 1st cracking (cra1), 2nd cracking (cra2) and desorption (des) step are –0.37, 0.54, –0.53, 0.17, 0.52 and 0.25 eV, and –0.37, 0.54, –0.53, 0.22, 0.58 and 0.19 eV, respectively, for the sites.

The results in Fig. 5 show that both the propane adsorption (ads), and H diffusion (diff) steps displayed a negative energy barrier for their forward reactions. The results imply that the steps are barrierless. In contrast, the other steps like hydrogen abstraction (suf), first cracking (cra1), second cracking (cra2), and desorption (des) steps showed a positive activation energy (or energy barrier), which indicated that they would demand energy for these steps to proceeds.

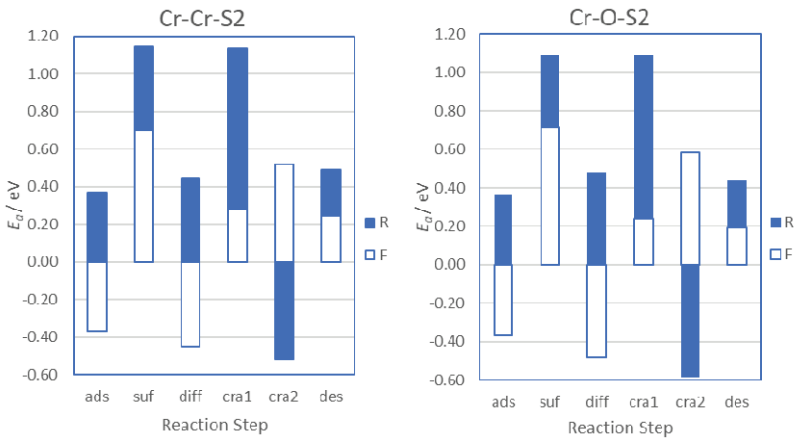

Fig. 5. Energy barriers, E_a / eV, for the surface reaction steps across: a) Cr–Cr and b) Cr–O path sites activated at the beta-carbon (S2) atom of the propane.

The evaluation of the entire energy barriers in the Cr-Cr (S1), Cr-O (S1), Cr–Cr (S2) and Cr–O (S2) reaction routes indicate that H abstraction (*i.e.*, propane activation to give isopropyl) shows the highest energy barrier followed by the 2nd cracking step. Across the S1 route, Cr–Cr sites displayed the lowest barrier (0.17 eV) for the first cracking step (cracking initiation) that promotes crack-

ing while Cr–O shows a higher barrier (0.22 eV) in Fig. 4. For the S2 route, the Cr-Cr sites displayed a higher barrier of 0.28 eV, while the Cr–O site displayed 0.24 eV in Fig. 5. This implies that across all reaction's routes, the Cr–Cr sites in the S1 route showed the lowest barrier (that will require the least energy) for the cracking to get initiated. The reaction routes along the path of the S1 scheme indicated that the path which interacted through the Cr–Cr sites would be thermodynamically feasible.

The findings indicate that the activity of Cr–Cr along the route of the S1 scheme will tend to promote propane cracking due to its lower energy barrier in its routes. It could also imply that surface with more Cr sites will better crack propane. Furthermore, it indicates that the Cr site remains an active component in the cracking of propane. That is why the surface dominated with Cr sites tends to promote deep dehydrogenation or cracking, which has been traced to the activity of the site. These findings were found to agree with the report of Jibril,[28] which indicates that the activeness of the Cr site greatly influences the dehydrogenation of propane into propylene.

Evaluation of thermodynamic feasibility of a different reaction route or path and the identification of potential rate-limiting steps in the cracking process

The assessment of the six elementary steps, involved in the cracking of propane across the Cr–Cr and Cr–O sites on the route of S1, indicate that the propane adsorption (ads), H abstraction (suf), H diffusion (diff), and second cracking steps displayed a similar trend.

However, it was observed that the 1st cracking step displayed a lower barrier for the Cr–Cr site, while a higher barrier was identified for the Cr–O. Similarly, a lower barrier was recorded for the Cr–Cr site while a higher barrier was displayed for the Cr–O site for both 2nd cracking and desorption steps. The findings are evident in Fig. 6, which displayed the profiles for the different reaction routes. The reaction routes along the path of the S1 scheme indicated that the path which interacted through the Cr–Cr sites would be thermodynamically feasible.

The study of propane cracking along the route of S2 indicated that participation of the Cr–Cr site displayed lower energy profiles in all steps of the reaction. It is graphically displayed in Fig. 7. The findings obtained from the results presented the reaction profiles in Fig. 7 indicated that the Cr–Cr sites would be more thermodynamically feasible when compared to Cr–O site in the assessment of scheme S2 routes due to its lower energy barriers displayed.

In general, it was primarily found that most of the surface species adsorbed on Cr–Cr sites displayed negative energy compared to those adsorbed on Cr–O sites, which is evident in Figs. 6 and 7. The findings, however, imply that species tend to be more stable on the Cr–Cr site than on the Cr–O sites. In other words, it can be said that the binding force holding the species to the Cr–Cr sites is

stronger than on the species adsorbed across the Cr–O sites. This force has made desorption energy barrier to be lower for Cr–O sites when compared to Cr–Cr sites. This strong force on the Cr–Cr sites, thereby promotes further cracking, which end-up leading to the coking of the sites.

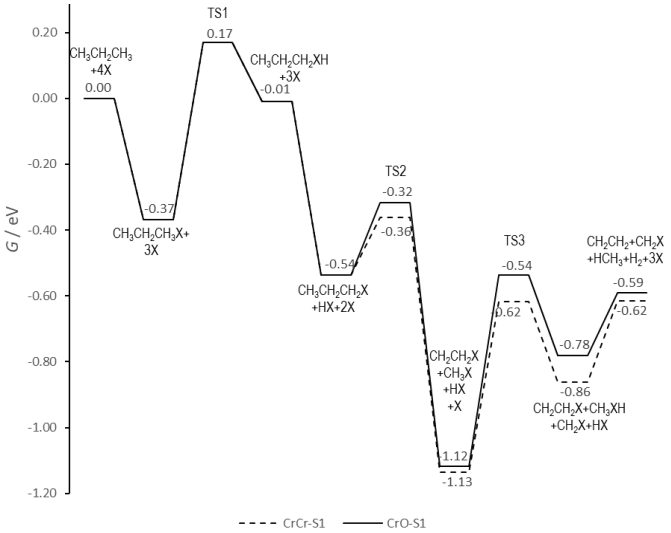

Fig. 6. Propane cracking reaction path across Cr–Cr (broken lines) and Cr–O (continuous line) sites using the reaction scheme S1.

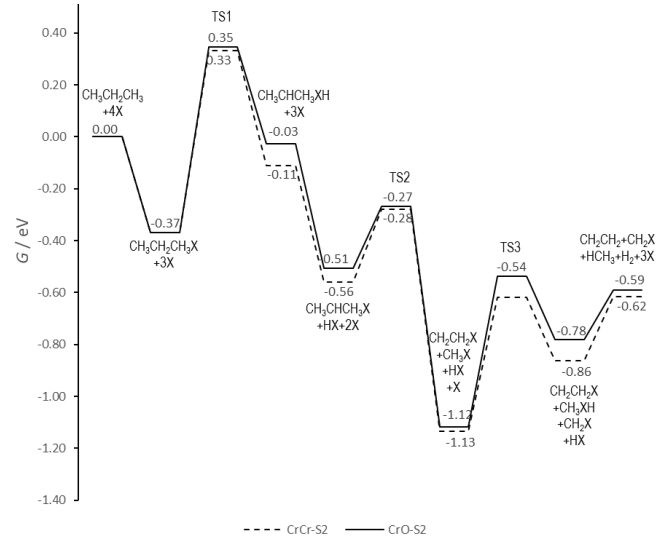

Fig. 7. Propane cracking reaction path across Cr–Cr (broken lines) and Cr–O (continuous line) sites using the reaction scheme S2.

As a way of preventing cracking or coking during H abstraction processes when cracking of the molecules or species is not desired, this study suggests, Cr site substitution, as a way to aid in alleviating the production of undesired products such as coke, methylene (CH_2), methyl (CH_3) and ethyl (C_2H_5) during the use of chromium oxide catalyst. Another way of preventing the cracking when it is not desired, Stephanie *et al.*[10] in their studies identified the co-feeding of propane with hydrogen, which will primarily prevent cracking.

Therefore, the most thermodynamically favored reaction pathway, for the cracking or scission of propane into small hydrocarbons on chromium oxide, would be Cr–Cr (S1) as it was found to have the lowest energy barrier for the H abstraction and also showed a lower energy barrier for the cracking initiation step. These findings indicate that Cr–Cr (S1) will effectively promote the cracking of propane. The H abstraction step (where C–H bond activation of propane at the alpha (or terminal) carbon takes place on Cr site) would be the potential rate-determining step (RDS) due to its significant energy barrier displayed in its profile for Cr–O (S1) in Fig. 4. This finding showed a similar RDS to that of Yu-Jue *et al.*,[29] which confirms the first C–H activation step (*i.e.*, first abstraction step) as its RDS for propane dehydrogenated on vanadium oxide. However, the 1st cracking step's lower energy barrier enables cracking to hold with less energy demand along such a reaction route.

CONCLUSIONS

The investigation into the cracking of propane to small hydrocarbon on a chromium oxide catalyst via the use of a DFT study approach was carried out. The study was done in order to understand the reaction routes that promote the production of products like coke, methylene (CH_2), methyl (CH_3), ethyl (C_2H_5) and many others when such kind of products are not desired.

The study identified that the reaction route where propane gets activated at the alpha-carbon (S1) across the Cr–Cr sites, as the most thermodynamically feasible reaction route, which would be the best at promoting the production of cracked products. Moreover, the H abstraction (*i.e.*, C–H bond activation) was found to be RDS along that reaction route. It was also identified that the strong force that binds species strongly to Cr sites aid in promoting the cracking of the species.

The understanding gained from this investigation reveals the reaction path that has to be inhibited the production of propylene, BTX and many others where crack species/products are not desired. It is therefore recommended that the dormancy of Cr sites across the surface of the catalyst could be reduced *via* the use of oxygen/oxidants or substitution of some Cr sites with metals that would best promote the desired products.

NOMENCLATURE

F	Forward reaction	E_a	Activation energy or energy barrier
R	Reverse reaction	E_{elect}	Electronic energy
ads	Adsorption step	S_{config}	Configurational entropy
suf	H abstraction	ZPE	Zero-point energy
diff	H diffusion	T	Temperature
cra1	1st cracking step	$\nu_{n,i}$ or ν_i	Wavenumbers of species
cra2	2nd cracking step	k_g	Boltzmann constant
des	Desorption step	h	Planck constant
vib.	Vibration effect/contribution	m	Mass of specie
transl	Translation effect/contribution	P_0	Standard pressure
rot	Rotation effect/contribution	$I_{r,linear}$, I_a, I_b, I_c	Moment of inertia
R	Gas constant	ρ_r	Symmetry number of the species
ΔG	Reaction energy	^{o}	Standard state
G	Gibbs energy		
H_i	Enthalpy (where i is either vib (v), transl (t) or rot (r))		
s_i	Entropy (where i is either vib (v), transl (t) or rot (r))		

SUPPLEMENTARY MATERIAL

The additional data are available electronically at the pages of journal website: http://www.shd.org.rs/JSCS/, or from the corresponding author on request.

Acknowledgement. The first author wishes to acknowledge the support of the Petroleum Technology Development Fund Abuja, Nigeria, for funding his program.

И З В О Д

ИЗРАЧУНАВАЊЕ ТЕОРИЈОМ ФУНКЦИОНАЛА ГУСТИНЕ МЕХАНИЗМА КРЕКОВАЊА ПРОПАНА НА ХРОМ (III)–ОКСИДУ КЛАСТЕРСКИМ ПРИСТУПОМ

TOYESE OYEGOKE[1,2], FADIMATU NYAKO DABAI[1], ADAMU UZAIRU[3] и BABA EL-YAKUBU JIBRIL[1]

[1]Chemical Engineering Department, Faculty of Engineering, ABU Zaria, Nigeria, [2]Laboratoire de Chimie, ENS Lyon, l'Universite de Lyon, 69007, Lyon, France u [3]Chemistry Department, Faculty of Physical Sciences, ABU Zaria, Nigeria

Таложење кокса на катализатору и производња нежељених производа током трансформисања пропана у пропилен представља велики изазов наменском приступу производње пропилена. Механизам који доприноси решавању овог проблема је теоријски проучаван преко реакционих путева крековања. Спроведена студија користи DFT и кластерски приступ, да би се разумеле реакције које доприносе коксовању катализатора, као и у потрази за кинетичким и термодинамичким подацима реакционог механизма који је присутан у процесима на Cr_2O_3. Идентификовани су ступањ који одређује брзину реакције (RDS) и могући путеви који лако промовишу производњу малих угљоводоника као што су етилен, метан и многи други. Студија сугерише, супституцију Cr-места или додавање кисеоника, као начин да се помогне спречавање дубоке дехидрогенизације код конверзије пропана у пропилен. Ова информација ће помоћи да се побољша перформанса Cr_2O_3 катализатора и даље побољша принос производа.

(Примљено 21. маја, ревидирано 18. јула, прихваћено 20. јула 2020)

REFERENCES

1. S. Asadi, L. Vafi, R. Karimzadeh, *Micropor. Mesopor. Mat.* **255** (2018) 253 (https://dx.doi.org/10.1016/j.micromeso.2017.07.018)
2. H. A. Wittcoff, B. G. Reuben, J. S. Plotkin, *Industrial Organic Chemicals*, John Wiley & Sons, Hoboken, FL, 2000, p. 211 (https://dx.doi.org/10.1002/0471651540)
3. S. Budavari, *Propylene - The Merck Index*, Merck & Co., Kenilworth, NJ, 1996, p. 1
4. Y. Ren, F. Zhang, W. Hua, Y. Yue, Z. Gao, *Catal. Today* **148** (2009) 3 (https://dx.doi.org/10.1016/j.micromeso.2017.07.018)
5. J. C. Philip, *Survey of Industrial Chemistry*, Springer, Berlin, 2001, p. 2
6. L. Yan, Z. H. Li, J. Lu, K. N. Fan, *J. Phys. Chem., C* **112** (2008) 51 (https://dx.doi.org/10.1021/jp807864z)
7. Y. Ming-Lei, Y. A. Zhu, X. G. Zhou, Z. J. Sui, D. Chen, *ACS Catal.* **2** (2012) 1247 (https://dx.doi.org/10.1021/cs300031d)
8. N. Lauri, H. Karoliina, *ACS Catal.* **3** (2013) 3026 (https://dx.doi.org/10.1021/cs400566y)
9. H. Timothy, *Computational study of the catalytic dehydrogenation of propane on Pt and Pt3Ga catalyst*, Ghent University, Ghent, 2015, p. 15
10. S. Saerens, M. K. Sabbe, V. V. Galvita, E. A. Redekop, M.-F. Reyniers, G. B. Marin, *ACS Catal*. **7** (2017) 7495 (https://dx.doi.org/10.1021/acscatal.7b01584)
11. T. Oyegoke, F. N. Dabai, A. Uzairu, B. Jibril, *B. J. Pure Appl. Sci.* **11** (2018) 178 (https://dx.doi.org/10.4314/bajopas.v11i1.29S)
12. J. Zhang, Z. R-Jia, C. Q-Yu, S. Z-Jun, Z. X-Gui, Z. Y-An, *Cat. Today* (2020), in press (https://dx.doi.org/10.1016/j.cattod.2020.02.023)
13. E. Araujo-Lopez, L. Joos, B. D. Vandegehuchte, D. I. Sharapa, F. Studt, *The J. of Phys. Chem. C* **124** (2020) 3171 (https://dx.doi.org/10.1021/acs.jpcc.9b11424)
14. Y. Xie, R. Luo, G. Sun, S. Chen, Z. J. Zhao, R. Mu, *RSC Chem. Sci.* **11** (2020) 3845 (https://dx.doi.org/10.1039/C8CY00564H)
15. J. H. Warren, *A guide to molecular mechanics and quantum chemical calculations*, Wavefunction, Irvine, CA, 2003, p. 89
16. P. Brown, J. Forsyth, E. Lelievre-Berna, F. Tasset, *J. Phys.: Condens. Matter* **14** (2002) 1957 (https://dx.doi.org/10.1088/0953-8984/14/8/323)
17. W. Yanbiao, G. Xinxin, W. Jinla, *Phys. Chem. Chem. Phys.* **12** (2010) 2471 (https://dx.doi.org/10.1039/B920033A)
18. C. Compere, D. Costa, L. Jolly, E. Mauger, C. Gessner–Prettre, *New J. Chem.* **24** (2000) 993 (https://dx.doi.org/10.1039/B005313I)
19. S. Veliah, K. Xiang, R. Pandey, J. Recio, J. Newsam, *J. Phys. Chem., B* **102** (1997) 1126 (https://dx.doi.org/10.1021/jp972546m)
20. T. Oyegoke, F. N. Dabai, A. Uzairu, B. Y. Jibril, *Eur. J. Mat. Sci. Eng*. **5** (2020) 173 (https://dx.doi.org/10.36868/ejmse.2020.05.04.173)
21. N. M. Laurendeau, *Statistical Thermodynamics: Fundamentals and Applications*, Cambridge University Press, Cambridge, 2005
22. I. Kennedy, H. Geering, M. Rose, A. Crossan, *Entropy* **21** (2019) 454 (https://dx.doi.org/10.3390/e21050454)
23. T. L. Hill, *An Introduction to Statistical Thermodynamics,* Dover Publications Inc., New York, 1960
24. C. T. Campbell, L. H. Sprowl, L. Árnadóttir, *J. Phys. Chem.* **120** (2016) 10283 (https://dx.doi.org/10.1021/acs.jpcc.6b00975)
25. A. Savara, *J. Phys. Chem., C* **117** (2013) 15710 (https://dx.doi.org/10.1021/jp404398z)

26. L. H. Sprowl, C. T. Campbell, L. Arnadottir, *J. Phys. Chem., C* **121** (2017) 17 (https://dx.doi.org/10.1021/acs.jpcc.7b03318)
27. L. H. Sprowl, C. T. Campbell, L. Arnadottir, *J. Phys. Chem., C* **120** (2016) 9719 (https://dx.doi.org/10.1021/acs.jpcc.5b11616)
28. B. Y. Jibril, *Appl. Catal., A* **264** (2004) 193 (https://dx.doi.org/10.1021/ie000285o)
29. D. Yu-Jue, Z. H. Li, K. N. Fan, *J. Mol. Catal., A* **379** (2013) 122 (https://dx.doi.org/10.1016/j.molcata.2013.08.011)
30. P. Wang, S. N. Steinmann, G. Fu, C. Michel, P. Sautet *ACS Catal.* **7** (2017) 1955 (https://dx.doi.org/10.1021/acscatal.6b03544)
31. F. Maldonado, A. Stashans, *Surface Rev. Lett.* **23** (2016) 1650037 (https://dx.doi.org/10.1142/S0218625X16500372)
32. Z. J. Zhao, T. Wu, C. Xiong, G. Sun, R. Mu, L. Zeng, J. Gong, *Angew. Chem. Int. Ed.* **57** (2018) 6791 (https://dx.doi.org/10.1002/anie.201800123).

Journal of the Serbian Chemical Society
JSCS-info@shd.org.rs • www.shd.org.rs/JSCS
J. Serb. Chem. Soc. 86 (3) S84–S86 (2021)
Supplementary material

SUPPLEMENTARY MATERIAL TO

Density functional theory calculation of propane cracking mechanism over chromium (III) oxide by cluster approach

TOYESE OYEGOKE[1,2]*, FADIMATU NYAKO DABAI[1], ADAMU UZAIRU[3] and BABA EL-YAKUBU JIBRIL[1]

[1]*Chemical Engineering Department, Faculty of Engineering, ABU Zaria, Nigeria,* [2]*Laboratoire de Chimie, ENS Lyon, l'Universite de Lyon, 69007, Lyon, France and* [3]*Chemistry Department, Faculty of Physical Sciences, ABU Zaria, Nigeria*

J. Serb. Chem. Soc. 86 (3) (2021) 283–297

LIST OF RELEVANT MODELS EMPLOYED IN THIS STUDY

a) Enthalpy contributions

$$H_{\text{linear}}(T)=\left[\frac{5}{2}RT\right]_{\text{trans}}+[RT]_{\text{rot}}+\left[RT\sum_{\text{i}}\frac{h\nu_{\text{i}}}{k_{\text{B}}T}\frac{e^{-\frac{h\nu_{\text{i}}}{k_{\text{B}}T}}}{1-e^{\frac{h\nu_{\text{i}}}{k_{\text{B}}T}}}\right]_{\text{vib}} \quad (1)$$

$$H_{\text{non-linear}}(T)=\left[\frac{5}{2}RT\right]_{\text{trans}}+\left[\frac{3}{2}RT\right]_{\text{rot}}+\left[RT\sum_{i}\frac{h\nu_{i}}{k_{B}T}\frac{e^{-\frac{h\nu_{\text{i}}}{k_{\text{B}}T}}}{1-e^{\frac{h\nu_{\text{i}}}{k_{\text{B}}T}}}\right]_{\text{vib}} \quad (2)$$

$$\text{ZPE}=\frac{1}{2}\sum\nu_{\text{n, i}} \quad (3)$$

b) Entropy contributions

$$s_{\text{linear}}(T)=R\left[ln\frac{\{(2\pi m/h^2\})^{\frac{3}{2}}(k_{\text{B}}T)^{\frac{5}{2}}}{P_{\text{o}}}+\frac{5}{2}\right]_{\text{trans}}+R\left[ln\frac{8\pi^2k_{\text{B}}TI_{\text{r, linear}}}{h^2\rho_{\text{r}}}+1\right]_{\text{rot}}+$$
$$+\left[R\sum_{i}\frac{\frac{h\nu_{i}}{k_{B}T}}{e^{\frac{h\nu_{\text{i}}}{k_{\text{B}}T}}-1}-R\sum_{\text{i}}ln\left(1-e^{\frac{h\nu_{\text{i}}}{k_{\text{B}}T}}\right)\right]_{\text{vib}} \quad (4)$$

* Corresponding author. E-mail: ToyeseOyegoke@gmail.com, Toyese.Oyegoke@ens-lyon.fr

$$s_{\text{non-linear}}(T) = R\left[ln\frac{(2\pi m/h^2)^{\frac{3}{2}}(k_{\text{B}}T)^{\frac{5}{2}}}{P_{\text{o}}} + \frac{5}{2} \right]_{\text{trans}} + R\left[ln\frac{8\pi^2(2\pi k_{\text{B}})^{\frac{3}{2}}(T)^{\frac{3}{2}}(I_{\text{a}}I_{\text{b}}I_{\text{c}})^{\frac{1}{2}}}{h^3\rho_{\text{r}}} + \frac{3}{2} \right]_{\text{rot}} + \left[R\sum_{\text{i}} \frac{h\nu_{\text{i}}}{k_{\text{B}}T} - R\sum_{\text{i}} ln\left(1 - e^{\frac{h\nu_{\text{i}}}{k_{\text{B}}T}}\right) \right]_{\text{vib}} \quad (5)$$

$$S_{config} = R\left[\ln\left(\frac{1-\theta}{\theta}\right) - \frac{ln(1-\theta)}{\theta} \right] \quad (6)$$

$$S_{\text{config}} = 1.39R \quad (7)$$

TABLE S-I. The activation and reaction energies across Cr-Cr, Cr-O sites for scheme S1

Step	E_a / eV				ΔG / eV			
	CrCr-S1		CrO-S1		CrCr-S1		CrO-S1	
	F	R	F	R	F	R	F	R
ads	-0.37	0.37	-0.37	0.37	-0.37	0.37	-0.37	0.37
suf	0.54	0.18	0.54	0.18	0.36	-0.36	0.36	-0.36
diff	-0.53	0.53	-0.53	0.53	-0.53	0.53	-0.53	0.53
cra1	0.17	0.77	0.22	0.80	-0.60	0.60	-0.58	0.58
cra2	0.52	-0.52	0.58	-0.58	0.52	-0.52	0.58	-0.58
des	0.25	-0.25	0.19	-0.19	0.25	-0.25	0.19	-0.19

TABLE S-II. The activation and reaction energies across Cr-Cr, Cr-O sites for scheme S2

Step	E_a / eV				ΔG / eV			
	CrCr-S2		CrO-S2		CrCr-S2		CrO-S2	
	F	R	F	R	F	R	F	R
Ads	-0.37	0.37	-0.37	0.37	-0.37	0.37	-0.37	0.37
Suf	0.70	0.45	0.72	0.38	0.26	-0.26	0.34	-0.34
Diff	-0.45	0.45	-0.48	0.48	-0.45	0.45	-0.48	0.48
cra1	0.28	0.86	0.24	0.85	-0.58	0.58	-0.61	0.61
cra2	0.52	-0.52	0.58	-0.58	0.52	-0.52	0.58	-0.58
des	0.25	0.25	0.19	0.25	0.25	-0.25	0.19	-0.19

TABLE S-III. Free energies of the species computed

Species	Chemical formula	Symbols	H^o / eV	S^o / eV K^{-1}	G^o / eV
1st Dehy. CrCr	TS (C_3H_7*H)	TS11	3.1223	0.0017	2.6166
1st Dehy. CrO	TS (C_3H_7*H)	TS12	2.9888	0.0016	2.5210
1st Dehy. CrCr	TS (C_3H_7*H)	TS21	3.1213	0.0015	2.6845
1st Dehy. CrO	TS (C_3H_7*H)	TS22	3.1076	0.0014	2.6985
Cracking of propyl-1, CrCr	TS (C_2H_4*CH_3)	TScp1CrCr	2.7798	0.0016	2.2955
Cracking of propyl-1, CrO	TS (C_2H_4*CH_3)	TScp1CrO	2.7942	0.0015	2.3414
Cracking of propyl-2, CrCr	TS (C_2H_4*CH_3)	TScp2CrCr	2.8599	0.0016	2.3795
Cracking of propyl-2, CrO	TS (C_2H_4*CH_3)	TScp2CrO	2.7539	0.0012	2.3903
H Diff., CrO	TS (H*CH_3)	TS_Cat_Cr(M)O(H)_o	1.4611	0.0012	1.1083
Methane	CH_4	M	1.3356	0.0021	0.7112
Cracking of methyl, Cr	TS (H*CH_2)	TS_Cat_Cr(M)	1.3292	0.0008	1.0794
Cracking of methyl, O	TS (H*CH_2)	TS_Cat_O(M)	1.0145	0.0012	0.6684

TABLE S-IV. Free energies of the species computed (Note: "*" signifies that it is surface species)

Species	Chemical formula	Symbols	H^o / eV	S^o / eV K^{-1}	G^o / eV
Catalyst	Cr_2O_3	X	0.3390	0.00031	0.2450
Propane	C_3H_8	R	2.9814	0.0029	2.1062
Phys. Propane	*C_3H_8	RX	3.4571	0.0049	1.9828
Propyl-1&H, CrCr	$CH_3CH_2CH_2$**H	UHX11	3.2556	0.0033	2.2601
Propyl-1&H, CrO	$CH_3CH_2CH_2$**H	UHX12	3.3686	0.0034	2.3418
Propyl-2&H, CrCr	CH_3CH*CH_3H	UHX21	3.2461	0.0034	2.2392
Propyl-2&H, CrO	CH_3CH*CH_3*H	UHX22	3.3644	0.0035	2.3234
Hydrogen, Cr	*H	HX1	0.5841	0.0023	-0.1063
Hydrogen, O	*H	HX2	0.6949	0.0025	-0.0611
Propyl-1, CrCr	$CH_3CH_2CH_2$*	UX11	3.0783	0.0032	2.1216
Propyl-1, CrO	$CH_3CH_2CH_2$*	UX12	3.1534	0.0033	2.1625
Propyl-1, OCr	$CH_3CH_2CH_2$*	UX21	3.0740	0.0033	2.0991
Propyl-1, OO	$CH_3CH_2CH_2$*	UX22	3.1344	0.0033	2.1509
Hydrogen gas	H_2	H2	0.3661	0.0015	-0.0857
Ethylene	C_2H_4	ET	1.5018	0.0024	0.7760
Methyl, CrO	*CH_3	Cat_cr(M)_o	1.4670	0.0028	0.6443
Ethyliene, CrCr	*C_2H_4	Cat_Cr(Ey)Cr_o	1.9491	0.0028	1.1235
Ethyliene, CrO	*C_2H_4	Cat_O(Ey)Cr_o	1.9828	0.0028	1.1400
Methyl & H, OO	H*CH_3	Cat_O(M)O(H)_o	1.7226	0.0030	0.8273
Methyl & H, CrO	H*CH_3	Cat_Cr(M)O(H)_o	1.7482	0.0030	0.8671
H Diff., CrO	TS (H*CH_3)	TS_Cat_Cr(M)O(H)_o	1.4611	0.0012	1.1083
Methane	CH_4	M	1.3356	0.0021	0.7112
Methyliene, Cr	CH_2	Cat_Cr(My)Cr	1.1254	0.0027	0.3339
Methyliene, O	CH_2	Cat_O(My)Cr	1.1671	0.0027	0.3595

Journal of the Serbian Chemical Society
JSCS-info@shd.org.rs • www.shd.org.rs/JSCS
J. Serb. Chem. Soc. *86* (3) 299–311 (2021)
JSCS–5422
Original scientific paper

Electrochemical formation of ion-conducting oxo-phosphate-molybdate polymer on aluminium

HUSSEIN HUSSEIN[1]*, SWETLANA POPOVA[2], IRINA FROLOVA[2] and MARINA LOPUKHOVA[2]

[1]*Department of Chemistry and Chemical Technology of Materials, Yuri Gagarin State Technical University of Saratov, Saratov, Russia and* [2]*Engels Technological Institute (branch) of Yu. Gagarin Saratov State Technical University, Engels, Russia*

(Received 13 September, revised 27 November, accepted 8 December 2020)

Abstract: The state of the electrochemical behaviour of the Al electrode in aqueous solutions containing $Na_2MoO_4 + H_3PO_4$ + chitosan was investigated by methods of currentless chronopotentiometry, chronoamperometry, optical and scanning electron microscopy. The modification of the surface polymolybdate phosphate layers was carried out in a potentiostatic mode in the potentials range from –1 to –3 V and polarization time (from 15 to 90 min). The elemental composition of the surface layer of the metal before and after cathodic polarization were investigated. The electrochemical formation of matrix polymeric structures from ion-conducting (H^+, Na^+) heteronuclear polymolybdate and polyphosphate-molybdate complexes of double salts $Na_6Al_nMo_{7-n}O_{24}$ and $Na_{2y}Al_2(MoO_4)_y(PO_4)_{3-y}$ was established. The rate of hydrogen and sodium intercalation into the structure of the polyoxophosphate-molybdate layer increased sharply with an increase of the potential range from –1.3 to –3.0 V. The addition of chitosan into the solution enhances the film-forming effect of surface ion-conducting oxo-phosphate – molybdate polymeric layer.

Keywords: energy carrier; hydrogen sorption; polymolybdate phosphate; aluminum hydrides; hydrogen; chronopotentiometry.

INTRODUCTION

The problem of hydrogen storage has remained in the focus of scientific research for many decades.[1,2] Hydrogen is the most abundant element in the universe, it has the highest energy density per unit mass. Being an energy carrier, mainly derived from water, hydrogen turns back into water when burned. This ensures the ecological safety of hydrogen production for the environment, its energy and economic competitiveness. In this regard, electrochemical methods[3,4] of hydrogen production can be very effective. Therefore, research on the problem

* Corresponding author. E-mail: hussein-2010@mail.ru
https://doi.org/10.2298/JSC20913081H

of developing an electrochemical technology for generating hydrogen and its accumulation and storage is urgent and requires the search and study of the properties of hydride-forming metals and alloys, as well as methods for controlling the kinetics of hydrogen sorption and the sorption capacity of the hydrogen-sorbing material.[5–7] A directed effect on the surface and bulk properties of the sorbing material, on the concentration of structural defects and the hydrogen sorption capacity can be made by the electrochemical modification using the method of cathode incorporation.[5,6,8,9]

Recently, scientists and technologists have shown particular interest in aluminum,[10–15] due to its low specific gravity, non-toxicity, high purity of hydrogen generated by the reaction of aluminum with water, the ease of formation and the ability to use commercial aluminum alloys. It is also important that the alkali formed during the reaction acts as a catalyst and it can be completely recovered, and finally, the used devices can be recycled.

The standard electrode potential of aluminum is –1.676 V. Aluminum is a reactive metal with a high affinity for oxygen.[16] The strongest activators of aluminum[7] in the alkaline medium are OH ions. The thickness of the formed oxide layers can vary from 50 to 100 Å. The presence of pores facilitates the occurrence of chemical and electrochemical reactions and the localization of products in the pores of the oxide layer.[16,17] The dependence of the stationary potential Al on the pH medium in acidic solutions from 1 to ~6 is described by the equation: $E_{stat} = –0.26–0.063pH$. The corrosion resistance of Al under atmospheric conditions is explained by the presence of a natural film of Al_2O_3 or $Al_2O_3{\times}H_2O$ on its surface with a thickness from 0.005 to 0.015 μm. The electrochemical modification allows to vary the composition of the oxide film, its structure and properties.[8,9,11,15,17]

The activation of the surface oxide layer by the modification with the atoms of other elements is accompanied by the separation of the aluminum-oxygen layers and the formation of a spinel-type structure, in which aluminum ions in tetrahedral spaces are replaced by ions of the incorporated metal.[8,9,17,18]

Studies show that the main factor determining the properties of aluminum oxide, if we imagine its composition in the form of a hydroxo-anionic complex $n(Al_2O_{3-x})m(An^{z-})p(OH^-)q(H_2O)$ is the nature of the electrolyte.[5,6,8,11,16] The channel (tunnel) structure should facilitate the sorption or incorporation of particles of various substances. In this case, the nature of the anion in the electrolyte solution has a significant effect on the adhesion of the reaction product with the metal surface.[5,8,15]

In the group of hydroxy acids, the adhesion turned out to be the highest in phosphoric acid due to the largest pore diameter in the formed oxide layer, mainly because of the occurrence of chemical bonds between the incorporated particles and structural elements of the aluminum oxide.[6,17,19]

Due to the distorted tetrahedral shape of the structural cell, the phosphates have a high deformation and polarization ability and, accordingly, a high degree of chemical adhesion on the aluminum oxide. The increase in the electrical conductivity of such a modified oxide layer, by alloying with a third component, can be explained by the following factors:[15,16]

– higher transport properties of the modified layer (Na_2O, Al_4O_3) due to the disappearance of anisotropy and disordering of the cation sublattice;

– the formation of cation vacancies V_C;

– the increase in the size of migration channels.

If we take into account, the dependence of the dissociation reaction of phosphoric acid on p*K*a the results are as follows:

$$H_3PO_4 \leftrightarrows H^+ + H_2PO_4^-, \quad pKa_1 = 2.03 \tag{1}$$

$$H_2PO_4^- \leftrightarrows H^+ + HPO_4^{2-}, \quad pKa_2 = 7.2 \tag{2}$$

$$HPO_4^{2-} \leftrightarrows H^+ + PO_4^{3-}, \quad pKa_3 = 12.03 \tag{3}$$

then $H_2PO_4^-$ should possess the highest adsorption, presumably because of the formation of a chemical bond of the O–M type with the surface metal atoms of the electrode. A slight increase in the adsorption of $H_2PO_4^-$, observed during the cathodic polarization, can be explained by their reorientation by hydrogen atoms to the metal surface: $(HO)_2PO_2^-$. Thus, polar anions of the $H_2PO_4^-$ type can be adsorbed either through hydrogen atoms or through oxygen atoms.

If cathodic polarization is applied to the metal being treated, the discharge of H^+ and, accordingly, the growth of pH of the near-electrode layer will significantly accelerate, providing the formation of a precipitate of hardly soluble phosphates, for example, during cathodic polarization in a phosphating solution.[20–22] The stretching vibration of the P–OH group detected by IR spectroscopy at a frequency of $\nu = 1010$ cm^{-1} indicates the presence of a substance with the composition $Al_2(HPO_4)_3$ in the surface layer. Metals (aluminum, titanium) behave similarly during the cathodic polarization in solutions containing phosphoric acid (or its soluble salts) and the additives of molybdates, tungstates of alkali metals.[18,20–23]

In this regard, inorganic compounds are of interest, the porous structure of which are based on a tetrahedral phosphate framework capable of trapping cations in their cavities. The transfer of cations along the channels of such structures at a high rate is possible, provided that the width of the narrowest point in the crystallographic channel is greater than the doubled sum of the radii of the mobile cation and oxygen. Moreover, the cationic conductivity can be significantly increased by varying the lattice parameters due to the heterovalent substitutions in the sublattices of both the alkali metal and phosphorus. With the addition of the Mo^{6+} into the phosphorus sublattice, the electrical conductivity increases, and the higher is the Mo^{6+} content, the greater is conductivity.[16] An

increase in ionic conductivity in solid solutions Me_xPO_4 (Me = Na to Cs) at heterovalent substitutions is explained by the formation of vacancies in the alkali metal sublattice associated with the solubility of the additive. Besides, the size of the modifying cation cannot be neglected.[18]

It is also possible to improve the conductivity by creating compositions with a flexible structure that can withstands a wide range of substitutions in cationic and anionic groups, with the formation of substitutional solid solutions containing a large number of mobile cations, including multiply charged ones.[18,19] In the case of heterovalent substitution of, for example, a part of phosphorus (V) by silicon (IV), a deficiency of positive charge occurs, which is compensated by the incurporation of an additional amount of Na^+, which are statistically distributed over 18-fold positions, which leads to high ionic conductivity.[16,18]

Thus, the presence of ionic conductivity in phosphates allows us to expect that the formation of a phosphate-containing coating on aluminum should not prevent reversible intercalation-deintercalation of alkali and alkaline-earth metal ions.[13,15] Moreover, due to various iso- and heterovalent substitutions in the sublattice of the structure-forming element (Al) and phosphorus, due to its inevitable deformation, it becomes possible to obtain materials with the desired functional properties. In this regard, it seems relevant to study the effect of the elemental composition of the polymeric multinuclear phosphate-containing oxide of the molybdate coating, formed by heterovalent substitution under cathodic polarization on the capacitive characteristics of the Al electrode, when an organic polymer with a high film-forming effect, biopolymer chitosan, is added into the electrolyte composition.

Due to the ability to form non-covalent complexes with other polyelectrolytes, high sorption activity with ions of various metals, the ability to retain both the solvent and substances dissolved in its structure, chitosan is one of the promising research objects that have found application in various branches of science and technology, biotechnology and medicine. Of particular interest is its ability to form fibers and films. Chitosan films favourably differ in their strength, elasticity, uniformity in thickness, and transparency.[23–27]

When modified, in particular, with phosphoric acid, the ability of chitosan to form fibers and films increases, as well as its sorption properties.[24–28] Phosphoric acid, as a strong nucleophile (reagent), can affect the position of OH groups connected with the terminal glycosidic center of the chitosan molecule. Probably, the phosphoric acid anion can form a stable complex with the terminal glycosidic center of chitosan. In this complex, the position of the OH group is fixed in the configuration that makes the greatest contribution to the specific rotation (Fig. 1).

The study of the effect of chitosan on the electrochemical behaviour of polyphosphate molybdate complexes on metal electrodes through the stage of the

formation of polyelectrolyte complexes in the solution and their subsequent adsorption on the electrode is a promising direction[29] in electrochemistry of heteronuclear polyelectrolyte structures, which determines the kinetics of cathodic incorporation of alkali metals and hydrogen into the electrode metal by the mechanism of intercalation – deintercalation.

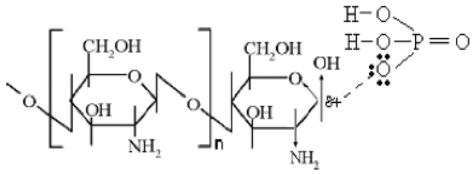

Fig. 1. Formation of a complex of chitosan with phosphoric acid.

EXPERIMENTAL

The method of the preparation of the working solution included the following operations: chitosan (previously ground) was completely dissolved in phosphoric acid at 40±0.5 °C.[27] The temperature was maintained using a U-15 laboratory recording thermostat. A thin stream of phosphoric acid with chitosan dissolved in it was added and thoroughly mixed until homogeneous in a flask half filled with distilled water. Then sodium molybdate was dissolved in a small amount of water, thoroughly mixed and added into a volumetric flask.

For the electrochemical treatment of the system Al/Na_2MoO_4 (0.01 M) + H_3PO_4(1 M) + chitosan (4 g/l), the solutions were prepared in volumetric flasks 1000 ml: Na_2MoO_4 $2H_2O$ (2.42 g), H_3PO_4 (57.65 g) and chitosan (4 g). It was carried out using a potentiostat-galvanostat P-8S (LLC "Elins"), combined with a computer and equipped with a program developed by the manufacturer. The potential of the chloride silver electrode in the test solutions was measured and expressed relative to a standard silver chloride reference electrode (C_{Cl} = 1 M, at t =25 °C, $E^0_{Cl-/AgCl/Ag}$ = 0.222 V). Besides the effect of the potential and the duration of electrolysis, the effect of the degree of chitosan dispersion was investigated by varying the grinding time of chitosan flakes within 30 to 60 min, using a Philips electric mill.[24,27] The surface of the modified electrodes was investigated using the methods of current-free chronopotentiometry, optical microscopy[29] in the direct and reflected light[30,31] (microscope MINIMED 5021 and Axio Ymager A2m, manufactured by ZEISS, Germany). The elemental composition of the surface layer of modified electrodes was determined by scanning electron microscopy.[30–32] All studies were carried out at the temperature of 20±2 °C. Each experiment was repeated 3 times and the average statistical value of the fixed current (or potential) value was determined.[33]

The objects under study were aluminum foil plates Al: 97.5 % (impurities P 1.52 %, Mn: 0.56 %, Fe: 0.42 %), which were preliminarily subjected to degreasing with ethanol and mechanical polishing with sandpaper (or glass powder of double decantation).[34] Reagents used in the work were $Na_2MoO_4{\cdot}2H_2O$ of grade "h" GOST 10931-71, H_3PO_4 of grade "chda" GOST 6552-80, flake chitosan produced by OOO "Chitosan Technologies" (Engels, Saratov region) with molecular weight 120 kDa, size of flakes 0.1 to 3.0 mm. All solutions were prepared in bidistilled water.

The modification of the surface polymolybdate phosphate layers[29] was carried out in a potentiostatic mode in the range of potentials from –1 to –3 V and at different polarization time (15 to 90 min). The electrodes were immersed in the studied solutions of

$Na_2MoO_4 \cdot 2H_2O$ (0.01 mol/l) and the mixtures with H_3PO_4 (1 mol/l) without and with the addition of chitosan (4 g/l), the dispersed time was 30, 40 and 60 min, the molecular weight 250. Electrochemical treatment was carried out using Elins R-301 potentiostat-galvanostat (manufactured by Elins LLC), combined with a computer and equipped with a program developed by the manufacturer, which allowed to convert the digital record into graphic dependences to determine the polarization characteristics (current-free potential *E*, current density and polarization time under the specified experimental conditions). The current-free potential was recorded for 300 s before and after cathodic polarization in a solution of a given composition, until a stationary value did not change over time.

RESULTS AND DISCUSSION

According to visual observations, after a few seconds of cathodic polarization current, small gas bubbles appear on the aluminum electrode in Na_2MoO_4 (0.01 M) solution at a potential of –1.3 V, which accumulate on the electrode surface. As the cathode potential shifts to the negative side to –1.4 and further, the rate of the bubble formation and their number increase. At $E_{c.p}$ = -2.0 V, the hydrogen evolution begins immediately and in large quantities when the cathodic polarization potential is switched on up to –3 V (Figs. 2 and 3). The currentless potential *E* (Fig. 4) significantly shifts to the negative side.

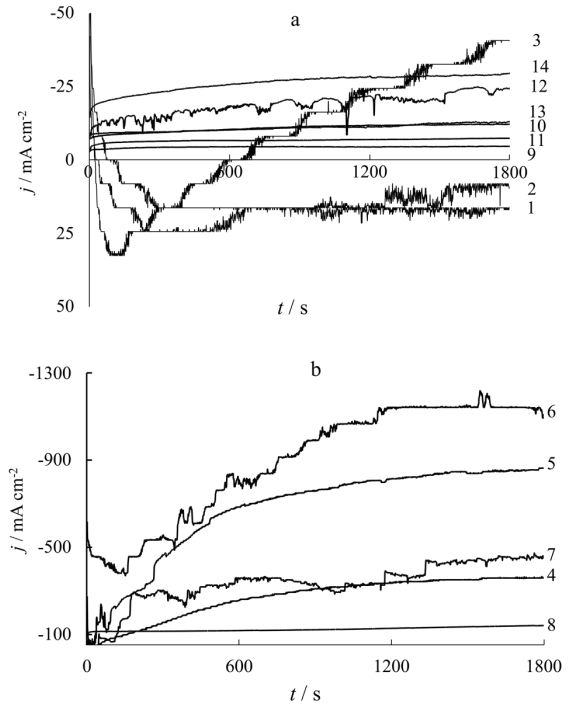

Fig. 2. Cathodic chronoamperograms of the Al cathode at potentials $-E_c$ / V: 1) 1; 2) 1.1; 3) 1.2; 4) 1.3; 5) 1.6; 6) 1.5; 7) 1.6; 8) 1.8; 9) 2; 10) 2.2; 11) 2.4; 12) 2.6; 13) 2.8; 14) 3.0 in Na_2MoO_4 (0.01 M) solution for 30 min.

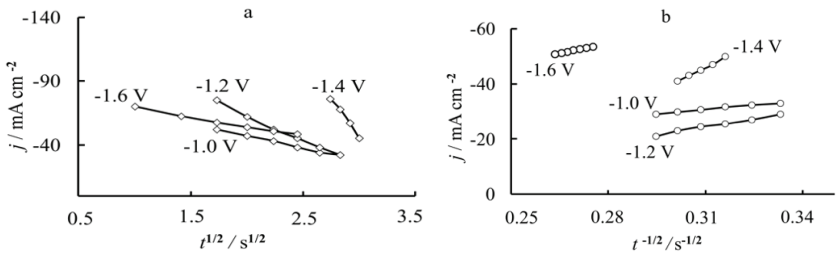

Fig. 3. Dependence a) j–$t^{1/2}$, b) j–$t^{-1/2}$ at the initial stage of the cathode polarization of Al in solution Na_2MoO_4 (0.01 M).

In the investigated potential range, two areas of current density can be distinguished (Fig. 2, curves 1–7 and curves 9–14) which differ in the mechanism of phase formation: the diffusion-kinetic mechanism of incorporation in the first case and the crystallization-chemical mechanism in the second one.[5-7,9] It is important that in the first case the fixed value of the current density is 2 to 3 times higher than in the second one.

When H_3PO_4 (1 M) is added into Na_2MoO_4 (0.01 M) solution, the crystallization-chemical mechanism predominates on the Al electrode (Fig. 4) in the potential range from –1.0 to –2.0 V, both the electrode surface and the near-electrode layer of the solution turn blue.[19] The analysis of the j–t curves in the coordinates j–$t^{1/2}$ and j–$t^{-1/2}$ (Fig. 3) made it possible to calculate the diffusion-kinetic characteristics (Table I).[29,35]

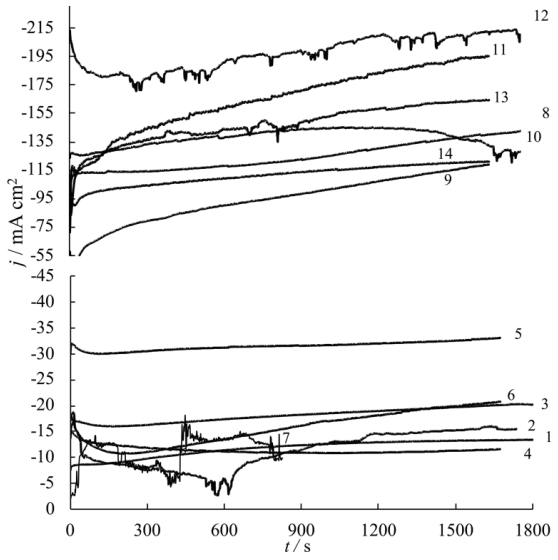

Fig. 4. Cathodic chronoamperograms of the Al cathode at potentials $-E_k$ / V: 1) 1; 2) 1.1; 3) 1.2; 4) 1.3; 5) 1.6; 6) 1.5; 7) 1.6; 8) 1.8; 9) 2; 10) 2.2; 11) 2.4; 12) 2.6; 13) 2.8; 14) 3.0 in solution: Na_2MoO_4 (0.01 M) + H_3PO_4 (1 M) for 30 min.

TABLE I. Influence of the potential of cathodic treatment on the diffusion-kinetic characteristics of the cathodic process at Al electrode in Na_2MoO_4 (0.01 mol)

E / mV	$j_{(t=0)}$ mA cm^{-2}	$K^{I}_{p} = \frac{\Delta i}{\Delta\sqrt{t}}$ mA·cm^{-2} s$^{-1/2}$	$K^{II}_{p} = \frac{\Delta i}{\Delta(1/\sqrt{t})}$ mA·cm^{-2} s$^{1/2}$	$C_0D^{1/2}$ mol cm^{-2}s$^{-1/2}$
–1	–42.8	22	100	0.002
–1.2	54	51	225	0.004
–1,4	60	222	100	0.009
–1.6	64	21	310	0.006
–2.2	7	1.4	0.2	$4.2\cdot10^{-6}$
–2.8	20	0.7	233	0.004

This discovered effect of the interface boundary Al/Na_2MoO_4+H_3PO_4 was explained by the molybdate ions property (nature): the molybdate ions pronounced ability increases with their polycondensation in the acidic medium. In the structure of heteropolyanions $[PMo_{12}O_{40}]^{3-}$ formed in the case of molybdenum, phosphorus is located in the center of a tetrahedron surrounded by 12 octahedrons, arranged in 4 groups containing three octahedra, in which each phosphorus atom has 4 oxygen atoms common to 3 octahedrons (MoO_6), 24 oxygen atoms in polyanion common to 2 octahedra (MoO_6) and 12 atoms are not bonded to others.

In the structures of heteropolyanions $[PMo_{12}O_{40}]^{3-}$, $[PMo_{11}O_{39}]^{7-}$, $[P_2Mo_{18}O_{62}]^{6-}$, $[P_2\ Mo_{17}O_{61}]^{10-}$, $[P_2Mo_5O_{23}]^{6-}$, $[HP_2Mo_5O_{23}]^{5-}$ a phosphorus atom occupies a central place.

The currentless potential E (Fig. 5) shifts significantly to the negative side. Studies of the morphology of the surface layer (Fig. 6) have shown that with the addition of a film-forming substance, chitosan, into the solution (Na_2MoO_4 (0.01 M) + solution H_3PO_4 (1 M)), a film-forming effect characteristic of chitosan is clearly observed, which rises with an increase in the duration and potential

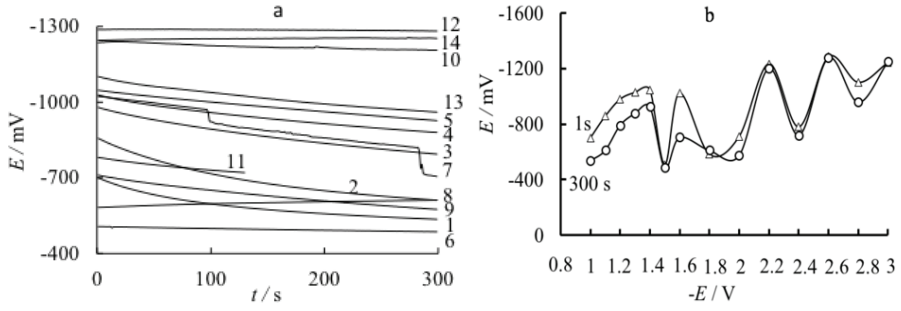

Fig. 5. The currentless potential ($E_{c/l}$, t) for the Al cathode; a) the dependence of $E_{c/l}$ on the E_{CP}; b) for t of 1 and 300 s after cathodic polarization in the solution: Na_2MoO_4 (0.01 mol/l) at different potentials E_c/V: 1) –1.0; 2) –1.1; 3) –1.2; 4) –1.3; 5) –1.4; 6) –1.5; 7) –1.6; 8) –1.8; 9) –2; 10) –2.2; 11) –2.4; 12) –2.6; 13) –2.8; 14) –3.0.

of cathodic polarization, and the concentration of chitosan in the solution (Fig. 7). The catalytic effect of chitosan on the formation of a fiber structure precipitate is more clearly seen (Fig. 6, optical microscopy).

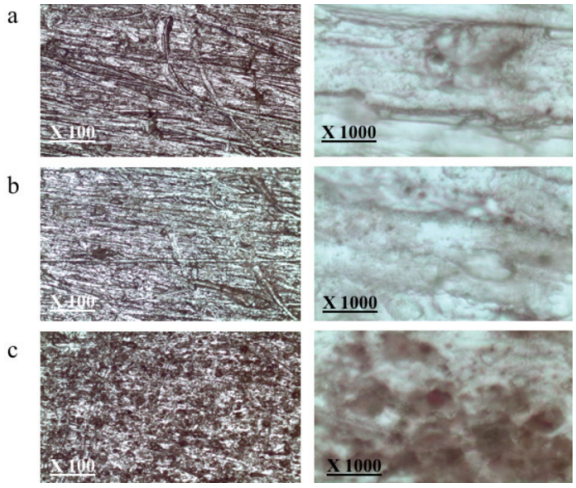

Fig. 6. Influence of the polarization duration on the morphology of the Al electrode surface in the electrolyte of the studied composition Na_2MoO_4 (0.01M) + H_3PO_4 (1 M) + chitosan (4 g/l; t_{grind} = 60 min) at $E_{c.p}$ = –2.6 V and polarization time: a) 30; b) 45; c) 90 min.

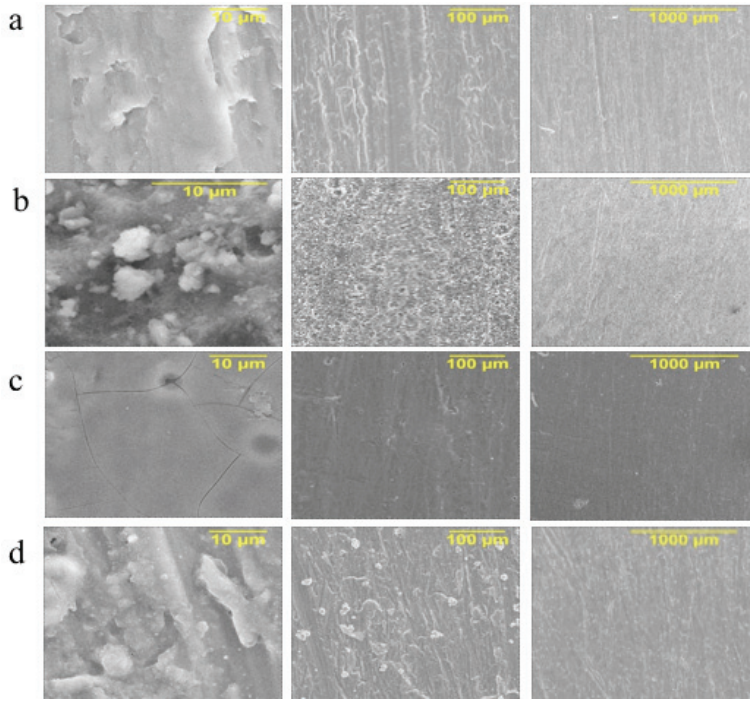

Fig. 7. Morphology of the Al electrode surface after cathodic treatment at E_c = –2.6 V and t_{cp} = 90 min in solutions: a) initial electrode, b) Na_2MoO_4 (0.01 M), c) Na_2MoO_4 (0.01 M) + + H_3PO_4 (1 M) and d) Na_2MoO_4 (0.01 M) + H_3PO_4 (1 M) + chitosan (4 g /l, t_{grind} = 60 min).

The value of $E_{c/l}$ of the Al of electrode as before as after cathodic polarization shifts to the region of less negative values from –0.9 to –0.6 V at the first second (to the moment the electrode is immersed in the solution) and from–0.7 to –0.45 V after 300 s when the stationary state is established on the electrode (Fig 5b).

After cathodic treatment, depending on the value of the cathodic potential (-1.2 to –3.0 V), the electrode potential shifts significantly to the range of less negative values – at the time adding H_3PO_4 to Na_2MoO_4 solution (Table II). The H_3PO_4 addition shows structural action and as result, more aquability proportional change as before as after cathodic polarization at region E_c from –1.0 to –3.0 V.

TABLE II. Currentless potentials *E*/mV of the Al electrode after cathodic treatment at different potentials, depending on the composition of the solution at the first and 300th s after opening the circuit

Cathodic treatment potential, V	Na_2MoO_4 (0.01 M)		Na_2MoO_4 (0.01 M) + + H_3PO_4 (1 M)		Na_2MoO_4 (0.01M) + H_3PO_4 (1 M) + + chitosan (4 g/l; t_{grind} = 60 min)	
	at 1s	at 300 s	at 1 s	at 300 s	at 1 s	at 300 s
–1.0	–699	–537	–626	–363		
–1.1	–856	– 612	–642	–213		
–1.2	–978	–793	–614	–214		
–1.3	–1028	–879	–706	–212		
–1.4	–1047	–926	–647	–230		
–1.5	–507	–488	–759	–237		
–1.6	–1024	–705	–655	–227		
–1.8	–582	–612	–582	–238		
–2.0	–711	–576	–716	–202		
–2.2	–1235	–1205	–618	–225		
–2.4	–800	–720	–653	–218		
–2.6	–1286	–1281	–213	–151	–556	–232
–2.8	–1101	–959	–780	179		
–3.0	–1243	–1252	–726	–185		

The nature of the dependence of *E* on the value of the $E_{c.p}$ allows us to discuss about the formation of phases of variable composition, and about the accumulation of hydrogen and sodium in their composition as the $E_{c.p}$ shifts to the negative side.

As can be seen from Table III, with the higher duration of polarization, the amount of the oxide-containing phase in the surface layer increases. These can be aluminum oxides Al_2O_3, Na_2O, nAl_2O_3), (MoO_3), MoO_4^{2-}, phosphates, phosphate derivatives of chitosan, embedded in a single heteropolymer fibrous-type structure, which is in good agreement with the results of the investigation of the morphology of the modified electrode surface (Figs. 6 and 7).

With the addition of chitosan additives (4 g/l) the solution becomes cloudy at the phase boundary and the precipitate of the forming phase becomes looser but retains its fibrous structure.

TABLE III. Elemental composition of the modified layer on the surface of the Al electrode after cathodic treatment in the solution Na_2MoO_4 (0,01 M) + H_3PO_4 (1 M) + chitosan (4 g/l; t_{grind} = 60 min) at E_c = –2.6 V and different polarization times (t_{cp} / min). Average values over 5 points; τ_p – polarization time

τ_p / min	Content, wt.%						
	C	O	Al	P	Mo	Na	Mn
30	28.56	49.29	14.0	6.8	1.2	0.08	0.03
60	18.6	42.8	20.5	11.4	6.3	0.24	0.33
90	4.0	50.84	17.0	13.9	4.25	0.27	0.01

CONCLUSION

When adding phosphoric acid H_3PO_4(1M) to the solution, the equilibrium of the reaction of the formation of polynuclear complexes:

$$Mo_7O_{24}^{6-} + Na^+ \rightarrow [NaMo_7O_{24}]^{5-} \quad (4)$$

shifts strongly to the right and the concentration of mononuclear complexes MoO_4^{2}, $HMoO_4^-$, H_2MoO_4 (respectively $NaMoO_4^-$ and Na_2MoO_4) does not exceed 1–3 %. The protonated cations $H_4PO_4^+$ present in the solution are involved in the formation of polymeric heteronuclear formations with molybdate ions of the polyelectrolyte structure. Phosphate-molybdates of the alkali metal in the crystalline state are substitutional solid solutions $Na_{1-y}Ti_2(MoO_4)_y(PO_4)_{3-y}$ in the range $0 \leq y \geq 0.6$. The introduction of chitosan (4 g/l) into the solution of Na_2MoO_4 and H_3PO_4 is accompanied by a sharp increase in the film-forming effect.

Under the conditions of cathodic polarization, Na^+ accumulating near the electrode surface, under the action of a concentration gradient migrate through the layer of electrochemical adsorption products deep into the electrode and, at the boundary with metallic aluminum, participate in the formation of an interstitial phase according to the vacancy mechanism:

$$xH^+ + xe^- + Al\square \rightarrow H_xAl. \quad (5)$$

$$xNa^+ + xe^- + Al\square \rightarrow Na_xAl, \quad (6)$$

Al□ – Al vacancy

At potentials more negative than –1 V in aqueous solutions, the formation of aluminum hydrides with the participation of H_2O or directly:

$$xH_2O + xe^- + Al\square \rightarrow H_xAl + xOH^- \quad (7)$$

$$Na_xAl + xH_2O \rightarrow H_xAl + xNaOH \quad (8)$$

The existence of two potential regions, which are established, confirms the occurrence of two different processes with the participation of the $[NaMo_7O_{24}]^{5-}$ polynuclear complexes on the electrode in the adsorbed layer. The product of surface adsorption of polynuclear complexes could be double salts such as $Na_6Al_nMo_{7-n}O_{24}$ and $Na_{1-y}Al_2(MoO_4)_y(PO_4)_{3-y}$ which have the properties of substitutional solid solutions.

И З В О Д

ЕЛЕКТРОХЕМИЈСКО ФОРМИРАЊЕ ЈОНСКИ ПРОВОДНОГ ПОЛИМЕРА ОКСО-ФОСФАТ-МОЛИБДАТА НА АЛУМИНИЈУМУ

HUSSEIN HUSSEIN[1], SWETLANA POPOVA[2], IRINA FROLOVA[2] и MARINA LOPUKHOVA[2]

[1]*Department of Chemistry and Chemical Technology of Materials, Yuri Gagarin State Technical University of Saratov, Saratov, Russia и* [2]*Engels Technological Institute (branch) of Yu. Gagarin Saratov State Technical University, Engels, Russia*

Електрохемијско понашање алуминијумске електроде у воденом раствору који је садржао Na_2MoO_4, H_3PO_4 и хитосан је испитивано методама хронопотенциометрије на отвореном колу, хроноамперометрије, оптичке и скенирајуће електронске микроскопије. Модификација површине полимолибдат-фосфат слојева је извршена у потенциостатком режиму на потенцијалима између −1 и −3 V током различитих времена поларизације (од 15 до 90 min). Одређиван је елементарни састав површинског слоја метала пре и после катодне поларизације. Утврђено је да је електрохемијски формирана полимерна матрична структура од јонски проводних (H^+, Na^+) хетеронуклеарних полимолибдата и полифосфат-молибдатних комплекса двоструких соли $Na_6Al_nMo_{7-n}O_{24}$ и $Na_{2y}Al_2(MoO_4)_y(PO_4)_{3-y}$. Брзина интеркалације водоника и натријума у структуру полиоксо-фосфатно-молибдатних слојева нагло расте са повећањем негативне вредности потенцијала. Додатак хитосана у раствор поспешује ефекат формирања филма на површини јонски проводног оксо-фосфат-молибдатног полимерног слоја.

(Примљено 13. септембра, ревидирано 27. новембра, прихваћено 8. децембра 2020)

REFERENCES

1. B. P. Tarasov, M. V. Lototskii, V. A. Yartys, *Russ. J. Gen. Chem.* **77** (2007) 694 (https://dx.doi.org/10.1134/s1070363207040329)
2. V. N. Ageev, I. N. Beckman, O. P. Burmistrova, *Interaction of Hydrogen with Metals*, Nauka, Moscow, 1987, p. 296 (https://b-ok.cc/ireader/3065144)
3. W. X. Chen, *Int. J. Hydrogen Energy* **26** (2001) 603 (https://doi.org/10.1016/S0360-3199(00)00119-1)
4. K. Young, J. Nei, *Materials* **6** (2013) 4574 (https://doi.org/10.3390/ma6104574)
5. S. S. Popova, L. A. Alekseeva, B. N. Kabanov, *Russ. J. Electrochem*. **22** (1986) 1427
6. S. S. Popova, N. A. Sobgaida, *Izv. Vyssh. Uchebn. Zaved. Khim. Khim. Tekhnol.* **45** (2002) 84
7. N. G. Krapivny, *Russ. J. Electrochem*. **17** (1981) 678
8. W. X. Chen, *Intern. J. Hydrogen Energy* **26** (2006) 603 (https://doi.org/10.1016/S0360-3199(00)00119-1)
9. A. V. Zvyaginceva, *ISJAEE* **21** (2015) 145 (https://doi.org/10.15518/isjaee.2015.21.018)
10. E. O. Chudotvorova, P. I. Bestuzhev, V. V. Kozlyakov, in *Proceedings of The III International Scientific and Practical Conference*, Minsk, 2016, Belarus, Collection of Abstracts, 2016, p. 43

11. A. V. Reznichenko, V. V. Rybalchenko, F. Z. Badaev, S. G. Ponomarev, A. A. Vasin, *J Chem. Eng. Process. Technol.* **8** (2017) 347(https://doi.org/10.4172/2157-7048.1000347)
12. Z. Ragaiy, L. Brenda, G. Diaz, C. S. Fewox, C. Ashley, J. Stowe, R. G. Gray, G. H. Andrew, *Chem. Comm*. **25** (2009) 3717 (https://doi.org/10.1039/B901878F)
13. C. C. Wang, Y. C. Chou, C. Y. Yen, *Procedia Eng.* **36** (2012) 105 (https://doi.org/10.1016/j.proeng.2012.03.017)
14. H. Z. Wang, D. Y. C. Zeung, M. K. H., M. Ni, *Renew. Sustain. Energy Rev.* **13** (2009) 845 (https://doi.org/10.1016/j.rser.2008.02.009)
15. H. Zou, , S. Chen, , Z. Zhao, W. Lin, *J. Alloys Compd*. **578** (2013) 380 (https://doi.org/10.1016/j.jallcom.2013.06.016)
16. R. Ripan, I. Chetyanu, *Inorganic chemistry*. *Vol. 2. Chemistry of Metals*, M publishing house Mir, Moscow, 1972, p.872
17. I. O. Grigorieva, A. F.Dresvyannikov, A. S. Zifirov, *Bullet. Kazan Tech. Univ*. **16** (2013) 271
18. A. Mueller, S. Roy, *Usp. Khim.* **71** (2002) 1101 (https://doi.org/10.1070/rc2002v071n12abeh000751)
19. N. A. Perekhrest, K. N. Pimenova, V. D. Litovchenko, *J. Appl. Chem*. **65** (1992) 1163
20. O. A. Stadnik, N. D. Ivanova, E. I. Boldyrev, L. I. Zheleznova, *Ukr. Chem. J.* **74** (2009) 55
21. E. E. Tekutskaya, I. Ya. Turyan, V. I. Kravtsov, V. V. Kondrat'ev, *Russ. J. Electrochem*. **27** (1991) 407
22. E. E. Tekutskaya, V. I. Kravtsov, *Ind. Lab. Diagn. Mater.* **64** (1998) 8
23. M. A Krayukhina. , N.A. Samoilova, I. A. Yamskov, *Usp. Khim.* **77** (2008) 854 (https://doi.org/10.1070/RC2008v077n09ABEH003750)
24. Ya. A. Kamenchuk, E. A. Zelichenko, V. V. Guzeev, *Perspektivnye materialy* **6** (2009) 66
25. V. Scheveleva, L. A. Zemskova, A. V. Voight, V. G. Kuryavy, *Khimicheskie Volokna* **2** (2008) 44
26. T. S. Khakamov, D. V. Feoktistov, L. A. Badykova, P. G. Kornilaev, R. R. Shavaleev, R. K. Mudarisova, *Russ. J. Appl. Chem.* **86** (2013) 1417 (https://doi.org/10.1134/S1070427213090175)
27. S. S. Popova, O. G. Kovalenko, V. V. Kurchavova, K. A. Belousov, *Perspektivnye materialy* **11** (2013) 35
28. S. S. Popova, H. A. Hussein, I. I. Frolova, V. F, Abdullin, *Electrochem. Energetic* **20** (2020) 99 (https://doi.org/10.18500/1608-4039-2020-20-2-99-111)
29. S. S. Popova, *Methods of investigation of kinetics of electrochemical processes*, Saratov State Technical University, Saratov, 2008, p.106
30. O. N. Lyubiev, *Numerical methods in electrochemistry*, NPI Publishing House, Novocherkassk, 1982, p.68
31. V. L. Mironov, *Fundamentals of scanning probe microscopy: Textbook for senior students of higher educational institutions*, Institute for Physics of Microstructures of the Russian Academy of Sciences, Nizhny Novgorod, 2004, p. 110
32. V. M. Zolotarev, N. V. Nikonorov, A. I. Ignatiev, *Modern methods for the study of optical materials Part 2*, ITMO University, St. Petersburg, 2013, p.166
33. J. I. Goldstein, H. Yahowitz, D. E. Newbury, E. Lilshin, J. W. Colby, J. R. Coleman, *Practical Scanning Electron Microscopy: Electron and Ion Microprobe Analysis*, Plenum Press, New-York, 1975, p.598 (https://doi.org/ 10.1007/978-1-4613-4422-3)
34. L. V. Baranova, E. L. Demina, *Metallographic etching of metals and alloys: Handbook*, Metallurgy, Moscow, 1968, p. 256
35. S. P. Chizhik, L. K. Grigorieva, R. N. Kuklin, *Doklady Akad. Nauk SSSR* **321** (1991) 1221.

Journal of the Serbian Chemical Society
JSCS-info@shd.org.rs • www.shd.org.rs/JSCS
J. Serb. Chem. Soc. *86* (3) 313–326 (2021)
JSCS–5423
Original scientific paper

Experimental study of the effect of single walled carbon nanotube/water nanofluid on the performance of a two-phase closed thermosyphon

MOHAMMAD CHEHRAZI and BAHAREH KAMYAB MOGHADAS*

Department of Chemical Engineering, Shiraz Branch, Islamic Azad University, Shiraz, Iran

(Received 28 June, revised 26 October, accepted 29 October 2020)

Abstract: Thermosyphons are one of the most efficient heat exchanger apparatus that are used extensively in different industries. One of the most common uses of this device is energy recovery, which is essential due to the energy crisis. Several parameters, such as geometric dimensions, type of working fluid and type of the body, affect the efficiency of a thermosyphon. In this work, the effect of type and concentration of single-walled carbon nanotube nanofluid (SWCNT/water) on the efficiency of heat transfer in a two-phase closed thermosyphon (TPCT) was investigated. For this purpose, a system with a two-phase closed thermosyphon was initially constructed. Then SWCNT/water nanofluids at 0.2, 0.5 and 1 % weight concentration were used as the working fluid in the thermosyphon system. The results of the current experiments showed that the addition of a nanofluid at any weight concentration and an increase in input power increases the performance of the system. In addition, the heat resistance of the TPCT was reduced when the level of SWCNT and input power increased. Hence, for the prepared nanofluid samples, the minimum thermal resistance was obtained at 1 wt. % SWCNT and 120 W. Moreover, the Nusselt number increased with increasing input power and decreased with increasing concentration. In all experiments, all the prepared nanofluid samples had a significantly better thermal performance in comparison with pure water.

Keywords: energy recovery; SWCNT/water-based nanofluid; efficiency; thermal resistance; TPCT.

INTRODUCTION

Apparatuses such as heat pipes are one of the most utilized tools ever known. It could be noted that this system can transmit large quantities of heat at a slight temperature difference in a small cross-section over relatively long dis-

* Corresponding author. E-mail: kamyab@iaushiraz.ac.ir; kamyab_bahareh@yahoo.com
https://doi.org/10.2298/JSC200628070C

tances between the hot and cold source, quickly without the need of external power. Perhaps, for this reason, the heat pipe is reminisced as a superconductor.

By investigating nanofluids, it has been shown that these materials, which are a stable and homogenized suspension consisting of a base fluid and additional nanoparticles as an additive, lead to notable enhancement in the thermal performance of this kind of heat exchangers.[1–4] Additionally, studies showed that compared to fluids without nanoparticles, nanofluids have a significantly higher thermal conductivity.[5–9]

Kang *et al.*[6] assayed a nanofluid containing diamond nanoparticles in ethylene glycol as a base fluid. Their result showed an improvement of thermal conductivity of up to 70 % for nanofluid 1 % UDD in ethylene glycol compare to the base fluid. Moreover, Godson *et al.*[7] demonstrated that Ag/water-based nanofluid leads to an enhancement of 80 % at 0.9 vol. % in thermal conductivity compared to pure water. Zeinali Heris *et al.*[9–11] investigated the addition of CuO/water--based and Al_2O_3/water-based nanofluid effects on convective heat transfer *via* a roundish tube. Their results led to this fact that by increasing the density of nanofluids, the heat transfer coefficient improves accordingly. Hence Al_2O_3/water--based nanofluids showed better enhancement than CuO/water-based solutions. Noie *et al.*[12] in Ferdowsi Engineering University of Mashhad investigated the heat transfer improvement in a thermosyphon using an Al_2O_3/water-based nanofluid. They investigated the thermal efficiency of a thermosyphon in various volume concentrations of the nanofluid. The results showed that increasing the nanofluid concentration to 3 % by volume concentration would increase the thermal efficiency by up to 14.7 % in comparison with pure water. According to the results of Kang *et al.*,[13] compared to pure water, the thermal proficiency of an Ag/water-based nanofluid in a heat pipe was comparatively higher. The thermal resistance decreased by 10–80 % compared to DI-water at an input power of 30––60 W. Furthermore, Jia *et al.*[14] studied the heat transfer performance of SiO_2/ /water-based nanofluids at various concentrations on pulsating heat pipes (PHP), which showed that high concentrations of SiO_2/water reduced the PHP efficiency compared to pure water. This is because of the increase in thermal resistance and evaporator section temperature at high concentrations of SiO_2/water nanofluid. The results of Xu *et al.*[15] showed that hybrid nanofluid 25 % Al_2O_3 + 75 % TiO_2/water-based and the single nanofluid TiO_2/water-based exhibited better thermal performance than deionized water in a TPCT. Another study by Das *et al.*[16] was performed to characterize the thermal performance of a water-based TiO_2 nanofluid with ethylene glycol as a surfactant, and their results evidenced that the use of the nanofluid improved the thermal proficiency of a circular finned thermosyphon by about 20.12 % for 0.30 vol. % TiO_2 nanofluid compared to deionized water as the working fluid.

One of the essential categories of material properties is its thermal properties. The thermal properties of carbon nanotubes are significantly important in various fields of technology, particularly due to the high thermal conductivity of diamond and graphite and the similarities between them. Scientists are interested in studying these properties and found some results in terms of the thermal conductivity of carbon nanotubes in their experimental studies. It has been predicted that carbon nanotubes have a higher thermal conductivity than graphite and diamond at room temperature.[17] Hence, it is necessary to study the performance of carbon nanotubes on the thermal efficiency of thermosyphons because of their thermal properties. Liu *et al.*[18] confirmed the thermal performance improvement and thermal resistance reduction by using CNT/water-based suspension in a weight concentration of 2 % and an operating pressure of 7.4 kPa. Their research showed a 150 % enhancement in heat transfer compared to water at the optimal pressure and concentration. The results of experiments by Choi and Eastman[19] showed that a MWCNT/water-based nanofluid could increase the thermal conductivity more than the base fluid. In addition, Choi *et al.*[19] determined the effective thermal conductivity of MWCNT in oil suspensions. They reported that the measured conductivity enhancements for a 1.0 vol. % nanotubes/oil-based suspension are noticeably greater than those predicted by theoretical models and are about 160 %. Shanbedi *et al.*[20] researched multiwalled carbon nanotubes and also suggested the thermal efficiency of a MWCNT/water-based suspension increase, and the Nusselt number and thermal resistance of the thermosyphon diminish on increasing the density of the nanofluid, which led to an increase in the conduction heat transfer by these nanoparticles.

Single-walled carbon nanotubes (SWCNT) are one of the most important types of carbon nanotubes, and the properties vary considerably with different types of SWCNTs. In addition, the results of Pettes and Shi[21] showed the thermal conductivity of CNTs on the number of walls, and the dependency of the thermal conductivity of CNTs decreases with increasing the number of walls, accordingly. This is attributed to consequential decrease in the concentration of CNTs with increasing number of walls. Despite the advantages of CNTs, some factors; such as poor solubility and instability of aqueous and organic suspensions of CNTs, difficulty in working with them due to their extremely small size, relatively expensive, the current production processes of CNTs, and confined understanding of how CNTs work, has limited their applications. The current work intends to investigate the effects of the addition of (SWCNT) to water as the operating fluid in a two-phase closed thermosyphon, on the Nusselt number, thermal resistance, thermal efficiency, vacuum pressure drop, and evaporator mean temperature. Considering the desirability of the results of experiments and research, the possibility of increasing the efficiency of thermosyphons and pre-

venting the waste of energy in thermal engineering applications will be more than ever possible.

EXPERIMENTAL

In these experiments, single-walled carbon nanotubes with a purity of over 95 %, a length of 5–30 μm, an internal diameter of 0.9–2 nm, and an outer diameter of 1–3 nm were used to prepare a nanofluid that was purchased from VCN Materials Co., Ltd. One of the difficulties of carbon nanotubes is their stability in polar fluids. Arabic gum was used as a surfactant to stabilize the suspension of carbon nanotubes in water. Arabic gum stabilizes carbon nanotubes in polar solvents such as water, due to the creation of non-covalent bondings. Hence, according to reports,[23] in this current study, Arabic gum (AG) was used at a concentration of 0.5 % by weight. Then SWCNT/water nanofluid containing AG was prepared at concentrations of 0.2, 0.5 and 1 % by weight. In order to prepare these concentrations of nanofluid, a balance (AND model GF-1000) with an accuracy of 0.001 g was used. Finally, for further uniformity of the suspension, a sonicator (bath type, operating frequency, and power source of the sonicator are 43 kHz and AC 100–120 V/AC 220–240 V 50/60 Hz, respectively) was used for 5 h. Substances and their weight fractions for prepared nanofluid samples are given in Table I.

Table. I. Substance and weight fraction in different samples of nanofluid

Sample No.	Content of nanoparticles in nanofluid wt. %	Substance for preparation of the nanofluid
1	0.2	SWCNT with purity of 95 %
2	0.5	+ 0.5 wt. % Arabic gum
3	1	

Due to the stability of prepared suspension and the absence of sediment formation in the samples, tests were performed several days after the preparation of the nanofluids. In addition, to evaluate the stability of the nanofluid, transmission electron microscopy (TEM) analysis was provided by the nanofluid manufacturer. After several days from the preparation of the nanofluid until the test, no sediment was observed in the samples. A TEM image of SWCNT/ /water nanofluid is shown in Fig. 1.

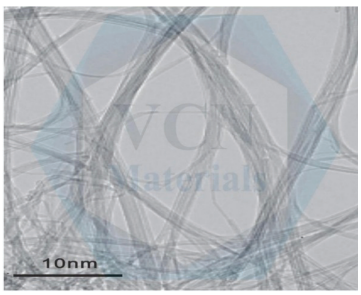

Fig. 1. TEM image of a SWCNT/water sample.

The TPCT set up used in this study is schematically depicted in Fig. 2a, and the constructed apparatus is pictured in Fig. 2b. The primary part of this system is fabricated by a 20 mm×450 mm copper tube with a wall thickness of 1 mm, including the evaporator, adiabatic, and the condenser sections, which are 160, 90 and 200 mm in length, respectively, as

illustrated in Fig. 2a. In addition, the diameter of the casing used in the condenser section is 40 mm. At the outer surface of the copper tube, precisely in the evaporator and condenser sections, four thermocouples (ARVAN model TG-4) were installed to study the process of temperature change in the TPCT system. These K-type thermocouples were positioned at a distance of 5, 10, 15 and 35 cm from the end of the evaporator section, respectively, and were able to measure temperatures in the range of –200 to 1350 °C. Moreover, to observe the temperature changes of the cooling water in the condenser section, two thermometers (CEM DT-131) with an accuracy of 0.1 °C with a temperature range from 0 to 100 °C were used before the inlet and after the outlet of the condenser part. The flow rate of the cooling water was controlled and monitored by a flowmeter (Rotameter LZS-15) with an accuracy of 5 L h^{-1} in the outlet of the condenser at 15 L h^{-1}. Also, a vacuum pump (Hamer 2RS-5 VE 2100) that makes a vacuum near –85 kPa was used to exhaust the non-condensate gases before testing from the thermosyphon and a pressure gauge to measure the TPCT vacuum pressure. Furthermore, an electrical element with the power of 1000 watts was used to heat the evaporator section. This electrical element was metal and fitted in series with an ammeter (AKB DT-9205A) with an accuracy of 0.01 A and power supply (Variac TDGC2-1KVA) in the circuit. The apparatus was insulated by 2 cm of fiberglass to prevent heat dissipation while considering the thermocouples are adequately protected. Because by contacting the electrical element with these parts, the registered temperatures are unrealistic and higher than expected.

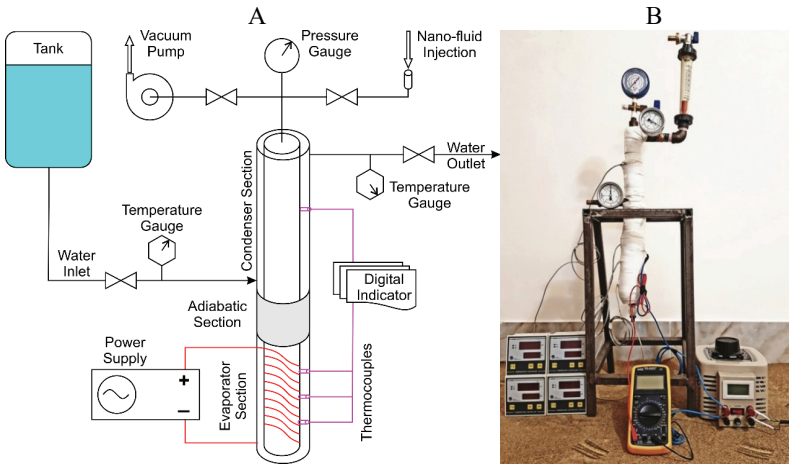

Fig. 2. A – Schematic of TPCT; B – constructed apparatus.

The experimental method was as follows: first, to remove non-condensable gases such as air, the thermosyphon was vacuumed to about –85 kPa by a vacuum pump. The operating fluid of deionized water, with or without the nanoparticles, was then charged into the thermosyphon. In these experiments, a constant filling ratio (FR) of 60 % was used in the system. This ratio is defined as the volume of fluid to the total volume of the evaporator section fraction. The experiment was initially started up with a 30 W input power following up to 30, 45 60, 90 and finally 120 W afterward with different SWCNT nanofluid concentrations of 0.2, 0.5,and 1.0 wt. % accordingly.

Data processing

The heat transfer rate from the condenser section can be determined as:[11,23]

$$Q_{out} = \dot{m}C_p(T_{out}-T_{in}) \quad (1)$$

where the variables of $\dot{m}$, C_p, T_{in} and T_{out} indicate the mass flow rate of the cooling water, the specific heat of the cooling water, inlet temperature, and outlet temperature of the cooling, respectively. The total heat transfer alongside the evaporator section by the electrical element is expressed as follows:[12,24]

$$Q_{in} = VI \quad (2)$$

where, V is defined as voltage, and I is defined as electric current of the power supply for various input powers.

Also, an equation is defined to estimate the thermal efficiency of thermosyphon in the following form:[12]

$$\eta = \frac{Q_{out}}{Q_{in}} \quad (3)$$

Also, the Nusselt number for a TPCT could be defined as follows:[25,26]

$$Nu = \frac{Q_{net,conv}}{Q_{net,cond}} \quad (4)$$

where $Q_{net,conv}$ indicates the amount of net convective heat transfer and $Q_{net,cond}$ indicates the net conductive heat transfer amount. The amount of the net convective heat transfer is obtained by Eq. (1), while the net conductive heat transfer amount is determined as:[24]

$$Q_{net,cond} = \pi r^2 K_{nf} \frac{\Delta T}{L} \quad (5)$$

where r is the radius, and L is the length of the TPCT, K_{nf} is the thermal conductivity coefficient of the nanofluid, and ΔT is the temperature difference between the condenser and the evaporator section.

Therefore, according to these definitions, the Nusselt number of TPCT is calculated from:

$$Nu = \frac{\dot{m}C_P(T_{out}-T_{in})}{\pi r^2 K_{nf}\Delta T / L} \quad (6)$$

In Eq. (6), only K_{nf} is unknown. Various models have been presented for the estimation of the nanofluid thermal conductivity. However, all of these models are valid only for compounds containing spherical or oval-shaped particles with a small axis ratio. While carbon nanotubes can be considered as oval-shaped nanoparticles with a large axial ratios. Moreover, the existing models cannot explain the effect of CNT spatial distribution on the coefficient of thermal conductivity. Accordingly, Xue[27] presented an equation based on the Maxwell model to calculate the thermal conductivity of CNT containing nanofluids, including the effect of a large axis ratio and spatial distribution of carbon nanotubes. The, Xue equation is defined to estimate the thermal conductivity coefficient:

$$K_{nf} = \frac{(1-\nu)+2\nu\alpha\ln(\gamma)}{(1-\nu)+2\nu\beta\ln(\gamma)}K_{bf} \quad (7)$$

where

$$\alpha = \frac{K_{CNT}}{K_{CNT} - K_{bf}}, \beta = \frac{K_{bf}}{K_{CNT} - K_{bf}}, \gamma = \frac{K_{bf} + K_{CNT}}{2K_{bf}}$$

and ν describes the volume fraction of the nanotubes of the nanofluid. Therefore, considering the volume fraction of carbon nanotubes used in this study were 0.095, 0.238 and 0.476 for nanofluid with a concentration of 0.2, 0.5 and 1 % by weight, respectively. While, K_{bf}, K_{nf}, and K_{CNT} are the thermal conductivity of pure water, nanofluid, and carbon nanotubes, respectively.

The thermal resistance (R_{th}) for the TPCT was obtained from:[18,28]

$$R_{th} = \frac{T_e - T_c}{Q} \tag{8}$$

where, T_e and T_c are defined as the temperatures of the evaporator and condenser section, respectively, and Q indicates the amount of the heat transferred from the condenser section.

In this study, the uncertainty could be estimated by Holman Correlation as follows:[29]

$$\text{Max } E_\eta = \pm\left\{\left(E_{Q_{out}}\right)^2 + \left(-E_{Q_{in}}\right)^2\right\}^{0.5} \tag{9}$$

$$\text{Max } E_{Q_{out}} = \pm\left\{\left(E_{\dot{m}}\right)^2 + \left(E_{C_P}\right)^2 + \left(E_{(T_{out} - T_{in})}\right)^2\right\}^{0.5} \tag{10}$$

$$\text{Max } E_{Q_{in}} = \pm\left\{\left(E_V\right)^2 + \left(E_I\right)^2\right\}^{0.5} \tag{11}$$

Since the maximum precision of the voltmeter, ammeter and thermometer is 1 V, 0.01 A and 0.1 °C, respectively, the maximum uncertainties in the obtained thermal efficiency is 3.5 %.

RESULTS AND DISCUSSION

The thermal efficiency results of the two-phase closed thermosyphon (TPCT) were observed. The factors of the thermal efficiency, thermal resistance, and the Nusselt number are investigated under different operating conditions, as the essential factors affecting the thermal performance of a closed thermosyphon. The effect of parameters such as sample type and nanofluid concentration under various input powers on the thermal performances of two-phase closed thermosyphons (TPCT) were investigated, and the respective diagrams with complete discussion are given. In addition, the temperature distribution on the external surface of the core cylinder of the TPCT, which can be a good indication of the thermal resistance and the vacuum pressure drop in the thermosyphon, are discussed.

In this research, experiment operations were performed at 30, 45, 60, 90 and 120 W input powers in accordance with three weight (volume) concentrations of the SWCNT/water suspension (nanofluid) of 0.2 % (0.095 %), 0.5 % (0.238 %), and 1 % (0.476 %) CNT concentrations. A 3D and linear diagram for the variability of thermal efficiency with a constant input power at a different weight fraction of nanoparticles for the five diverse input powers used in this study are shown in Fig. 3. Thermal efficiency increases with increasing input power and weight fraction of nanoparticles. This enhancement of thermal efficiency depends

on the heat transfer behavior of the nanostructure. Nanoparticles, with their Brownian motion, result in a noticeable rise in the rate of the heat transfer between the fluid and nanotube wall.[11] Therefore, as the nanofluid weight fraction increases, the TPCT thermal efficiency also increases, because the addition of nanostructure into the base fluid enhances the particle collisions in the TPCT. As shown in Fig. 3, the thermal efficiency in the lower concentrations is significantly increased, but at higher concentrations, the increase is less. For example, in the range of 30 to 45 W for input power at a concentration of 0.2 wt. %, the thermal efficiency of the TPCT was increased by about 10 %. According to Fig. 3, it was observed that the nanofluid sample with a concentration of 1 wt. % of SWCNT obtained the highest efficiencies at all input powers, and the maximum efficiency of about 89 %. was reported for an input power of 120 W. In this study, for an input power of 120.75 W (voltage = 75 V, I = 1.61 A) and concentration of 1 wt. %, the temperature of the inlet (T_{in}) and outlet (T_{out}) cooling water reached 19 and 25.1 °C, respectively. According to Eq. (1) and at a mass flow rate of cooling water of 0.00415 kg s^{-1}, the Q_{out} obtained about 107.09 W. By substituting the values of Q_{out} and Q_{in} in Eq. (3), the obtained thermal efficiency of thermosyphon was about 0.89.

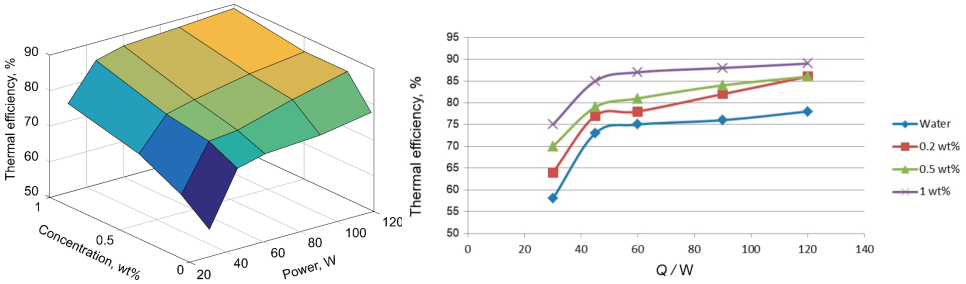

Fig. 3. The TPCT thermal efficiency *vs*. input power and concentration of nanofluid.

The dimensionless Nusselt number in a thermosyphon represents the ratio of the heat transferred through displacement to that transferred through conduction, which is obtained from Eq. (6). In this study, the variation of the Nusselt number under different concentrations of carbon nanotubes and various input power is shown in Fig. 4.

According to Fig. 4, the Nusselt number decreases with increasing concentration of carbon nanotubes in the nanofluid. For example, a nanofluid with 0.2 wt.% of CNT, the Nusselt number at 30 W is about 145.19, while at a concentration of 0.5 and 1.0 wt. % of CNT, these values are about 70.22 and 30.26 at the same input power, respectively. According to Eq. (7), with increasing concentration of carbon nanotubes, the coefficient of thermal conductivity for the nanofluid (K_{nf}) increases and considering the definition of the Nusselt number in

Eq. (6) by increasing the denominator, the Nusselt number decreases consequently, which represents the increase in heat transfer through the conduction mechanism.

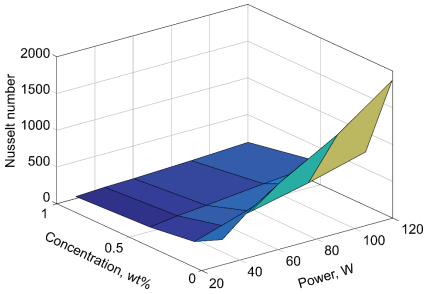

Fig. 4. The thermosyphon Nusselt number versus input power and concentration of nanofluid.

Increasing in the input power, the thermal resistance of the TPCT decreases, whereas, according to Eq. (8), the thermal resistance has an inverse relation to power. However, the reduction of thermal resistance at lower power is more than at a higher power. In addition, by increasing the concentration of SWCNT in the nanofluid, the resistance against the thermal proficiency of the thermosyphon is reduced. For example, at an input power of 30 W, the highest and the lowest thermal resistance are related to water (2.34 °CW^{-1}) and nanofluid 1.0 wt. % of CNT (1.71 °C W^{-1}), respectively. In this study, at an input power of 30.24 W (voltage = 36 V, I = 0.84 A), the average evaporator temperature, condenser temperature, and temperature difference of condenser section obtained about 62.9, 21.8 and 1 °C for water and 61.2, 22.3 and 1.3 °C for nanofluid 1.0 wt. %, respectively. The variation of thermal resistance against the input power of the TPCT is plotted in Fig. 5.

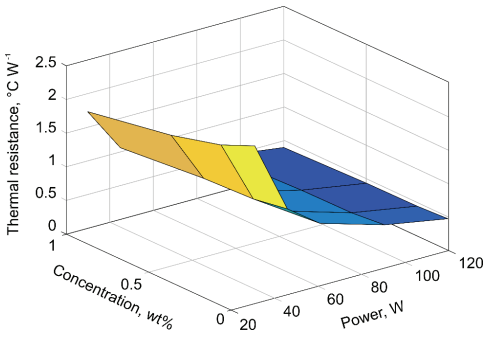

Fig. 5. The thermal resistance of TPCT (in the condenser section) *vs*. input power and concentration of the nanofluid.

Bubble formation at the liquid–solid interface of the TCPT is considered to be the primary cause of the thermal resistance. The larger size of these bubbles leads to the creation of higher amounts of thermal resistance, which interferes with the heat transfer from the solid surface to the fluid. In the presence of nano-

particles dispersed in the fluid, the vapor bubbles will explode at the first moments of formation. Therefore, much smaller vapor bubbles should be did not contain any nanoparticles, which consequently reduces the thermal resistance of the TPCT.[29–33]

Variations in the vacuum pressure drop of the operating fluid are shown in Fig. 6 for each test. It was observed that with increasing nanofluid concentration, the vacuum pressure drop increased, because at higher pressure, the boiling point of the fluid was even higher, and the thermal proficiency of thermosyphon was reduced. In this study, the maximum vacuum pressure drop was obtained for a SWCNT concentration of 1 wt. %. Although the nanofluid had the highest thermal efficiency, it also had the biggest top vacuum pressure drop.

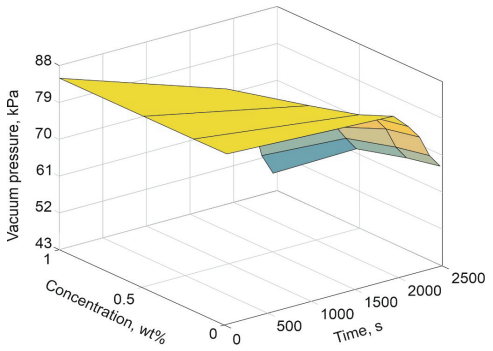

Fig. 6. Vacuum pressure drop *vs.* experiment time and concentration of the nanofluid.

The average temperature of the evaporator section against various input power with various concentrations of SWCNT is plotted in Fig. 7. According to the results of experiments, one could expect the power of 90 and 120 W as the density of nanofluid rises, while the evaporator section average temperature decreases too. For example, at an input power of 45 W, the evaporator section is at average temperature for water, whereas the nanofluid of 0.2, 0.5, and 1 wt. % heats to about 63.9, 63.8, 63.7 and 62.9 °C, respectively. According to Eq. (8), the thermal resistance is directly related to the variations of temperature between the evaporator and condenser section. Hence, with a reduction of the average temperature of the evaporator section, the temperature difference between the evaporator and condenser section evidently decreased, which represents a reduction of the thermal resistance in the TPCT. The thermal resistance of the thermosyphon core surface, the evaporation and condensation process thermal resistances, and the two-phased flow resistance alongside the length of the TPCT form the overall thermal resistance of a thermosyphon totally in between the evaporation core and the condenser section.[20] The surface properties of the interior surfaces of the thermosyphon, such as wettability and roughness, effect the bubbles formation and, consequently, the thermal resistance in the evaporator and condenser section. Using nanofluids, by increasing thermal conductivity and

density of the liquid and decreasing the diameter of the released bubbles, leads to reduced thermal resistance and temperature in the evaporator section.[12,24,29,30] On the other hand, the reason of increasing temperature in the evaporator section at high input power (90 and 120 W) and low concentrations (0.2 and 0.5 wt. %) could be related to an increase in the number of bubbles at high input power and the inability of the nanofluid to explode these bubbles at low concentrations.

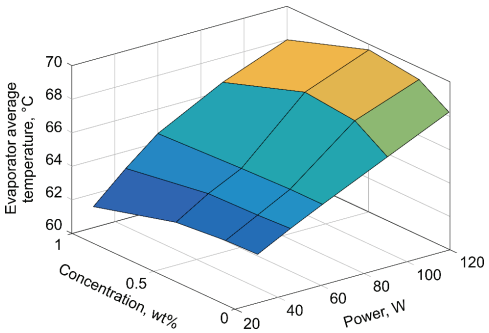

Fig. 7. The average temperature distribution of the evaporator section of the TPCT *vs*. input power and concentration of the nanofluid.

A comparison between the performance of MWCNT & SWCNT in the TPCT

The research carried out on the performance of MWCNT/water nanofluid as the operating fluid in a TPCT[20] indicates that at a concentration of 1 wt. % (R = 0.43) and 90 W input power, which has the highest thermal efficiency, the thermal resistance in condenser section decreased to about 12.24 % compared to the water as the base fluid (R = 0.49). While this reduction for SWCNT/water nanofluid at a concentration of 1 wt. % (R = 0.52) and the same input power compared to water (R = 0.63) is about 17.46 %. In addition, improvement in the thermal efficiency of the thermosyphon at an input power of 90 W is about 12.19 % after applying MWCNT/water nanofluid at a concentration of 1 wt. % (η = 0.8944) compared to pure water (η = 0.7972). While this improvement in thermal efficiency for SWCNT/water nanofluid at a concentration of 1 wt. % (η = 0.88) and the same input power is about 15.78 % compared to water (η = 0.76). Moreover, to achieve steady-state conditions and a thermal efficiency of 89 % needs about 5200 s when using MWCNT/water nanofluid, while the time for SWCNT/water nanofluid to achieve to this thermal efficiency is about 2215 s.

CONCLUSIONS

In this research, the experiments were carried out with a TPCT initiated by input powers of 30, 45, 60, 90 and 120 W along with SWCNT concentrations of 0.2, 0.5 and 1.0 wt. % in the operating nanofluid. The purpose of the current research was to explore the effect of the addition of SWCNT nanoparticles into the operating fluid of a TPCT on the thermal efficiency and its leading parameters, such as vacuum pressure drops, the average temperature of the TCPT

evaporator, Nusselt number, and the thermal resistance of the apparatus. In this section, the most relevant results of this research are mentioned. The results show that SWCNT/water nanofluids at all concentrations lead to improved thermal proficiency of a TPCT. By increasing the density of the nanofluid and electrical power, the thermal efficiency of the TCPT also increases, the improvement in thermal efficiency being more significant at lower input power. Additionally, by increasing the concentration of SWCNT in the operating nanofluid, the Nusselt number of the TPCT decreases, which, together with input power increase, will lead to a reduction in the thermal resistance. The minimum thermal resistance will occur at a concentration of 1 wt. %. Moreover, by condensing the nanofluid, the vacuum pressure drop in the TPCT increases. Also, by increasing the concentration of nanofluids at all amounts of input power, the average temperature of the evaporator section is reduced (except 90 and 120 W at a concentration of 0.2 and 0.5 wt. %), which is confirmed by a reduction in the thermal resistance at the evaporator section. Furthermore, on comparing the performance of the MWCNT/ /water and SWCNT/water nanofluids on a TPCT, it was observed that SWCNT nanofluid has higher thermal efficiency that leads to a greater reduction in thermal resistance at a TPCT.

NOMENCLATURE

C_p	water specific heat, J kg^{-1} K^{-1}
I	current, A
K_{bf}	base fluid thermal conductivity, W m^{-1} K^{-1}
K_{CNT}	carbon nanotube thermal conductivity, W m^{-1} K^{-1}
K_{nf}	nanofluid thermal conductivity, W$m^{-1}K^{-1}$
L	length of evaporator section, m
$\dot{m}$	water mass per unit time, kg s^{-1}
Nu	Nusselt number
Q_{in}	input heat transfer by evaporation, W
$Q_{net,\ cond}$	net conductive heat transfer, W
Q_{out}	output heat transfer by condensation, W
r	radius, m
R_{th}	thermal resistance, K W^{-1} or °C W^{-1}
T_e	evaporator temp, °C
T_c	condenser temp, °C
T_i	inlet temp of cooling water, K
T_o	outlet temp of cooling water, K
V	voltage, V
ΔT	temperature difference (T_e–T_c), °C
$Q_{net,conv}$	net convective heat transfer, W
Greek letters	
η	efficiency of two-phase closed thermosiphon
ν	volume concentration (%)

ИЗВОД

ЕКСПЕРИМЕНТАЛНО ИСПИТИВАЊЕ УГЉЕНИЧНИХ НАНОЦЕВИ СА ЈЕДНОСТРУКИМ ЗИДОМ/ЕФЕКАТ ВОДЕНОГ НАНОФЛУИДА НА ПЕРФОРМАНСЕ ДВОФАЗНОГ ЗАТВОРЕНОГ ТЕРМОСИФОНА

MOHAMMAD CHEHRAZI и BAHAREH KAMYAB MOGHADAS

Department of Chemical Engineering, Shiraz Branch, Islamic Azad University, Shiraz, Iran

Термосифони су међу најефикаснијим апаратима за размену топлоте који се користе у различитим индустријама. Једна од најчешћих употреба ових уређаја је регенерација енергије, што је изузетно битно, с обзиром на енергетску кризу. Неколико параметара, као што су геометријске димензије, тип радног флуида, тип тела термосифона, утиче на ефикасност термосифона. У овом експерименту испитиван је утицај типа и концентрације воденог нанофлуида са угљеничним наноцевима са једноструким зидом (*single-walled carbon nanotube nanofluid* – SWCNT) на ефикасност преноса топлоте у двофазном затвореном термосифону (*two-phase closed thermosyphon*). За ову сврху, најпре је конструисан двофазни затворени термосифон. Затим су водени SWCTN нанофлуиди са тежинским концентрацијама 0,2; 0,5 и 1 % коришћени као радни флуид у термосифонском систему. Резултати експеримената су показали да додатак нанофлуида било које концентрације и повећање улазне снаге побољшавају перформанце система. Такође, топлотни отпор двофазног затвореног термосифона опада са повећањем нивоа SWCNT и улазне снаге. Тако, за припремљене узорке нанофлуида, најмања вредност топлотног отпора је добијена за 1 % SWCNT и 120 W. Такође , Нуселтов број расте са повећањем улазне снаге и смањује се са повећањем концентрације. У свим експериментима, сви припремљени узорци нанонфлуида су имали значајно боље топлотне перформансе у поређењу са чистом водом.

(Примљено 28. јуна, ревидирано 26. октобра, прихваћено 29. октобра 2020)

REFERENCES

1. M. Ramezanizadeh, M. A. Nazari, M. H. Ahmadi, E. Açıkkalp, *J. Mol. Liq.* **272** (2018) 395 (https://doi.org/10.1016/j.molliq.2018.09.101)
2. H. Karami, S. Papari-Zare, M. Shanbedi, H. Eshghi, A. Dashtbozorg, A. Akbari, C. B. Teng, *Int. Commun. Heat Mass* **108** (2019) 104302 (https://doi.org/10.1016/j.icheatmasstransfer.2019.104302)
3. A. O. Borode, N.A. Ahmed, P. A. Olubambi, *Nano-Struct. Nano-Objects* **20** (2019) 100394 (https://doi.org/10.1016/j.nanoso.2019.100394)
4. E. Živković, S. Kabelac, S. Šerbanović, *J. Serb. Chem. Soc.* **74** (2009) 427 (https://doi.org/10.2298/JSC0904427Z)
5. S. U. Choi, J. A. Eastman, *International Mechanical Engineering Congress and Exposition*, in *Enhancing Thermal Conductivity of Fluids with Nanoparticles*, San Francisco, CA, 1995, p. 12
6. H. U. Kang, S. H. Kim, J. M. Oh, *Exp. Heat Transf.* **19** (2006) 181 (https://doi.org/10.1080/08916150600619281)
7. L. Godson, B. Raja, D. M. Lal, S. Wongwises, *Exp. Heat Transf.* **23** (2010) 317 (https://doi.org/10.1080/08916150903564796)
8. H. R. Goshayeshi, M. R. Safaei, M. Goodarzi, M. Dahari, *Powder Technol.* **301** (2016) 1218 (https://doi.org/10.1016/j.powtec.2016.08.007)
9. S. Zeinali Heris, M. N. Esfahani, G. Etemad, *J. Enhanc. Heat Transf.* **13** (2006) 279 (https://doi.org/10.1615/JEnhHeatTransf.v13.i4.10)

10. S. Zeinali Heris, G. Etemad, M. Nasr Esfahany, *Int. Commun. Heat Mass* **33** (2006) 529 (https://doi.org/10.1016/j.icheatmasstransfer.2006.01.005)
11. S. Zeinali Heris, M. Nasr Esfahany, G. Etemad, *Int. J. Heat Fluid Flow* **28** (2007) 203 (https://doi.org/10.1016/j.ijheatfluidflow.2006.05.001)
12. S. H. Noie, S. Zeinali Heris, M. Kahani, S. M. Nowee, *Int. J. Heat Fluid Flow* **30** (2009) 700 (https://doi.org/10.1016/j.ijheatfluidflow.2009.03.001)
13. S. W. Kang, W. C. Wei, S. H. Tsai, S. Y. Yang, *Appl. Therm. Eng.* **26** (2006) 2377 (https://doi.org/10.1016/j.applthermaleng.2006.02.020)
14. H. J. Jia, L. Jia, Z. Tau, *J. Therm. Sci.* **22** (2013) 484 (https://doi.org/10.1021/ma302119t)
15. Q. Xu, L. Liu, J. Feng, L. Qiao, Ch. Yu, W. Shi, Ch. Ding, Y. Zang, Ch. Chang, Y. Xiong, Y. Ding, *Int. J. Heat Mass Transf.* **149** (2020) 119189 (https://doi.org/10.1007/s11630-020-1273-7)
16. S. Das, A. Giri, S. Samanta, *Energy Source, A* (2020) 1 (https://doi.org/10.1080/15567036.2020.1727998)
17. S. Berber, Y. K. Kwon, D. Tomanek, *Phys. Rev. Lett.* ***84*** (2000) 4613 (https://doi.org/10.1103/PhysRevLett.84.4613)
18. Z. H. Liu, X. F. Yang, G. S. Wang, G. L. Guo, *Int. J. Heat Mass Transf.* **53** (2010) 1914 (https://doi.org/10.1016/j.ijheatmasstransfer.2009.12.065)
19. S. U. Choi, Z. G. Zhang, W. Yu, F. E. Lockwood, E. A. Grulke, *Appl. Phys. Lett*. **79** (2001) 2252 (https://doi.org/10.1063/1.1408272)
20. M. Shanbedi, S. Zeinali Heris, M. Baniadam, A. Amiri, *Exp. Heat Transf.* **26** (2013) 26 (https://doi.org/10.1080/08916152.2011.631078)
21. M. T. Pettes, L. Shi, *Adv. Funct. Mater.* **19** (2009) 3918 (https://doi.org/10.1002/adfm.200900932)
22. D. Wen, Y. Ding, *J. Thermophys. Heat Transf.* **18** (2004) 481 (https://doi.org/10.2514/1.9934)
23. Y. Yang, E. A. Grulke, Z. G. Zhang, G. Wu, *J. Appl. Phys.* **99** (2006) 114307. (https://doi.org/10.1063/1.2193161)
24. S. H. Noie, *Appl. Thermal Eng.* **25** (2005) 495 (https://doi.org/10.1016/j.applthermaleng.2004.06.019)
25. S. Maki, T. Tagawa, H. Ozoe, *J. Heat Transf.* **124** (2002) 667 (https://doi.org/10.1115/1.1482082)
26. H. Salehi, S. Zeinali Heris, S. H. Noie, *J. Enhanced Heat Transf.* **18** (2011) 261 (https://doi.org/10.1615/JEnhHeatTransf.v18.i3.70)
27. Q. Z. Xue, *Physica B* **368** (2005) 302 (https://doi.org/10.1016/j.physb.2005.07.024)
28. S. Khandekar, Y. M. Joshi, B. Mehta, *Int. J. Ther. Sci.* **47** (2008) 659 (https://doi.org/10.1016/j.ijthermalsci.2007.06.005)
29. J. D. Holman, *Experimental Methods for Engineers*, 5th ed., Ch. 3, McGraw-Hill, New York, 1989
30. H. Sardarabadi, S. Z. Heris, A. Ahmadpour, M. Passandideh-Fard, *Energy Conv. Manage.* **188** (2019) 321 (https://doi.org/10.1016/j.enconman.2019.03.070)
31. M. M. Sarafraz, I. Tlili, Z. Tian, M. Bakouri, M. R. Safaei, *Physica A* **534** (2019) 122146 (https://doi.org/10.1016/j.physa.2019.122146)
32. C. Li, Z. Wang, P. Wang, Y. Peles, N. Koratkar, G. P. Peterson, *Small* **4** (2008) 1084 (https://doi.org/10.1002/smll.200700991)
33. S. J. Kim, I. C. Bang, J. Buongiorno, L. W. Hu, *Int. J. Heat Mass Transf.* **50** (2007) 4105 (https://doi.org/10.1016/j.ijheatmasstransfer.2007.02.002).

Journal of the Serbian Chemical Society
JSCS-info@shd.org.rs • www.shd.org.rs/JSCS
J. Serb. Chem. Soc. *86* (3) 327–340 (2021)
JSCS–5424
Original scientific paper

Role of EDTA capped cobalt oxide nanomaterial in photocatalytic degradation of dyes

MEENA SINGH[1], DIPTI VAYA[2]*, RAVI KUMAR[3] and BIJOY K. DAS[1]

[1]*Department of Applied Science, The NorthCap University, Sector 23A, Gurugram-122017, India,* [2]*Department of Chemistry, Amity School of Applied Sciences, Amity University Haryana, Gurugram-122413, India and* [3]*Department of Chemistry, NIT, Srinagar, Jammu and Kasmir-190006, India*

(Received 11 July, revised 4 October, accepted 16 November 2020)

Abstract: Dyes released from textile, paint, and various other industries in wastewater have posed long term environmental damage. Functional nanomaterials provide a hope and opportunities to treat these effluent wastes in a rapid and efficient way due to their large surface area to volume ratios. Synthesis of 2,2',2",2"'-(ethane-1,2-diyldinitrilo)tetraacetic acid (EDTA) capped cobalt oxide nanomaterial, as a photocatalyst, has been investigated and used for the rapid and efficient removal of malachite green (MG) and crystal violet (CV) dyes. The morphological, structural, optical, chemical and thermal properties of the synthesized nanomaterial were analysed using different characterization tools such as scanning electron microscopy, transmission electron microscopy, X-ray diffraction, ultra violet–visible and Fourier transform infrared (FT-IR) spectroscopy and thermogravimetric analysis. The prepared EDTA capped cobalt oxide nanomaterials display better photocatalytic degradation, 56.3 % for MG and 37.9 % for CV in comparison to the pure cobalt oxide, 47.7 and 27.6 %, respectively, under visible light illumination. The kinetics of the degradation followed the pseudo-first order and it corresponds to Freundlich adsorption isotherm model. The incremental photodegradation of these two dyes was attributed by morphology of the nanomaterial which favour effective electron/hole separation.

Keywords: photocatalytic activity; crystal violet; malachite green; adsorption isotherm.

INTRODUCTION

Dye stuffs represent a class of synthetic organic pigments; these are one of the many causes for growing ecological issues. Coloured dyeing wastewaters emanating from industries are largely non-biodegradable and also carcinogenic in nature. They also problems with creating the aquatic creatures and adversely

* Corresponding author. E-mail: diptivaya08@gmail.com
https://doi.org/10.2298/JSC200711074S

affect water ecosystem.[1] Therefore, degradation of dyes has attracted attention and substantial efforts have been committed to the specific remediation techniques. These techniques could degrade bio-recalcitrant organic contaminants into non-toxic form before their discharge into water to decrease the pollution load on mainstream water.

A number of methods such as biodegradation, ozonation, chemical degradation, oxidation, reduction, precipitation, flocculation, photolysis, adsorption, and advanced oxidation process, *etc.*[2,3] have been used to investigate the removal of the dyeing from wastewater. However, heterogeneous photocatalysis, using semiconductor oxides under UV/Vis light, expresses immense potential to convert these organic pollutants into reasonably harmless end products such as CO_2, H_2O and inorganic ions with the possibility of regeneration.[4] Photocatalysis offers good advantage over other conventional methods, as it uses a renewable and ecologically favourable source of energy like sunlight and has many other benefits such as easily controlled simple instrumentation and non-selective oxidation. Semiconducting materials, including TiO_2,WO_3, Ta_2O_5, TiO_2, ZnO, ZrO_2, CdS, MoS_2, Fe_2O_3, ZnS and CdS have been used as heterogeneous photocatalysts for the efficient photodegradation of several organic pollutants present in waste water.[5]

The applicability of heterogeneous catalysts can be improved by modulating their particle size, morphology, size distribution and dispersion. Nanomaterials possessing attractive physical and chemical properties, such as higher surface area to volume ratio and new interfacial properties, that could be used to enhance the photocatalytic process.[6] The semiconductor metal oxide nanoparticles show size dependent optical properties.[7,8]

Magnetic spinel p-type semiconductor Co_3O_4 is a technologically important oxide. A number of different methods for the synthesis of cobalt oxide nanoparticles such as coprecipitation, sol–gel, thermal decomposition, pulsed laser deposition and solution combustion[9–13] were reported. The sol–gel method has acquired more curiosity among researchers in the synthesis of nanoparticles as it offers controlled consolidation, shape modulation and patterning of the nanostructures.[14,15] However, literature survey shows that very small nanoparticles have an extremely high surface area to volume ratio hence, they agglomerate easily to minimize their surface, but size can be controlled by tuning their surface, which can be achieved by capping.[8,16] The nature and the critical concentration of the capping agents controls the morphology of the synthesized nanoparticles.[17]

MG and CV are typical basic triarylmethane cationic dyes. They are used extensively as colouring agents in industries.[18,19] The cationic dyes are more poisonous as they can easily enter the cells through the negatively charged cells membrane surfaces and accumulate in the cytoplasm.[20,21] Both dyes are carcinogenic and pose environmental risks, as MG dye and its reduced form has adverse

effects on the reproductive and the immune system[22] and CV is a mutagen and mitotic poison.[23] The excess inhalation of these dyes cause irritation of the respiratory tracts, vomiting, diarrhoea, headache, dizziness and its long term exposure might damage the mucous membrane and the gastrointestinal tract.[24]

The activity of cobalt oxide nanoparticles is influenced by several factors such as crystallinity, particle size, surface area and method of preparation. The studies reflect Co_3O_4 used in applications such ceramics, pigments, electrochemical devices, solid state sensors, lithium ion batteries, gas sensors, magnetic storage and supercapacitors.[25–27] However, its photocatalytic property has been occasionally observed.[28,29]

The target of the present study is to synthesize photocatalytic active EDTA supported stable cobalt oxide nanomaterial by green chemistry approach and its application in the effectively degradation of MG and CV dyes in aqueous solution. The possible mechanism for photocatalytic degradation of the dyes based on experimental results has also been proposed.

EXPERIMENTAL

All chemicals are analytical grade purchased from Merck and Fischer Scientific. Deionised water was used in all experiments.

Synthesis of EDTA capped cobalt oxide nanomaterial

EDTA supported cobalt oxide nanomaterials were synthesized using the sol–gel method. In brief, aqueous $Co(NO_3)_2{\cdot}H_2O$ of 0.2 M was taken as precursor and 1.0 M NaOH solution was added to it slowly in drops under continuous stirring until basic medium (pH 9) was achieved. Stoichiometric ratio of aqueous solution of capping agent EDTA was prepared and then mixed dropwise with the above basic solution. Thereafter, the reaction mixture was refluxed at 70–80 °C for 15 h until a gel-like compound was formed. The gel was ripened for 12 h and afterwards heated at 200 °C in air oven for 2–3 h to get EDTA supported cobalt oxide nanomaterial (ECO). Finally, ECO was ground in mortar and pestle and stored in desiccators. Similar method is used for the synthesis of cobalt oxide nanomaterials without using EDTA (CO).

Characterization of nanomaterials

The structural and phase crystallinity of the ECO was done using PXRD on Bruker AXS D8 Advance with Cu X-ray wavelength 1.5406 Å at a 2θ scan rate of 0.5°/min, the surface morphology and particles size was investigated using SEM (Zeiss EVO 18) and TEM (Jeol JEM 2100). Functionalities and thermal properties of the capping molecule were investigated using FT-IR spectroscopy and TGA (STA 8000 Perkin Elmer). FT-IR spectra were recorded in the wave number range of 4000 to 400 cm^{-1} using KBr pellets. UV–Vis-NIR spectrophotometer (Cary 5000 Series) was used to record the absorbance spectra of the solid sample. Light intensity was measured by solarimeter.

Photocatalytic activity

MG (C.I. 93405) and CV (C.I. 42555) are organic dyes with chemical formulas $C_{23}H_{25}N_2Cl$ and $C_{25}H_{30}N_3Cl$. Prior to start the photocatalytic activity, the optimization parameters of reaction have been measured, these are: pH 7.5, dye concentration = 10^{-5} M, catalyst amount = 20 mg, light intensity = 60 W cm^{-2}. Then aqueous solutions of optimum concentrat-

ion of dyes (10^{-5} M) and catalyst ECO was taken in beakers. These are placed in dark to attain adsorption and absorption equilibrium and then put under the simulated sunlight of 60 W cm^{-2}. A water filter was used to cut off thermal radiations from the light. Aliquot samples of 5 mL were pipette out at regular interval of 10 min and their absorbance value was monitored at a wavelength of λ_{max} = 610 nm for MG and 590 nm for CV. These values track the photocatalytic progress of these two dyes. Control photocatalysis test with pure cobalt oxide catalyst (CO) was also performed concurrently under similar conditions for comparison. The degradation efficiency of dyes over CO and ECO samples were estimated by:

$$\text{Degradation, \%} = 100\frac{A_0 - A_t}{A_0} \quad (1)$$

where, A is initial absorbance and A_t is absorbance of the dye at t time. Photocatalysis experiments were performed at room temperature. Blank experiments were carried out by irradiating the aqueous solutions of the dyes in the absence of catalyst sample.

RESULT AND DISCUSSION

PXRD of the synthesized nanomaterial measured at 2θ of 20–80° (Fig. 1). These diffraction peaks best matched with Co_3O_4 nanomaterial with JCPDS card No. 09-418. Sample of ECO exhibits few more peak due to capping material, *i.e.*, sodium tetraacetate. From Fig. 1a and b, series of well defined peaks are: 20.06 (111), 31.4 (220), 37.04 (311), 45.06 (400), 59.3 (511) and 65.38° (440), measured which show FCC phase of Co_3O_4 material with Fd3m space group. Sharpness of majority of peaks indicated good degree of crystallinity. In addition, broadening of few peaks was explained by nanometer size range of Co_3O_4. The crystallite size, D, of the nanoparticles was estimated by the Debye–Scherrer formula:

$$D = K\lambda/\beta\cos\theta \quad (2)$$

where, K = Scherrer constant (*i.e.*, 0.94), λ = 0.15406 nm, β = full width at half-maximum (FWMH) of the (311) PXRD peak and θ = Bragg diffraction angle. The computed crystallite sizes were found to be 70 and 43 nm for CO and ECO nanomaterials.

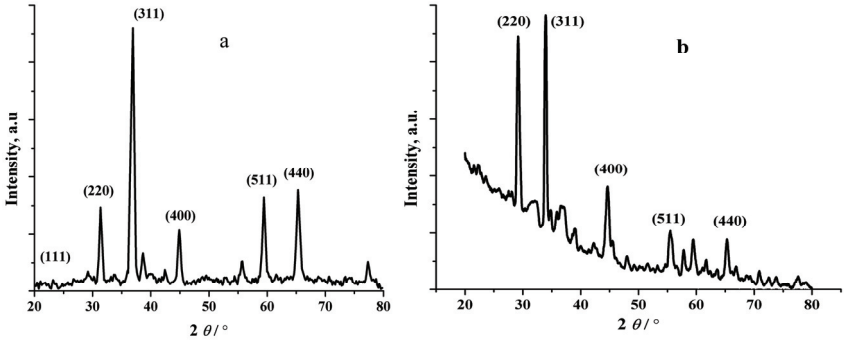

Fig. 1. PXRD of: a) CO and b) ECO.

SEM photograph of CO and ECO revealed the surface texture, porosity and structure of the synthesized nanomaterial. EDTA is an outstanding metal ion chelating agent with six coordinating sites, *i.e.*, two nitrogen and four hydroxyl groups. Hence, surface functionalization through coordination bonds ceased the nucleation growth of the particles and also effectively stabilized them against further oxidation. Nanomaterials exhibited polyhedral shapes with dimensions range from 200 to 300 nm (Fig. 2b). Their porous morphology exposed greater surface area and more reactive sites. CO powder (Fig. 2a) had no particular morphology and the particles are present as highly agglomerated structures.

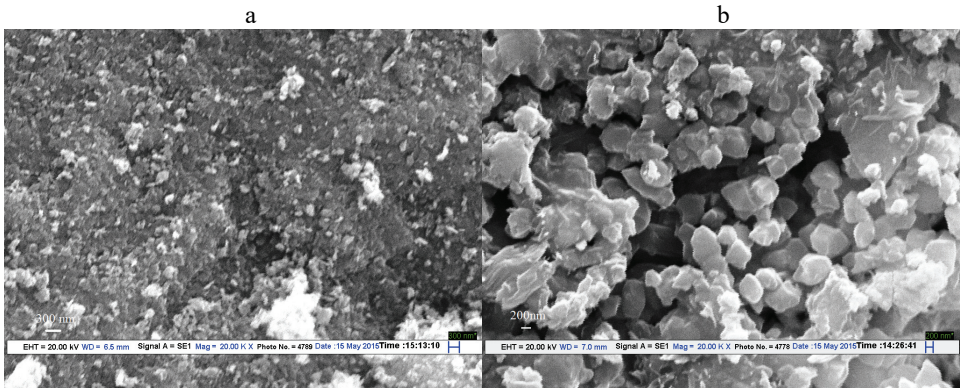

Fig. 2. SEM micrographs of: a) CO and b) ECO.

TEM images of Fig. 3a–d of ECO revealed that the cobalt oxide is capped. Fig. 3c, indicates that the average nanosize of embedded cobalt oxide is 40 nm with nearly spherical morphology matches with XRD crystalline size. SAED pattern of ECO nanomaterial was shown in Fig. 3d where the appearance of diffraction rings and bright spots represent the good degree of crystallinity. This data matches very well with the reported XRD patterns.

The absorption curve (Fig. 4) of ECO and CO for the samples represent two strong absorption bands in 250–350 nm and 400–580 nm wavelength ranges. The first band may be assigned to the charge transfer process from O^{2-} to Co^{2+} while the second one represents O^{2-} to Co^{3+}.[30] It is explicable from the optical absorption spectra that the absorption onset is almost the same for the uncapped and capped samples, as well as the absorption peaks, are without any significant blue shift, probably due to uneven distribution of the synthesized particles. ECO showed lower absorption than CO, suggested the morphological changes of the nanoparticles. This suggested slight variation in band gap which is confirmed by Tauc plot. The value of band gap is determined to be 1.80 and 2.80 eV for ECO and CO, respectively, by plotting graph between energy verses $(\alpha hc/\lambda)^2$. It has also been suggested that the absorption also depends on particle size as reported.[15]

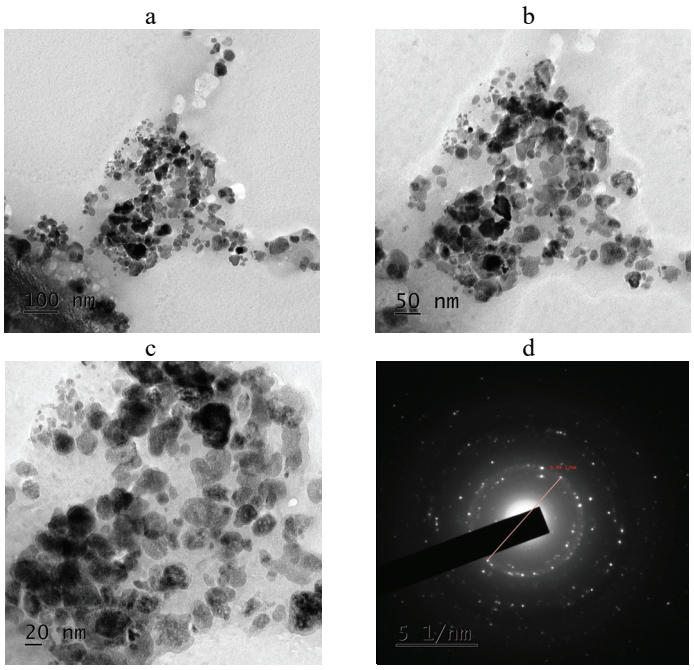

Fig. 3. a–c) Images of TEM at different scales; d) SAED image of TEM.

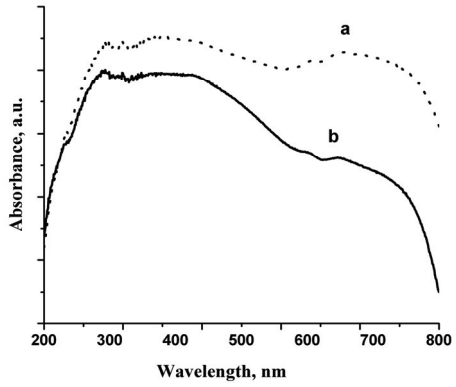

Fig. 4. Optical absorption spectra of: a) CO and b) ECO.

In distinction with the FT-IR spectra of pure EDTA, ECO spectrum is highly resolved (Fig. 5a and b). The spectrum of ECO as represented is broad and few peaks with low transmittance, confirming the complexation of EDTA. The sharp strong absorption band at 1700 cm^{-1} of –C=O stretch of COOH shifted to 1630 cm^{-1} as compare to pure EDTA.[31] This shifting confirmed that EDTA has been encapsulated the Co_3O_4 nanocrystals through esterification between carboxylate group present in EDTA and hydroxyl groups on the Co_3O_4 nanomaterial surface[32–35] and develop a partial single bond character to the –C=O. The broad

absorption band in the higher frequency region of ECO spectrum around 3457 cm^{-1} was associated with hydrogen bond –OH stretching vibration mode of EDTA. The –CN stretch at 1192 cm^{-1} in pure EDTA,[31] shifted to 1177 cm^{-1} in ECO. The sharp and strong absorption band at 1383 cm^{-1} would be the bending vibrations of –CH of methylene groups of EDTA. The sharp peak was at 847 cm^{-1} due to –CH and –OH out of plane bending vibrations. The sharp band around 588 cm^{-1} and shoulder at 662 cm^{-1} characteristics of Co–O stretching and O–Co–O bridging vibrations, respectively, are present in the spectrum of CO even stronger than ECO.

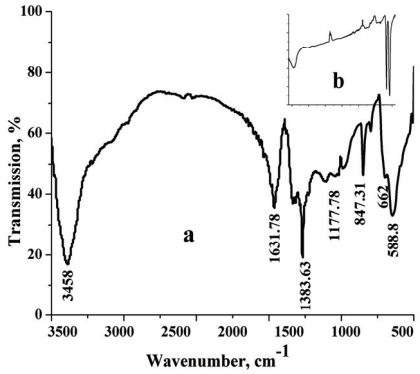

Fig. 5. FTIR spectra of: a) CO and b) ECO.

TGA analysis of ECO performed from room temperature to 700 °C. ECO sample represent 2 steps of thermal degradation. ECO sample exhibited 15 % loss due to moisture removal till 200 °C. After 200 °C sudden reduction of mass is occurred between 210–350 °C, which is attributed to the decomposition of ligand, *i.e.*, EDTA and removal of nitrous oxide, acid moieties as shown in Fig. 6. Above 600 °C again mass reduced due to the formation of CoO from Co_3O_4.

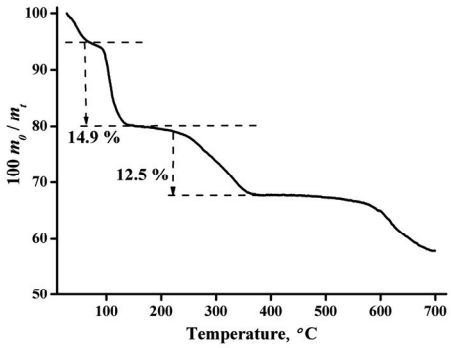

Fig. 6. TGA graph of ECO.

A number of isotherm models such as Langmuir, Freundlich, *etc.* have already been reported to explain the relationship between the amount of ads-

orbate per unit mass of adsorbent. Here, Langmuir and Freundlich isotherm models were used for the isotherm studies by varying the concentration of MG solution from 10 to 150 mg L^{-1}. The well-known linearized equation of Langmuir isotherm model is represented as:

$$\frac{C_e}{Q_e} = \frac{1}{Q_o K_L} + \frac{1}{Q_o} C_e \tag{3}$$

where C_e is the equilibrium concentration in mg L^{-1}, Q_e is the amount of adsorbate adsorbed at equilibrium in mg g^{-1} and Q_o / mg g^{-1} and K_L / L mg^{-1} are the Langmuir constants related to the adsorption capacity and the rate of adsorption, respectively. When C_e/Q_e *vs.* C_e was plotted, a straight line with slope $1/Q_o$ and intercept $1/(Q_o K_L)$ is obtained as shown in Fig. 7a. From these, Langmuir constants Q_o and K_L were calculated and are listed in Table I. The lower value of correlation coefficients R^2 displays that the adsorption does not follows Langmuir isotherm model.

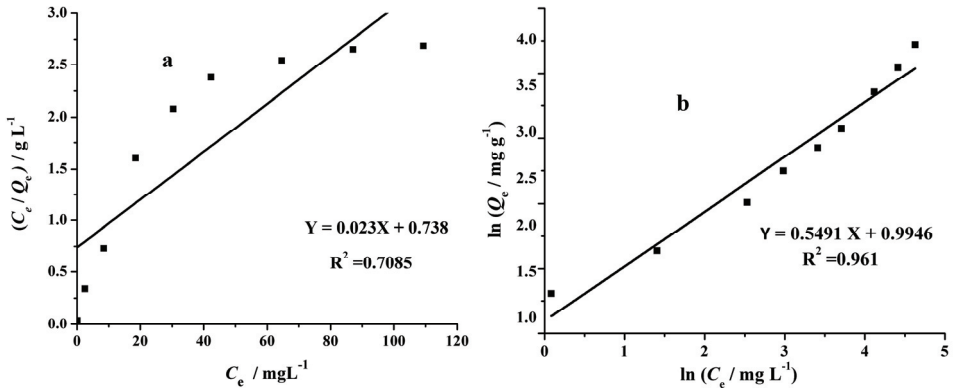

Fig. 7. Adsorption isotherms; a) Langmuir b) Freundlich.

The Freundlich isotherm model reflects as multilayer adsorption. The linearized form of Freundlich isotherm:

$$\ln Q_e = \ln K_F + \frac{1}{n} \ln C_e \tag{4}$$

where, Q_e and C_e are the same as in Langmuir isotherm, K_F and n are the Freundlich constants K_F is related to the binding energy of the adsorbent and n is the heterogeneity factor, which measure the deviation from linearity of the adsorption. The adsorption will be favourable if the value will be in the range of 1 to 10. The plot between ln Q_e *vs.* ln C_e gives a straight line with slope $1/n$ and intercepts ln K_F as representing in Fig. 7b. The values of Freundlich constants are given in Table I. Both the isotherm experiments were carried out at room temperature. Based on the higher values of correlation coefficients R^2, the adsorption

data are depicted better by the Freundlich isotherm model than by the Langmuir isotherm model.

Table I. Coefficient of adsorption isotherm model with malachite green over ECO

Langmuir adsorption isotherm	Freundlich adsorption isotherm
Q_o = 43.47 mg g^{-1}	K_F = 9.876 (mg/g) (L/mg)$^{1/n}$
K_L = 0.0377 L mg^{-1}	1/n = 0.5491
R^2 = 0.7083	R^2 = 0.961

The photocatalysis of dyes was monitored by noting the decrease in absorbance of the dyes in presence samples under visible light irradiation. It was observed that the relative absorption intensity decreases as the visible light illumination contact period increases, which imply that the MG and CV dyes decompose gradually and their concentration decreases, while the rate of decrease was greater for MG than compared to CV. Initially, the rate of reaction increases with increase pH till 7.5, then the rate declines with increase in the pH value. This change happens due to the surface charge of catalyst and the point of zero charge which vary with change in pH.

The rate constant for the photodegradation of each dye was calculated from the plot of the absorbance and irradiation time. The rate constant of the photodegradation was determined using the expression:

$$k = \frac{1}{t} \ln \frac{A_o}{A_t} \tag{5}$$

where k and t are rate constant and time. The photocatalyst ECO was found to be more efficient in mineralization of MG dye (56.3 % in 100 min) in Table II and Fig.8a with higher reaction rate constant, when compared to CV (Table II and Fig. 8b). Also, the significant degradation of MG to 56.3 % was achieved in shorter time interval of less than 100 min of irradiation, whereas it took 190 min for CV to degrade 37.9 % (Table II). The degradation rate values were higher for both the dyes when compared with CO sample and also no self-decomposition of the dyes took place in absence of catalyst under the above similar conditions. Table III represent comparison with previous literature.

Under same photocatalyst, MG degradation was higher than CV, which exhibited that photocatalytic activity depends on the distinctive chemical structures of the dyes.

As reported by Ju *et al.* the degradation mechanism of CV and MG dye in aqueous solution followed a five step path: cleavage of central carbon atom, consequent decomposition of the p-π conjugated structure, *N*-demethylation reactions, adduct reactions, loss of benzene rings and ring opening reactions.[39,40] The probable mechanism is suggested in Scheme 1. CV first gets degraded into MG which further breaks down. Both dyes have para quinoid ring chromophores and

phenyl rings substituted at para position by positively charged *N*,*N*′-dimethyl amino auxochromes.

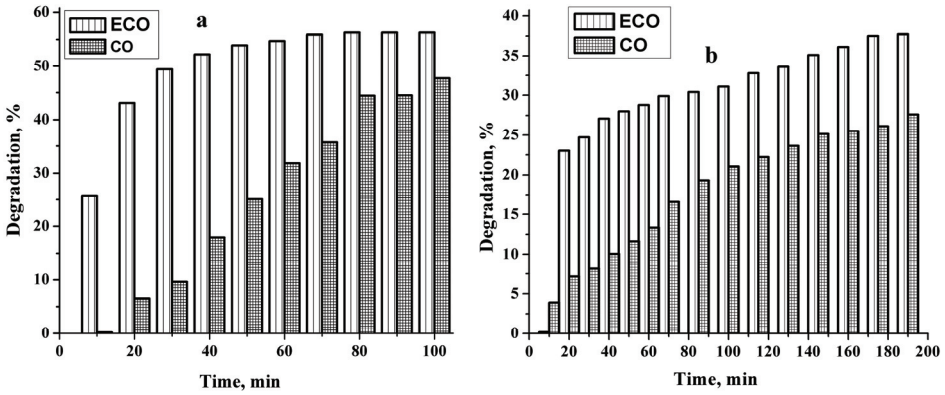

Fig. 8. Percentage degradation of: a) MG and b) CV dye in the presence ECO and CO.

TABLE II. Rate constants and degradation of dyes

Sample	MG Dye		CV dye	
	Rate constant, min^{-1}	Degradation, %	Rate constant, min^{-1}	Degradation, %
ECO	2.15×10^{-2}	56.3	4.0763×10^{-3}	37.9
CO	5.89×10^{-3}	47.7	2.9017×10^{-3}	27.6

TABLE III. Comparison of degradation of dyes

Co_3O_4 nanocatalyst, catalyst loading	Methodology	Pollutant dye	Time min	Degradation %
CoAc, urea and PEG, 0.5 g L^{-1} [36]	Hydrothermal	Methyl violet	120	50
Cobalt chloride, EG, PVP and hydrazine, 20 mg L^{-1} [29]	Hydrothermal	Methyl orange	100	70
Cobalt chloride, EG and sodium acetate, 10 mg L^{-1} [37]	Hydrothermal	Methyl orange	120	55
Cobalt nitrate, 1 g L^{-1} [38]	Sol–gel	Methylene blue	120	10

MG has two substituted rings while CV has three substituted rings which affect their spatial configuration. The two substituted rings in MG are coplanar whereas in CV the three rings are twisted out of the plane of the central conjugated ring which makes it more stable[41] suggesting that a large energy barrier is to be crossed to degrade CV into MG. EDTA, being a hexadentate ligand and effective capping agent has also been confirmed earlier with ZnO.[41] It is therefore critical to the formation of a protective layer as it gets chemisorbed as carboxylate onto the surface of cobalt oxide nanoparticles, altering their surface properties, which not only stabilizes them against agglomeration and aggregation but also prevents their aerial oxidation. As reported in literature the EDTA molecules

cap and confine the particle size to a great extent.[42] Porous structures on the surface allow greater adsorption of dye molecules and shorter diffusion path length of photogenerated charge carriers.[12] All the above factors contributed to the better performance of ECO for photocatalytically degradation the MG dye.

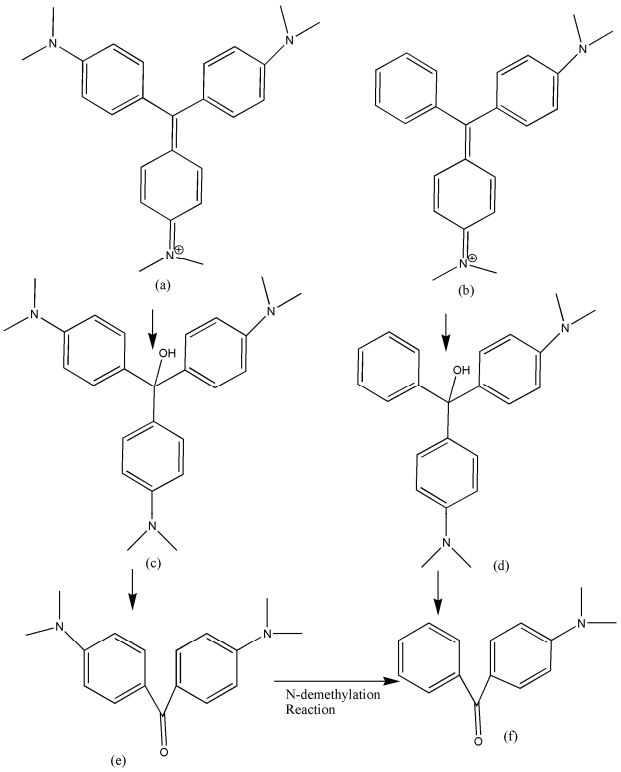

Scheme 1. Probable degradation mechanism of MG and CV dye (a – MG; b – CV; c and d – carbinol base; e – bis(4-(dimethylamino)phenyl)methanone; f – 4-dimethylaminobenzophenone).[39]

CONCLUSION

ECO and CO were synthesized by a sol–gel route and utilized as catalysts for the photocatalytic degradation of MG and CV dyes to reduce their toxicity. The nanomaterial revealed crystalline morphologies and good optical properties.

The ECO nanomaterial is found superior than CO and exhibited higher capacity for removal of MG and CV dyes from aqueous solution under visible light irradiations. This is due to the distinctive morphology, high surface area and high crystalline of synthesized EDTA supported Co_3O_4. The different rate of degradation of dyes was based on the specific stero-configuration of MG and CV dyes. Therefore, it could be concluded that ECO is one of the excellent active catalyst

for the removal of cationic basic dyes from water, especially MG. Photocatalytically degradation of dyes follow pseudo first order kinetics and are presented by the Freundlich adsorption isotherm.

Acknowledgements. The authors thank IIT Delhi and DST-SAIF, Kochi for sample analysis. DV would also like to acknowledge the support provided under the DST-FIST Grant No.SR/FST/PS-I/2019/68 of Govt. of India.

ИЗВОД

УЛОГА НАНОМАТЕРИЈАЛА КОБАЛТ-ОКСИДА КАПТИРАНОГ СА EDTA У ФОТОКАТАЛИТИЧКОЈ РАЗГРАДЊИ БОЈА

MEENA SINGH[1], DIPTI VAYA[2], RAVI KUMAR[3] и BIJOY K. DAS[1]

[1]*Department of Applied Science, The NorthCap University, Sector 23A, Gurugram-122017, India,* [2]*Department of Chemistry, Amity School of Applied Sciences, Amity University Haryana, Gurugram-122413, India и* [3]*Department of Chemistry, NIT, Srinagar, Jammu and Kasmir-190006, India*

Боје из текстила, фарби и других индустријских производа загађују одпадне воде. Функционални наноматеријали обезбеђују начин да се отпадне воде ефикасно и брзо пречисте, захваљујући томе што имају велику површину у односу на запремину. Испитивана је синтеза кобалт оксида каптираног са етилендиаминтетрасирћетном киселином (EDTA) и његова примена на уклањање малахитне зелене (MG) и кристално љубичасте (CV) боје. Карактеризација синтетисаног наноматеријала испитана је SEM, TEM, XRD, TGA, FT-IR и UV–Vis техникама. Наведени наноматеријал показује бољу фотокаталитичку деградацију боја од самог кобалт оксида. Кинетика деградације је псеудо-првог реда и одговара Фројндлиховој апсорпционој изотерми. Фотодеградација две наведене боје се објашњава морфологијом наноматеријала који омогућава ефикасну електрон/ /шупљина сепарацију.

(Примљено 11 јула, ревидирано 4. октобра, прихваћено 16. новембра 2020)

REFERENCES

1. J. H. Huang, K. L. Huang, S. Q. Liu, A. T. Wang, C. Yan, *Colloids Surfaces, A* **330** (2008) 55 (https://doi.org/10.1016/j.colsurfa.2008.07.050)
2. R. Kabbout, S. Taha, *Phys. Proc.* **55** (2014) 437 (https://doi.org/10.1016/j.phpro.2014.07.063)
3. M. B. Kasiri, N. Modirshahla, H. Mansouri, *Int. J. Ind. Chem.* **4** (2013) 3 (https://doi.org/10.1186/2228-5547-4-3)
4. L. Saikia, D. Bhuyan, M. Saikia, B. Malakar, D. K. Dutta, P. Sengupta, *Appl. Catal., A* **490** (2015) 42 (https://doi.org/10.1016/j.apcata.2014.10.053)
5. M. R. Hoffmann, S. T. Martin, W. Choi, D. W. Bahnemannt, *Chem. Rev.* **95** (1995) 69 (https://doi.org/10.1021/cr00033a004)
6. C. Hariharan, *Appl. Catal., A* **304** (2006) 55 (https://doi.org/10.1016/j.apcata.2006.02.020)
7. E. A. Meulenkamp, *J. Phys. Chem., B* **102** (1998) 5566 (https://doi.org/10.1021/jp980730h)
8. K. S. Babu, A. R. Reddy, K. V. Reddy, *Mater. Res. Bull.* **49** (2014) 537 (https://doi.org/10.1016/j.materresbull.2013.09.024)
9. K. Sinkó, G. Szabó, M. Zrínyi, *J. Nanosci. Nanotechnol.* **11** (2011) 4127 (https://doi.org/10.1166/jnn.2011.3875)

10. S. Farhadi, J. Safabakhsh, P. Zaringhadam, *J. Nanostruct. Chem.* **3** (2013) 69 (https://doi.org/10.1186/2193-8865-3-69)
11. R. K. Gupta, A. K. Sinha, B. N. Raja Sekhar, A. K. Srivastava, G. Singh, S. K. Deb, *Appl. Phys., A* **103** (2011) 13(https://doi.org/10.1007/s00339-011-6311-6)
12. R. Edla, N. Patela, M. Orlandi, N. Bazzanella, V. Bello, C. Maurizio, G. Mattei, P. Mazzoldi, A. Miotello, *Appl. Catal., B* **166**–**167** (2015) 475 (https://doi.org/10.1016/j.apcatb.2014.11.060)
13. W. Wen, J. M. Wu, J. P. Tu, *J. Alloys Compd.* **513** (2012) 592 (https://doi.org/10.1016/j.jallcom.2011.11.019)
14. S. Baruah, J. Dutta, *Sci. Technol. Adv. Mater.* **10** (2009) 013001 (https://doi.org/10.1088/1468-6996/10/1/013001)
15. H. N. Azlina, J. N. Hasnidawani, H. Norita, S. N. Surip, *Acta Phys. Pol., A* **129** (2016) 842 (https://doi.org/10.12693/APhysPolA.129.842)
16. E. G. Goh, X. Xu, P. G. McCormick, *Scr. Mater.* **78**–**79** (2014) 49 (https://doi.org/10.1016/j.scriptamat.2014.01.033)
17. P. Chandrasekaran, G. Viruthagiri, N. Srinivasan, *J. Alloys Compd.* **540** (2012) 89 (https://doi.org/10.1016/j.jallcom.2012.06.032)
18. K. P. Singh, S. Gupta, A. K. Singh, S. Sinha, *J. Hazard. Mater.* **186** (2011) 1462 (https://doi.org/10.1016/j.jhazmat.2010.12.032)
19. W. Cheng, S. Wang, L. Lu, W. Gong, X. Liu, B. Gao, H. Zhang, *Biochem. Eng. J.* **39** (2008) 538 (https://doi.org/10.1016/j.bej.2007.10.016)
20. O. J. Hao, H. Kim, P. C. Chiang, *Crit. Rev. Environ. Sci. Technol.* **30** (2000) 449 (https://doi.org/10.1080/10643380091184237)
21. S. Li, *Bioresour. Technol.* **101** (2010) 2197 (https://doi.org/10.1016/j.biortech.2009.11.044)
22. K. V. K. Rao, *Toxicol. Lett.* **81** (1995) 107 (https://doi.org/10.1016/0378-4274(95)03413-7)
23. M. Saquib, M. Muneer, *Dyes Pigments* **56** (2003) 37.(https://doi.org/10.1016/S0143-7208(02)00024-4)
24. S. Ameen, M. S. Akhtar, M. Nazim, H. S. Shin, *Mater. Lett.* **96** (2013) 228 (https://doi.org/10.1016/j.matlet.2013.01.034)
25. L. Wang, B. Liu, S. Ran, H. Huang, X. Wang, B. Liang, D. Chen, G. Shen, *J. Mater. Chem.* **22** (2012) 23541 (https://doi.org/10.1039/c2jm35617a)
26. L. Man, B. Niu, H. Xu, B. Cao, J. Wang, *Mater. Res. Bull.* **46** (2011) 1097 (https://doi.org/10.1016/j.materresbull.2011.02.045)
27. S. Vijayakumar, A. Kiruthika Ponnalagi, S. Nagamuthu, G. Muralidharan, *Electrochim. Acta* **106** (2013) 500 (https://doi.org/10.1016/j.electacta.2013.05.121)
28. S. Bazgir, S. Farhadi, *Int. J. Nanodimension* **8** (2017) 284 (http://www.ijnd.ir/article_656340.html)
29. X. Zhao, Z. Pang, M. Wu, X. Liu, H. Zhang, Y. Ma, Z. Sun, L. Zhang, X. Chen, *Mater. Res. Bull.* **48** (2013) 92 (https://doi.org/10.1016/j.materresbull.2012.10.001)
30. S. Farhadi, G. Nadri, M. Javanmard, *Int. J. Nanodimension* **7** (2016) 201 (http://www.ijnd.ir/article_649420.html)
31. T. Umamath, J. A. Selvi, S. A. Kanimozhi, S. Rajendran, A. J. Amalraj, *Ind. J. Chem. Technol.* **15** (2008) 560 (http://nopr.niscair.res.in/handle/123456789/2870)
32. R. Y. Hong, T. T. Pan, H. Z. Li, *J. Magn. Magn. Mater.* **303** (2006) 60 (https://doi.org/10.1016/j.jmmm.2005.10.230)
33. R. Hong, T. Pan, J. Qian, H. Li, *Chem. Eng. J.* **119** (2006) 71 (https://doi.org/10.1016/j.cej.2006.03.003)

34. J. C. Liu, J. H. Jean, C. C. Li, *J. Am. Ceram. Soc.* **89** (2006) 882 (https://doi.org/10.1111/j.1551-2916.2005.00858.x)
35. Z. Li, Y. Zhu, *Appl. Surf. Sci.* **211** (2003) 315 (https://doi.org/10.1016/S0169-4332(03)00259-9)
36. D. E. Zhang, L. Z. Ren, X. Y. Hao, B. Bin Pan, M. Y. Wang, J. J. Ma, F. Li, S. A. Li, Z. W. Tong, *Appl. Surf. Sci.* **355** (2015) 547 (https://doi.org/10.1016/j.apsusc.2015.04.018)
37. Y. Chen, L. Hu, M. Wang, Y. Min, Y. Zhang, *Colloids Surfaces, A* **336** (2009) 64 (https://doi.org/10.1016/j.colsurfa.2008.11.018)
38. M. Pudukudy, Z. Yaakob, *Chem. Pap.* **68** (2014) 1087 (https://doi.org/10.2478/s11696-014-0561-7)
39. Y. Ju, J. Fang, X. Liu, Z. Xu, X. Ren, C. Sun, S. Yang, Q. Ren, Y. Ding, K. Yu, L. Wang, Z. Wei, *J. Hazard. Mater.* **185** (2011) 1489 (https://doi.org/10.1016/j.jhazmat.2010.10.074)
40. Y. Ju, S. Yang, Y. Ding, C. Sun, A. Zhang, L. Wang, *J. Phys. Chem., A* **112** (2008) 11172 (https://doi.org/10.1021/jp804439z)
41. S. Meena, D. Vaya, B. K. Das, *Bull. Mater. Sci.* **39** (2016) 1735 (https://doi.org/10.1007/s12034-016-1318-4)
42. B. Ajitha, Y. A. Kumar Reddy, P. S. Reddy, H. J. Jeon, C. W. Ahn, *RSC Adv.* **6** (2016) 36171 (https://doi.org/10.1039/c6ra03766f).